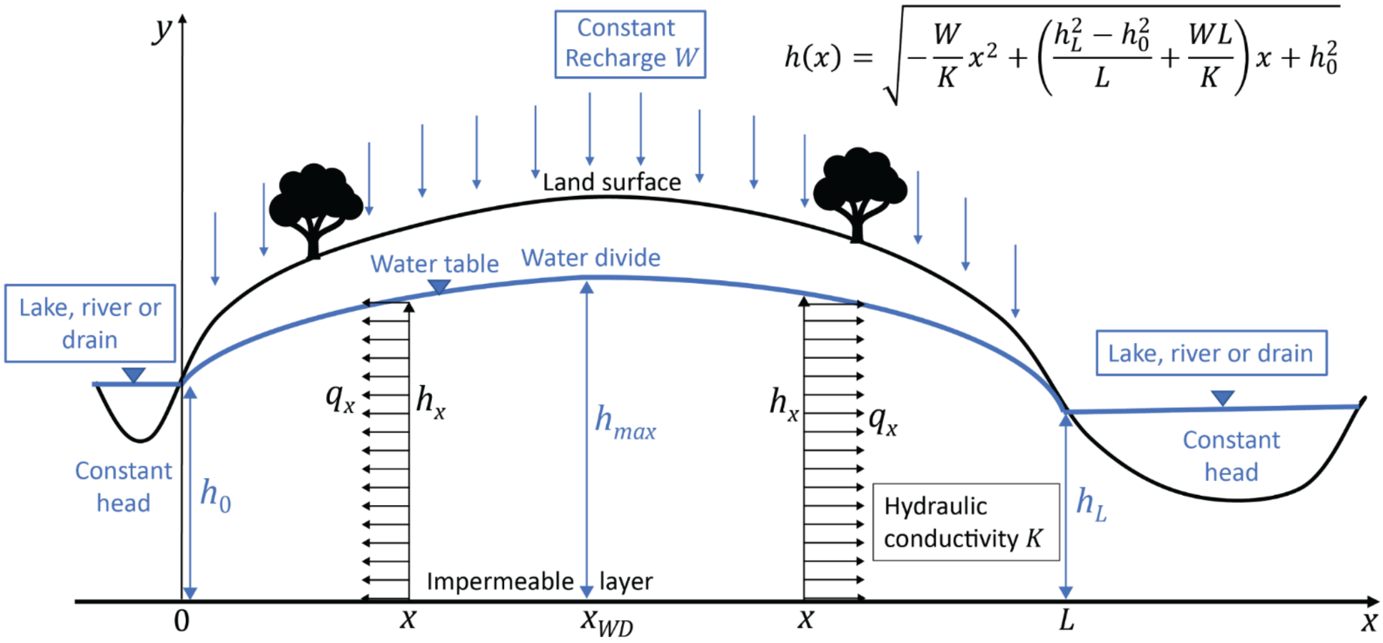

Analytical Hydrogeology of Inland and Coastal Unconfined Dupuit-Type Aquifers

Romain Chesnaux

THE GROUNDWATER PROJECT

Analytical Hydrogeology of Inland and Coastal Unconfined Dupuit-Type Aquifers

The Groundwater Project

Romain Chesnaux

Full Professor
Université du Québec à Chicoutimi
Québec/Canada

Analytical Hydrogeology of Inland and Coastal Unconfined Dupuit-Type Aquifers

The Groundwater Project
Guelph, Ontario, Canada

The Groundwater Project relies on private funding for book production and management of the Project.

Please consider sponsoring the Groundwater Project so that our books will continue to be freely available. https://gw-project.org/donate/↗

Thank you.

Published by the Groundwater Project, Guelph, Ontario, Canada, 2026.

Analytical Hydrogeology of Inland and Coastal Unconfined Dupuit-Type Aquifers / Romain Chesnaux
169 pages
DOI: https://doi.org/10.62592/IDJD7328↗
ISBN: 978-1-77470-151-5

Please consider signing up for the GW-Project mailing list to stay informed about new book releases, events, and ways to participate in the GW-Project. When you sign up for our email list, it helps us build a global groundwater community. Sign up↗.

APA (7th ed.) Citation
Chesnaux, R. (2026). Analytical Hydrogeology of Inland and Coastal Unconfined Dupuit-Type Aquifers. The Groundwater Project. https://doi.org/ 10.62592/IDJD7328↗.

THE GROUNDWATER PROJECT

Cover Image: Conceptual model of a Dupuit-type flow system in an unconfined aquifer, Romain Chesnaux, 2026

Dedication

To my beloved Maryse, Josée, Lorène and Anaïs, to the memory of my father who instilled in me a love of science, and to all my students. To Corsica and Morocco, the inspiring places where this book was written.

Table of Contents

The Groundwater Project Foreword

The 2022 United Nations (UN) World Water Day theme "*Groundwater – Making the Invisible Visible*" was pivotal in raising global awareness about groundwater as an invaluable resource, and the year concluded with the UN Water Summit on Groundwater at the UNESCO headquarters. One of the key outcomes of the Summit was a call for governments and other stakeholders to scale up their efforts to better manage groundwater.

Groundwater makes up 99% of all liquid fresh water on Earth, underpinning its importance in providing drinking water to the world, sustaining food production, and maintaining healthy ecosystems. Many important global organizations have concluded that there is a freshwater crisis and given that nearly all freshwater is groundwater, the freshwater crisis is a groundwater crisis. During drought in many locales, groundwater is the only freshwater available, putting even more pressure on groundwater resources.

According to the World Health Organization and UNICEF (WHO/UNICEF, 2025↗), 2.1 billion people (1 in 4) live without safely managed drinking water and 3.4 billion people (4 in 10) live without safely managed sanitation. With groundwater directly supporting 8 of the 17 UN Sustainable Development Goals, groundwater is an invaluable resource. Safe and reliable access to groundwater directly supports the 2026 UN World Water Day (March 22) Theme "*Water and Gender Equality*" focusing on ensuring that women and girls have equal rights and leadership in water management.

The Groundwater Project (GW-Project), a registered Canadian charity founded in 2018, pioneers in advancing the understanding of groundwater by providing groundwater education to everyone. Recognizing that the world needs more highly skilled groundwater scientists to solve the water crisis, the GW-Project plays a pivotal role in creating the knowledge base for building the much-needed human capacity for the development and management of groundwater.

The GW-Project gained global recognition with publication of 64 original books, 94 translated books (in 59 languages), 7 interactive groundwater educational tools/modules, and over 50 high-quality educational videos, all made possible by a dedicated international group of over 1000 volunteer professionals from a broad range of disciplines throughout 70 countries on six continents. Academics, practitioners, and retirees contribute by writing and/or reviewing books aimed at diverse levels of readers including children, youth, undergraduate and graduate students, groundwater professionals, and the general public.

The GW-Project operates with the philosophy that high-quality groundwater education should be freely accessible for everyone, and to that end our publications are available free-of-charge on our website↗. We thank our corporate sponsors and private donors for making this possible. Please consider sponsoring the GW-Project so we can continue to provide groundwater education free of charge.

The Groundwater Project *Board of Directors*, January 2026

Foreword

The essence of hydrogeology lies in the conceptual thinking used to solve complex groundwater problems. Conceptual models provide the foundational framework for selecting data-collection methods and executing quantitative analysis.

The author, Dr. Romain Chesnaux, is a full professor at the Université du Québec à Chicoutimi. He has published over a hundred peer-reviewed articles covering a wide spectrum of topics, while maintaining a lifelong commitment to the unique and enduring role of analytical solutions in hydrogeology education and problem-solving.

Analytical Hydrogeology of Inland and Coastal Unconfined Dupuit-Type Aquifers offers valuable methods for assessing groundwater flow in inland freshwater systems, as well as groundwater flow, seawater intrusion, and effects of sea level rise in coastal freshwater systems adjacent to saltwater bodies.

Visual thinking and communication in this book serve as an exemplary guide for using sketches to visualize flow systems, which is a crucial skill both for mathematical thinking and communicating complex ideas.

This book preserves elegance in a digital age by demonstrating how analytical models represent the formal foundation of quantitative hydrogeology. Analytical modeling is a disciplined way of thinking that must not be lost while commercial numerical models are increasingly dominant in practice and in research.

It must not be forgotten that analytical solutions remain a precious resource that makes it possible to analyze results obtained from computer simulations, including machine-learning programs and AI tools. They may also play a vital role in contexts where technological and financial resources do not allow full deployment of numerical tools and processes, such as in the Majority World and research centers with limited means.

John Cherry, The Groundwater Project Leader

Guelph, Ontario, Canada, June 2026

Preface

This guide, composed of seven sections, is intended for practitioners in hydrogeology, for undergraduate and graduate students in Earth sciences/hydrogeology or civil/environmental engineering, and for academic researchers.

The aim of the guide is not to present or recall the basics of hydrogeology that are already extensively addressed in many textbooks. Rather, the guide focuses on compiling and presenting a series of analytical solutions for solving practical problems in Dupuit-type flow systems in both inland and coastal aquifers. These solutions can be included in the toolbox of professional practitioners and can be applied for consulting work. They can also be used by graduate students and by researchers to improve their knowledge of quantitative hydrogeology and for solving practical problems at an academic level. All the equations can be solved with Excel spreadsheets.

Analytical solutions for solving groundwater flow in Dupuit-type aquifers are provided for solving groundwater flow equations and for calculating groundwater velocity and transit time, groundwater recharge, and groundwater volumes in unconfined Dupuit-type aquifers. A particular application is proposed for assessing seawater intrusion and the impacts of climate change for different scenarios.

Acknowledgments

I deeply appreciate the thorough and useful reviews of and contributions to this book by the following individuals:

- John Molson, Full Professor, Université Laval, Québec, Canada;
- Christopher Neville, Chief Hydrogeologist, S.S. Papadopoulos & Associates, Inc., Canada;
- Alain Rouleau, Professor Emeritus, Université du Québec à Chicoutimi, Québec, Canada;
- An anonymous reviewer.

I am grateful for Amanda Sills and the Formatting Team of the Groundwater Project for their oversight and copyediting of this book. I especially thank Claire Tiedeman (retired, U.S. Geological Survey) and Eileen Poeter (Colorado School of Mines, Golden, Colorado, USA) for an exceptional effort in an extremely conscientious and elegant review, edit and production of this book. I am grateful to John Cherry for our initial discussions, encouragement and expert advice regarding the contribution and relevance of the project for this book. I also thank the Université du Québec à Chicoutimi (UQAC) for its continuous support during my career as well as my dear departmental colleagues (département des Sciences Appliquées).

1 Introduction

1.1 Teaching Hydrogeology: Trying to Reveal "A Hidden Resource"

When I teach hydrogeology, my first introduction to the students is to declare that most of the material and methods that are presented to them are conceptual. Groundwater is hidden below our feet in underground voids and pore spaces contained within *geological boxes*. For these reasons, no one can ever directly access this hidden world. Only by drilling boreholes—mere pinheads in the context of geological scale—do we have limited and expensive access to the underground world. Therefore, to better understand and describe groundwater, we conceptualize these hydrogeological systems by establishing models. By design, these models are a simplified representation of reality. Because the necessary simplifications and assumptions of models fail to perfectly represent reality, the definition of every model is uncertain. Hence, one of the biggest challenges for hydrogeologists involves establishing the most accurate models to understand and predict groundwater flow as well as contaminant transport. A thousand different models can represent the same unique reality. The hydrogeologist faces the difficult choice of deciding which model or group of models will best describe and predict groundwater flow systems in a particular geological system.

This introduction may lead to wondering whether hydrogeology is or is not an exact science (Poeter, 2007). Such an argument may appear as a provocation. Yet, all models are misleading in the sense that they all exist with limiting assumptions and are always based on a simplified representation of reality. Knowing that, hydrogeological modeling uses several independent methods or tools and compares their results. When differences are small, our degree of confidence in the results is increased.

1.2 Groundwater Flow Modeling: Physical, Mathematical and Artificial Intelligence

There are four types of models that can be developed by hydrogeologists.

1. Physical models are experimental sandbox models that allow reconstructing the subsurface using appropriate hydraulic boundary conditions. Typically, these physical bench-scale models represent groundwater flow at small scales.
2. Mathematical models include a description of the physics of groundwater flow with mathematical equations that can be solved either analytically or numerically.
3. Models obtained from machine learning—a subfield of artificial intelligence—consist of designing and implementing parametric and nonparametric methods to generate models to then solve groundwater problems. These machine learning models are possible when hydrogeologists have access to large amounts of data acquired in real time.

4. Models based on theory-guided machine learning, sometimes referred to as physics-informed machine learning, consist of integrating theoretical knowledge into the learning process of machine-learning models. In this case, the learning process includes mathematical equations that govern groundwater flow and transport. Such models based on theory-guided machine learning are therefore hybrid models because they include machine learning processes with respect to the physics of groundwater flow.

1.3 Analytical vs Numerical Modeling: The Pros and Cons

In hydrogeology, with two equations, a wide range of groundwater flow problems in an aquifer system can be solved: 1) the continuity equation, which is based on the principle of mass conservation; and 2) Darcy's law. Combining these two equations yields the hydraulic diffusion equation, which solves the basic groundwater flow problem by calculating the hydraulic head field—representing the total energy of water—at any location in space and time. The hydraulic diffusion equation is then solved with the knowledge of key hydraulic properties—hydraulic conductivity, storativity of the aquifer, and a consideration of the boundary conditions of the aquifer system. Two challenges must be overcome by the hydrogeologist: 1) developing a conceptual model of the aquifer system including its geological composition as well as its physical and hydraulic boundaries; and 2) defining the hydraulic properties of the aquifer system components considering that hydraulic properties may vary in space (heterogeneity) and may vary with direction (anisotropy).

Considering that most aquifer systems are naturally *heterogeneous* and *anisotropic*, and considering the high level of uncertainty in defining the values of the hydraulic parameters, it is extremely difficult for hydrogeologists to determine these values with confidence and, therefore, to obtain accurate models.

Numerical models are employed to address more complex problems by solving a discrete form of the hydraulic diffusion equation. Analytical models can be employed for simple settings and systems with linear responses, or when assumptions are made to simplify (e.g., linearize) the problem so that it can be solved directly with basic mathematical tools. Numerical models can handle more complex systems than analytical models because they are more versatile with respect to the spatial and temporal variation in parameters, geometry, and boundary conditions. Indeed, numerical models allow for more flexibility regarding the inclusion of variable temporal conditions (steady-state versus transient), variable dimensionality (one-, two-, and three-dimensions), as well as heterogeneous and anisotropic hydraulic properties. By contrast, analytical solutions are developed for simpler conditions, usually steady-state, one or two dimensions, homogeneous and isotropic hydraulic properties. These restrictive assumptions render the solution easier to obtain but may also represent an oversimplification of reality.

Among the advantages of numerical models is that they are more representative of the complexity of the aquifer natural environments. Among the limitations of numerical modeling, though, is the amount of knowledge that the modeler must have on the aquifer parameters (input data), such as detailed aquifer-property data. The level of accuracy of these input data may be poor. In this case that would mean that the results obtained (output data) from the numerical model would also be of poor value. Numerical models are also more costly, they require more user expertise, they can be time consuming to develop and run, and their solution is for discrete points in space and time, requiring interpolation to estimate the values between those points. In contrast, analytical models provide a continuous solution with a solution for every point in space and time. Analytical solutions are less expensive and faster to develop. Although these solutions may be oversimplified and based on limited input data, they can still provide useful results if their assumed conditions—physical processes, boundary conditions, aquifer properties, flow directions, etc.—are consistent with the site conceptual model.

A good approach, when possible, is to use a combination of analytical and numerical models and compare the independent results. The modeler then has a rapid estimate of the solution from the analytical model while waiting for the development of the numerical model. Also, the modeler will be able to reach a higher degree of confidence in the models established and be able to decide if a simpler analytical model could be used.

Based on the author's experience, simpler models are often better models. Some modelers, especially those with limited experience, try to develop detailed models because they believe that more comprehensive models will be more representative of reality and will therefore be more accurate. This approach can be misleading at best and may in fact be less accurate. This mistake is easy to make considering that numerical error or uncertainty can be hidden, particularly when complex three-dimensional figures are generated which may seem impressive but are difficult to compare and may mask numerical error. Most importantly, a modeler must acknowledge all model assumptions and limitations to clients. For example, the most complex and detailed numerical model with the most parameters and processes may yield inaccurate results, especially if the parameters, boundary conditions, and other input data have a low accuracy or high uncertainty.

One can never assume accurate results when the quality and accuracy of the input data are not sufficiently known. When limited input data are available, it is usually better to simplify the model and not lose confidence by making excessive assumptions. Ultimately, if possible, consider replacing a numerical model with an analytical model, which can often provide more accurate results than a data-poor numerical model.

1.4 Why Do Analytical Solutions Still Have a Role to Play? And How Can They Be Applied?

Even though numerical modeling and theory-guided machine learning are popular and powerful tools, they should nevertheless not replace the rest of the tools in a hydrogeologist's toolbox. Hydrogeologists who use analytical solutions should not be perceived as "old school" modelers because analytical solutions still have and will continue to have a valuable role. Analytical models are efficient tools that should continue to be considered by professionals—in engineering and hydrogeological consulting—and by researchers and students. Indeed, analytical solutions are easy to use, inexpensive in terms of time and money, and can provide valuable insights on the basic behavior of groundwater flow (Haitjema 2006).

Solving an analytical model usually only requires a free, 'back-of-the-envelope' calculation or an Excel spreadsheet. Analytical solutions can also give a rapid estimate of the general order of magnitude of a calculated groundwater quantity.

Analytical models are useful for building understanding as well as for solving groundwater problems. For instance, when students learn to pose and solve equations, they must first understand the problem they want to describe and model. To succeed in this task, they must thoroughly understand the hydrogeological system instead of simply putting data into a black box, which a numerical model may appear to be. This aspect is very important as I have seen many students using numerical models without fully understanding what they can or cannot do.

Instead, solving an analytical model requires students to understand what they are doing. The modeler needs to decide when analytical solutions can be employed, and which assumptions and simplifications can be made for the problem to be solved. Analytical solutions are a valuable check on many numerical results. A simple analytical solution often suffices. Nevertheless, the task of applying closed-form solutions to a problem may be tricky and may still require a thorough analysis and conceptualization of the hydrogeological system to be modeled.

For all the reasons discussed previously, several researchers still advocate the use of analytical solutions in hydrogeology. I am one of them. We should remember that our science is young and that analytical models developed in the mid-nineteenth century are still being used. Moreover, we should continue to develop more analytical approaches despite already being deeply engaged in the era of numerical solutions and artificial intelligence.

1.5 Objectives of this Book and Short Description of its Contents

This book provides simple analytical solutions that can be directly applied (as closed-form solutions) by practitioners for solving a variety of practical problems. The guide is intended for people at all levels who already know the fundamentals of hydrogeology (e.g., curious readers, students, professionals, researchers). Therefore, rather than recalling the basics of hydrogeology—already extensively well presented in many textbooks—this is a guide to directly applicable solutions for solving problems of groundwater flow in Dupuit-type unconfined aquifers.

This guide presents a compilation of simple analytical solutions for practical application in hydrogeology that have been developed and published by the author over the last two decades. The guide proposes the use of the Dupuit-Forchheimer model for solving multiple problems of regional groundwater flow systems under different conditions and for solving different problems. Practical examples are given as illustration. The solutions are also versatile since they can apply either in unconsolidated deposits or fractured-rock aquifers as long as the Dupuit-type conditions are respected.

Section 2 introduces the Dupuit-Forchheimer models that can handle most of our modeling needs involving natural groundwater flow in aquifers at a regional scale when the horizontal velocity component dominates. To make the guide easy and practical for the reader, it has been divided into sections that refer to different Dupuit-type aquifer environments: inland aquifers and island inland aquifers (Section 3), coastal aquifers (Section 4), and oceanic island aquifers (Section 5). Each section follows a similar structure:

1. description of the context and hydraulic head profiles of the conceptual model;
2. closed-form analytical solutions for solving groundwater velocity, groundwater travel time, groundwater volume, and mean residence time;
3. applications of the solutions for calculating other variables like recharge; and
4. seawater intrusion and fresh groundwater volumes available in coastal and oceanic-island Dupuit-type aquifers (for Sections 4 and 5 only).

Section 6 specifically addresses the issue of climate change on oceanic Dupuit-type aquifers while investigating the impacts of climate change on groundwater resources. In particular, the usefulness of analytical solutions to predict the impact of climate change on coastal and island oceanic aquifers is illustrated with respect to the effects of climate change including sea-level rise and coastal erosion, as well as changes in recharge of oceanic aquifers. Finally, in Section 7, the guide presents a series of examples to illustrate the application and use of closed-form analytical solutions developed in the guide. These examples are based on a specific case and serve as an illustration of how closed-form solutions can be solved with Excel spreadsheets.

1.6 Practical Applications of the Closed-Form Analytical Solutions

The closed-form analytical solutions presented in this guide can be used for several applications. The main applications are suggested below. All the solutions can be solved with an Excel spreadsheet, making their use accessible and efficient for practitioners, engineers, and students.

- Groundwater flow in unconfined aquifers is characterized by the position and shape of the water table. The water table profile is controlled by both the hydraulic properties and the boundary conditions (side and surface conditions) of an unconfined Dupuit-type aquifer. The profile of the water table is controlled by the ratio (W/K), where W is the recharge rate of the aquifer and K is the hydraulic conductivity of the aquifer. Knowing the profile of the water table allows for the estimate of the ratio W/K and ultimately the estimate of one of the unknown variables when the other one is either known or can be estimated with another independent method.
- Groundwater velocities and travel time are groundwater variables that are important to characterize for many reasons. Travel times can provide a first estimate of the contaminant residence times in aquifers and the time required for a contaminant dissolved in groundwater to circulate from an upstream point to a downstream point in an aquifer. Knowing this time is crucial for anticipating possible contamination issues and for determining contaminant migration within an aquifer. The solutions presented in this guide have significant limitations because only advective transport in the saturated zone of the aquifer below the water table is considered with closed-form solutions for velocities and travel times. Dispersion and diffusion are neglected as well as mass transport in the vadose zone of the aquifer. Modelers must be aware of these limitations so they can evaluate the accuracy of the results for their study and whether travel times calculated with the closed-form solution would underestimate or overestimate the field travel times.
- Groundwater recharge is a crucial parameter for estimating the capacity of the aquifer to renew its groundwater. Recharge can be estimated from the water table profile as well as from groundwater travel time; relevant analytical solutions are presented in this guide.
- Estimating groundwater volumes is of interest not only in inland environment, but is of particular interest in oceanic environments to assess the quantity of freshwater that is available either in coastal or island oceanic aquifers.
- Mean groundwater residence time derived from groundwater volume and recharge allows for the estimate of the mean time for groundwater to circulate in the aquifer and to renew. Mean residence times also help with interpreting the groundwater chemistry signature—young versus mature groundwater.
- The effects of climate change are particularly critical in coastal or island oceanic aquifers, because coastal environments are highly populated and worldwide coastal populations rely on these aquifers for their water supply. This guide presents analytical solutions that allow for the anticipation of climate change impacts while evaluating changes in groundwater availability for various scenarios and environmental parameters.
- Finally, analytical solutions should be a prerequisite for every numerical modeling project, as numerical models should be verified as much as possible against analytical

solutions. The purpose of using analytical solutions for flow problems is to better understand the mechanics of a flow system, which is extremely valuable.

2 Dupuit-Type Flow Aquifers: Presentation and Assumptions

This section describes a Dupuit-type flow system and identifies the associated assumptions and limitations. It also explains how to verify if a real aquifer under study satisfies the assumptions so that it can be modeled according to the Dupuit conditions. Such verification is a prerequisite to using the equations and solutions provided to solve different hydrogeological problems in inland, oceanic, and island unconfined Dupuit-type aquifers.

2.1 Groundwater Flow in an Unconfined Aquifer

Unconfined aquifers are shallow permeable formations in contact with the atmosphere. They are bounded below by a lower permeability formation represented by an aquitard. Unconfined aquifers are composed of the saturated zone below the water table and the vadose zone above it. The vadose zone comprises the capillary fringe just above the water table and the unsaturated zone between the ground surface and the capillary fringe. Unconfined aquifers are bounded by surface water features—represented by rivers, lakes, or drains—and/or by no-flow boundaries—represented by low permeability materials or groundwater divides. Unconfined aquifers are recharged at their top by precipitation. The groundwater flow paths along the aquifer are directed and oriented according to the hydraulic heads represented by equipotential lines. Figure 1 shows the conceptual model of the general behavior of an unconfined aquifer.

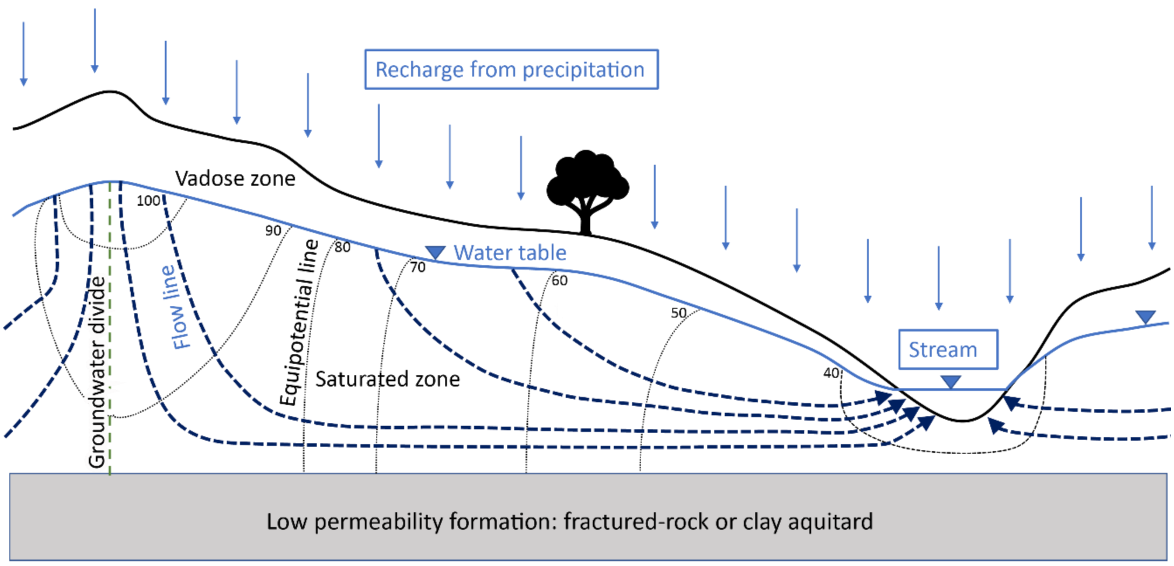

Figure 1 - Conceptual model of groundwater flow paths (dashed lines with arrows) in an unconfined aquifer (vertical cross-section). The numbers (40 to 100) are given as examples to represent the values of hydraulic head contours (equipotential lines shown as thin, dotted, gray lines) that govern the orientation and direction of the flow paths. Labels outlined by a rectangle are recharge or head boundaries. The cross section has significant vertical exaggeration.

2.2 Dupuit-Type Flow Description, Conditions and Assumptions

Dupuit (1863) was the first to quantitatively address regional groundwater flow. He simplified the system by ignoring vertical flow, thus reducing the problem to that of one-dimensional horizontal flow. The resulting simplified approach of Dupuit (1863) can be applied to saturated groundwater flow in a single dimension in unconfined aquifers when flow conditions are steady. Other assumptions of Dupuit-type flow are as follows.

- The aquifer is homogeneous and isotropic.
- The aquifer overlies a fully-horizontal, impervious substratum.
- The aquifer is recharged by surface infiltration, and discharges to a fixed-head boundary.
- The vertical component of groundwater velocity is neglected, and only the horizontal component of the velocity is considered. Horizontal flow dominates over vertical flow, and the equipotential lines are vertical. Thus, surface recharge is instantaneously uniformly distributed vertically over the aquifer thickness.
- The hydraulic head in the aquifer is represented by the phreatic surface (water table) elevation above the horizontal impervious substratum. It also represents the saturated thickness of groundwater below the water table; thus, the head datum is the base of the aquifer. Groundwater levels and piezometric levels are thus the same.
- Groundwater flow paths are perpendicular to the hydraulic head contours (equipotential lines) due to the steady-state flow conditions and the homogeneous and isotropic hydraulic conductivity of the aquifer.
- The flow is laminar.
- There is no influence of pumping or injecting; only natural flow is considered, without external human influence.

A rule of thumb for the Dupuit-Forchheimer approximation states that it is acceptable for an aquifer length L which is at least five times longer than the mean aquifer thickness (Kirkham, 1967).

2.3 Dupuit-Forchheimer Model of Groundwater Flow, Water Table Profile Calculation and Calculation of Groundwater Divide Position

Two decades after Dupuit (1863), Forchheimer (1886) presented a differential equation for the water table elevation in unconfined aquifers, referring to Dupuit's approximation. In the Dupuit-Forchheimer model (Dupuit, 1863; Forchheimer, 1886, 1901), saturated groundwater flow occurs within an unconfined aquifer underlain by an impervious boundary. The aquifer is bounded by two fully-penetrating fixed-head boundaries. The flow in this aquifer is considered horizontal and one-dimensional according to the Dupuit approximation, which ignores unsaturated flow and is essentially a 1D approach to solve vertical 2D plane problems in an unconfined aquifer (Strack, 1989). The slope of the tangent to the water table is assumed to be small; thus, the vertical component of the gradient vector is assumed to be negligible. The flow velocity is assumed constant throughout the depth of flow. A uniform, annual average rate of infiltration, W [LT^{-1}] is applied over the entire upper boundary of the aquifer, establishing a regional groundwater flow system. Flow is assumed to be at steady state, which implies that the downstream discharge equals the groundwater recharge and that the water table position does not change over time. The conceptual model of the Dupuit-type flow aquifer is presented in Figure 2.

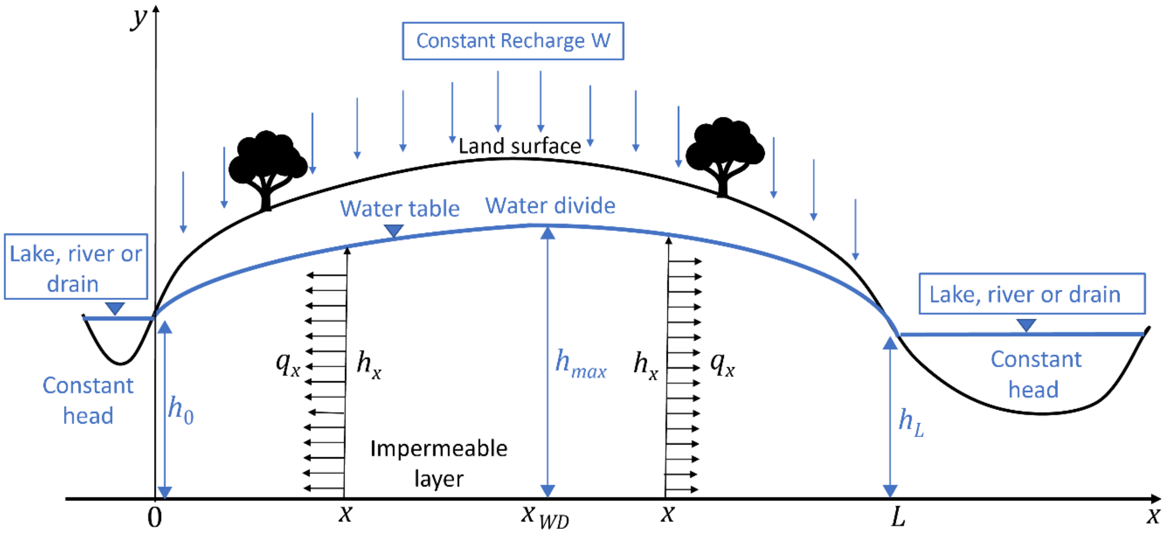

Figure 2 - Conceptual model of a Dupuit-type flow system in an unconfined aquifer—Case I with $0 < x_{WD} < L$.

The conceptual flow system can be described using the Dupuit-Forchheimer differential equation, which is a simplification of the general diffusivity equation, and can be written as shown in Equation (1).

$$\frac{\mathrm{d}}{\mathrm{d}x}\left(K\,h\,\frac{\partial h}{\partial x}\right) + W = 0 \tag{1}$$

where:

h = phreatic surface elevation or saturated thickness above the horizontal impervious substratum; also denoted hydraulic head [L]

W = recharge rate of the aquifer [LT^{-1}]

K = hydraulic conductivity of the aquifer [LT^{-1}]

The general solution to the Dupuit-Forchheimer equation for the phreatic surface elevation (h) versus distance (x) is given by Bear (1972) in Equation (2).

$$h(x) = \sqrt{-\frac{W}{K}x^2 + \left(\frac{h_L^2 - h_0^2}{L} + \frac{WL}{K}\right)x + h_0^2} \qquad (2)$$

where:

L = length of the aquifer [L]

h_0 and h_L = fixed upstream (x=0) and downstream (x=L) heads, respectively (as shown in the example given in Figure 1, where h_0>h_L)

As explained by Forchheimer (1901), the phreatic surface $h(x)$ in each case describes a semi-ellipse with a maximum elevation $h_{\max}$ at x_{WD}. The gradient dh/dx is zero at $h_{\max}$ so it is a groundwater divide. Equation (2) can be rearranged to determine the position of the groundwater divide, x_{WD} where dh/dx=0 as shown in Equation (3) (Bear, 1972).

$$x_{WD} = \frac{L}{2} + \frac{K}{2WL}(h_L^2 - h_0^2) \qquad (3)$$

The location of x_{WD} can be either between the two boundaries of the aquifer (between x=0 and x=L in Figure 2) or, when x_{WD}<0, beyond the upgradient boundary. These two situations are developed in Section 3.

2.4 Verifying if the Aquifer Under Study Satisfies the Dupuit-Type Flow Conditions

The Dupuit-type flow conditions in an unconfined aquifer can be verified by plotting h^2 versus x (a polynomial function of second degree) along a flow line when piezometric data from the aquifer are available. If the curve of h^2 versus x fits with a quadratic regression as presented in Figure 3 (parabolic curve), then it means that the water table elevation in the aquifer satisfies Equation (4) obtained from Equation (2) by squaring both sides.

$$h^2(x) = -\frac{W}{K}x^2 + \left(\frac{h_L^2 - h_0^2}{L} + \frac{WL}{K}\right)x + h_0^2 \qquad (4)$$

In these conditions, when groundwater flow in the aquifer satisfies the Dupuit flow conditions, the aquifer can be modeled as a Dupuit-type unconfined aquifer. The regression presented in Figure 3 could be representative of the model presented in Figure 2.

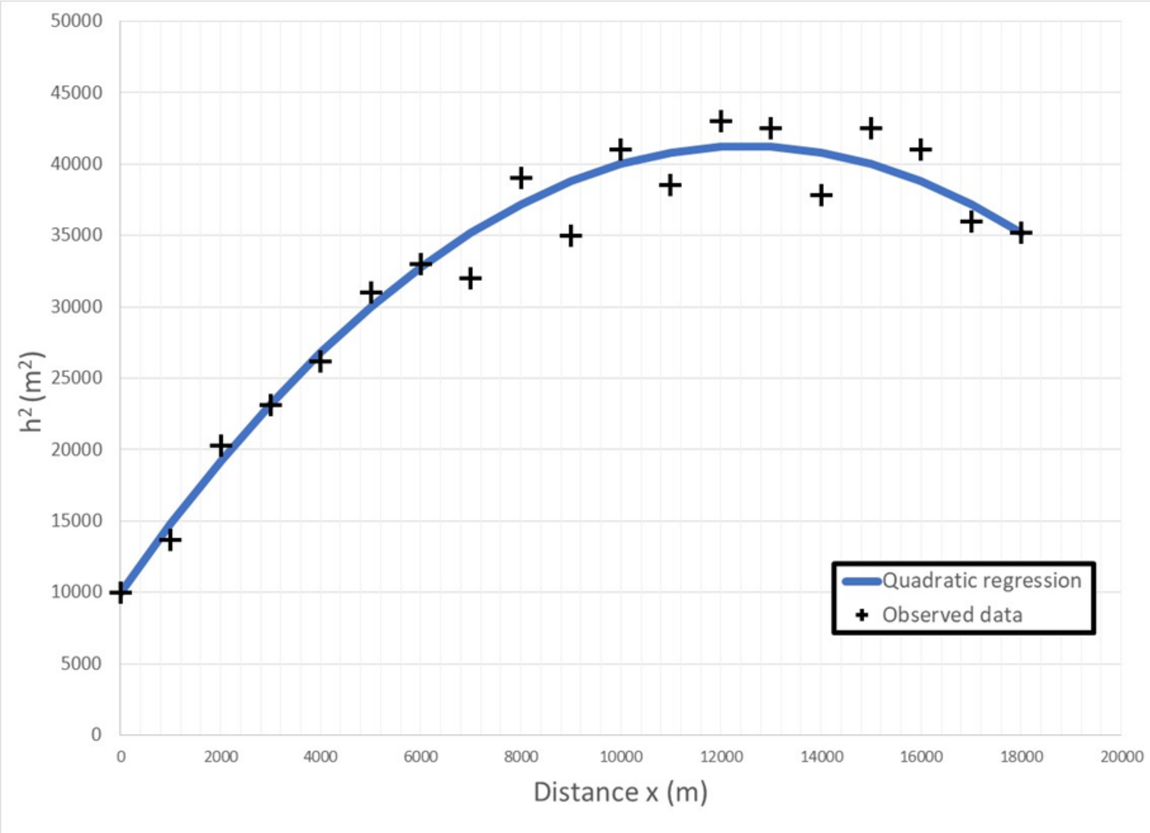

Figure 3 - Quadratic regression on the observed squared hydraulic head data along a flow line of an unconfined aquifer with h_0=$h(x$=$0)$=100 m, h_L=$h(x$=$L)$=187.6 m and L=18,000 m. In this conceptual graphic, the observed data of h^2 versus x fit a quadratic regression (h^2=ax^2+bx+c), which indicates that the unconfined aquifer agrees with the Dupuit assumptions and as such can be considered as a Dupuit-type aquifer. The constant values a, b, and c of the regression respectively represent the values of $-W/K$, $((h_L^2$-$h_0^2)/L) + (WL/K)$, and h_0^2.

2.5 Discussion on the Dupuit-Type Flow Conditions

Dupuit conditions can be satisfied both in unconsolidated deposits and fractured-rock aquifers. In practice, there are many situations where Dupuit-type flow models can be assumed because in most regional scale situations of natural groundwater flow in aquifers, the horizontal velocity component dominates over the vertical component (Chesnaux 2013; Haitjema 1995; Miled et al., 2023). Also, Haitjema and Brucker (2005) have demonstrated that the Dupuit-Forchheimer approximation is often valid in areas with properties typical of *usable aquifers*—aquifers from which adequate quantities of water can be pumped for public, domestic, or industrial use.

Figure 4 shows a conceptual unconfined aquifer in plan view at the scale of a watershed. When the Dupuit-type flow conditions are satisfied in the aquifer, then many cross-sections can be realized along different flow paths and interpreted according to the Dupuit-type flow model.

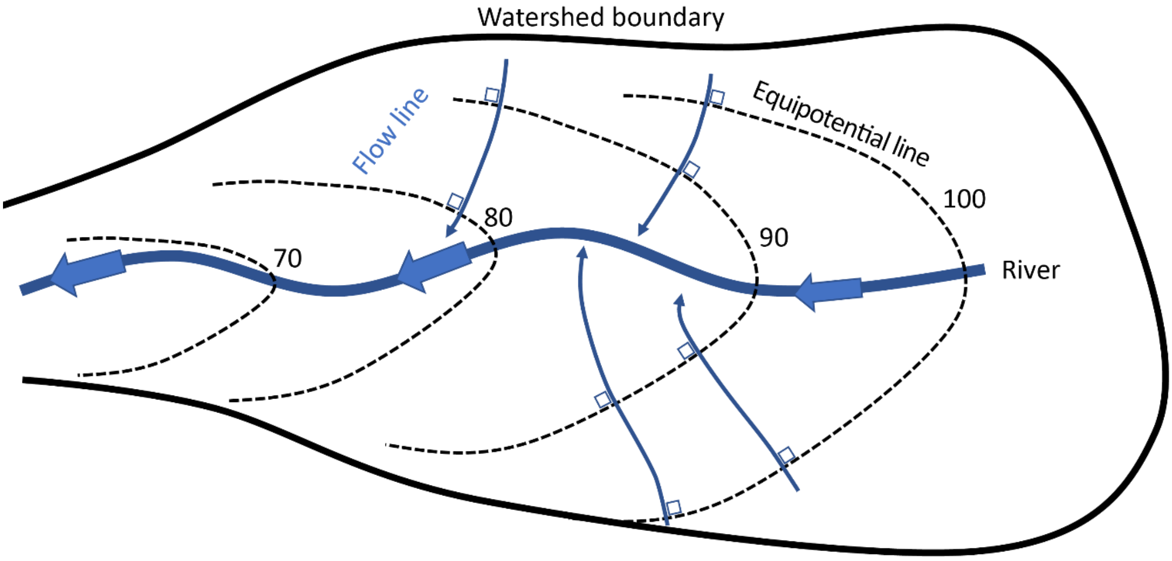

Figure 4 - Conceptual groundwater contour map of a watershed under steady-state flow conditions in a homogeneous and isotropic unconfined aquifer. In these conditions, flow lines are constructed at right angles to the equipotential lines as indicated by the squares at their intersection.

Finally, sloping aquifers are not considered in this book. It is only in the case of horizontal unconfined aquifers—those with a horizontal bottom boundary—where the analytical solutions presented in the following sections can be applied.

3 Inland and Inland-Island Dupuit-Type Aquifers

This section presents a series of closed-form analytical solutions for water table configurations, groundwater velocity, groundwater travel times, groundwater recharge, groundwater volumes, and groundwater mean residence times in inland Dupuit-type aquifers. The section also presents the solutions for the specific cases of inland-island aquifers with simplified geometries, both strip and circular.

3.1 Conversion of the Natural System into a Single Conceptual Model

In order to study groundwater flow in a Dupuit-type aquifer, a regional model as presented in Figure 2 will be converted into one or two systems bounded by an upstream no-flow boundary and a downstream fixed-head boundary, depending on the location of the groundwater divide. One such conversion is presented in Chesnaux and others (2005). Indeed, two scenarios can exist from the Dupuit model applied along a flow line: either the groundwater divide may physically exist between the two fixed-head boundaries as presented in Figure 2, or it may be *imaginary*, meaning it is external to the aquifer system, as presented in Figure 5. The scenario that prevails depends on the relative values of the fixed-head conditions at the boundaries of the Dupuit-type aquifer.

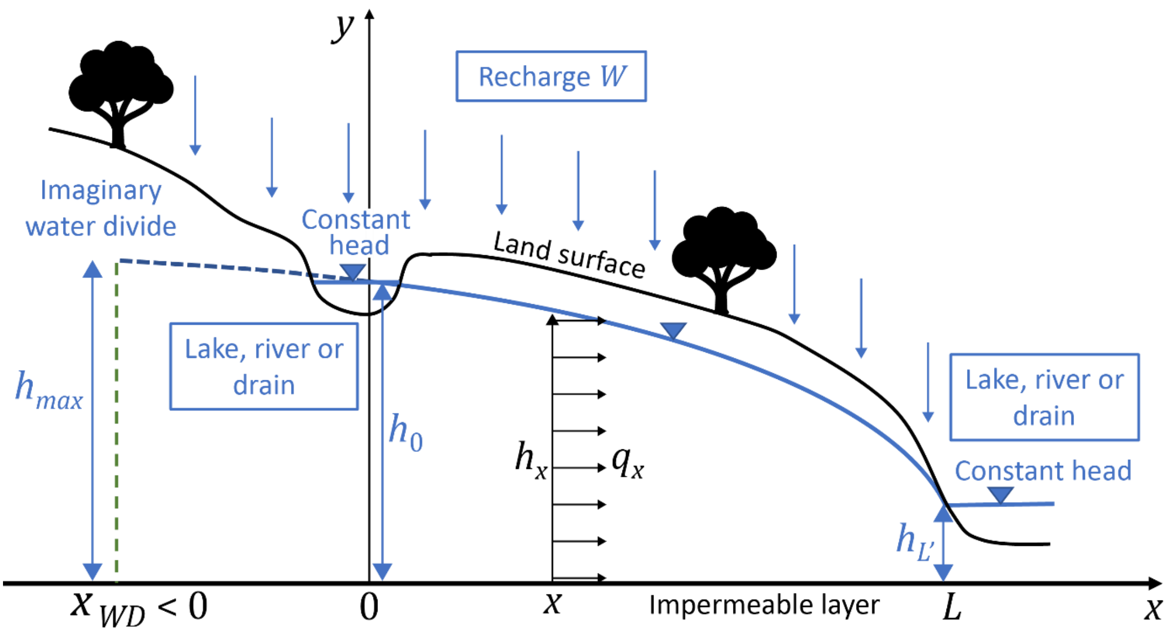

Figure 5 - Conceptual model with an imaginary groundwater divide beyond the upstream boundary (x_{WD} < 0)—Case II.

We define Case I as the flow system shown in Figure 2, with a flow divide between two fixed-head boundaries and Case II as an otherwise equivalent system without an internal flow divide where flow is unidirectional between the upstream and downstream constant head boundaries (Figure 5). In Case II, the flow divide is imaginary and is located upgradient of the constant head boundary at x=0, that is, at $x_{WD} < 0$.

After Forchheimer (1901), the phreatic surface $h(x)$ in each case describes a semi-ellipse with a maximum elevation $h_{\max}$ at x_{WD} either somewhere between the two boundaries (Case I—Figure 2) or beyond the upgradient boundary (Case II—Figure 5). The gradient $\mathrm{d}h/\mathrm{d}x$ is zero at $h_{\max}$. In Case II, x_{WD} is negative and located at what can be considered an imaginary location.

The particular location of the water divide depends on the relative magnitude of the boundary heads h_0 and h_L as well as the recharge rate and the hydraulic conductivity. From Equation (3), we can deduce that the condition of $h_0^2 - h_L^2 < \frac{WL^2}{K}$ (that is, x_{WD}>0) corresponds to Case I while $h_0^2 - h_L^2 > \frac{WL^2}{K}$ (that is, $x_{WD} < 0$) corresponds to Case II.

Each of the two cases must be transformed into a single flow system bounded by an upgradient impermeable boundary and a downgradient fixed head boundary as shown in Figure 6.

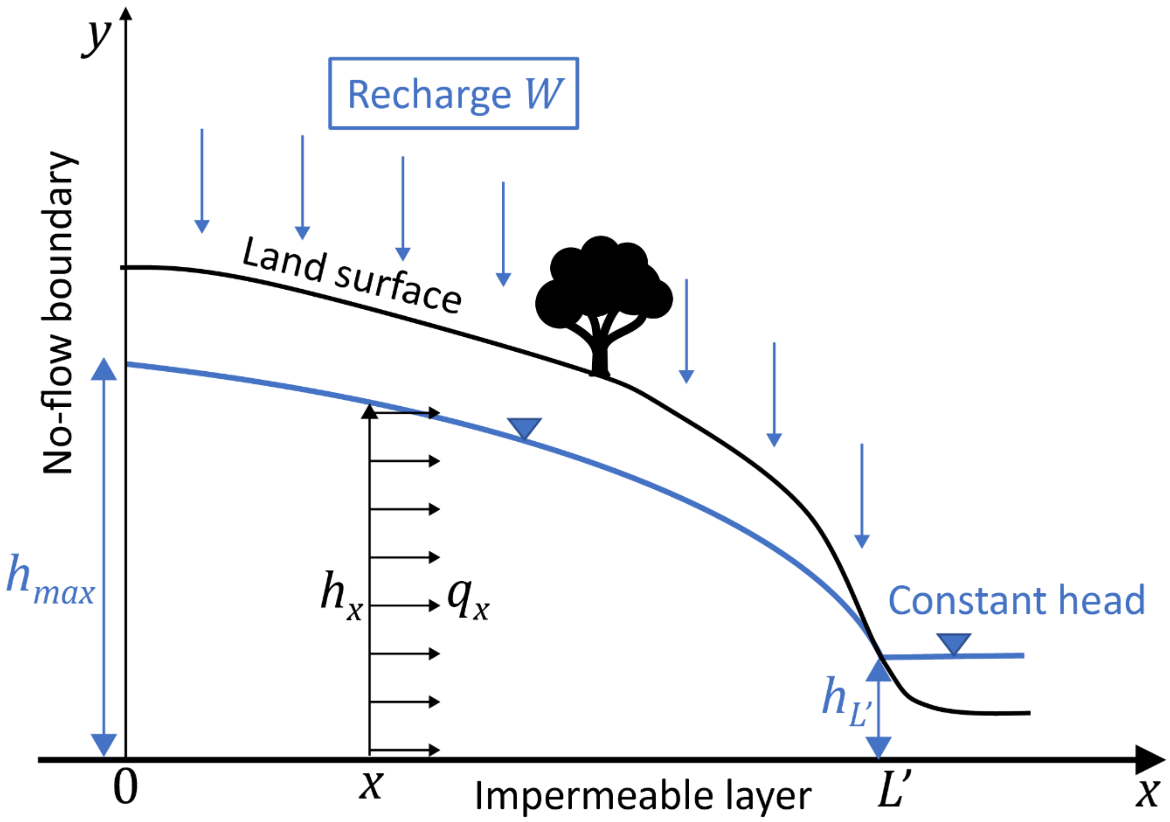

Figure 6 - Final transformed system for developing general analytical solutions.

To transform Case I, we first separate the regional system into the two subdomains on either side of the water divide. Both subdomains can then be reduced to the single problem shown in Figure 6, with a length L' of either x_{WD} for the left subdomain, or ($L-$

x_{WD}) for the right subdomain. We will take the origin (x=0) in the transformed system as representing the no-flow (impermeable or symmetric) upgradient boundary.

To transform Case II, we place the imaginary upgradient water divide at the origin of the transformed system. The Case II coordinates between x=0 and x=L will then map to the transformed system between x=$|x_{WD}|$ and x=L+$|x_{WD}|$, where L+$|x_{WD}|$= L', and L' represents the length of the transformed system (Figure 6). Groundwater flow is thus only meaningful with respect to the original Case II system between x=$|x_{WD}|$ and $x = L'$. If $|x_{WD}|$ =0, the solution reverts to Case I. Exercise 1 offers the opportunity to determine the location of the groundwater divide in an aquifer and to illustrate how the groundwater system can be transformed in different cases (Cases I and II).

To recapitulate, the analytical tools presented below for inland Dupuit-type aquifers can be applied to systems with constant groundwater recharge and all three of following lateral boundary conditions.

1. One no-flow boundary and one fixed head boundary condition.
2. Two fixed head boundary conditions and a flow divide within the system.
3. Two fixed head boundary conditions and a flow divide outside of the system.

3.2 Groundwater Velocity

In the following development, we will calculate the groundwater velocity within the transformed system of Figure 6 between x=0 and x=L.

We begin with Darcy's Law for groundwater flow, written as shown in Equation (5).

$$q_x = -K\frac{\mathrm{d}h}{\mathrm{d}x} \tag{5}$$

where:

q_x	=	Darcy flux [LT^{-1}]
K	=	saturated hydraulic conductivity [LT^{-1}]
h	=	hydraulic head [L]
$\mathrm{d}h/\mathrm{d}x$	=	hydraulic gradient [dimensionless]

According to the Dupuit theory (Dupuit, 1863), Darcy's law can be applied to describe groundwater discharge (Q_x) per unit width of aquifer [L^{2}T^{-1}] in the horizontal (x) direction, as shown in Equation (6).

$$Q_x = -Kh\frac{\mathrm{d}h}{\mathrm{d}x} \tag{6}$$

Since the flow depends on the recharge rate W, by continuity we have Equation (7).

$$\mathrm{d}Q_x = W\mathrm{d}x \tag{7}$$

For boundary conditions, we have q_x=0 at the left symmetry boundary at x=0 while at the right boundary (x=L'), we have h=$h_{L'}$.

Combining and integrating Equations (6) and (7) leads to the solution for the hydraulic head, h_I (with subscript I for "Inland"), versus the distance x (Equation (8)). Equation (8) is the equation of the Dupuit-Forchheimer ellipse (Dupuit, 1863).

$$h_I(x) = \sqrt{\frac{W}{K}(L'^2 - x^2) + h_{L'}^2} \tag{8}$$

where:

h_I	=	hydraulic head in an inland aquifer [L]
W	=	recharge rate of the aquifer [LT^{-1}]
K	=	hydraulic conductivity of the aquifer [LT^{-1}]
L'	=	length of the aquifer [L]
$h_{L'}$	=	fixed downstream (x=L') head [L]

Recognizing that the vertical component of the gradient is negligible, the groundwater velocity $v_x(x)$ can be expressed as $v_I(x)$. Combining Equations (6) and (8), we then obtain the expression of the fluid velocity for steady-state flow in an unconfined recharged inland aquifer (Equation (9)).

$$v_I(x) = \frac{q_x(x)}{n_e} = \frac{1}{n_e}\frac{Q(x)}{h_I(x)} = \frac{1}{n_e}\frac{Wx}{\sqrt{\frac{W}{K}(L'^2 - x^2) + h_{L'}^2}} \tag{9}$$

where:

$v_I(x)$	=	average linear velocity of a particle located at x in the inland aquifer [LT^{-1}] and [L]
n_e	=	effective porosity of the porous medium [dimensionless]

3.3 Groundwater Travel Times

This section presents the time required for a water particle to move along any flowline between the water table and an arbitrary downgradient x-coordinate. In the following development, we calculate the time required for a particle within the transformed system of Figure 6 to travel from the water table at position i to any arbitrary downgradient position x (Figure 7). For Case I, the particle departure point x_i is between zero and L' whereas for Case II, x_i is between $|x_{WD}|$ and L'.

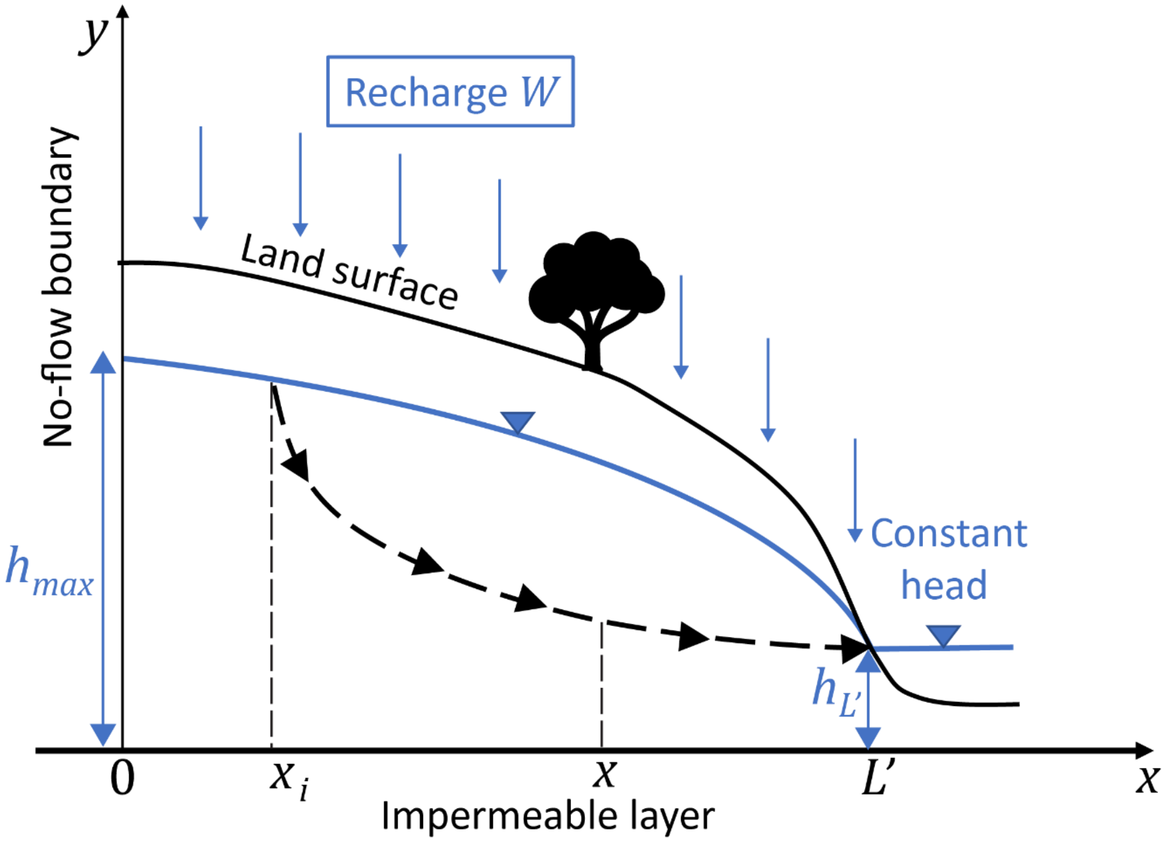

Figure 7 - A flow path in the transformed system of Figure 6 to represent the travel time calculated between two arbitrary points: x_i (the departure point at the water table) and x (Equations (18) and (19)). Downgradient of point x, the path continues to point L'.

Travel times are computed using the fluid velocity which is defined as in Equation (10).

$$v(x) = \frac{\mathrm{d}x}{\mathrm{d}t} \tag{10}$$

Equalizing Equations (9) and (10), separating variables x and t and integrating the resulting differential equation (with the variable of integration ξ) yields an expression for the travel time t [T] between two arbitrary positions x_i (at t=0, assuming the travel path begins at the water table) and x (at t; see Figure 7), as shown in Equation (11).

$$\frac{W}{n_e}\int_0^t \mathrm{d}\tau = \int_{x_i}^{x} \frac{\sqrt{\frac{W}{K}(L'^2-\xi^2)+h_{L'}^2}}{\xi}\, d\xi \tag{11}$$

We finally obtain the expression for t, as shown in Equation (12).

$$t(x) = \frac{n_e}{W}\int_{x_i}^{x} \frac{\sqrt{\frac{W}{K}(L'^2-\xi^2)+h_{L'}^2}}{\xi}\, d\xi \tag{12}$$

Equation (12) can be rewritten as Equation (13).

$$t(x) = \frac{n_e}{\sqrt{KW}} \int_{x_i}^{x} \sqrt{\left(\frac{\alpha}{\xi^2} \quad - 1\right)} \; d\xi$$

$$\text{with } \alpha = L'^2 + \frac{Kh_{L'}^2}{W} \qquad (13)$$

By using the following change of variables: $\gamma = \frac{\sqrt{\alpha}}{x}$, the integral expression in Equation (13) can be simplified to Equation (14).

$$t(x) = -n_e \sqrt{\frac{\alpha}{KW}} \int_{\frac{\sqrt{\alpha}}{x_i}}^{\frac{\sqrt{\alpha}}{x}} \frac{\sqrt{\gamma^2 - 1}}{\gamma^2} \; d\gamma \qquad (14)$$

Applying integration by parts, we obtain Equation (15).

$$t(x) = n_e \sqrt{\frac{\alpha}{KW}} \left(\left[\frac{\sqrt{\gamma^2 - 1}}{\gamma} \right]_{\frac{\sqrt{\alpha}}{x_i}}^{\frac{\sqrt{\alpha}}{x}} - \int_{\frac{\sqrt{\alpha}}{x_i}}^{\frac{\sqrt{\alpha}}{x}} \frac{d\gamma}{\sqrt{\gamma^2 - 1}} \right) \qquad (15)$$

If γ>1, then the indefinite integral of the function $\frac{1}{\sqrt{\gamma^2 - 1}}$ is the inverse hyperbolic cosine function $\cosh^{-1}(\gamma)$. To first verify if γ >1, we can write Equation (16).

$$\gamma = \frac{\sqrt{\alpha}}{x} = \sqrt{\frac{L'^2 + \frac{Kh_{L'}^2}{W}}{x^2}} \qquad (16)$$

Because $\frac{Kh_{L'}^2}{W} > 0$, and $L' \geq x$, then $L'^2 + \frac{Kh_{L'}^2}{W} > x^2$ and therefore γ>1. Under these conditions, $\cosh^{-1} \gamma = \ln(\gamma + \sqrt{(\gamma^2 - 1)})$ and we finally obtain the expression for $t(x)$, as shown in Equation (17).

$$t(x) = n_e \sqrt{\frac{\alpha}{KW}} \left[x \sqrt{\frac{1}{x^2} - \frac{1}{\alpha}} - x_i \sqrt{\frac{1}{x_i^2} - \frac{1}{\alpha}} + ln \left(\frac{\sqrt{\alpha}/_{x_i} + \sqrt{\alpha/_{x_i^2} - 1}}{\sqrt{\alpha}/_{x} + \sqrt{\alpha/_{x^2} - 1}} \right) \right] \qquad (17)$$

Equation (17) can be developed to yield Equation (18).

$$t(x) = n_e \sqrt{\frac{1}{WK}} \left[\sqrt{\alpha - x^2} - \sqrt{\alpha - x_i^2} - \sqrt{\alpha}\ ln \left(\frac{\sqrt{\alpha} + \sqrt{\alpha - x^2}}{\sqrt{\alpha} + \sqrt{\alpha - x_i^2}} \frac{x_i}{x} \right) \right] \tag{18}$$

Replacing α by its value $\alpha = L'^2 + \frac{Kh_{L'}^2}{W}$ in Equation (18) yields the closed-form analytical equation for calculating groundwater travel time t_I (with subscript *I* for "Inland") in the inland aquifer (Equation (19)).

$$t_I(x) = n_e \sqrt{\frac{1}{WK}} \left[\sqrt{L'^2 + \frac{Kh_{L'}^2}{W} - x^2} - \sqrt{L'^2 + \frac{Kh_{L'}^2}{W} - x_i^2} - \sqrt{L'^2 + \frac{Kh_{L'}^2}{W}}\ ln \left(\frac{\sqrt{L'^2 + \frac{Kh_{L'}^2}{W}} + \sqrt{L'^2 + \frac{Kh_{L'}^2}{W} - x^2}}{\sqrt{L'^2 + \frac{Kh_{L'}^2}{W}} + \sqrt{L'^2 + \frac{Kh_{L'}^2}{W} - x_i^2}} \frac{x_i}{x} \right) \right] \tag{19}$$

where:

t_I	=	travel time in the inland aquifer between position x_i and position x [T]
W	=	recharge rate of the aquifer [LT^{-1}]
K	=	hydraulic conductivity of the aquifer [LT^{-1}]
L'	=	length of the aquifer [L]
$h_{L'}$	=	fixed downstream ($x=L'$) head [L]
n_e	=	effective porosity of the porous medium [dimensionless]
x_i	=	departure point [L]

Equation (19) is the general analytical solution of the travel time for a particle flowing from position x_i at the water table to an arbitrary downgradient position x within an unconfined, horizontal inland aquifer under uniform surface recharge. This expression does not account for travel time in the vadose zone nor for vertical migration within the aquifer, which is small given that aquifer thickness is small relative to its length.

By replacing x with L' we obtain the result for the specific case of calculating the travel time of a groundwater particle flowing from position x_i where it enters as recharge to the aquifer discharge location at $x=L'$.

The closed-form analytical solution of travel time (Equation (19)) has been verified against numerical modeling (Chesnaux et al., 2005). Also, Equation (19) is now extensively used by scientists and practitioners to calculate groundwater travel time (Glass et al., 2018). The methodology and the analytical equation (Equation (19)) to calculate groundwater travel times is available in the INOWAS platform↗ (Glass et al., 2018; INOWAS, 2018). The platform provides a compilation of free web-based analytical tools for groundwater management. All tools run on a web server and can be accessed via standard browsers. All tools are also incorporated into a decision-support environment. The reader is invited to use the INOWAS platform to solve Equation (19) which is included in the platform. Finally, the platform provides detailed online support that contains the theoretical background of the tools, possible applications, and examples.

3.4 Groundwater Recharge

3.4.1 Calculating Recharge from Groundwater Travel Times Along a Flowline

Knowledge of groundwater travel time makes it possible to constrain recharge. Equation (19) can be used to calculate one of four parameters when the other three are known: effective porosity, hydraulic conductivity, recharge or groundwater travel time. In Equation (19), the term t_I can be replaced by the known value of groundwater travel time derived from hydrogeochemical dating (Chesnaux et al., 2018; Miled et al., 2023). An illustration is given in Chesnaux and others (2018) when the age of groundwater is obtained from the analysis of CFC and $\mathrm{SF_6}$ concentrations from groundwater samples taken at two different locations (x_1 and x_2) along a flowline. This time value is the essential parameter which makes it possible to adapt the initial Equation (19) by eliminating the need for the original x_i parameter.

The difference in age of water Δt between these two locations (x_1 and x_2) represents the travel time; this value is inserted into Equation (19) as a known variable. Equation (20) is derived from Equation (19) to calculate recharge using the difference in age Δt between two locations x_1 and x_2 along the flowline.

$$W_I^2 = \frac{WL'^2 + Kh_{L'}^2}{K} \frac{n_e^2}{(\Delta t)^2} \left[\sqrt{1 - \frac{x_2^2}{L'^2 + \frac{K}{W} h_{L'}^2}} - \sqrt{1 - \frac{x_1^2}{L'^2 + \frac{K}{W} h_{L'}^2}} + ln \left(\frac{x_2}{x_1} \frac{\sqrt{WL'^2 + Kh_{L'}^2} + \sqrt{WL'^2 + Kh_{L'}^2 - x_1^2 W}}{\sqrt{WL'^2 + Kh_{L'}^2} + \sqrt{WL'^2 + Kh_{L'}^2 - x_2^2 W}} \right) \right]^2 \qquad (20)$$

The recharge W_I (with subscript I for "Inland") in the inland aquifer can be calculated by solving Equation (20). W_I cannot be isolated from Equation (20) and in consequence it cannot be directly extracted and calculated. Solving W_I from Equation (20) requires the use of numerical or iterative methods—for example solvers built into commercial spreadsheets.

3.4.2 Calculating the Ratio of Recharge and Hydraulic Conductivity

Equation (4) can be used and solved to calculate the ratio of the recharge to hydraulic conductivity. As explained in Section 2.4, once the quadratic regression has been realized along a flowline for confirming the behavior of a Dupuit-type aquifer, then the equation of regression can be exploited to determine the properties of the aquifer. From Equation (4), when the Dupuit-Forchheimer assumptions are followed, it is possible to calculate the ratio a=W/K by plotting h^2 versus x (Figure 3).

In a 1D system with predominant flow along the x-axis, if static water levels are monitored in observation wells distributed along the groundwater flow path x-axis, saturated thicknesses $h_I(x)$ in the unconfined aquifer can be calculated at different positions. The coefficient W/K can then be extracted from the h^2 versus x curve after application of a quadratic regression (Chesnaux, 2013). Assuming steady-state conditions of the groundwater flow system, W/K is constant; knowing the average homogeneous and isotropic hydraulic conductivity K of the aquifer (i.e., the K component in the x-axis direction), it is then possible to calculate the average steady-state recharge of the aquifer. Such a method to assess the recharge of an unconfined aquifer is therefore limited by a certain number of assumptions. However, in specific cases of regional groundwater flow systems where most of these assumptions are satisfied, the approach can ensure good estimates of an aquifer recharge for a minimum of effort compared with other available methods.

3.5 Groundwater Volume

The volume V_I of groundwater per unit width of aquifer in an inland aquifer can be calculated by integrating the saturated freshwater aquifer thickness $h_I(x)$ (Equation (8)) between the boundaries of the aquifer (Figure 8) and by multiplying this volume of aquifer by its effective porosity n_e (Equation (21)). Use of the effective porosity—not the total porosity—in the calculation yields the volume available for flow in the voids of porous medium, not the total volume of the voids. This choice will be kept for the equations in the remainder of the book, but the effective porosity could be exchanged in the equations for total porosity depending on the purpose of the analysis conducted.

$$V_I = n_e \int_0^{L'} h(x)\, dx = n_e \int_0^{L'} \sqrt{\frac{W}{K}(L'^2 - x^2) + h_{L'}^2},\ dx \tag{21}$$

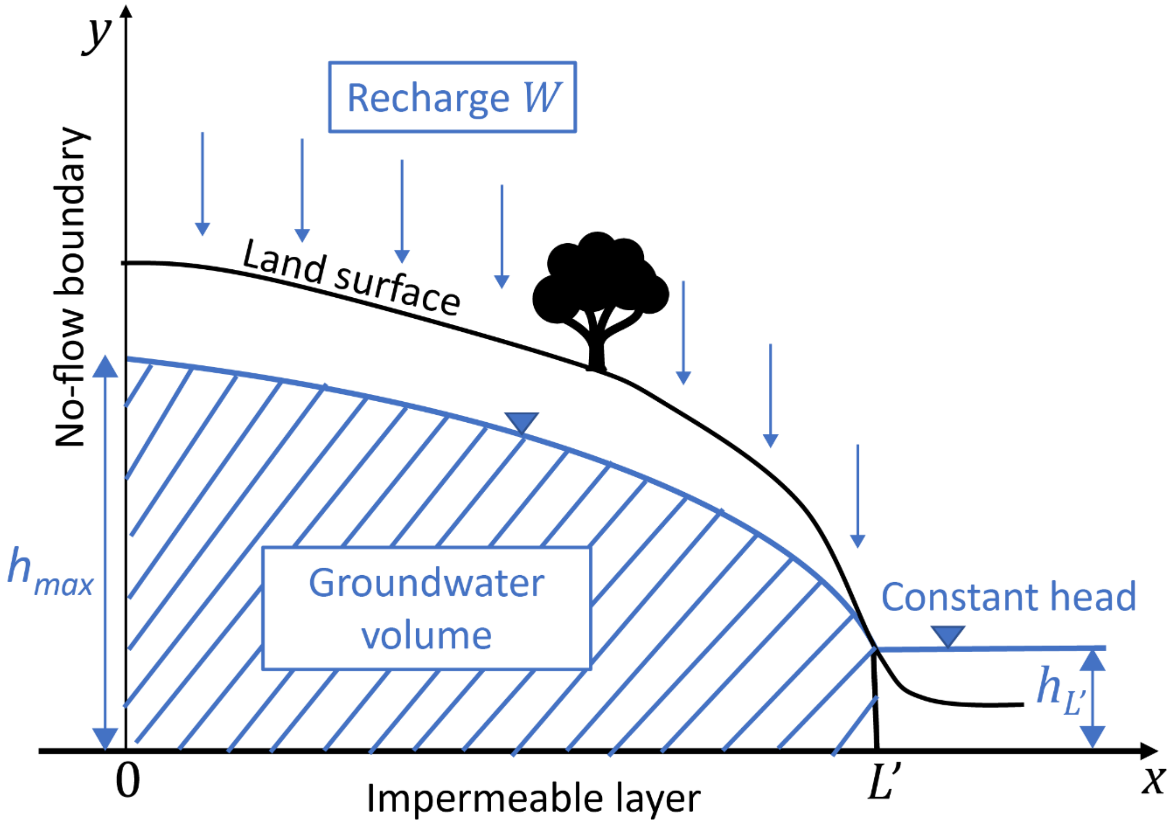

Figure 8 - Groundwater volume of an inland unconfined Dupuit-type aquifer

After integration, Equation (21) yields Equation (22). The function $\sqrt{a^2 - x^2}$ integrates as $\int \sqrt{a^2 - x^2}\, dx = \frac{x}{2}\sqrt{a^2 - x^2} + \frac{a^2}{2}\sin^{-1}\frac{x}{a} + c$ with a and c representing two constants, resulting in Equation (22).

$$V_I = n_e \sqrt{\frac{W}{K}} \left[\frac{x}{2} \sqrt{L'^2 + \frac{K}{W} h_{L'}^2 - x^2} + \frac{L'^2 + \frac{K}{W} h_{L'}^2}{2} \sin^{-1} \left(\frac{x}{\sqrt{L'^2 + \frac{K}{W} h_{L'}^2}} \right) \right]_0^{L'} \tag{22}$$

Developing Equation (22) yields Equation (23).

$$V_I = \frac{n_e}{2} \left(L' h_{L'} + \sqrt{\frac{W}{K}} \left(L'^2 + \frac{K}{W} h_{L'}^2 \right) \sin^{-1} \left(\frac{L'}{\sqrt{L'^2 + \frac{K}{W} h_{L'}^2}} \right) \right) \tag{23}$$

Equation (23) is the closed-form analytical solution for calculating V_I, the volume of freshwater available for flow contained in the inland aquifer per unit width of aquifer [L^2].

3.6 Groundwater Mean Residence Time

The mean residence time RT is a measure of the average time a particle of water spends in the aquifer. The mean residence time (Equation (25)) defined for steady-state conditions is equal to the groundwater volume divided by the inflow over the length of the aquifer, which is the product of the recharge and aquifer length as shown in the conceptual model presented in Figure 6, Figure 7, and Figure 8.

$$RT_I = \frac{V_I}{W\ L'} \tag{24}$$

In Equation (24), RT_I is the mean residence time of groundwater in the inland aquifer. Combining Equation (23) with Equation (24) yields Equation (25).

$$RT_I = \frac{n_e}{2W\ L'}\left(L'h_{L'} + \sqrt{\frac{W}{K}}\left(L'^2 + \frac{K}{W}h_{L'}^2\right)\sin^{-1}\left(\frac{L'}{\sqrt{L'^2 + \frac{K}{W}h_{L'}^2}}\right)\right) \tag{25}$$

Equation (25) is the closed-form analytical solution for the mean residence time of groundwater in an inland aquifer.

If the residence time can be independently evaluated with geochemical tracers and an estimate of hydraulic conductivity (K) is available, then the recharge (W) of the aquifer can be estimated from Equation (25).

Exercise 2 provides the opportunity to apply the main previously presented equations to a specific case to calculate different parameters of the flow system in an inland unconfined Dupuit-type aquifer.

3.7 Specific Case of Inland-Island Aquifers

The solutions developed earlier for inland aquifers are presented in this section for inland islands (i.e., islands in freshwater bodies) with specified simple geometries; cases of both strip islands and circular islands are considered to develop the closed-form solutions (Chesnaux and Allen, 2008). In the case of inland strip or circular islands, unlike the case of inland aquifers, there is no need to consider multiple scenarios of the groundwater divide location—real versus imaginary. Instead, the groundwater divide is located at the center of islands having strip or circular geometries.

3.7.1 Strip Inland Islands

For strip inland islands, the flow system is defined using coordinates (x, y), but the flow is considered horizontal and one dimensional according to the Dupuit approximation, and indicates that the hydraulic head is dependent only on x. The vertical plane, defined by x=0, represents the axis of symmetry of the island, and it represents the water divide—

where the hydraulic gradient is zero—since the down-gradient boundary is a hydraulic head that is the same at both sides of the island (Figure 9). The width of the island (the direction perpendicular to the page) is defined theoretically to be infinite. Its half-length is L—the total length of the island, therefore, is $2L$. Due to the symmetry of the island, the problem is solved between x=0 and x=L (Figure 9) which is equivalent to the inland aquifer model presented in Figure 6. Consequently, the equations for determining the hydraulic head profile, groundwater velocity, groundwater travel times, and recharge are the same as the equations developed for inland aquifers—Equations (8), (9), (19) and (20), respectively.

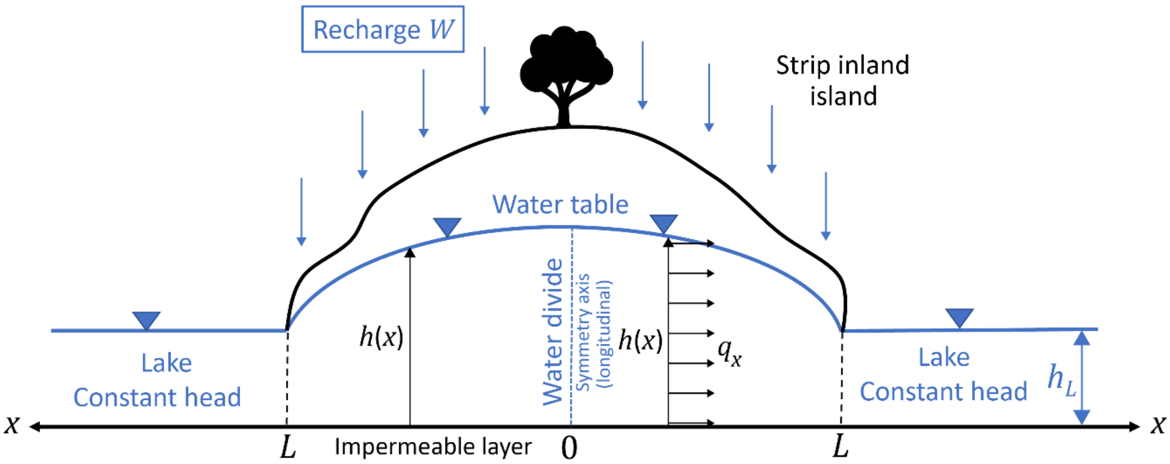

Figure 9 - Cross-sectional view and definition of variables for strip inland-islands.

Hydraulic head profile

The solution for the hydraulic head h_{SII} in the strip inland-island aquifer, h, versus the distance x is given by Equation (26), analogous to Equation (8).

$$h_{SII}(x) = \sqrt{\frac{W}{K}(L^2 - x^2) + h_L^2} \tag{26}$$

Groundwater velocity

The expression of the fluid velocity for steady-state flow in an unconfined recharged strip inland-island aquifer is given by Equation (27) analogous to Equation (9).

$$v_{SII}(x) = \frac{q_x(x)}{n_e} = \frac{1}{n_e}\frac{Q(x)}{h_{SII}(x)} = \frac{1}{n_e}\frac{Wx}{\sqrt{\frac{W}{K}(L^2 - x^2) + h_L^2}} \tag{27}$$

where:

$v_{SII}(x)$ = average linear velocity of a particle [LT^{-1}] located at x [L] in the strip inland island

n_e = effective porosity of the porous medium

Groundwater travel times

In the case of strip inland islands, the two points along a flow line for which travel time is calculated are characterized by their distances x_i (initial position) and x (Figure 10).

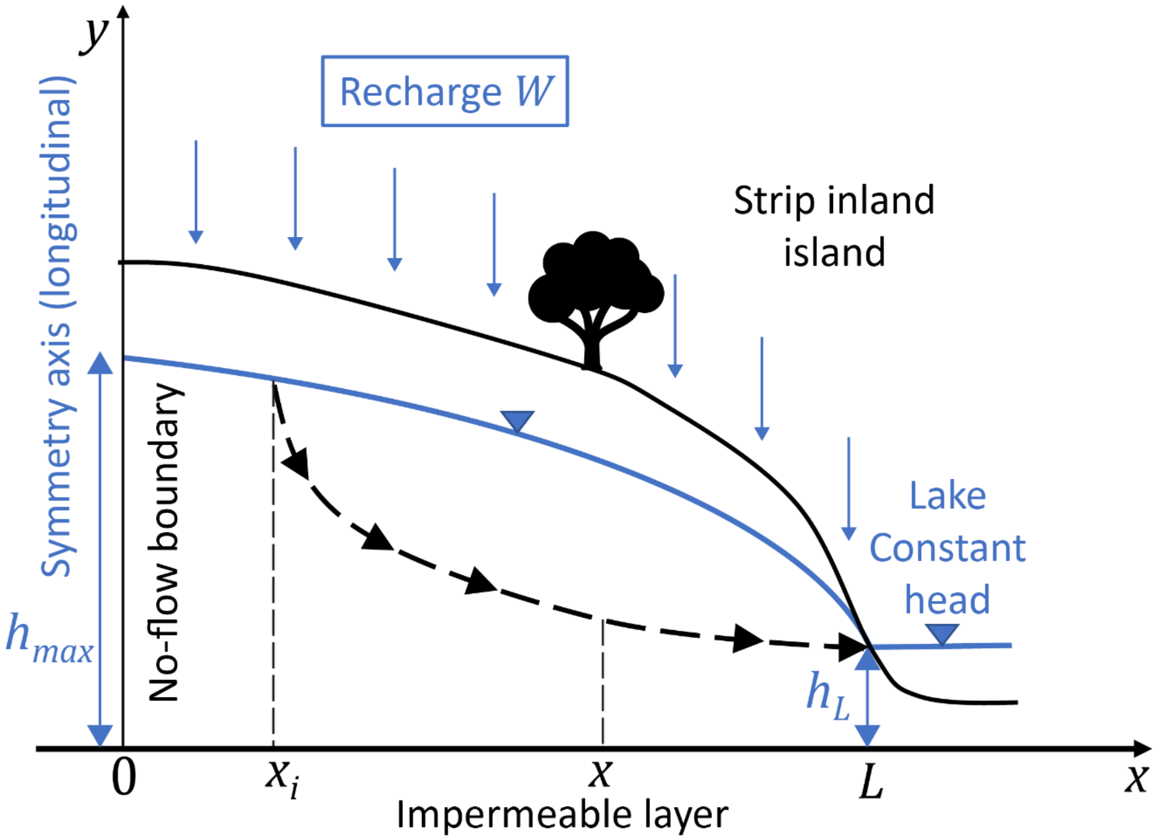

Figure 10 - A flow path to represent the travel time calculated between the two arbitrary points: x_i (the departure point at the water table) and x for the case of strip inland-islands (only one half-length of the island is represented on the figure). Downgradient of point x, the path continues to point L.

The closed-form analytical equation for calculating groundwater travel time position x_i from the water table to an arbitrary downgradient position x in strip inland-islands is given by Equation (28), analogous to Equation (19).

$$t_{SII}(x) = n_e\sqrt{\frac{1}{WK}}\left[\sqrt{L^2 + \frac{Kh_L^2}{W} - x^2} - \sqrt{L^2 + \frac{Kh_L^2}{W} - x_i^2} - \left(\sqrt{L^2 + \frac{Kh_L^2}{W}}\ ln\left(\frac{\sqrt{L^2+\frac{Kh_L^2}{W}}+\sqrt{L^2+\frac{Kh_L^2}{W}-x^2}}{\sqrt{L^2+\frac{Kh_L^2}{W}}+\sqrt{L^2+\frac{Kh_L^2}{W}-x_i^2}}\ \frac{x_i}{x}\right)\right)\right] \tag{28}$$

where:

$t_{SII}(x)$ = travel time between position x_i and position x [T] in the strip inland-island aquifer

Groundwater recharge

Equation (29), analogous to Equation (20), allows the calculation of the recharge W_{SII} in the strip inland-island aquifer using the difference in age Δt between two locations x_1 and x_2 along a flowline.

$$W_{SII}^2 = \frac{WL^2 + Kh_L^2}{K}\ \frac{n_e^2}{(\Delta t)^2}\left[\sqrt{1 - \frac{x_2^2}{L^2 + \frac{K}{W}h_L^2}} - \sqrt{1 - \frac{x_1^2}{L^2 + \frac{K}{W}h_L^2}} + ln\left(\frac{x_2}{x_1}\frac{\sqrt{WL^2 + Kh_L^2} + \sqrt{WL^2 + Kh_L^2 - x_1^2W}}{\sqrt{WL^2 + Kh_L^2} + \sqrt{WL^2 + Kh_L^2 - x_2^2W}}\right)\right]^2 \tag{29}$$

Groundwater volume

Equation (30), analogous to Equation (23), allows the calculation of the groundwater volume V_{SII} in the strip inland-island aquifer per unit width of island (Figure 11). Considering the axis of symmetry of the strip island, Equation (23) is multiplied by 2 to obtain the total volume per unit width of aquifer.

$$V_{SII} = n_e\left(Lh_L + \sqrt{\frac{W}{K}}\left(L^2 + \frac{K}{W}h_L^2\right)\sin^{-1}\left(\frac{L}{\sqrt{L^2 + \frac{K}{W}h_L^2}}\right)\right) \tag{30}$$

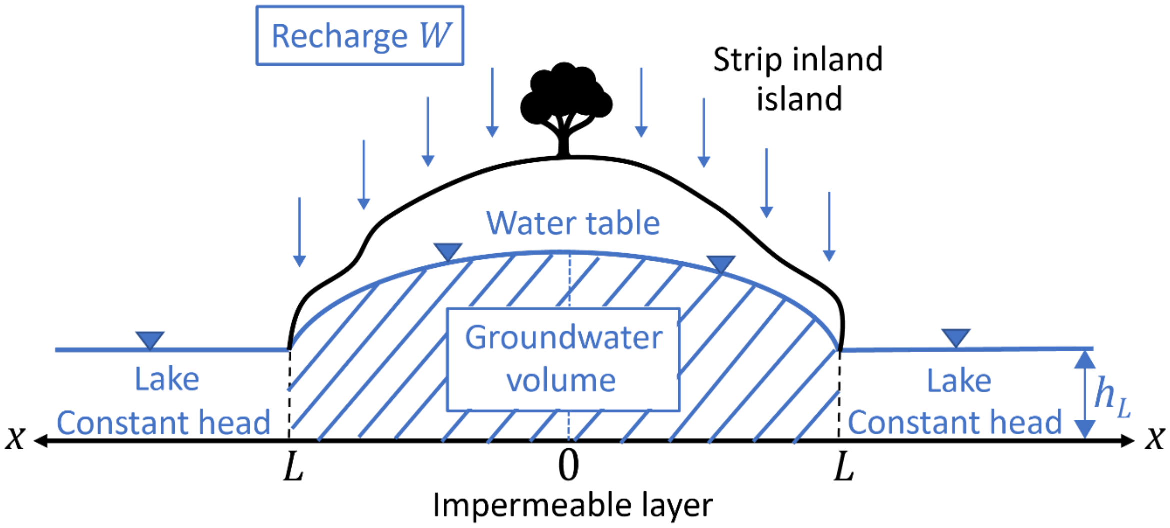

Figure 11 - Groundwater volume in strip inland-island, unconfined, Dupuit-type aquifers.

Groundwater mean residence time

Equation (31), identical to Equation (25), allows the calculation of the mean residence time RT_{SII} of groundwater in a strip inland-island aquifer.

$$RT_{SII} = \frac{n_e}{2WL}\left(Lh_L + \sqrt{\frac{W}{K}}\left(L^2 + \frac{K}{W}h_L^2\right)\sin^{-1}\left(\frac{L}{\sqrt{L^2 + \frac{K}{W}h_L^2}}\right)\right) \tag{31}$$

3.7.2 Circular Inland Islands

The groundwater flow system for circular inland islands is defined using polar coordinates (r, α) for the horizontal plane and a vertical axis of elevation centered on the axis of symmetry (center of the island). Circular islands have radial symmetry, which implies that the hydraulic head does not depend on the angle α, but only on the radial coordinate r. The upgradient boundary is represented by the axis of symmetry (defined as the origin, where r=0) and consists of a no-flow boundary—in this case, a water divide—where the hydraulic gradient is zero. The radius of the island is noted by R (Figure 12).

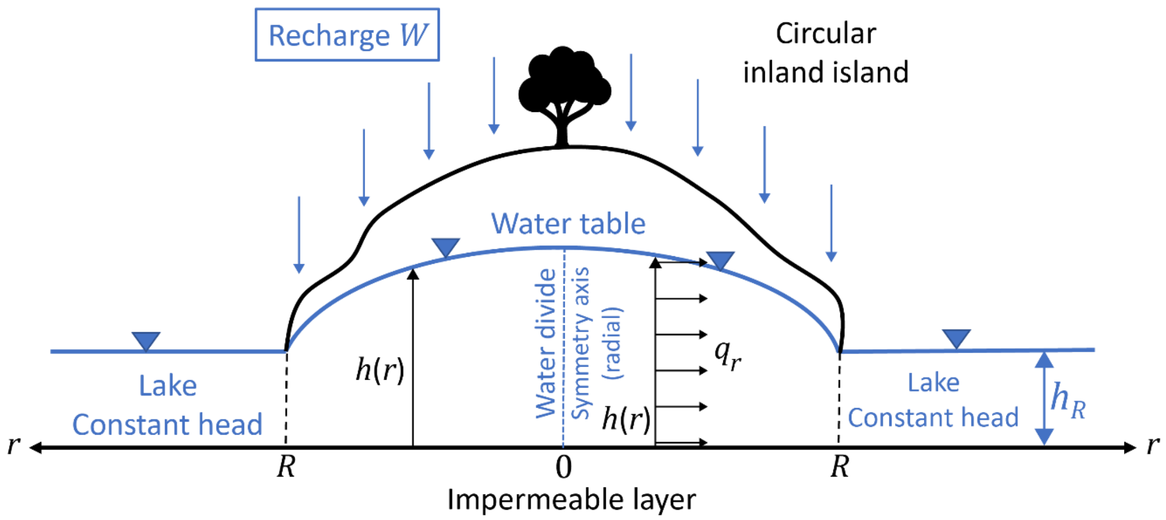

Figure 12 - Cross-sectional view and definition of variables for circular inland islands.

Hydraulic head profile

We begin with Darcy's Law for groundwater flow, written as shown in Equation (32).

$$q_r = -K\frac{\mathrm{d}h}{\mathrm{d}r} \tag{32}$$

where:

q_r	=	Darcy flux in the circular inland-island [LT^{-1}]
K	=	saturated hydraulic conductivity [LT^{-1}]
h	=	hydraulic head [L]
$\mathrm{d}h/\mathrm{d}r$	=	hydraulic gradient [dimensionless]

According to the Dupuit theory, Darcy's law is applied to describe groundwater discharge (Q_r) [L^3T^{-1}] in the radial (r) direction (Figure 12), as shown in Equation (33).

$$Q_r = -2\pi Krh\frac{\mathrm{d}h}{\mathrm{d}r} \tag{33}$$

When the horizontal bottom of the aquifer is at elevation zero, then $h(r)$ represents the saturated thickness at r, the hydraulic head at r, and the water table elevation. The flow rate depends on the recharge rate W [LT^{-1}], yielding, by continuity, Equation (34).

$$Q_r = \pi W r^2 \tag{34}$$

Equating Equations (33) and (34), and considering a specified head boundary $h=h_R$ at $r=R$, after integration, the solution (Equation (35)) is obtained for the saturated thickness, h_{CII}, for circular inland islands as a function of the distance, r, as follows.

$$h_{CII}(r) = \sqrt{\frac{W}{2K}(R^2 - r^2) + h_R^2} \tag{35}$$

Groundwater velocity

We consider a water particle flowing from r_i at time t=0 to r at time t. Travel times in the circular inland island v_{CII} are computed using the water velocity, which is defined in Equation (36).

$$v_{CII}(r) = dr/dt \tag{36}$$

This velocity can then be written as equal to the mean velocity of water given by Darcy's law:

$$v_{CII}(r) = \frac{v_{Darcy}}{n_e} = -\frac{K}{n_e}\frac{dh_{CII}}{dr} \tag{37}$$

The expression of the fluid velocity for steady-state flow in an unconfined recharged circular inland-island aquifer is given by Equation (38), obtained from Equation (37).

$$v_{CII}(r) = \frac{q_r(r)}{n_e} = \frac{1}{n_e}\frac{Q(r)}{2\pi r h_{CII}(r)} = \frac{1}{2n_e}\frac{Wr}{\sqrt{\frac{W}{2K}(R^2 - r^2) + h_R^2}} \tag{38}$$

where:

$v_{CII}(r)$ = average linear velocity of a particle [LT^{-1}] located at r [L] in the circular inland-island

n_e = effective porosity of the porous medium

Groundwater travel times

In the case of circular inland islands, the two points along a flow line for which travel time is calculated are characterized by their radial distances r_i (initial position) and r (Figure 13).

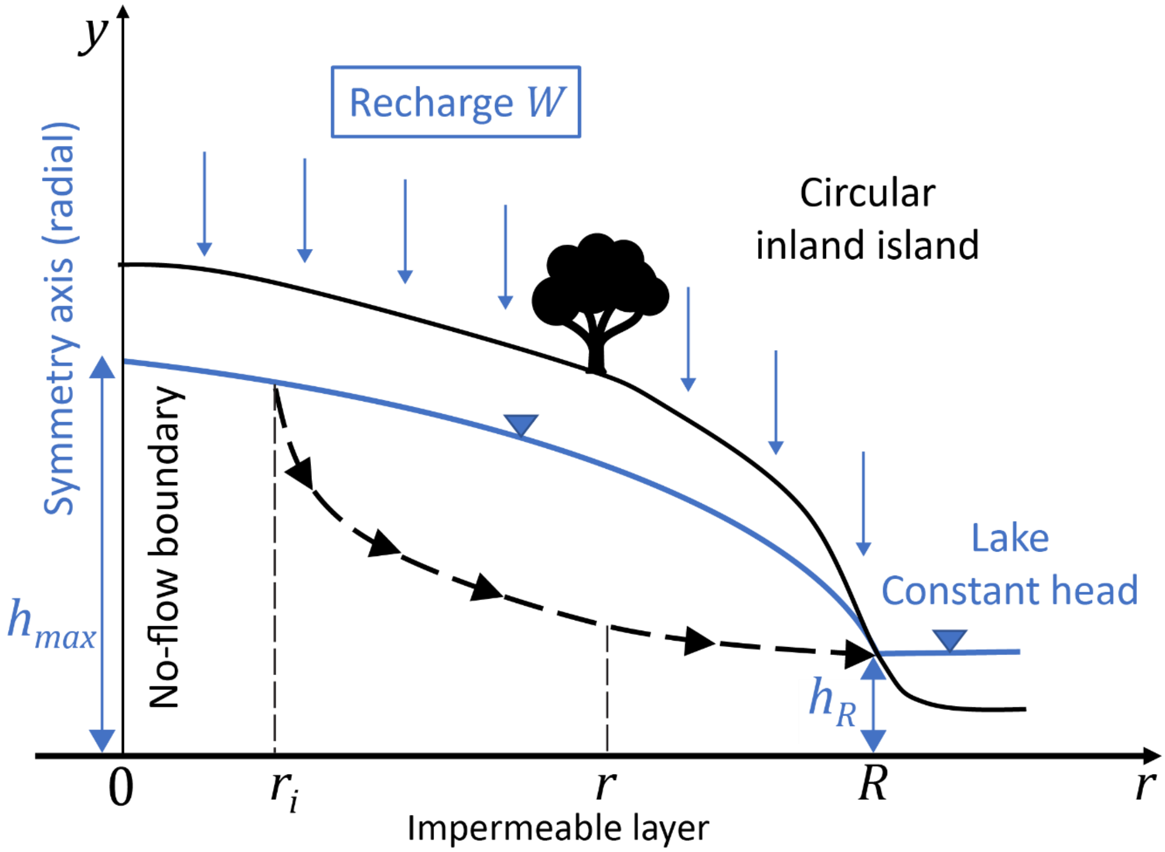

Figure 13 - A flow path to represent the travel time calculated between the two arbitrary points: r_i (the departure point at the water table) and r for the case of circular inland-islands (only one half-diameter of the island is represented on the figure). Downgradient of point x, the path continues to point R.

Combining Equations (28), (29), and (30), and separating the variables r and t, yields the differential equation of fluid flow, which is integrated between r_i at t=0 and r>r_i at time t>0, as shown in Equation (39).

$$\int_0^t d\tau = t_{CII}(r) = n_e \sqrt{\frac{2}{WK}} \int_{r_i}^{r} \frac{\sqrt{(R^2 + 2Kh_R^2/W) - \rho^2}}{\rho}\, d\rho \tag{39}$$

where:

τ and ρ = the integration variables for t_{CII} (travel time in a circular inland-island) and r, respectively

Integration of Equation (39) yields Equation (40).

$$t_{CII}(r) = n_e\sqrt{\frac{2}{WK}}\left[\sqrt{{C_{CII}}^2 - r^2} - \sqrt{{C_{CII}}^2 - r_i^2} - C_{CII}\, ln\left(\frac{C_{CII} + \sqrt{{C_{CII}}^2 - r^2}}{C_{CII} + \sqrt{{C_{CII}}^2 - r_i^2}}\frac{r_i}{r}\right)\right] \quad (40)$$

where:

C_{CII} = constant equal to $C_{CII} = \sqrt{R^2 + 2Kh_R^2/W}$

Equation (40) is the general closed-form solution of the travel time of a particle of water between the initial position r_i and a position r in a circular inland-island aquifer that is unconfined, horizontal, and recharged by infiltration.

Finally, replacing C_{CII} by its value in Equation (40) yields the closed-form analytical equation for calculating groundwater travel time (Equation (41)).

$$t_{CII}(r) = n_e\sqrt{\frac{2}{WK}}\left[\sqrt{R^2 + \frac{2Kh_R^2}{W} - r^2} - \sqrt{R^2 + \frac{2Kh_R^2}{W} - r_i^2} - \sqrt{R^2 + \frac{2Kh_R^2}{W}}\, ln\left(\frac{\sqrt{R^2+\frac{2Kh_R^2}{W}} + \sqrt{R^2+\frac{2Kh_R^2}{W} - r^2}}{\sqrt{R^2+\frac{2Kh_R^2}{W}} + \sqrt{R^2+\frac{2Kh_R^2}{W} - r_i^2}}\frac{r_i}{r}\right)\right] \quad (41)$$

where:

$t_{CII}(r)$ = travel time between position r_i and position r [T] in the circular inland-island aquifer

Groundwater recharge

W_{CII} in a circular inland-island aquifer is calculated using the difference in age Δt between two locations r_1 and r_2 along a flowline, as shown in Equation (42).

$$W_{CII}^2 = \frac{WR^2 + Kh_R^2}{2K} \frac{n_e^2}{(\Delta t)^2} \left[\sqrt{1 - \frac{r_2^2}{R^2 + \frac{2K}{W} h_R^2}} - \sqrt{1 - \frac{r_1^2}{R^2 + \frac{2K}{W} h_R^2}} + ln\left(\frac{r_2}{r_1} \frac{\sqrt{WR^2 + 2Kh_R^2} + \sqrt{WR^2 + 2Kh_R^2 - r_1^2 W}}{\sqrt{WR^2 + 2Kh_R^2} + \sqrt{WR^2 + 2Kh_R^2 - r_2^2 W}} \right) \right]^2 \quad (42)$$

Groundwater volume

The total volume V_{CII} of groundwater in a circular inland island can be calculated by integrating the saturated freshwater aquifer thickness $h(r)$ (Equation (35)) between the boundaries of the aquifer (Figure 14) and by multiplying this volume of aquifer by the effective porosity n_e of the aquifer (Equation (43)).

$$V_{CII} = n_e \int_0^R 2\pi r h(r)\,\mathrm{d}r = 2\pi n_e \int_0^R r\sqrt{\frac{W}{2K}(R^2 - r^2) + h_R^2}\,\mathrm{d}r \tag{43}$$

After integration, Equation (43) yields Equation (44). The function $r\sqrt{a^2 - r^2}$ integrates as $\int r\sqrt{a^2 - r^2}\,dr = -\frac{(a^2 - r^2)^{3/2}}{3} + c$ with a and c being constants, yielding Equation (44).

$$V_{CII} = 2\pi n_e \left[-\frac{\left(R^2 + \frac{2K}{W}h_R^2 - r^2\right)^{3/2}}{3} \right]_0^R \tag{44}$$

Developing Equation (44) yields Equation (45).

$$V_{CII} = \frac{2\pi n_e}{3}\left[\left(R^2 + \frac{2K}{W}h_R^2\right)^{3/2} - h_R^3\left(\frac{2K}{W}\right)^{3/2}\right] \tag{45}$$

Equation (45) is the closed-form analytical solution for calculating V_{CII}, the total volume of freshwater contained in the circular inland-island aquifer [L^3].

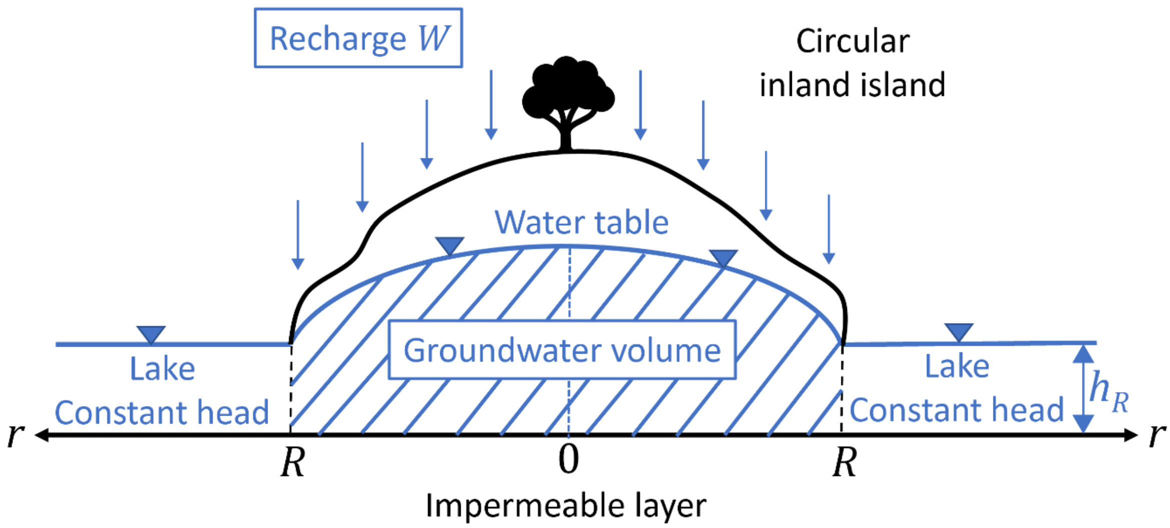

Figure 14 - Groundwater volume in circular inland-island unconfined Dupuit-type aquifers.

Groundwater mean residence time

The mean residence time RT_{CII} in a circular inland island (Equation (46)) defined for steady-state conditions is equal to the total groundwater volume divided by the inflow rate in the aquifer which corresponds to the total recharge which equals $\pi R^2 W$.

$$RT_{CII} = \frac{V_{CII}}{\pi R^2 W} \tag{46}$$

Combining Equation (45) with Equation (46) yields Equation (47).

$$RT_{CII} = \frac{2n_e}{3R^2W}\left[\left(R^2 + \frac{2K}{W}h_R^2\right)^{3/2} - h_R^3\left(\frac{2K}{W}\right)^{3/2}\right] \tag{47}$$

Equation (47) is the closed-form analytical solution for solving the mean residence time of groundwater in a circular inland-island aquifer.

3.8 Advantages and Limitations of Using Analytical Solutions

The closed-form analytical solutions presented in this section for inland unconfined Dupuit-type aquifers are useful for several reasons.

1. They can be used for direct practical applications, providing quick and free evaluations of the water table location, groundwater velocity, groundwater travel time as well as aquifer recharge. All of these variables are critical for improving groundwater knowledge and for managing groundwater resources.
2. The solutions are versatile because they can be used for unconsolidated and fractured-rock aquifers; however, the high degree of spatial heterogeneity in hydraulic conductivity and recharge that is typical of fractured-rock aquifers indicates that caution should be used in applying the analytical solutions to these flow systems.
3. The solutions can be solved with a simple Excel spreadsheet or using the free INOWAS web-based platform (INOWAS, 2018).
4. In particular, estimates of groundwater velocity and travel time can be used to determine advective transport of contaminant plumes and to conservatively approximate contaminant fate in aquifer systems.
5. Travel times and capture zones are essential parameters used to delineate groundwater and wellhead protection zones and to design groundwater remediation systems.
6. Assessing aquifer recharge is useful for managers to assess the quantity of groundwater that can be supplied by aquifers to satisfy human activities.
7. The analytical solutions can be used to verify or validate numerical models, keeping in mind the assumptions of the analytical solutions.
8. The solutions can be used for estimating how climate change and a change of aquifer recharge can affect groundwater velocity and travel time.

9. Sensitivity analyses can be conducted on the solutions to anticipate the effects of parameter uncertainty and changes in recharge, boundary conditions and hydraulic conductivity.
10. The closed form solutions facilitate understanding hydrogeological processes in an education context; they are useful to teachers for preparing course notes and for students for understanding subsurface hydraulics.

It is important to keep in mind the assumptions and limitations of using such closed-form analytical solutions when considering the Dupuit-type flow conditions and limitations, even though for most regional unconfined aquifers, Dupuit-type conditions are observed. Ultimately, it is the modeler who is responsible to verify if the Dupuit assumptions apply to a particular aquifer. It is also important to remember that groundwater flow in the vadose zone is not reflected in the Dupuit model and that consequently groundwater travel times in the vadose zone are ignored.

4 Oceanic Coastal Dupuit-Type Aquifers

This section presents a series of closed-form analytical solutions for oceanic coastal Dupuit-type aquifers: specifically, for seawater intrusion, water table configurations, groundwater velocity, groundwater travel times, fresh groundwater volumes, and mean groundwater residence times. The solutions are valid in cases of regional flow where the aquifer is not under the influence of pumping or injection.

4.1 Description of a Regional Dupuit-Type Coastal Aquifer Model with Seawater Intrusion

4.1.1 Coastal Seawater Intrusion Model

The case of Dupuit-type coastal aquifers is like the case of inland Dupuit-type aquifers as presented in Section 2 (Figure 2). Moreover, the same assumptions apply regarding Dupuit-type flow. The system has a uniform hydraulic conductivity of K and uniform rainfall recharge, with W the volumetric recharge rate per unit area. This time, however, the unconfined aquifer is in contact with the ocean (with a seashore angle θ) and is subject to saltwater intrusion. In general, an aquifer of length L is bounded by an inland fixed-head boundary (value of H_0 at x=0) and a fixed-head boundary of sea level at the ocean (H_L=0 at x=L). A groundwater divide occurs at x=x_{WD}. As in the case of inland Dupuit-type aquifers, this groundwater divide can be either situated between x=0 and x=L if it physically exists, or it can be imaginary when it is external to the aquifer system (in this case, $x_{WD} < 0$). These two different cases are further explained in the next section.

When in contact with the ocean, the fresh groundwater of a coastal aquifer—which is supplied by terrestrial recharge—interacts with the seawater. *Seawater interface* refers to the location where the fresh groundwater and the seawater interact. Because seawater is denser than freshwater, the seawater forms a wedge under the freshwater as shown on the righthand side of the conceptual model in Figure 15. The inland location where the interface intersects the base of the aquifer is called the *interface toe*, located at x=x_T. The saltwater interface is assumed to be sharp and is regarded as a no-flow boundary.

As a consequence of the interaction between inland freshwater and intrusive seawater, one can assume that the aquifer is composed of the two different zones represented in Figure 15. The inland zone ($0 \leq x \leq x_T$), without the interface, is located to the left of the saltwater toe location (x_T), whereas the seawater intrusion zone ($x_T \leq x \leq L$), containing the interface, is located to the right of x_T. In both the inland and seawater intrusion zones, the hydraulic heads are represented by the water table elevation above the base of the aquifer, which also represents the sum of the elevation of the water table above sea level $h(x)$ [L] and the elevation of sea level above the base of the aquifer S [L] along the x-axis (Figure 15).

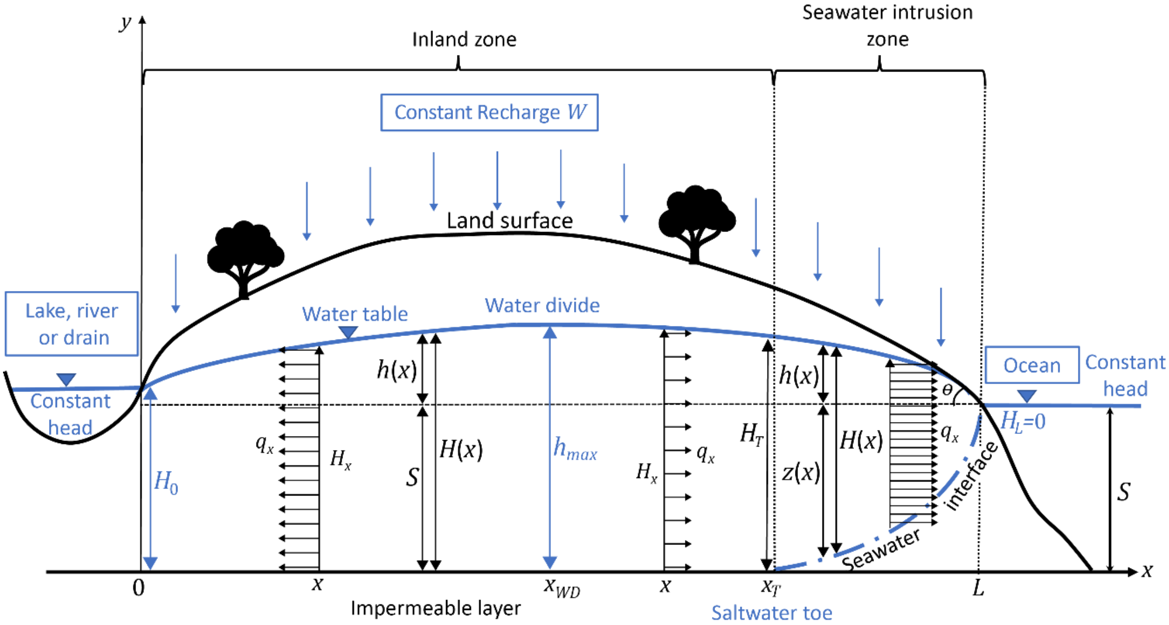

Figure 15 - Conceptual model of a Dupuit-type flow system occurring in a coastal unconfined aquifer interacting with seawater—Case I with $0 < x_{WD} < x_T$.

In the seawater intrusion zone ($x_T \leq x \leq L$), the depth to the interface below sea level $z(x)$ [L] is obtained from the Badon Ghijben-Herzberg relation (Drabbe & Badon Ghijben, 1889; Herzberg, 1901), which is commonly denoted the Ghyben-Hertzberg relation (Equation (48)).

$$z(x) = \frac{\rho_f}{\rho_s - \rho_f} h(x) = \frac{\rho_f}{\Delta\rho} h(x) \tag{48}$$

where:

h	=	water table elevation above sea level [L]
z	=	depth of the seawater interface below sea level [L]
ρ_f	=	density of freshwater [ML^{-3}]
ρ_s	=	density of saltwater [ML^{-3}]
$\Delta\rho$	=	$\rho_s - \rho_f$ [ML^{-3}]

Usually, the density of seawater ρ_s is taken as 1.025 and the density of freshwater ρ_f as 1.000. As such, the Ghyben-Hertzberg relation (Equation (48)) tells us that at any point within the seawater intrusion zone of the coastal aquifer, the depth of the interface below sea level ($z(x)$) will be $(\rho_f/(\rho_s - \rho_f))\ h(x)=(1/(1.025-1))\ h(x)=40$ times the elevation of the water table above sea level at that location. In the seawater intrusion zone ($x_T \leq x \leq L$), the total freshwater saturated thickness, $H(x)$, is the sum of the depth of the seawater interface below sea level ($z(x)$) and the water table elevation above the sea level ($h(x)$); that is, $H(x)=z(x) + h(x)$.

In the inland zone ($0 \leq x \leq x_T$), the total freshwater saturated thickness of the aquifer above the horizontal base of the aquifer (the impermeable substratum) $H(x)$ also represents the hydraulic head. The hydraulic head therefore is the sum of the difference in elevation between the sea level and the base of the aquifer (noted as S) and of the water table elevation above the sea level ($h(x)$); that is, $H(x)=S+h(x)$. The same definition of the hydraulic head applies in the seawater intrusion zone ($x_T \leq x \leq L$), i.e., the hydraulic head is equal to $S+h(x)$.

4.1.2 Groundwater Divide Location

As with the case of inland Dupuit-type aquifers, determining the groundwater divide location considers two cases as shown in Figure 15 and Figure 16. Case I applies to the flow system containing a flow divide between two fixed-head boundaries (Figure 15), whereas Case II applies to an otherwise equivalent system without an internal flow divide—where flow is unidirectional between the upstream and downstream constant head boundaries (Figure 16). In Case II, the flow divide is imaginary and is located upgradient of the constant head boundary at $x=0$ meaning that x_{WD} is negative (Figure 16).

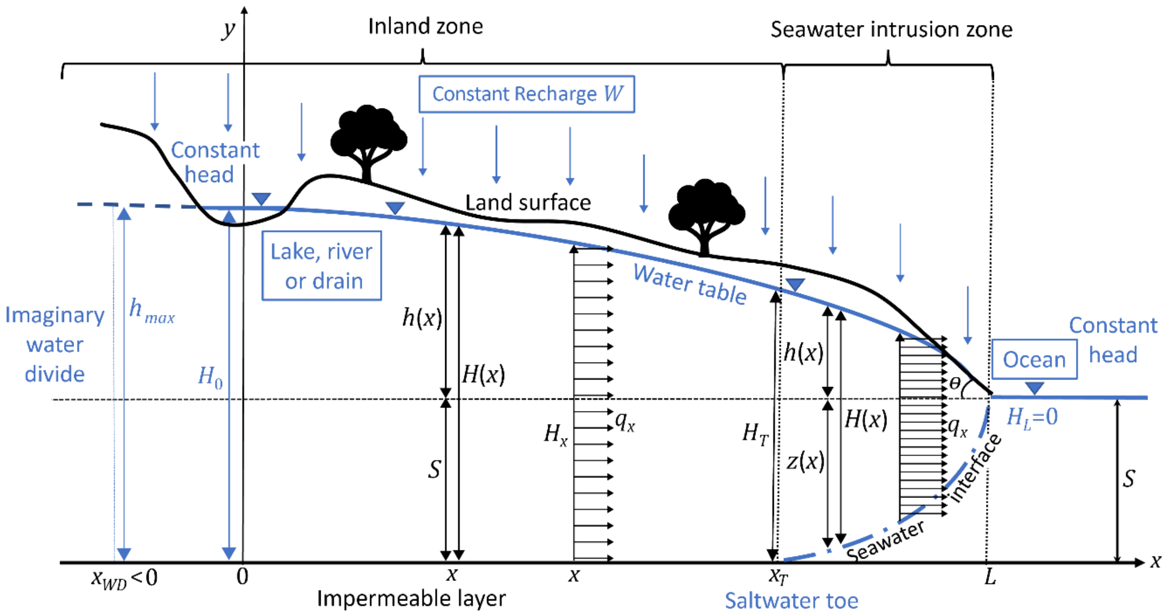

Figure 16 - Conceptual model of a coastal aquifer with an imaginary groundwater divide beyond the upstream boundary (x_{WD} < 0)—Case II.

In Case I and Case II the groundwater divide is located at a position x_{WD} upstream of the saltwater toe, meaning that $x_{WD} < x_T$. In both Cases (Figure 15 and Figure 16)), groundwater flow in the inland zone occurs between two fixed-head boundaries, H_0 at x=0 and H_T at x=x_T. This configuration satisfies the conditions of the Dupuit-type flow system that can be described by the Dupuit-Forchheimer differential equation solved by Bear (1972), yielding Equation (2) as presented in Section 2.

Substituting the two fixed-head boundary conditions H_0 and H_T into Equation (2) yields Equation (49) describing the hydraulic head profile between x=0 and x=x_T.

$$H(x) = \sqrt{-\frac{W}{K}x^2 + \left(\frac{H_T^2 - H_0^2}{x_T} + \frac{Wx_T}{K}\right)x + H_0^2} \tag{49}$$

Equation (49) can be used to determine the position of x_{WD} where $\mathrm{d}H/\mathrm{d}x=0$. The groundwater divide location can then be expressed as in Equation (50), which is analogous to Equation (3) (Bear, 1972).

$$x_{WD} = \frac{x_T}{2} + \frac{K}{2Wx_T}(H_T^2 - H_0^2) \tag{50}$$

where:

x_{WD} = water divide location [L]
x_T = saltwater toe location [L]
H_0 = fixed-head boundary at x=0 [L]
H_T = fixed-head boundary at x=x_T [L]

The value of H_T is calculated with Equation (48) using $H_T=H(x_T)=z(x_T)+h(x_T)=S(\rho_s/\rho_f)$ with S [L] being the depth below sea level of the aquifer basement. Replacing H_T by $S(\rho_s/\rho_f)$ in Equation (50) yields Equation (51) that gives the groundwater divide location x_{WD} as a function of the position of the saltwater toe x_T, depending on the sea level height S above the datum.

$$x_{WD} = \frac{x_T}{2} + \frac{K}{2Wx_T}\left(\frac{S^2\rho_s^2}{\rho_f^2} - H_0^2\right) \tag{51}$$

According to Equation (51), Case I where $0 \leq x_{WD} < x_T$ means that $H_0^2 - \frac{S^2\rho_s^2}{\rho_f^2} < \frac{Wx_T^2}{K}$ and Case II where $x_{WD} < 0$ means that $H_0^2 - \frac{S^2\rho_s^2}{\rho_f^2} > \frac{Wx_T^2}{K}$.

If the location of the saltwater toe x_T is not known a priori, a first assumption would be to neglect the influence of seawater intrusion on the location of the groundwater divide x_{WD}. With such an assumption, we would consider Dupuit-type flow occurring between $x=0$ where $H(x=0)=H_0$ and $x=L$ where $H(x=L)=S$. In this case, Equation (51) would transform into Equation (52).

$$x_{WD} = \frac{L}{2} + \frac{K}{2WL}(S^2 - H_0^2) \tag{52}$$

By this equation, Case I ($0 < x_{WD} < L$) yields $H_0^2 - S^2 < \frac{WL^2}{K}$ and Case II ($x_{WD} < 0$) yields $H_0^2 - S^2 > \frac{WL^2}{K}$.

4.2 Conversion of the Natural System into a Single Conceptual Model

Just as in the case of inland Dupuit-type aquifers, the regional model of a coastal aquifer will be converted into one or two systems bounded by an upstream no-flow boundary and a downstream boundary with fixed-head equal to sea level, S. Two scenarios can exist: Case I in which the groundwater divide physically exists between the two fixed-head boundaries, as shown in Figure 15; or Case II in which it is imaginary—meaning that it is external to the aquifer system, as shown in Figure 16. As discussed earlier, these two Cases depend on the relative values of the fixed-head conditions at the boundaries of the Dupuit-type coastal aquifer.

Each of the two Cases I and II must be transformed into a single flow system bounded by an upgradient no-flow boundary and a downgradient fixed head boundary as shown in Figure 17.

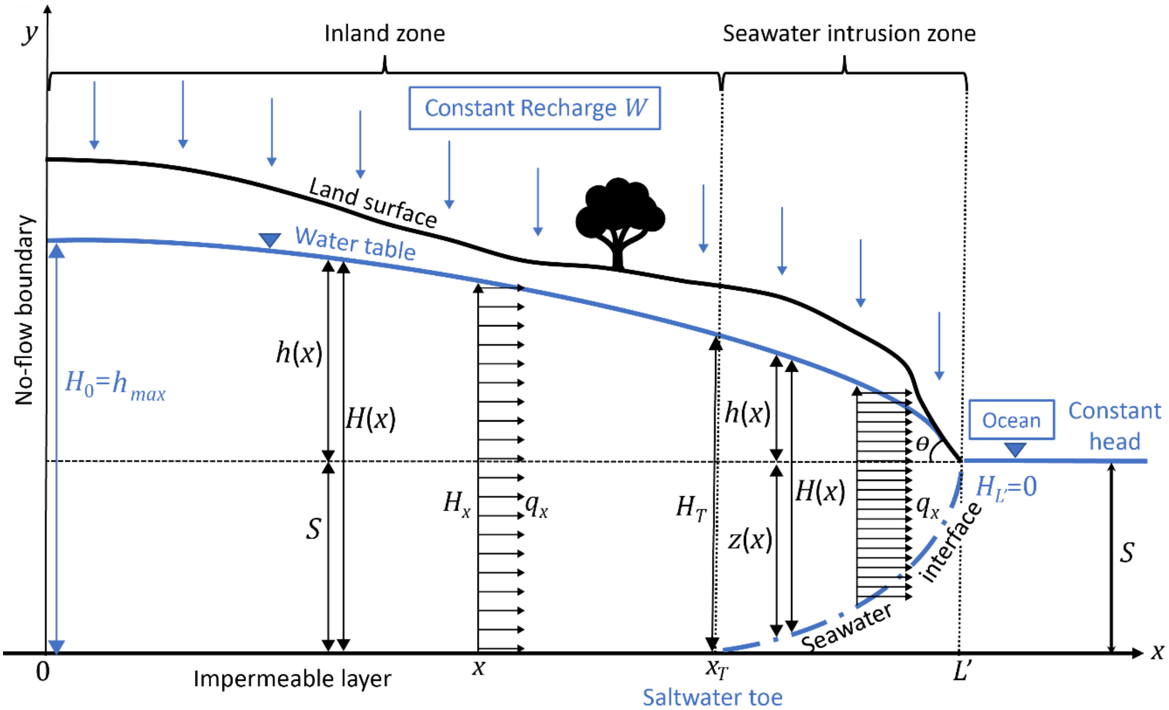

Figure 17 - Final transformed system of a coastal aquifer for developing general analytical solutions.

To transform Case I, first the regional system must be separated into the two subdomains on either side of the water divide. The right subdomain where seawater intrusion occurs can then be reduced to the single problem shown in Figure 17 with a length L' of (L-x_{WD}) (Figure 15 shows the length L). The origin (x=0) in the transformed system represents the no-flow upgradient boundary that was located at x_{WD} in Figure 15.

To transform Case II, the imaginary upgradient water divide is placed at the origin of the transformed system. Case II coordinates that are between x=0 and x=L (Figure 16) will then map to the transformed system between x=|x_{WD}| and x=L+|x_{WD}|, where L+|x_{WD}|=L', and L' represents the length of the transformed system (Figure 17). Groundwater flow in the coastal aquifer is thus only meaningful with respect to the original Case II system between $x=|x_{WD}|$ *and* $x=L'$. If $|x_{WD}|=0$, the solution reverts to Case I.

The aquifer system can also be bounded naturally by a physical no-flow boundary—an *impermeable boundary*. This physical upstream boundary could correspond, for example, to an inland contact between the aquifer and a clay layer or a rock mass or another geological layer with a relative hydraulic conductivity of at least 100 times lower than the hydraulic conductivity of the coastal aquifer. In this case, the no-flow inland boundary would be taken at $x=0$ in the flow system presented in Figure 17.

4.3 Regional Groundwater Flow Solutions and Determination of the Position of The Saltwater Toe

The coastal groundwater flow system presented in Figure 17 is solved in this section for the two different zones separated by a saltwater toe: 1) the seawater intrusion zone, which is the coastal region containing the saltwater/freshwater interface; and 2) the inland zone, which is the region without the interface. The location of the saltwater toe separating the two zones is also calculated.

One-dimensional equations for groundwater flow in inland unconfined aquifers have been addressed by Dupuit (1863); whereas those for coastal aquifers (Figure 16 and Figure 17) have been addressed by Fetter (1972). The steady-state regional flow solutions for both inland and oceanic unconfined aquifers are given in the context of Dupuit's assumptions: 1) the equipotential surfaces are vertical—the velocity is uniform over the depth; and 2) the aquifer is considered bounded at the bottom by a horizontal impermeable layer.

4.3.1 Groundwater Flow and Water Table Profile in the Seawater Intrusion Zone

The development of Fetter (1972) for the equations of flow in the seawater intrusion zone uses coordinates (x, y), but the flow is considered horizontal and one-dimensional according to the Dupuit approximation, and indicates that the hydraulic head is dependent only on x. The vertical plane, defined by $x=0$, represents the groundwater flow divide (where the hydraulic gradient is zero) of the aquifer (Figure 17). The length of the aquifer is L', which suggests that the problem to be solved lies between $x=0$ and $x=L'$ (Figure 17). The groundwater divide position—i.e., a no-flow condition—is either fixed (impermeable interface due to a geological contact with an aquitard) or estimated from data defining the position of the water table mound (a symmetric flow divide) as presented earlier.

According to the Dupuit theory, Darcy's law is applied to describe groundwater discharge (Q_x) per unit width of the aquifer [L^2T^{-1}] in the horizontal (x) direction (Figure 17), as shown in Equation (53).

$$Q_x = -K\, H\, \frac{\mathrm{d}(S+h)}{dx} = -K\,(h+z)\frac{\mathrm{d}h}{\mathrm{d}x} = -K\left(1+\frac{\rho_f}{\Delta\rho}\right)h\,\frac{\mathrm{d}h}{\mathrm{d}x} \quad (53)$$

where:

K	=	saturated hydraulic conductivity [LT^{-1}]
H=h+z	=	freshwater saturated thickness of the unconfined aquifer in the seawater intrusion zone [L]
S+h	=	hydraulic head in the seawater intrusion zone of the unconfined aquifer [L]
dh/dx	=	hydraulic gradient [dimensionless]

The flow depends on the recharge rate W [LT^{-1}] of the aquifer, yielding by continuity, Equation (54).

$$\mathrm{d}Q_x = W\,\mathrm{d}x \quad (54)$$

Combining Equations (53) and (54), and using Equation (48), and integrating to consider the boundary conditions $\mathrm{d}h/\mathrm{d}x=0$ *at* $x=0$ *and* $h(L')=0$, the solution for the water table elevation above sea level, $h_{SIZ}(x)$ (subscript SIZ means *Seawater Intrusion Zone*) for $x_T \le x \le L'$ is expressed in Equation (55).

$$h_{SIZ}(x) = \sqrt{\frac{\Delta\rho}{\rho_s}\frac{W}{K}}\sqrt{L'^2 - x^2} \qquad \textit{with } x_T \le x \le L' \quad (55)$$

The solution for the freshwater saturated thickness $H_{SIZ}(x)$ of the unconfined aquifer in the seawater intrusion zone is obtained by combining Equations (48) and (55) and is expressed in Equation (56).

$$H_{SIZ}(x) = h(x) + z(x) = \left(1+\frac{\rho_f}{\Delta\rho}\right)h(x) = \sqrt{\frac{\rho_s}{\Delta\rho}\frac{W}{K}}\sqrt{L'^2 - x^2} \qquad \textit{with } x_T \le x \le L' \quad (56)$$

4.3.2 Determination of the Saltwater Toe Location

The toe of the seawater wedge at position x_T [L] is located at the intersection of the saltwater/freshwater interface and the horizontal base of the aquifer—the *aquifer basement*. Solving Equations (48) and (55) for $z(x_T)=S$, the expression of x_T is obtained (Equation (57)).

$$x_T = \sqrt{L'^2 - \frac{\rho_s \Delta\rho}{\rho_f^2} \frac{K}{W} S^2} \tag{57}$$

Equation (57) shows that a higher recharge rate W will push the saltwater tongue to move seawards, while increasing hydraulic conductivity K will cause the toe to move further inland. It also shows that the interface position depends on the ratio K/W.

4.3.3 Groundwater Flow and Water Table Profile in the Inland Zone

In the inland zone where $0 \leq x < x_T$, the water table profile is solved using the equation of the Dupuit-Forchheimer ellipse (Dupuit, 1863), in a similar manner to solving Equation (8) for inland aquifers. For boundary conditions in the inland zone, we have $q_x=0$ at the left symmetry boundary while at the right boundary ($x=x_T$), we have $H=H_T$ (Figure 17) with $H_T=S+h_{SIZ}(x_T)=S(1+\Delta\rho/\rho_f)=S(\rho_s/\rho_f)$ according to Equation (48).

Equation (58), which is analogous to Equation (8), describes $H_{IZ}(x)$ (subscript IZ means *Inland Zone*), the saturated thickness, representing the hydraulic head in the inland zone as a function of x when $0 \leq x \leq x_T$.

$$H_{IZ}(x) = \sqrt{\frac{W}{K}\left(x_T^2 - x^2\right) + H_T^2} \qquad with\ 0 \leq x \leq x_T \tag{58}$$

Replacing x_T with its definition in Equation (57) and H_T with $S(\rho_s/\rho_f)$ gives the closed-form solution of the hydraulic head H_{IZ} in the inland zone (Equation (59)).

$$H_{IZ}(x) = \sqrt{\frac{W}{K}\left(L'^2 - x^2\right) + \frac{\rho_s}{\rho_f} S^2} \qquad with\ 0 \leq x \leq x_T \tag{59}$$

When $S=0$, then $H(x)=h(x)$ and Equation (59) refers to the case of an inland aquifer when the downstream fixed-head boundary condition is equal to 0 (Equation (8) when $h_L=0$).

4.4 Groundwater Velocities

Two cases must be developed for calculating the groundwater velocities in the coastal aquifer, depending on whether groundwater flow occurs in the inland zone or the seawater intrusion zone.

4.4.1 Groundwater Velocity in the Seawater Intrusion Zone

Recognizing that the vertical component of the gradient is negligible, the groundwater velocity $v_x(x)$ in the seawater intrusion zone can be expressed as $v_{SIZ}(x)$. Combining Equations (53) and (56), we obtain the expression of the fluid velocity for steady-state flow in the inland zone for $x_T \leq x \leq L'$ (Equation (60)).

$$v_{SIZ}(x) = \frac{Q_x(x)}{n_e} = \frac{1}{n_e}\frac{q(x)}{H_{SIZ}(x)} = \frac{1}{n_e}\frac{Wx}{\sqrt{\frac{\rho_s}{\Delta\rho}\cdot\frac{W}{K}}\cdot\sqrt{L'^2 - x^2}}$$
$$= \frac{1}{n_e}\sqrt{\frac{\Delta\rho W K}{\rho_s}}\frac{x}{\sqrt{L'^2 - x^2}} \qquad (60)$$
$$\text{with } x_T \leq x \leq L'$$

where:

$v_{SIZ}(x)$ = average linear velocity of a particle of water [LT^{-1}] located at x [L] in the seawater intrusion zone

4.4.2 Groundwater Velocity in the Inland Zone

Again, recognizing that the vertical component of the gradient is negligible, the groundwater velocity $v_x(x)$ in the inland zone can be expressed as $v_{IZ}(x)$. Combining Equations (5), (6), (7), and (59), and considering that $dH(x)=d(S+h(x))=dh(x)$, we obtain the expression of the fluid velocity for steady-state flow in the inland zone for $0 \leq x \leq x_T$ as shown in Equation (61).

$$v_{IZ}(x) = \frac{q_x(x)}{n_e} = \frac{1}{n_e}\frac{Q(x)}{H_{IZ}(x)} = \frac{W}{n_e}\frac{x}{\sqrt{\frac{W}{K}\left(L'^2 - x^2\right) + \frac{\rho_s}{\rho_f}S^2}} \qquad (61)$$
$$\text{with } 0 \leq x \leq x_T$$

where:

$v_{IZ}(x)$ = average linear velocity of a particle of water [LT^{-1}] located at x [L] in the inland zone

4.5 Groundwater Travel Times

There are three different scenarios for calculating the groundwater travel times of water particles between a departure point x_i and a downgradient position x (arrival point). The three different scenarios depend on the respective locations of the departure and arrival points in the transformed flow system shown in Figure 17.

- Scenario 1: Migration of a groundwater particle only occurs within the seawater intrusion zone where both x_i and x are located between x_T and L'.

- Scenario 2: Migration of a groundwater particle only occurs within the inland zone where both x_i and x are located between 0 and x_T.
- Scenario 3: Migration of a groundwater particle occurs within both the inland zone and the seawater intrusion zone. In this case, x_i is in the inland zone ($0 < x_i < x_T$) whereas x is in the seawater intrusion zone ($x_T < x < L'$).

4.5.1 Groundwater Travel Time in the Seawater Intrusion Zone

Equalizing Equations (10) and (60), separating variables x and t, and integrating the resulting differential equation (with the variable of integration ξ) yields an expression for the travel time t_{SIZ}[T] in the seawater intrusion zone between two arbitrary positions x_i (at t=0, assuming the travel path begins at the water table) and x (at t) (Figure 18), as shown in Equation (62).

$$\int_0^{t_{SIZ}} d\tau = \int_{x_i}^{x} \frac{d\xi}{v_{SIZ}} = n_e \sqrt{\frac{\rho_s}{\Delta\rho W K}} \int_{x_i}^{x} \frac{\sqrt{L'^2 - \xi^2}}{\xi} \, d\xi \tag{62}$$

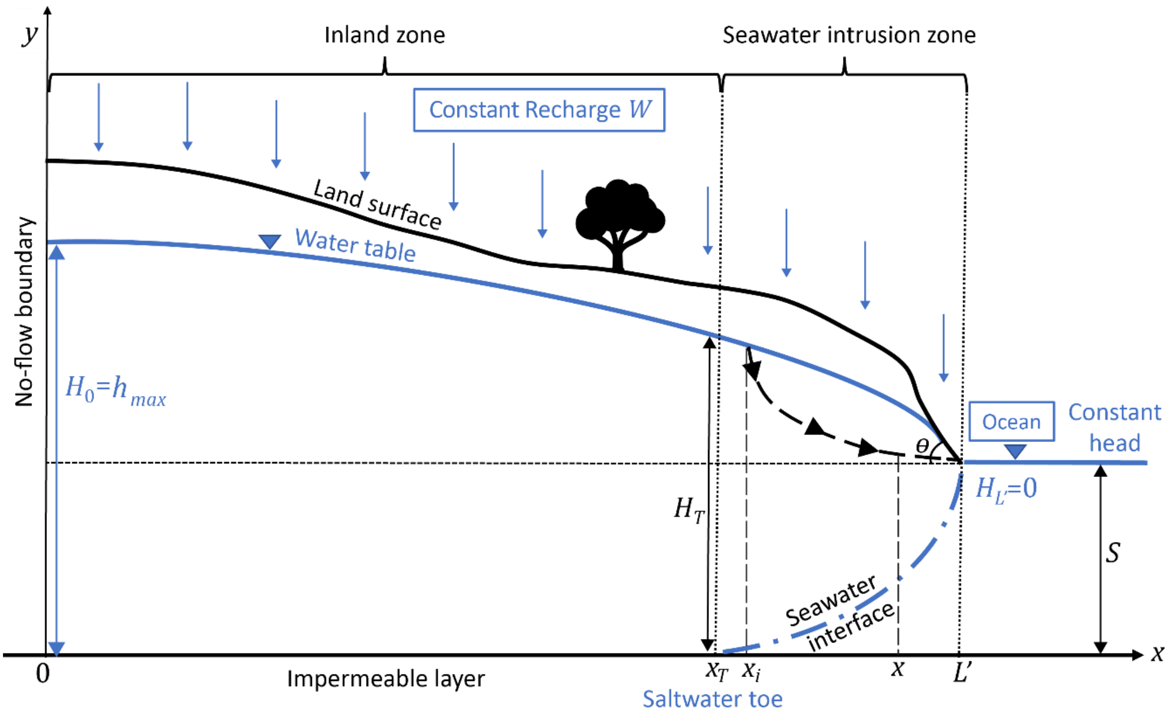

Figure 18 - Conceptual travel path of a groundwater particle in the seawater intrusion zone traveling between position x_i and position x where $x_T \leq x_i \leq L'$ and $x_i \leq x \leq L'$. Downgradient of point x, the path continues to point L'.

After integration we obtain the expression for t, as shown in Equation (63).

$$t_{SIZ}(x) = n_e \sqrt{\frac{\rho_s}{\Delta\rho W K}} \left[\sqrt{L'^2 - x^2} - \sqrt{L'^2 - x_i^2} - L' \, ln \left(\frac{L' + \sqrt{L'^2 - x^2}}{L' + \sqrt{L'^2 - x_i^2}} \frac{x_i}{x} \right) \right] \tag{63}$$

$$with\ x_T \leq x_i \leq L' \text{ and } x_i \leq x \leq L'$$

Equation (63) represents the closed-form analytical solution for groundwater travel time when $x_T \leq x_i \leq L'$ *and* $x_i \leq x \leq L'$.

By replacing x by L' we obtain the result for the specific case of calculating the travel time of a groundwater particle flowing between position x_i in the freshwater recharge zone to its discharge at the ocean (at x=L').

4.5.2 Groundwater Travel Time in the Inland Zone

Equalizing Equations (10) and (61), separating variables x and t and integrating the resulting differential equation (with the variable of integration ξ) yields an expression for the travel time t_{IZ} [T] in the inland zone between two arbitrary positions x_i (at t=0, assuming the travel path begins at the water table) and x (at t), which is a position upgradient of the saltwater toe, as shown in Equation (64).

$$\int_0^{t_{IZ}} d\tau = \int_{x_i}^{x} \frac{d\xi}{v_{IZ}} = \frac{n_e}{W} \int_{x_i}^{x} \frac{\sqrt{\frac{W}{K}(L'^2 - \xi^2) + \frac{\rho_s}{\rho_f} S^2}}{\xi}\, d\xi \tag{64}$$

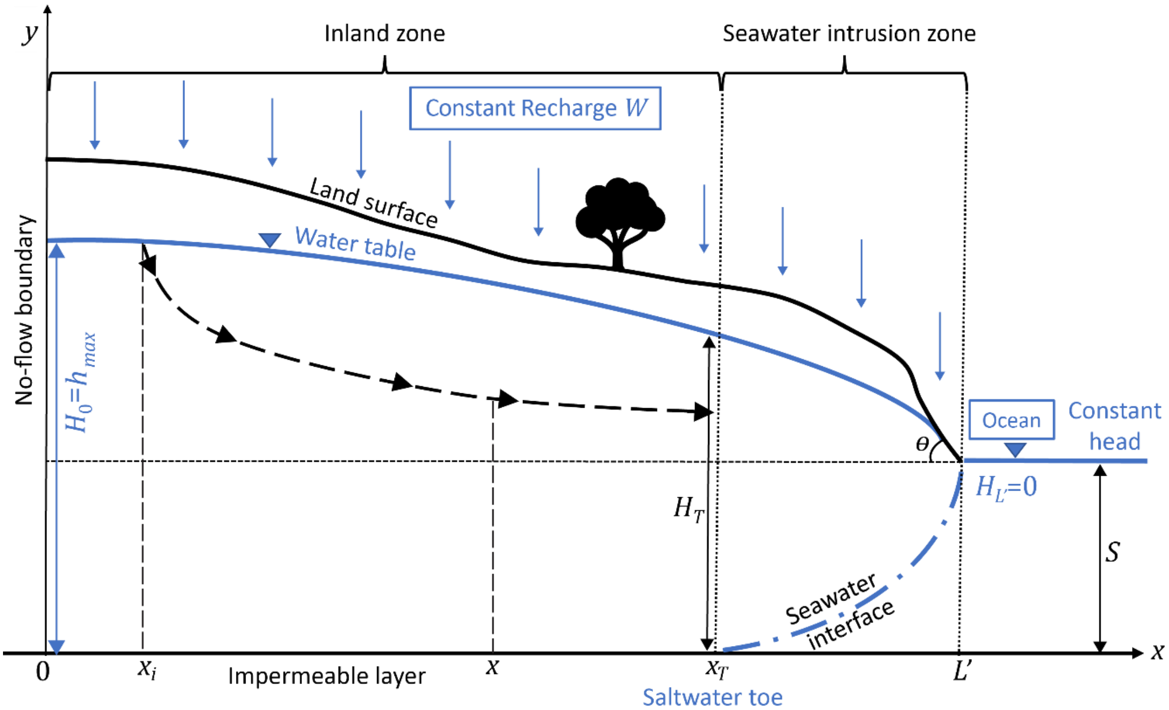

Figure 19 - Conceptual travel path of a groundwater particle in the inland zone traveling between position x_i and position x where $0 \leq x_i \leq x_T$ and $x_i \leq x \leq x_T$. Downgradient of point x, the path continues to point x_T.

After integration we obtain the expression for t, as shown in Equation (65).

$$t_{IZ}(x) = n_e\sqrt{\frac{1}{WK}}\left[\sqrt{L'^2 + \left(\frac{K}{W}\frac{\rho_s}{\rho_f}S^2\right) - x^2} - \sqrt{L'^2 + \left(\frac{K}{W}\frac{\rho_s}{\rho_f}S^2\right) - x_i^2}\right.$$
$$\left. - \sqrt{\left(L'^2 + \left(\frac{K}{W}\frac{\rho_s}{\rho_f}S^2\right)\right)}\, ln\left(\frac{\sqrt{L'^2 + \left(\frac{K}{W}\frac{\rho_s}{\rho_f}S^2\right)} + \sqrt{L'^2 + \left(\frac{K}{W}\frac{\rho_s}{\rho_f}S^2\right) - x^2}}{\sqrt{L'^2 + \left(\frac{K}{W}\frac{\rho_s}{\rho_f}S^2\right)} + \sqrt{L'^2 + \left(\frac{K}{W}\frac{\rho_s}{\rho_f}S^2\right) - x_i^2}}\frac{x_i}{x}\right)\right] \quad (65)$$

with $0 < x_i \leq x_T$ and $x_i \leq x \leq x_T$

Equation (65) represents the closed-form analytical solution for groundwater travel time in the inland zone when $0 < x_i \leq x_T$ and $x_i \leq x \leq x_T$.

By replacing x with x_T we obtain the result for the special case of calculating the travel time of a groundwater particle flowing between position x_i of recharge, to the position of the saltwater toe (at $x{=}x_T$) before entering the seawater intrusion zone of the coastal aquifer.

4.5.3 Groundwater Travel Time for a Particle of Water Circulating in Both the Inland and Seawater Intrusion Zones

A groundwater particle departing from position x_i in the inland zone and discharging to position x in the seawater intrusion zone will first travel from $x{=}x_i$ to $x{=}x_T$ in the inland zone and then travel from $x{=}x_T$ to x in the seawater intrusion zone, where $0 < x_i \leq x_T$ and $x_T \leq x \leq L'$. Therefore, the equation for groundwater travel time in the coastal aquifer t_{CA} (with subscript CA meaning *Coastal Aquifer*) is obtained from combining Equation (65) (with $x{=}x_T$) and Equation (63) (with $x_i{=}x_T$). The value of x_T is also replaced by its expression given in Equation (57) to obtain Equation (66).

$$t_{CA}(x) = t_{IZ}(x_T) + t_{SIZ}(x) =$$

$$n_e\sqrt{\frac{1}{WK}}\left[\sqrt{L'^2+\left(\frac{K}{W}\frac{\rho_s}{\rho_f}S^2\right)-x_T^2}-\sqrt{L'^2+\left(\frac{K}{W}\frac{\rho_s}{\rho_f}S^2\right)-x_i^2}-\sqrt{\left(L'^2+\left(\frac{K}{W}\frac{\rho_s}{\rho_f}S^2\right)\right)}\,ln\left(\frac{\sqrt{L'^2+\left(\frac{K}{W}\frac{\rho_s}{\rho_f}S^2\right)}+\sqrt{L'^2+\left(\frac{K}{W}\frac{\rho_s}{\rho_f}S^2\right)-x_T^2}}{\sqrt{L'^2+\left(\frac{K}{W}\frac{\rho_s}{\rho_f}S^2\right)}+\sqrt{L'^2+\left(\frac{K}{W}\frac{\rho_s}{\rho_f}S^2\right)-x_i^2}}\,\frac{x_i}{x_T}\right)\right]+$$

$$n_e\sqrt{\frac{\rho_s}{\Delta\rho WK}}\left[\sqrt{L'^2-x^2}-\sqrt{L'^2-x_T^2}-L'\,ln\left(\frac{L'+\sqrt{L'^2-x^2}}{L'+\sqrt{L'^2-x_T^2}}\,\frac{x_T}{x}\right)\right] \tag{66}$$

with $0 < x_i \leq\ x_T$ and $x_T \leq x \leq L'$

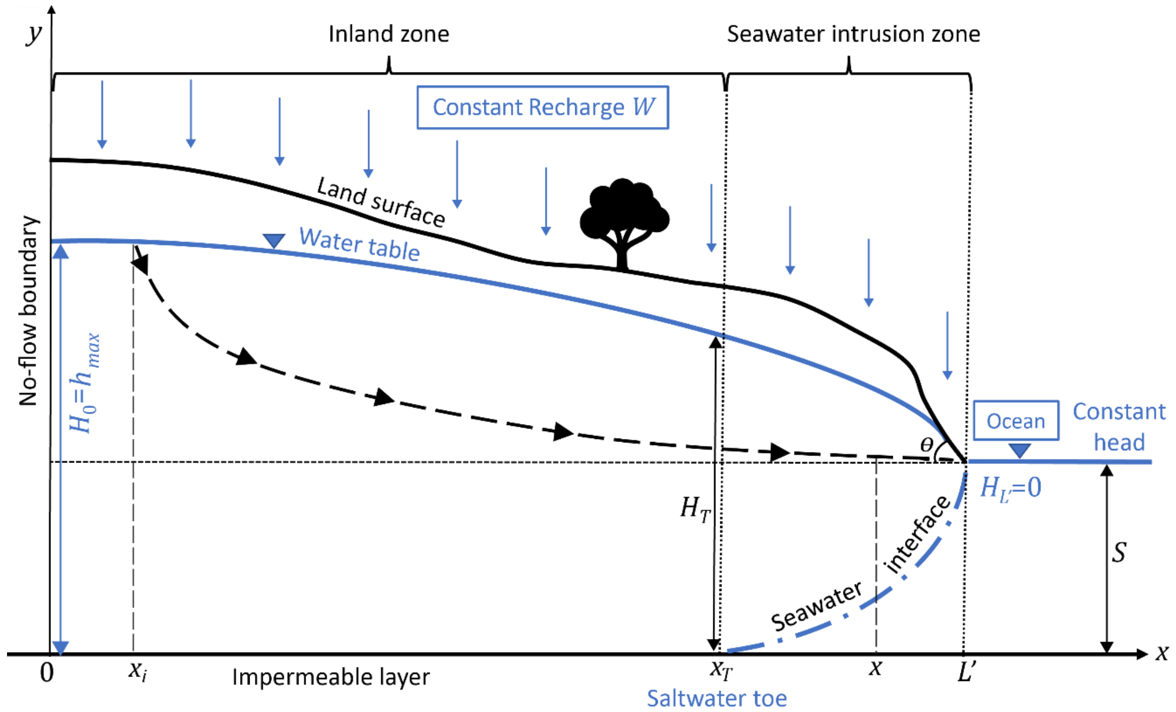

Figure 20 - Conceptual travel path of a groundwater particle within both the inland zone and the seawater intrusion zone. In this case, x_i is in the inland zone ($0 \leq x_i \leq x_T$) whereas x is in the seawater intrusion zone ($x_T \leq x \leq L'$).

The value of x_T is then replaced in Equation (66) by its expression given in Equation (57) to obtain Equation (67).

$$t_{CA}(x) = n_e\sqrt{\frac{1}{WK}}\left[S\frac{\rho_s}{\rho_f}\sqrt{\frac{W}{K}} - \sqrt{L'^2 + (\frac{K}{W}\frac{\rho_s}{\rho_f}S^2) - x_i^2} - \sqrt{\left(L'^2 + (\frac{K}{W}\frac{\rho_s}{\rho_f}S^2)\right)}\ ln\left(\frac{\frac{\sqrt{L'^2+(\frac{K}{W}\frac{\rho_s}{\rho_f}S^2)}+S\frac{\rho_s}{\rho_f}\sqrt{\frac{W}{K}}}{\sqrt{L'^2+(\frac{K}{W}\frac{\rho_s}{\rho_f}S^2)}+\sqrt{L'^2+(\frac{K}{W}\frac{\rho_s}{\rho_f}S^2)-x_i^2}}}{\frac{x_i}{\sqrt{L'^2-\frac{\rho_s\Delta\rho}{\rho_f^2}\frac{K}{W}S^2}}}\right)\right] +$$

$$n_e\sqrt{\frac{\rho_s}{\Delta\rho WK}}\left[\sqrt{{L'}^2 - x^2} - S\sqrt{\frac{\rho_s\Delta\rho}{\rho_f^2}\frac{K}{W}} - L'\ ln\left(\frac{\frac{L'+\sqrt{{L'}^2-x^2}}{L'+S\sqrt{\frac{\rho_s\Delta\rho}{\rho_f^2}\frac{K}{W}}}}{\frac{\sqrt{L'^2-\frac{\rho_s\Delta\rho}{\rho_f^2}\frac{K}{W}S^2}}{x}}\right)\right] \tag{67}$$

$$with\ 0 < x_i \leq x_T\ and\ x_T \leq x \leq L'$$

Equation (67) represents the closed-form analytical solution for groundwater travel time where $0 < x_i \leq x_T$ and $x_T \leq x \leq L'$.

By replacing x with L' we obtain the result for the special case of calculating the travel time of a groundwater particle flowing between position x_i from the inland recharge zone to its discharge to the ocean (at $x=L'$) after flowing through the entire length of the seawater intrusion zone of the coastal aquifer.

4.6 Freshwater Volumes

Fresh groundwater volume is critical for coastal aquifers. The volume of fresh groundwater per unit width of aquifer can be calculated by integrating the saturated freshwater aquifer thickness $H(x)$ between the boundaries of the aquifer (Figure 21). Two different zones must be considered, the inland zone between $x=0$ and $x=x_T$ and the seawater intrusion zone between x_T and L'.

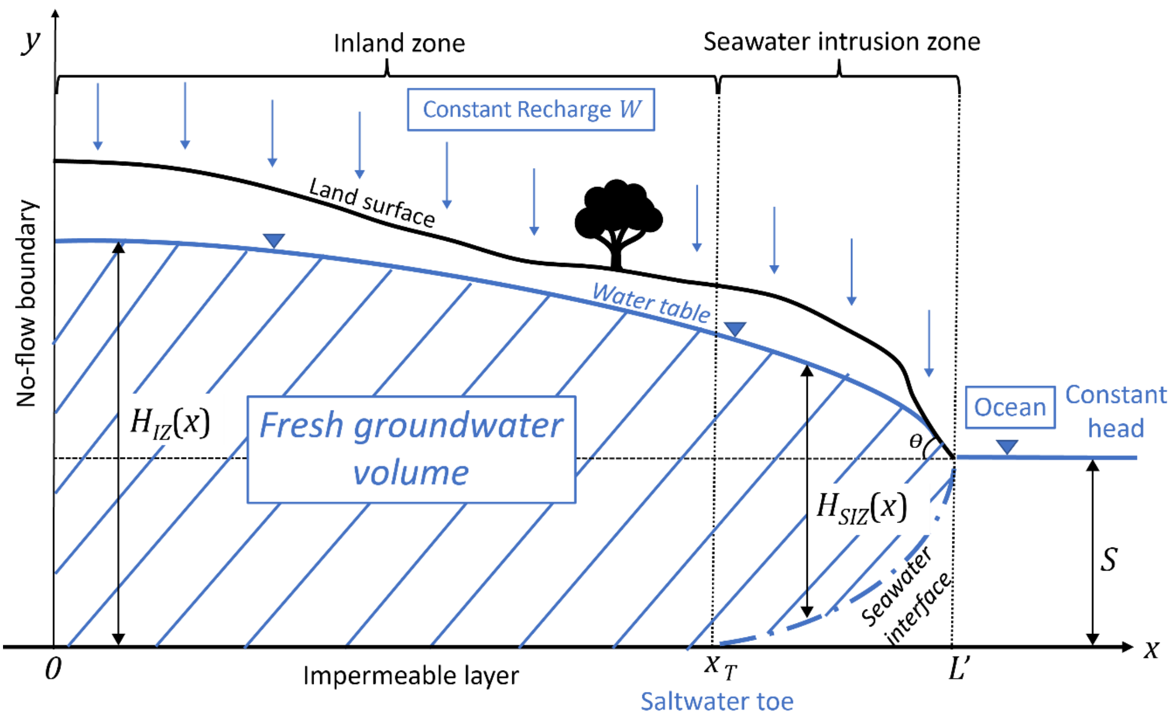

Figure 21 - Freshwater volume of a coastal aquifer.

4.6.1 Fresh Groundwater Volume in the Seawater Intrusion Zone

The freshwater volume V_{SIZ} in the seawater intrusion zone can be calculated by integrating the expression for $H_{SIZ}(x)$ (Equation (56)), the freshwater saturated thickness in this zone, and multiplying by the effective porosity n_e of the aquifer to give the total fresh groundwater volume (contributing to groundwater flow) contained in the coastal aquifer per unit width of aquifer. The expression to be integrated is given in Equation (68).

$$V_{SIZ} = n_e \int_{x_T}^{L'} H_{SIZ}(x)\, \mathrm{d}x = n_e \sqrt{\frac{\rho_s}{\Delta\rho} \frac{W}{K}} \int_{x_T}^{L'} \sqrt{L'^2 - x^2}\, \mathrm{d}x \tag{68}$$

After integration, Equation (68) yields Equation (69). The function $\sqrt{a^2 - x^2}$ integrates as $\int \sqrt{a^2 - x^2}\, \mathrm{d}x = \frac{x}{2} \sqrt{a^2 - x^2} + \frac{a^2}{2} sin^{-1} \frac{x}{a} + c$, where a and c are constants.

$$V_{SIZ} = n_e \sqrt{\frac{\rho_s}{\Delta\rho} \frac{W}{K}} \left[\frac{x}{2} \sqrt{L'^2 - x^2} + \frac{L'^2}{2} sin^{-1}\left(\frac{x}{L'}\right)\right]_{x_T}^{L'} \tag{69}$$

Developing Equation (69) yields Equation (70).

$$V_{SIZ} = \frac{n_e}{2} \sqrt{\frac{\rho_s}{\Delta\rho} \frac{W}{K}} \left[L'^2 \left(\frac{\pi}{2} - sin^{-1}\left(\frac{x_T}{L'}\right)\right) - x_T \sqrt{L'^2 - x_T{}^2}\right]$$
$$\text{with } x_T = \sqrt{L'^2 - \frac{\rho_s \Delta\rho}{\rho_f^2} \frac{K}{W} S^2} \tag{70}$$

Replacing x_T by its value given in Equation (57) gives Equation (71).

$$V_{SIZ} = \frac{n_e}{2} \sqrt{\frac{\rho_s}{\Delta\rho} \frac{W}{K}} \left[L'^2 \left(\frac{\pi}{2} - sin^{-1}\left(\frac{\sqrt{L'^2 - \frac{\rho_s \Delta\rho}{\rho_f^2} \frac{K}{W} S^2}}{L'}\right)\right) - S \sqrt{L'^2 - \frac{\rho_s \Delta\rho}{\rho_f^2} \frac{K}{W} S^2} \sqrt{\frac{\rho_s \Delta\rho}{\rho_f^2} \frac{K}{W}}\right] \tag{71}$$

Equation (71) is the closed-form analytical solution for calculating V_{SIZ} [L^2], the volume of freshwater contained in the saturated seawater intrusion zone per unit width of the coastal aquifer.

4.6.2 Fresh Groundwater Volume in the Inland Zone

The freshwater volume V_{IZ} in the inland zone can be calculated by integrating Equation (59) between x=0 and x=x_T and multiplying by the effective porosity n_e of the aquifer to give the total fresh groundwater volume contained in the inland zone per unit width of aquifer. The expression to be integrated is given in Equation (72).

$$V_{IZ} = n_e \int_0^{x_T} H_{IZ}(x)\, \mathrm{d}x = n_e \int_0^{x_T} \sqrt{\frac{W}{K} \left(L'^2 - x^2\right) + \frac{\rho_s}{\rho_f} S^2}\, \mathrm{d}x \tag{72}$$

Equation (72) can be transformed into Equation (73).

$$V_{IZ} = n_e \sqrt{\frac{W}{K}} \int_0^{x_T} \sqrt{L'^2 + (\frac{K}{W} \frac{\rho_s}{\rho_f} S^2) - x^2}\, \mathrm{d}x \tag{73}$$

After integration, Equation (73) yields Equation (74). The function $\sqrt{a^2 - x^2}$ integrates as $\int \sqrt{a^2 - x^2}\, dx = \frac{x}{2} \sqrt{a^2 - x^2} + \frac{a^2}{2} sin^{-1} \frac{x}{a} + c$, where a and c are constants.

$$V_{IZ} = \frac{n_e}{2}\sqrt{\frac{W}{K}}\left[x\sqrt{L'^2 + (\frac{K}{W}\frac{\rho_s}{\rho_f}S^2) - x^2} + \left(L'^2 + (\frac{K}{W}\frac{\rho_s}{\rho_f}S^2)\right) sin^{-1}\left(\frac{x}{\sqrt{L'^2 + \left(\frac{K}{W}\frac{\rho_s}{\rho_f}S^2\right)}}\right)\right]_0^{x_T} \tag{74}$$

Developing Equation (74) yields Equation (75).

$$V_{IZ} = \frac{n_e}{2}\sqrt{\frac{W}{K}}\left[x_T\sqrt{L'^2 + \left(\frac{K}{W}\frac{\rho_s}{\rho_f}S^2\right) - {x_T}^2} + \left(L'^2 + \left(\frac{K}{W}\frac{\rho_s}{\rho_f}S^2\right)\right) sin^{-1}\left(\frac{x_T}{\sqrt{L'^2 + \left(\frac{K}{W}\frac{\rho_s}{\rho_f}S^2\right)}}\right)\right] \tag{75}$$

$$\text{with } x_T = \sqrt{L'^2 - \frac{\rho_s \Delta\rho}{\rho_f^2}\frac{K}{W}S^2}$$

Replacing x_T by its value given in Equation (57) gives Equation (76).

$$V_{IZ} = \frac{n_e}{2}\sqrt{\frac{W}{K}}\left[S\frac{\rho_s}{\rho_f}\sqrt{\frac{K}{W}}\sqrt{L'^2 - \frac{\rho_s \Delta\rho}{\rho_f^2}\frac{K}{W}S^2} + \left(L'^2 + (\frac{K}{W}\frac{\rho_s}{\rho_f}S^2)\right) sin^{-1}\left(\frac{\sqrt{L'^2 - \frac{\rho_s \Delta\rho}{\rho_f^2}\frac{K}{W}S^2}}{\sqrt{L'^2 + (\frac{K}{W}\frac{\rho_s}{\rho_f}S^2)}}\right)\right] \tag{76}$$

Equation (76) is the closed-form analytical solution for calculating V_{IZ} [L^2], the volume of freshwater contained in the saturated inland zone per unit width of the coastal aquifer.

4.6.3 Total Fresh Groundwater Volume in the Coastal Aquifer (Seawater Intrusion Zone + Inland Zone)

The total volume of freshwater V_{CA} contained in the two zones of the coastal aquifer is obtained by the addition of Equations (70) and (75), as shown in Equation (77).

$$V_{CA} = V_{SIZ} + V_{IZ} = \frac{n_e}{2}\sqrt{\frac{\rho_s}{\Delta\rho}\ \frac{W}{K}}\ \left[L'^2\left(\frac{\pi}{2} - sin^{-1}\left(\frac{x_T}{L'}\right)\right) - x_T\sqrt{L'^2 - x_T{}^2}\right] + \frac{n_e}{2}\sqrt{\frac{W}{K}}\left[\begin{array}{c} x_T\ \sqrt{L'^2 + \left(\frac{K}{W}\ \frac{\rho_s}{\rho_f}\ S^2\right) - x_T{}^2} + \\ \left(L'^2 + \left(\frac{K}{W}\ \frac{\rho_s}{\rho_f}\ S^2\right)\right) sin^{-1}\left(\frac{x_T}{\sqrt{L'^2 + \left(\frac{K}{W}\frac{\rho_s}{\rho_f}S^2\right)}}\right) \end{array}\right] \tag{77}$$

$$with\ \ x_T = \sqrt{L'^2 - \frac{\rho_s \Delta\rho}{\rho_f^2}\ \frac{K}{W}\ S^2}$$

Replacing x_T by its value given in Equation (57) gives Equation (78).

$$V_{CA} = V_{SIZ} + V_{IZ} = \frac{n_e}{2}\sqrt{\frac{\rho_s}{\Delta\rho}\ \frac{W}{K}}\ \left[L'^2\left(\frac{\pi}{2} - sin^{-1}\left(\frac{\sqrt{L'^2 - \frac{\rho_s\Delta\rho}{\rho_f^2}\frac{K}{W}S^2}}{L'}\right)\right) - S\ \sqrt{L'^2 - \frac{\rho_s\Delta\rho}{\rho_f^2}\ \frac{K}{W}S^2}\ \sqrt{\frac{\rho_s\Delta\rho}{\rho_f^2}\ \frac{K}{W}}\right] + \frac{n_e}{2}\sqrt{\frac{W}{K}}\left[\begin{array}{c} S\ \frac{\rho_s}{\rho_f}\ \sqrt{\frac{K}{W}}\ \sqrt{L'^2 - \frac{\rho_s\Delta\rho}{\rho_f^2}\ \frac{K}{W}\ S^2} + \\ \left(L'^2 + (\frac{K}{W}\ \frac{\rho_s}{\rho_f}\ S^2)\right)\ sin^{-1}\left(\frac{\sqrt{L'^2 - \frac{\rho_s\Delta\rho}{\rho_f^2}\frac{K}{W}S^2}}{\sqrt{L'^2 + (\frac{K}{W}\frac{\rho_s}{\rho_f}S^2)}}\right) \end{array}\right] \tag{78}$$

Equation (78) is the closed-form analytical solution for calculating V_{CA}, the volume of freshwater contained in the coastal aquifer per unit width of aquifer [L^2].

4.7 Freshwater Residence Times

4.7.1 Fresh Groundwater Residence Time in the Seawater Intrusion Zone

The mean residence time RT_{SIZ} in the seawater intrusion zone (Equation (79)) defined for steady-state conditions is equal to the groundwater volume per unit width of aquifer (Figure 21) expressed by Equation (70) divided by the total inflow rate per unit width of aquifer in the seawater intrusion zone. This inflow rate corresponds to the length ($L'-x_T$) of the seawater intrusion zone multiplied by the recharge rate W.

$$RT_{SIZ} = \frac{V_{SIZ}}{W\,(L'-x_T)} = \frac{n_e}{2}\sqrt{\frac{\rho_S}{\Delta\rho}\,\frac{1}{WK}}\left[\frac{{L'}^2}{(L'-x_T)}\left(\frac{\pi}{2} - sin^{-1}\left(\frac{x_T}{L'}\right)\right) - x_T\sqrt{\frac{L'+x_T}{L'-x_T}}\right] \tag{79}$$

Replacing x_T by its value given in Equation (57) yields Equation (80).

$$RT_{SIZ} = \frac{V_{SIZ}}{W\,(L'-x_T)} = \frac{n_e}{2}\sqrt{\frac{\rho_S}{\Delta\rho}\,\frac{1}{wK}}\left[\frac{{L'}^2}{\left(L'-\sqrt{{L'}^2-\frac{\rho_S\Delta\rho}{\rho_f^2}\frac{K}{W}S^2}\right)}\left(\frac{\pi}{2}-sin^{-1}\left(\frac{\sqrt{{L'}^2-\frac{\rho_S\Delta\rho}{\rho_f^2}\frac{K}{W}S^2}}{L'}\right)\right)-\sqrt{{L'}^2-\frac{\rho_S\Delta\rho}{\rho_f^2}\,\frac{K}{W}\,S^2}\sqrt{\frac{L'+\sqrt{{L'}^2-\frac{\rho_S\Delta\rho}{\rho_f^2}\frac{K}{W}S^2}}{L'-\sqrt{{L'}^2-\frac{\rho_S\Delta\rho}{\rho_f^2}\frac{K}{W}S^2}}}\right] \quad (80)$$

Equation (80) is the closed-form analytical solution for the mean residence time [T] of groundwater in the seawater intrusion zone of an oceanic coastal aquifer.

4.7.2 Fresh Groundwater Residence Time in the Inland Zone

The mean residence time RT_{IZ} in the inland zone (Equation (81)) defined for steady-state conditions is equal to the groundwater volume per unit width of aquifer (Figure 21) expressed by Equation (75) divided by the total inflow rate per unit width of aquifer in the inland zone. This inflow rate corresponds to the length x_T of the inland zone multiplied by the recharge rate W.

$$RT_{IZ} = \frac{V_{IZ}}{W\, x_T} = \frac{n_e}{2}\sqrt{\frac{1}{WK}}\left[\sqrt{L'^2 + \left(\frac{K}{W}\frac{\rho_s}{\rho_f}S^2\right) - x_T{}^2} + \frac{\left(L'^2 + \frac{K}{W}\frac{\rho_s}{\rho_f}S^2\right)}{x_T} sin^{-1}\left(\frac{x_T}{\sqrt{L'^2 + \left(\frac{K}{W}\frac{\rho_s}{\rho_f}S^2\right)}}\right)\right] \tag{81}$$

Replacing x_T by its value given in Equation (57) yields Equation (82).

$$RT_{IZ} = \frac{V_{IZ}}{W\, x_T} = \frac{n_e}{2}\sqrt{\frac{1}{WK}}\left[S\frac{\rho_s}{\rho_f}\sqrt{\frac{K}{W}} + \frac{\left(L'^2 + \frac{K}{W}\frac{\rho_s}{\rho_f}S^2\right)}{\sqrt{L'^2 - \frac{\rho_s \Delta\rho}{\rho_f^2}\frac{K}{W}S^2}} sin^{-1}\left(\frac{\sqrt{L'^2 - \frac{\rho_s \Delta\rho}{\rho_f^2}\frac{K}{W}S^2}}{\sqrt{L'^2 + \left(\frac{K}{W}\frac{\rho_s}{\rho_f}S^2\right)}}\right)\right] \tag{82}$$

Equation (82) is the closed-form analytical solution for solving the mean residence time [T] of groundwater in the inland zone of an oceanic coastal aquifer.

4.7.3 Fresh Groundwater Residence Time in the Coastal Aquifer (Seawater Intrusion Zone + Inland Zone)

The mean residence time RT_{CA} in the coastal aquifer (Equation (83)) defined for steady-state conditions is equal to the groundwater volume per unit width of aquifer (Figure 21) expressed by Equation (77) divided by the total inflow rate per unit width of aquifer in the coastal aquifer. This inflow rate corresponds to the length L' of the coastal aquifer multiplied by the recharge rate W.

$$RT_{CA} = \frac{V_{CA}}{W\,L'} = \frac{n_e}{2L'}\sqrt{\frac{1}{WK}}\left[\sqrt{\frac{\rho_s}{\Delta\rho}}\left(L'^2\left(\frac{\pi}{2} - sin^{-1}\left(\frac{x_T}{L'}\right)\right) - x_T\sqrt{L'^2 - x_T{}^2}\right) + x_T\sqrt{L'^2 + \left(\frac{K}{W}\frac{\rho_s}{\rho_f}S^2\right) - x_T{}^2} + \left(L'^2 + \frac{K}{W}\frac{\rho_s}{\rho_f}S^2\right) sin^{-1}\left(\frac{x_T}{\sqrt{\left(L'^2 + \frac{K}{W}\frac{\rho_s}{\rho_f}S^2\right)}}\right)\right] \tag{83}$$

Replacing x_T by its value given in Equation (57) yields Equation (84).

$$RT_{CA} = \frac{n_e}{2L'}\sqrt{\frac{1}{WK}}\left[\sqrt{\frac{\rho_s}{\Delta\rho}}\left(L'^2\left(\frac{\pi}{2} - sin^{-1}\left(\frac{\sqrt{L'^2 - \frac{\rho_s\Delta\rho}{\rho_f^2}\frac{K}{W}S^2}}{L'}\right)\right) - S\sqrt{L'^2 - \frac{\rho_s\Delta\rho}{\rho_f^2}\frac{K}{W}S^2}\sqrt{\frac{\rho_s\Delta\rho}{\rho_f^2}\frac{K}{W}}\right) + S\frac{\rho_s}{\rho_f}\sqrt{\frac{K}{W}}\sqrt{L'^2 - \frac{\rho_s\Delta\rho}{\rho_f^2}\frac{K}{W}S^2} + \left(L'^2 + \frac{K}{W}\frac{\rho_s}{\rho_f}S^2\right) sin^{-1}\left(\frac{\sqrt{L'^2 - \frac{\rho_s\Delta\rho}{\rho_f^2}\frac{K}{W}S^2}}{\sqrt{L'^2 + \frac{K}{W}\frac{\rho_s}{\rho_f}S^2}}\right)\right] \tag{84}$$

Equation (84) is the closed-form analytical solution for solving the mean residence time [T] of groundwater in the seawater intrusion zone of an oceanic coastal aquifer.

Exercise 3⤵ provides the opportunity to apply the main previously presented equations to a specific case to calculate different parameters of the flow system in a coastal unconfined Dupuit-type aquifer.

5 Oceanic Island Dupuit-Type Aquifers

This section presents a series of closed-form analytical solutions for oceanic island Dupuit-type aquifers: specifically, for solving seawater intrusion, water table configurations, groundwater velocity, groundwater travel times, fresh groundwater volumes, and groundwater mean residence times. The solutions are valid in the case of regional flow where the aquifer is not under the influence of pumping or injection.

5.1 Description of the Regional Dupuit-Type Oceanic Island Aquifer Model: Freshwater Lens Model for Strip and Circular Islands

Contrary to coastal aquifers where the saltwater–freshwater interface intrudes inland in the form of a saltwater toe, the model for oceanic island aquifers consists of a freshwater lens that floats on top of the denser saltwater (Figure 22). This freshwater lens is replenished by precipitation that infiltrates into the subsurface and discharges to the ocean along the island's coast. The interface between freshwater and saltwater is treated as an impermeable boundary.

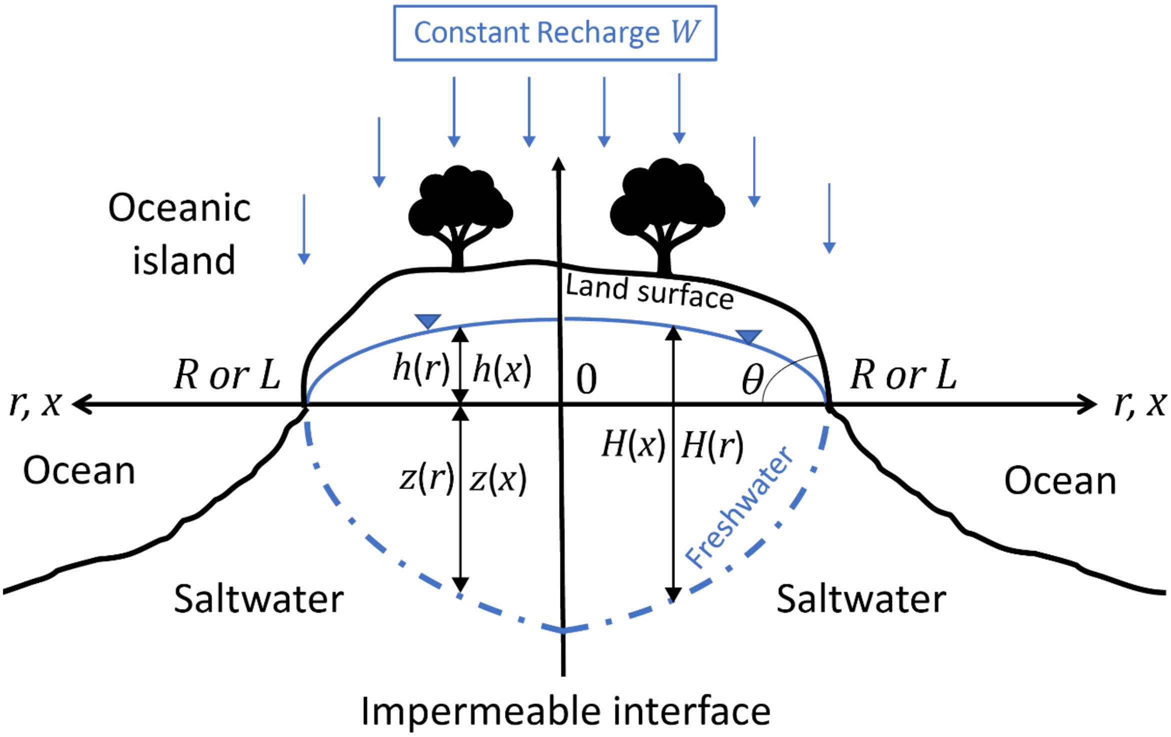

Figure 22 - Simplified conceptual model of a coastal unconfined aquifer of radius R for a circular island, and of half-length L for a strip island.

Limiting assumptions must be considered for developing the solutions—i.e., the island aquifer is unconfined, saturated, homogeneous and isotropic with a hydraulic conductivity represented by a unique value K that is constant and that can represent an equivalent average value for a system of multi-layered aquifers. Also, the aquifer is assumed to be uniformly recharged and, where it discharges into the ocean, the freshwater lens terminates. In this book, closed-form solutions are developed for a constant value of recharge. In Section 6.2.7 changes to in the magnitude of steady-state recharge are considered in a context of climate change.

Groundwater flow is one-dimensional and is assumed to be Dupuit-type. The transition zone between the freshwater lens and the saltwater is not considered; instead, a sharp interface between freshwater and saltwater is assumed. This is a simplification compared to field situations where often no sharp interface can be detected due to the presence of a mixing zone (Ferguson & Gleeson, 2012). Lastly, the assumption of steady-state is considered, but in field situations, the salinization of the coastal aquifer is gradual and the transition zone between saltwater and freshwater can develop and move over long periods of time.

Two cases of simple island geometries are considered to develop closed-form analytical solutions for Dupuit-type flow conditions: the islands are either strip or circular. In both cases, the center of the island represents the axis of symmetry. Circular islands have a radial symmetry with a radial coordinate r varying from 0 (center of the island) to R, the radius of the island (Figure 22). Strip islands have a transverse symmetry with a coordinate x varying from 0 (center of the island) to L, the half-length of the island (Figure 22).

The geometry of the freshwater lens is governed by the Ghyben-Hertzberg (Drabbe & Badon Ghijben, 1889; Herzberg, 1901) relation. For strip islands, the depth to the fresh-saline interface is given in Equation (85), which repeats Equation (48).

$$z(x) = \frac{\rho_f}{\rho_s - \rho_f} h(x) = \frac{\rho_f}{\Delta\rho} h(x) \tag{85}$$

where:

$h(x)$	=	elevation of the water table above sea level in the strip island [L]
$z(x)$	=	depth to the fresh-saline interface below sea level in the strip island [L]
ρ_f	=	density of freshwater [ML^{-3}]
ρ_s	=	density of saltwater [ML^{-3}]
$\Delta\rho$	=	$\rho_s - \rho_f$ [ML^{-3}]

For circular islands, the Badon Ghijben-Herzberg relation is given by Equation (86).

$$z(r) = \frac{\rho_f}{\rho_s - \rho_f} h(r) = \frac{\rho_f}{\Delta\rho} h(r) \tag{86}$$

where:

$h(r)$	=	elevation of the water table above sea level in the circular island [L]
$z(r)$	=	depth to the fresh-saline interface below sea level in the circular island [L]
ρ_f	=	density of freshwater [ML^{-3}]
ρ_s	=	density of saltwater [ML^{-3}]
$\Delta\rho$	=	$\rho_s - \rho_f$ [ML^{-3}]

5.2 Regional groundwater flow solutions

Groundwater flow in oceanic islands is more straightforward to solve than in coastal aquifers because in the case of an island, there is only one unique zone which consists of the freshwater lens.

One-dimensional equations for groundwater flow in oceanic islands have been presented by Fetter (1972). The steady-state regional flow solution for oceanic islands is given in the context of Dupuit's assumptions (Dupuit, 1863).

1) The equipotential surfaces are vertical; and

2) The velocity is uniform over the entire depth.

5.2.1 Strip Oceanic Islands

Flow in strip oceanic islands is defined using coordinates (x,y), but flow is considered horizontal and one-dimensional according to the Dupuit approximation, which implies that the hydraulic head is dependent only on x. The vertical plane at $x=0$ (Figure 23) represents the axis of symmetry of the island and also represents the water divide—where the hydraulic gradient is zero—because the downgradient boundary is a hydraulic head that is the same on both sides of the island. The width (transverse length) of the island (distance into the page in Figure 23) is defined theoretically to be infinite, whereas the half-length of the island is L (the total length of the island is $2L$). Due to the symmetry of the island, the problem is solved between $x=0$ and $x=L$ (Figure 23).

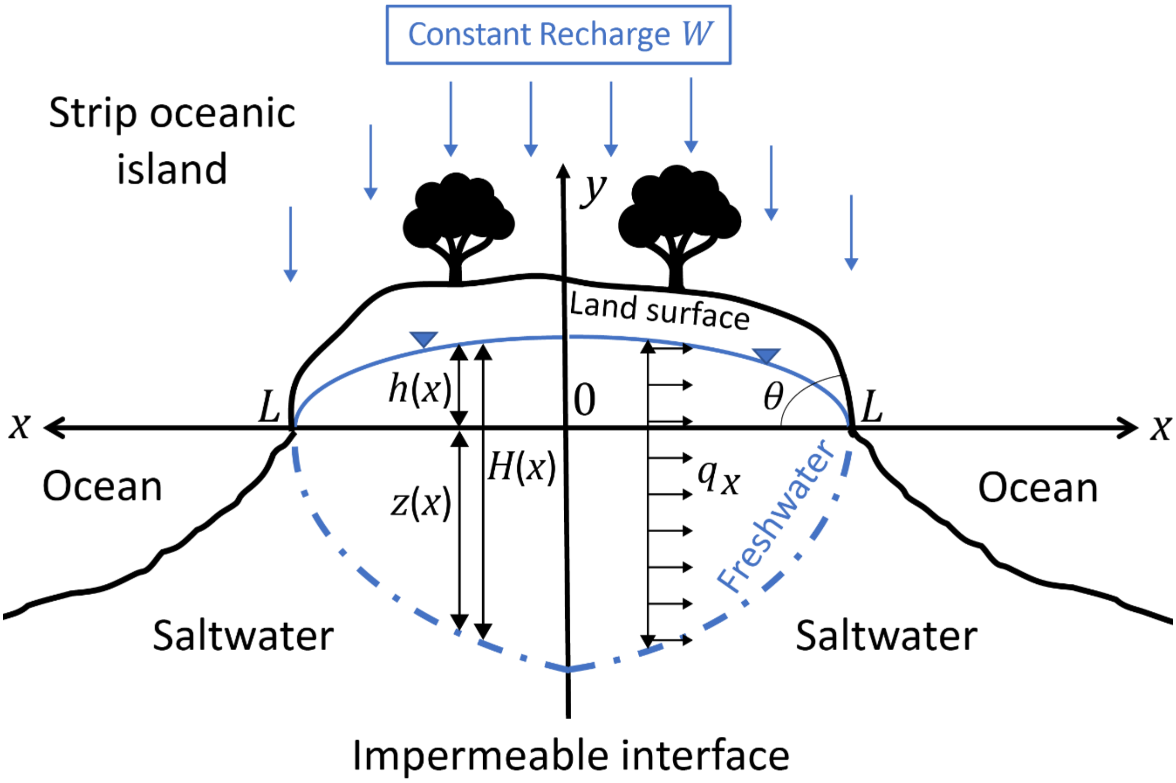

Figure 23 - Conceptual model of groundwater flow in a strip oceanic island.

The solution for the elevation of the water table above sea level, $h(x)$, is given by Fetter (1972) and is summarized below. The Fetter solution is based on combining Darcy's law, the expression of the recharge of the aquifer as a function of x, and the Ghyben-Hertzberg relation (Drabbe & Badon Ghijben, 1889; Herzberg, 1901) for the position of the freshwater–saltwater interface (Equation (85)).

According to the Dupuit theory, Darcy's law is applied to describe groundwater discharge (Q_x) per unit of length of the aquifer [L^2T^{-1}] in the horizontal (x) direction (Figure 23), as shown in Equation (87).

$$Q_x = -KH\frac{\mathrm{d}h}{\mathrm{d}x} = -K(h+z)\frac{\mathrm{d}h}{\mathrm{d}x} = -K\left(1+\frac{\rho_f}{\Delta\rho}\right)h\frac{\mathrm{d}h}{\mathrm{d}x} \tag{87}$$

where:

K	=	saturated hydraulic conductivity [LT^{-1}]
H=h+z	=	freshwater lens saturated thickness in the unconfined strip oceanic island [L]
$\mathrm{d}h/\mathrm{d}x$	=	hydraulic gradient [dimensionless]

The flow depends on the recharge rate W [LT^{-1}] of the aquifer, yielding by continuity, as shown in Equation (88).

$$\mathrm{d}Q_x = W\mathrm{d}x \tag{88}$$

Combining Equations (87) and (88), integrating, and imposing the boundary conditions $\mathrm{d}h/\mathrm{d}x=0$ at $x=0$ and $h(L)=0$, the solution for the water table elevation above sea level, $h(x)$ for $0 \leq x \leq L$ is expressed in Equation (89).

$$h(x) = \sqrt{\frac{\Delta\rho}{\rho_s}\frac{W}{K}}\sqrt{L^2 - x^2} \tag{89}$$

The closed-form analytical solution for the freshwater lens thickness $H_{SOI}(x)$ (with the subscript SOI meaning *Strip Oceanic Island*) in the strip oceanic island is finally obtained by combining Equations (85) and (89) and is expressed by Equation (90).

$$H_{SOI}(x) = h(x) + z(x) = \left(1 + \frac{\rho_f}{\Delta\rho}\right)h(x) = \sqrt{\frac{\rho_s}{\Delta\rho}\frac{W}{K}}\sqrt{L^2 - x^2} \tag{90}$$

5.2.2 Circular Oceanic Islands

Groundwater flow in circular oceanic islands is defined using polar coordinates (r,α) for a horizontal plane and a vertical axis of elevation at the center of the island (representing an axis of symmetry) (Figure 24). Circular islands have a radial symmetry, which implies that the hydraulic head does not depend on the angle α, but only on the radial coordinate r. The upgradient boundary is represented by the axis of symmetry (origin, r=0) and consists of a no-flow boundary—vertical impermeable boundary or water divide—where the hydraulic gradient is zero. The radius of the island is R (Figure 24).

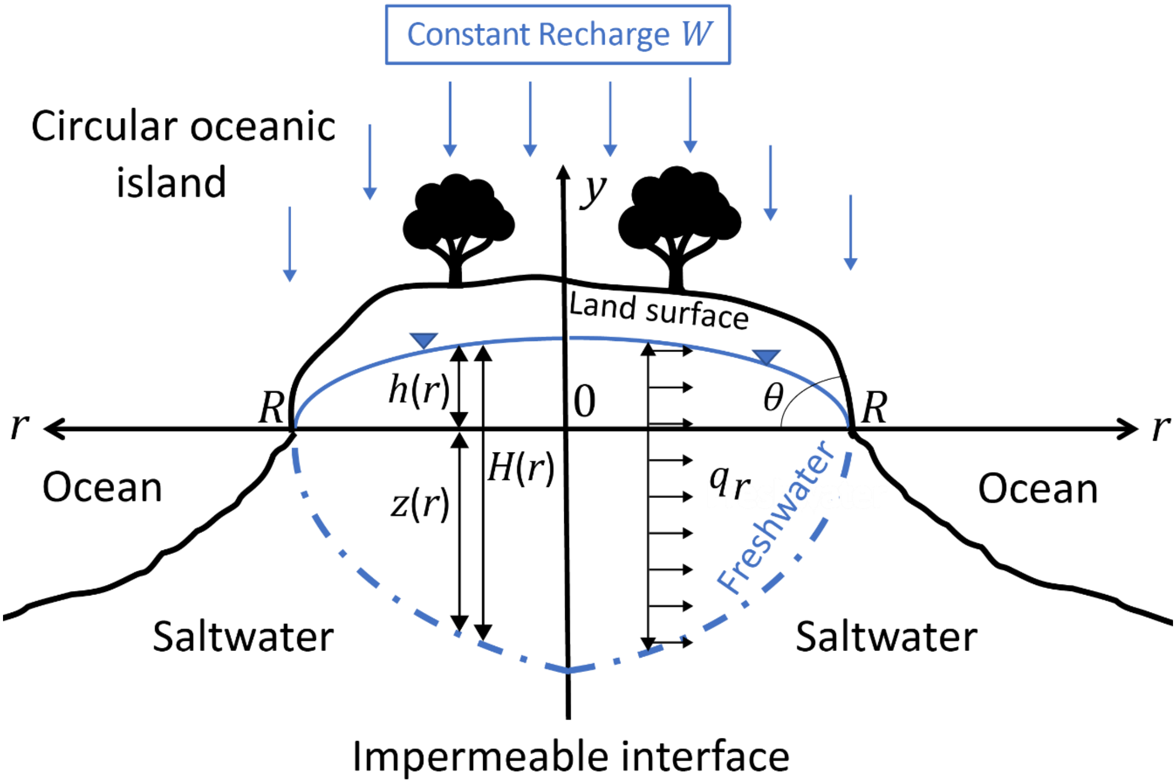

Figure 24 - Conceptual model of groundwater flow in a circular oceanic island.

The governing equation for the elevation of the water table above sea level is given by Fetter (1972), as summarized below. The Fetter solution is based on combining Darcy's law, the expression of the recharge of the aquifer as a function of x and the Ghyben-Hertzberg relation (Drabbe & Badon Ghijben, 1889; Herzberg, 1901), giving the position of the freshwater/saltwater interface (Equation (86)).

According to the Dupuit theory, Darcy's law is applied to describe groundwater discharge (Q_r) [L^3T^{-1}] in the radial (r) direction (Figure 24), as shown in Equation (91).

$$Q_r = -2\pi KrH\frac{\mathrm{d}h}{\mathrm{d}r} = -2\pi Kr(h+z)\frac{\mathrm{d}h}{\mathrm{d}r} = -2\pi Kr\left(1+\frac{\rho_f}{\Delta\rho}\right)h\frac{\mathrm{d}h}{\mathrm{d}r} \tag{91}$$

where:

K	=	saturated hydraulic conductivity [LT^{-1}]
H=h+z	=	freshwater lens saturated thickness in the unconfined circular oceanic island [L]
$\mathrm{d}h/\mathrm{d}r$	=	hydraulic gradient [dimensionless]

The flow depends on the recharge rate W [LT^{-1}] of the aquifer, yielding by continuity:

$$Q_r = \pi W r^2 \tag{92}$$

Equating Equations (91) and (92), integrating, and imposing the boundary conditions $dh/dr=0$ at $r=0$ and $h(R)=0$, the solution for the water table elevation above sea level, $h(r)$ for $0 \leq r \leq R$ is expressed in Equation (93).

$$h(r) = \sqrt{\frac{\Delta\rho}{\rho_s}\frac{W}{2K}}\sqrt{R^2 - r^2} \tag{93}$$

The closed-form analytical solution for the freshwater lens thickness $H_{COI}(r)$ (with subscript COI meaning *Circular Oceanic Island*) in the circular oceanic island is finally obtained by combining Equations (86) and (93) and is expressed in Equation (94).

$$H_{COI}(r) = h(r) + z(r) = \left(1 + \frac{\rho_f}{\Delta\rho}\right)h(r) = \sqrt{\frac{\rho_s}{\Delta\rho}\frac{W}{2K}}\sqrt{R^2 - r^2} \tag{94}$$

5.3 Groundwater Velocities

5.3.1 Strip Oceanic Islands

Recognizing that the vertical component of the gradient is negligible, the groundwater velocity $v_x(x)$ for strip oceanic islands can be expressed as $v_{SOI}(x)$. Combining Equations (87) and (90), we then obtain the expression of the fluid velocity for steady-state flow in the strip oceanic island for $0 \leq x \leq L$ (Equation (95)).

$$v_{SOI}(x) = \frac{q_x(x)}{n_e} = \frac{1}{n_e}\frac{Q(x)}{H_{SOI}(x)} = \frac{1}{n_e}\frac{W\,x}{\sqrt{\frac{\rho_s W}{\Delta\rho\, K}}\sqrt{L^2-x^2}} = \frac{1}{n_e}\sqrt{\frac{\Delta\rho W K}{\rho_s}}\frac{x}{\sqrt{L^2-x^2}} \tag{95}$$

where:

$v_{SOI}(x)$ = average linear velocity of a particle [LT^{-1}] located at x [L] in the strip oceanic island

n_e = effective porosity of the porous medium [dimensionless]

5.3.2 Circular Oceanic Islands

Recognizing that the vertical component of the gradient is negligible, the groundwater velocity $v_r(r)$ for circular oceanic islands can be expressed as $v_{COI}(r)$. Combining Equations (91) and (94), we then obtain the expression of the fluid velocity for steady-state flow in the circular oceanic island for $0 \leq r \leq R$ (Equation (96)).

$$v_{COI}(r) = \frac{q_r(r)}{n_e} = \frac{1}{n_e}\frac{Q(r)}{2\pi r H_{COI}(r)} = \frac{1}{n_e}\frac{\pi W r^2}{2\pi r\sqrt{\frac{\rho_s}{\Delta\rho}\frac{W}{2K}}\sqrt{R^2-r^2}} = \frac{1}{n_e}\sqrt{\frac{\Delta\rho W K}{2\rho_s}}\frac{r}{\sqrt{R^2-r^2}} \tag{96}$$

where:

$v_{COI}(r)$ = average linear velocity of a particle [LT^{-1}] located at r [L] in the circular oceanic island

n_e = effective porosity of the porous medium [dimensionless]

Equations (95) and (96) show that for the same distance R (circular island) and L (strip island), groundwater velocities in the circular island are about 1.41 times ($\sqrt{2}$) slower than velocities in the strip island.

5.4 Groundwater Travel Times

The groundwater travel time equations for strip and circular oceanic islands are presented in Chesnaux and Allen (2008).

5.4.1 Strip Oceanic Islands

In the case of strip oceanic islands, the groundwater travel time between a departing position x_i and a position x along the travel path to the ocean (Figure 25) is determined by integrating Equation (97).

$$\int_0^{t_{SOI}} \mathrm{d}\tau = \int_{x_i}^{x} \frac{\mathrm{d}\xi}{v_{SOI}(\xi)} \tag{97}$$

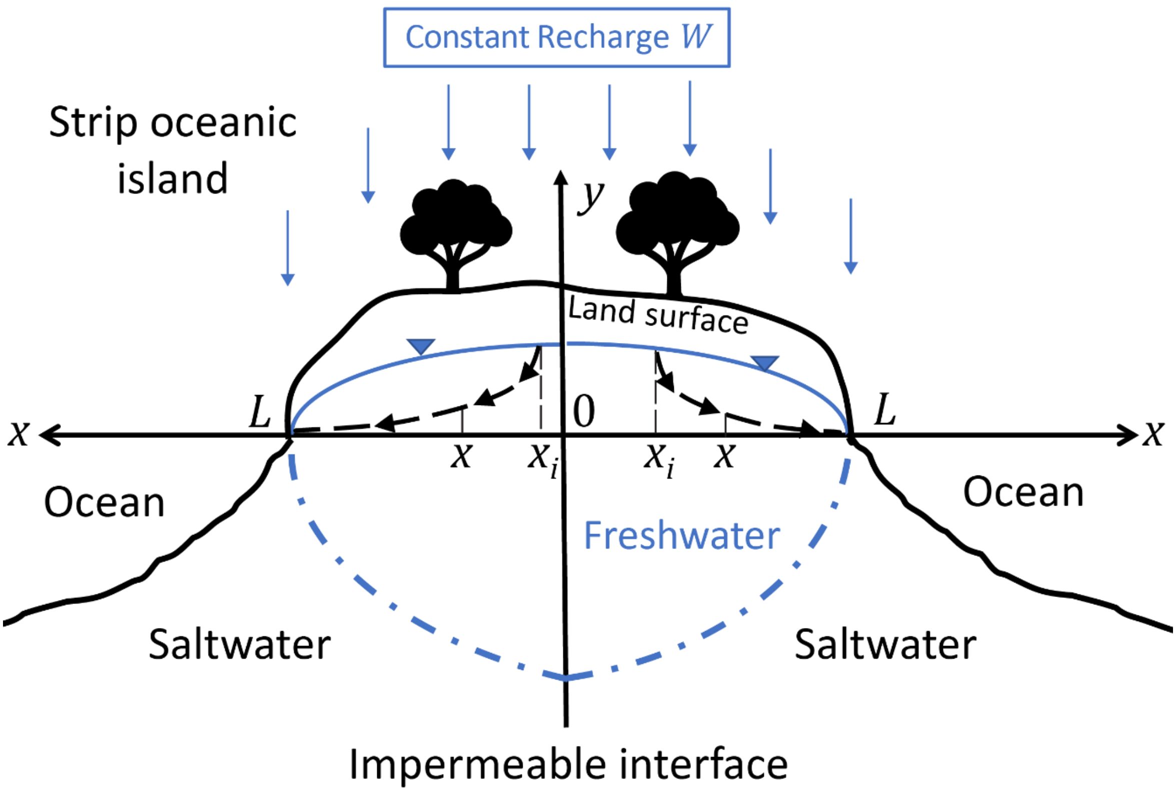

Figure 25 - Conceptual travel paths of groundwater particles in the freshwater lens of a strip oceanic island traveling between position x_i and position x—the paths of two different particles are shown as examples. Downgradient of point x, the paths continue to point L.

Combining Equation (95) and Equation (97) yields Equation (98).

$$t_{SOI} = \int_{x_i}^{x} \frac{\mathrm{d}\xi}{\frac{1}{n_e}\sqrt{\frac{\Delta\rho WK}{\rho_s}}\frac{\xi}{\sqrt{L^2-\xi^2}}} = n_e\sqrt{\frac{\rho_s}{WK\Delta\rho}}\int_{x_i}^{x}\frac{\sqrt{L^2-\xi^2}}{\xi}\mathrm{d}\xi \tag{98}$$

Integration of this equation yields Equation (99).

$$t_{SOI}(x) = n_e\sqrt{\frac{\rho_s}{WK\Delta\rho}}\left[\sqrt{L^2-x^2} - \sqrt{L^2-x_i^2} - L\,ln\left(\frac{L+\sqrt{L^2-x^2}}{L+\sqrt{L^2-x_i^2}}\frac{x_i}{x}\right)\right] \tag{99}$$

Equation (99) is the general closed-form solution of the travel time of water between the initial position x_i and a position x in a strip oceanic island aquifer that is unconfined, horizontal, and recharged by infiltration.

5.4.2 Circular Oceanic Islands

In the case of circular oceanic islands, the groundwater travel time between a departing position r_i and a position r along the travel path to the ocean (Figure 26) is determined by integrating Equation (100).

$$\int_0^{t_{COI}} \mathrm{d}\tau = \int_{r_i}^{r} \frac{\mathrm{d}\varphi}{v_{COI}(\varphi)} \tag{100}$$

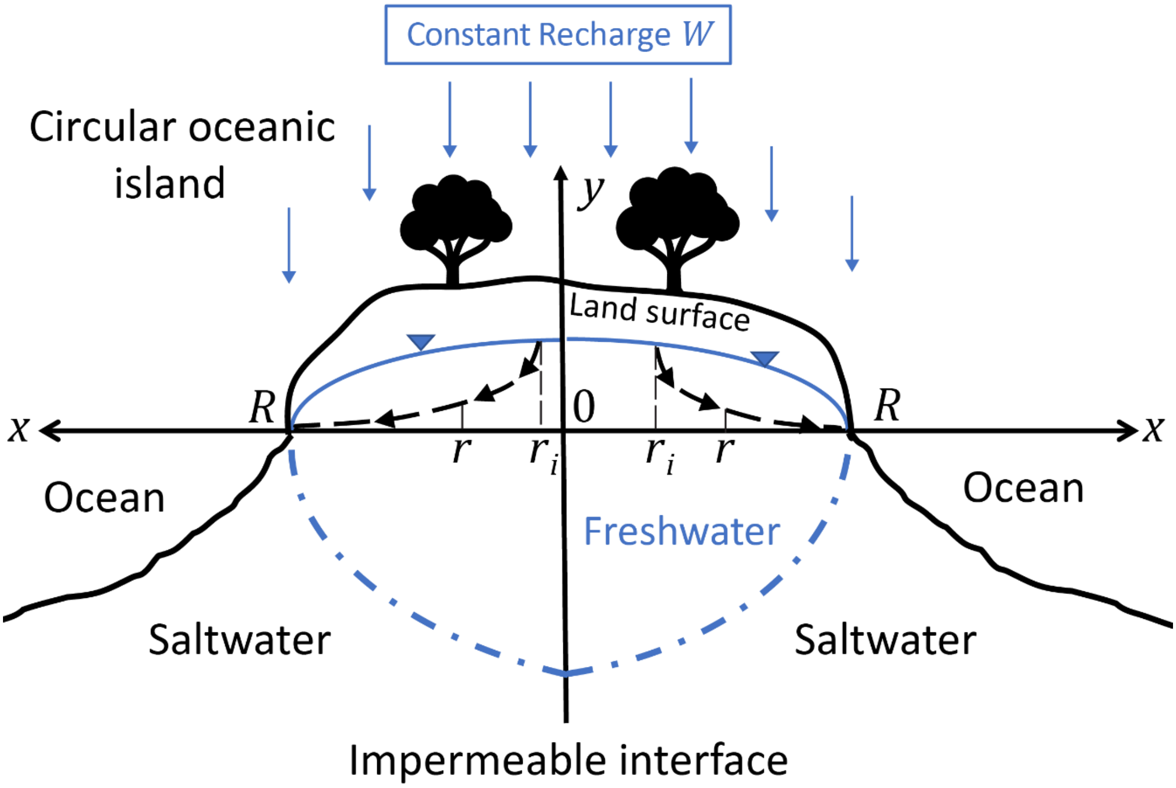

Figure 26 - Conceptual travel paths of groundwater particles in the freshwater lens of a circular oceanic island traveling between position r_i and position r (the paths of two different particles are shown as examples). Downgradient of point r, the paths continue to point R.

Combining Equation (96) with Equation (100) yields Equation (101).

$$t_{COI} = \int_{r_i}^{r} \frac{\mathrm{d}\varphi}{\frac{1}{n_e}\sqrt{\frac{\Delta\rho W K}{2\rho_s}}\frac{\varphi}{\sqrt{R^2-\varphi^2}}} = n_e\sqrt{\frac{2\rho_s}{WK\Delta\rho}}\int_{r_i}^{r}\frac{\sqrt{R^2-\varphi^2}}{\varphi}\mathrm{d}\varphi \qquad (101)$$

Integration of this equation yields Equation (102).

$$t_{COI}(r) = n_e\sqrt{\frac{2\rho_s}{WK\Delta\rho}}\left[\sqrt{R^2-r^2} - \sqrt{R^2-r_i^2} - R\ ln\left(\frac{R+\sqrt{R^2-r^2}}{R+\sqrt{R^2-r_i^2}}\frac{r_i}{r}\right)\right] \qquad (102)$$

Equation (102) is the general closed-form solution of the travel time of water between the initial position r_i and a position r in a circular oceanic island aquifer that is unconfined and recharged by infiltration.

Equations (99) and (102) show that for the same distance R (circular island) and L (strip island), groundwater travel times in the circular island are about 1.41 times ($\sqrt{2}$) longer than travel times in the strip island.

5.5 Freshwater Volumes

The calculations of volumes of fresh groundwater for strip and circular oceanic islands are presented in Chesnaux (2016).

5.5.1 Strip Oceanic Islands

The volume of the fresh groundwater lens per unit width of strip oceanic island aquifer V_{SOI} can be calculated by integrating the saturated freshwater aquifer thickness between the lateral boundaries of the aquifer (Figure 27).

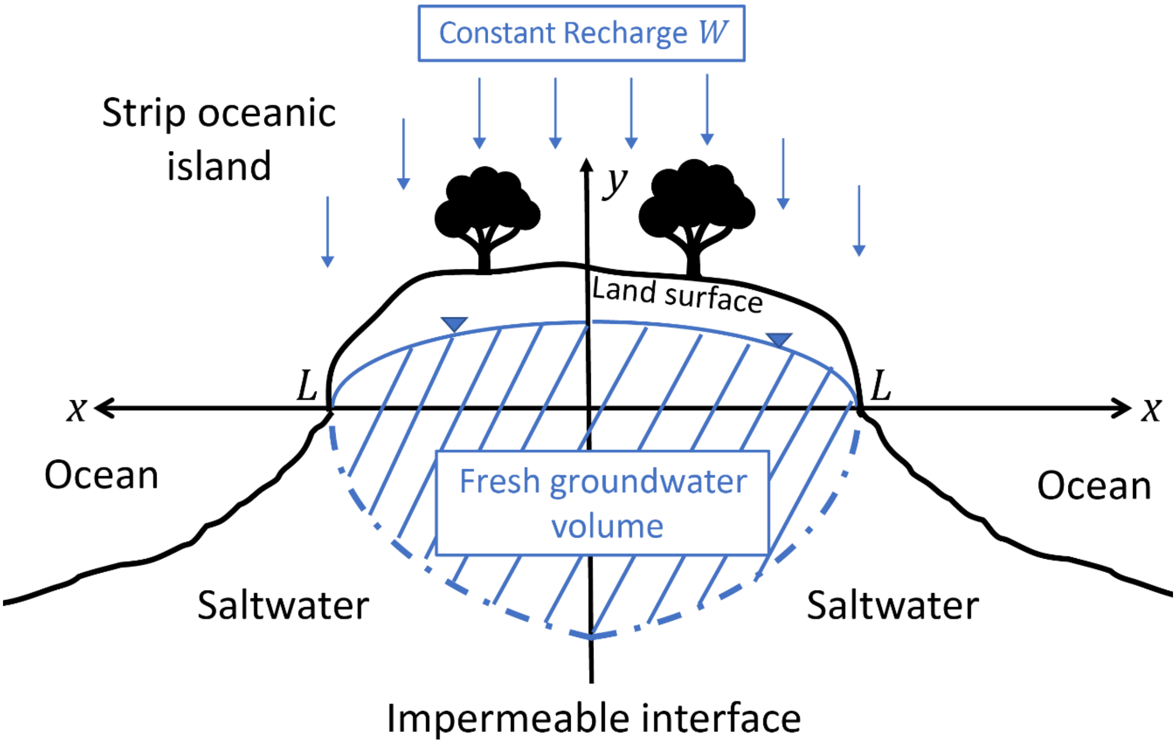

Figure 27 - Freshwater volume of a strip oceanic island aquifer.

The volume V_{SOI} can be calculated by integrating $H_{SOI}(x)$ over the island half-length L and multiplying by 2 to obtain the total volume between the lateral boundaries, as shown in Equation (103).

$$V_{SOI} = n_e \int_0^L 2[h(x) + z(x)]\,\mathrm{d}x = n_e \int_0^L 2H_{SOI}(x)\,\mathrm{d}x \tag{103}$$

Combining Equation (90) for $H_{SOI}(x)$ with Equation (103) gives Equation (104).

$$V_{SOI} = 2n_e \sqrt{\frac{\rho_s}{\Delta\rho}\frac{W}{K}} \int_0^L \sqrt{L^2 - x^2}\,\mathrm{d}x \tag{104}$$

After integration (change of variable), Equation (104) becomes Equation (105).

$$V_{SOI} = \frac{\pi n_e}{2}\sqrt{\frac{\rho_s}{\Delta\rho}\frac{W}{K}}\,L^2 \tag{105}$$

Equation (105) is the closed-form solution for calculating the volume of the freshwater lens in a strip oceanic island per unit width of the strip island.

5.5.2 Circular Oceanic Islands

The same approach is considered for the case of circular islands. The total volume V_{COI} can be calculated by integrating over the full extent of the island radius R, as shown in Equation (106) (Figure 28).

$$V_{COI} = n_e \int_0^R 2\pi r\,[h(r) + z(r)]\;\mathrm{d}r = n_e \int_0^R 2\pi r\; H_{COI}(r)\mathrm{d}r \tag{106}$$

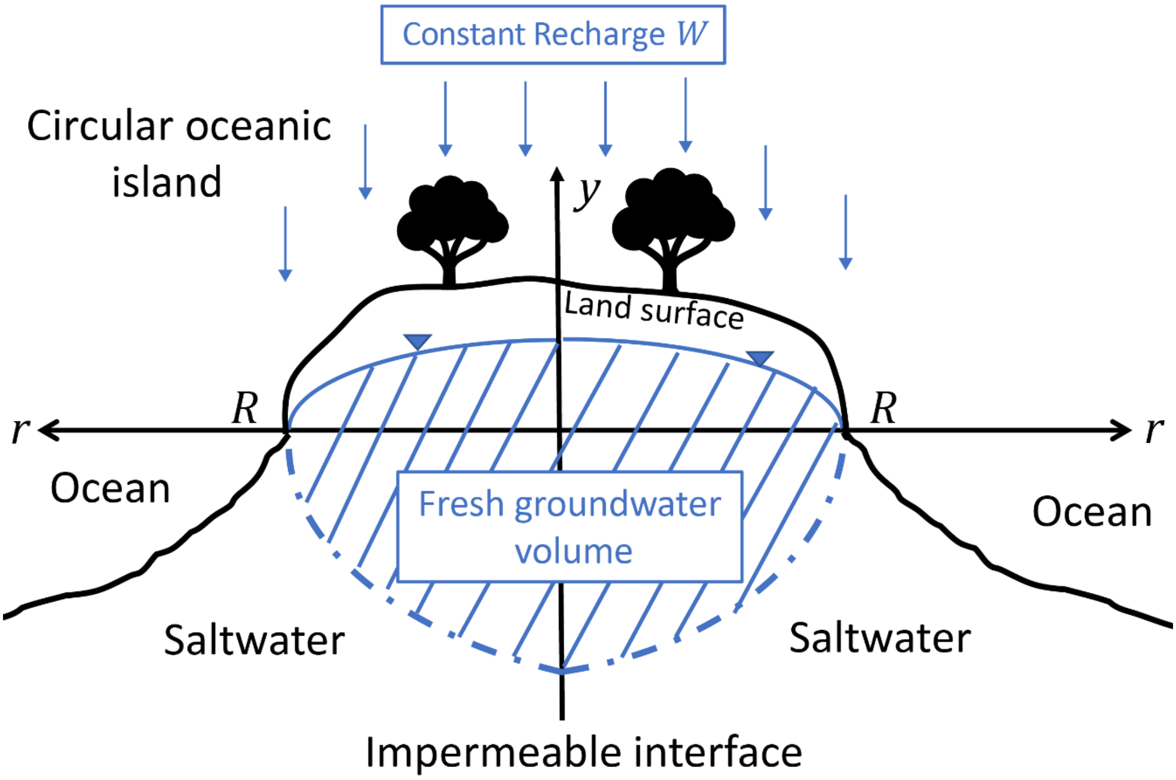

Figure 28 - Freshwater volume of a circular oceanic island aquifer.

Combining Equation (94) with Equation (106) gives Equation (107).

$$V_{COI} = \pi n_e\sqrt{2}\sqrt{\frac{\rho_s}{\Delta\rho}\frac{W}{K}}\int_0^R r\,\sqrt{R^2 - r^2}\;\mathrm{d}r \tag{107}$$

After integration, in a similar manner as for Equation (43) in Section 3, Equation (107) becomes Equation (108).

$$V_{COI} = \frac{\pi n_e \sqrt{2}}{3} \sqrt{\frac{\rho_s}{\Delta\rho} \frac{W}{K}} R^3 \tag{108}$$

Equation (108) is the closed-form solution for calculating the total volume of the freshwater lens in a circular oceanic island.

5.6 Freshwater Mean Residence Times

5.6.1 Strip Oceanic Islands

The mean residence time RT_{SOI} in a strip oceanic island is obtained from Equation (105) and presented in Equation (109).

$$RT_{SOI} = \frac{V_{SOI}}{WL} = \frac{\pi n_e}{2} \sqrt{\frac{\rho_s}{\Delta\rho} \frac{1}{WK}} L \tag{109}$$

5.6.2 Circular Oceanic Islands

The mean residence time RT_{COI} in a circular oceanic island is obtained from Equation (108) and presented in Equation (110).

$$RT_{COI} = \frac{V_{COI}}{\pi R^2 W} = \frac{n_e \sqrt{2}}{3} \sqrt{\frac{\rho_s}{\Delta\rho} \frac{1}{WK}} R \tag{110}$$

Exercise 4 provides the opportunity to apply the main previously presented equations to a specific case to calculate different parameters of the flow system in coastal island aquifers.

6 Analytical Solutions for Predicting the Effects of Sea-Level Rise and Coastal Erosion on Groundwater Resources in Oceanic Coastal and Island Aquifers

This section gives closed-form analytical solutions that allow for the evaluation of the impacts of land surface inundation due to climate change, for both coastal and oceanic island (strip or circular) aquifers and for multiple hydrogeological parameters. Solutions are presented for the *changes* in several critical measures: water table elevation, saltwater toe migration (in the case of coastal inland aquifers), groundwater velocities, groundwater travel times, groundwater volumes, groundwater mean residence times, and total groundwater recharge.

6.1 Effects of Climate Change: Land-Surface Inundation Resulting from Sea-Level Rise and Coastal Erosion

Sea-level rise and coastal erosion are processes that must be predicted by climatic models. The rates of sea-level rise and coastal erosion are used to determine the change of the position of the coastline. In coastal aquifers or oceanic island strip aquifers, this position is represented by the length L. This length is assumed to be L_0 at initial time and L_t at time t. Variation of the coastal position over a time period t due to climate change will then be represented by $\Delta L = L_t - L_0$ (Figure 29). For oceanic island circular aquifers, L is replaced with R. Jiao and Post (2019) and Chesnaux and others (2021) summarize the effects of sea level rise on oceanic aquifers.

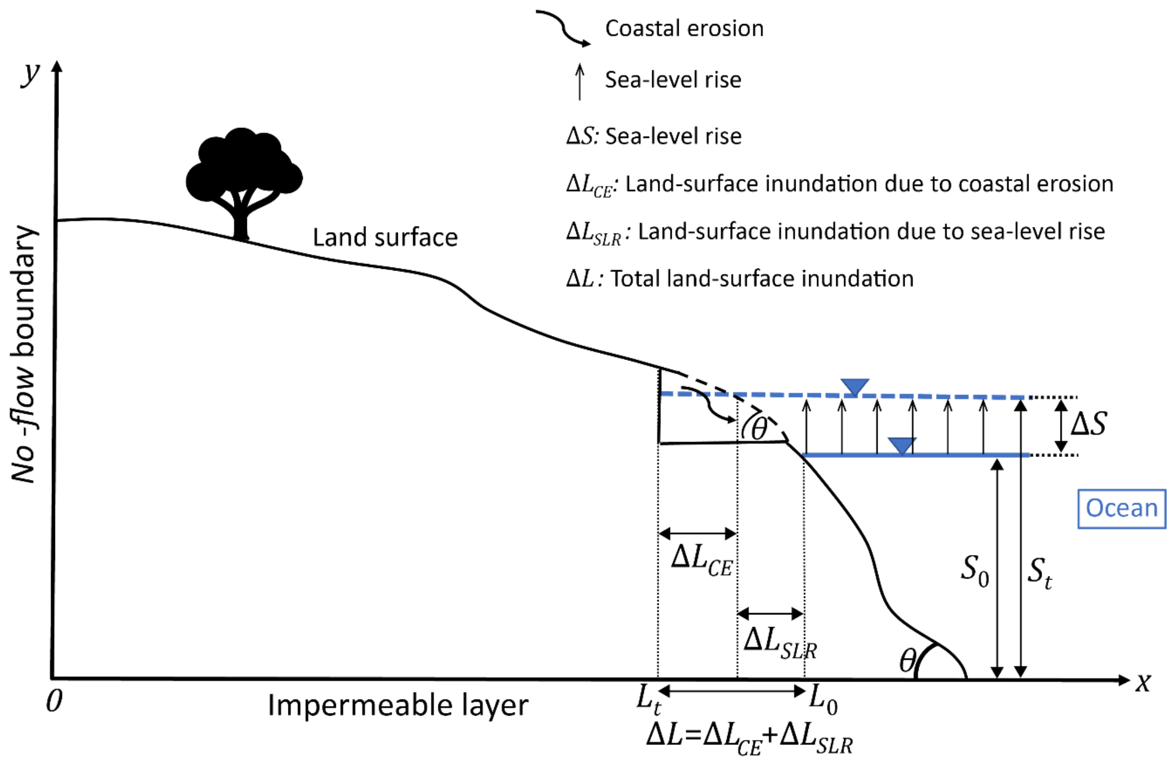

Figure 29 - Cumulative effects of sea-level rise and coastal erosion on land-surface inundation of oceanic coastal and island aquifers. The land-surface inundation is controlled by the seashore angle θ. Only the land surface, not the aquifer, is represented on this figure.

6.1.1 Sea-Level Rise

Defining S_t to be the sea level at time t and ΔS to be the change of sea level over time t, then $\Delta S = S_t - S_0$ where S_0 and S_t are initial sea level and final sea level after time t, respectively. If $\Delta S>0$, sea level has risen during t and conversely if $\Delta S<0$, sea level has dropped during t. A change of S (ΔS) over time t will cause a change of L ($\Delta L = L_t - L_0$) over time t depending on θ, the slope (angle of the shore face compared to the horizontal) of the coastal or oceanic island aquifer (Equation (111)). The sea shore angle is assumed constant over the entire width of the aquifer, however, the figures throughout Section 6 that represent conceptual models of inundation have a more realistic depiction of a land surface with varying slope, for illustration purposes.

$$\frac{\Delta S}{\Delta L} = -tan\theta \tag{111}$$

The resulting inundation of the coastline in the case of sea-level rise ΔS_{SLR} during t is $\Delta L_{SLR} = -\Delta S/tan\theta$, as ΔL_{SLR} is negative and ΔS is positive. In the special case where the seashore angle is 90 degrees—a vertical cliff—sea level rise has no effect on inland inundation.

6.1.2 Coastal Erosion

While sea-level rise is usually considered to represent the main impact of climate change on coastal aquifers, other impacts such as coastal erosion can also be expected.

Coastal erosion will diminish the length of coastal and oceanic island aquifers. The erosion rate can be defined as ΔL_{CE}. This erosion rate corresponds to the loss of coastal land (ΔL_{CE} is negative) during a given period. Usually, erosion is expressed as the length of coastal aquifer lost per year. This loss will cause the progression of seawater into the land, having comparable effects of sea-level rise. Indeed, both sea-level rise and erosion lead to land-surface inundation.

6.1.3 Total Land-Surface Inundation

The total land-surface inundation due to climate change, defined as ΔL (negative value), expresses the total loss of land due to the combination of sea-level rise (ΔL_{SLR}) and coastal erosion (ΔL_{CE}). ΔL can therefore be expressed as Equation (112).

$$\Delta L = \Delta L_{SLR} + \Delta L_{CE} = -\Delta S/tan\theta - \Delta L_{CE} \tag{112}$$

In special cases where the seashore angle is 90 degrees—as in the case of a vertical cliff—only coastal erosion contributes to inland flooding.

6.1.4 Consequences of Land-Surface Inundation on Groundwater

The total loss of coastline ΔL due to the cumulative effects of sea-level rise and coastal erosion (Figure 29) will not only cause inland inundation of saltwater but also a decrease in the total recharge to the aquifer because of the decrease in the amount of land surface capturing precipitation. The analytical closed-form solutions presented in the next sections allow for the direct calculation, in a context of sea-level rise, of the following groundwater conditions:

1) change in water table elevation of coastal aquifers;
2) change of the thickness of the fresh groundwater lens of oceanic island aquifers;
3) change of groundwater velocities, travel times and recharge in both coastal and oceanic island aquifers (strip and circular islands);
4) change of the fresh groundwater volumes in coastal aquifers;
5) change of the freshwater lens volumes in oceanic island aquifers (strip and circular islands); and
6) change of the groundwater residence time in oceanic aquifers.

The solutions for these changes are obtained from applying the previously introduced equations for calculating the groundwater conditions (which are outputs of the equations) in the above list. The new equations hold the same assumptions (Dupuit-type aquifers, steady-state conditions, and a sharp interface between freshwater and saltwater). Changes in the outputs can be calculated for different scenarios of climate change and sea-level rise that control the total land-surface inundation ΔL.

6.2 Case of Oceanic Coastal Aquifers

The closed-form analytical solutions presented in this section for oceanic coastal aquifers are based on those derived by Chesnaux (2015). The solutions presented here are more comprehensive because they also include the cumulative effects of coastal erosion and sea-level rise whereas the solutions of Chesnaux (2015) only include the effects of sea-level rise.

The solutions presented in Section 4 for groundwater conditions in both the inland zone and the seawater intrusion zone will be used in this section to develop the equations for the change of these conditions as a function of land-surface inundation caused by sea-level rise and coastal erosion.

An inclined shore renders the aquifer more susceptible to inundation and consequently to lateral seawater intrusion. The area of land surface contributing to recharge (W) diminishes, which in turn reduces groundwater replenishment by precipitation. Consequently, the total gradient decreases and seawater intrusion into the aquifer is amplified. In the following sub-sections, general closed-form analytical solutions are developed that quantify the consequences of sea-level rise on seawater intrusion by considering an inclined coast—and therefore considering inundation resulting from both sea-level rise and coastal erosion.

6.2.1 Change in Water Table Elevation

A change in water table position due to land-surface inundation will result in both a shift in elevation—assuming that if sea-level rises and/or the coastline withdraws due to shore erosion, the water table will rise—and a loss of aquifer surface area. This loss of surface area will cause a decrease in total recharge which in turn will change the length of the aquifer L and will affect the water table profile. Figure 30 presents a conceptual model for evaluating change in water table elevation with land-surface inundation in both inland and seawater intrusion zones. Importantly, the rise of the water table is due to the conditions at the boundary of the aquifer—a reduction of aquifer length and of total recharge. Such a rise is critical to anticipate eventual events of flooding of the coastal aquifer under study.

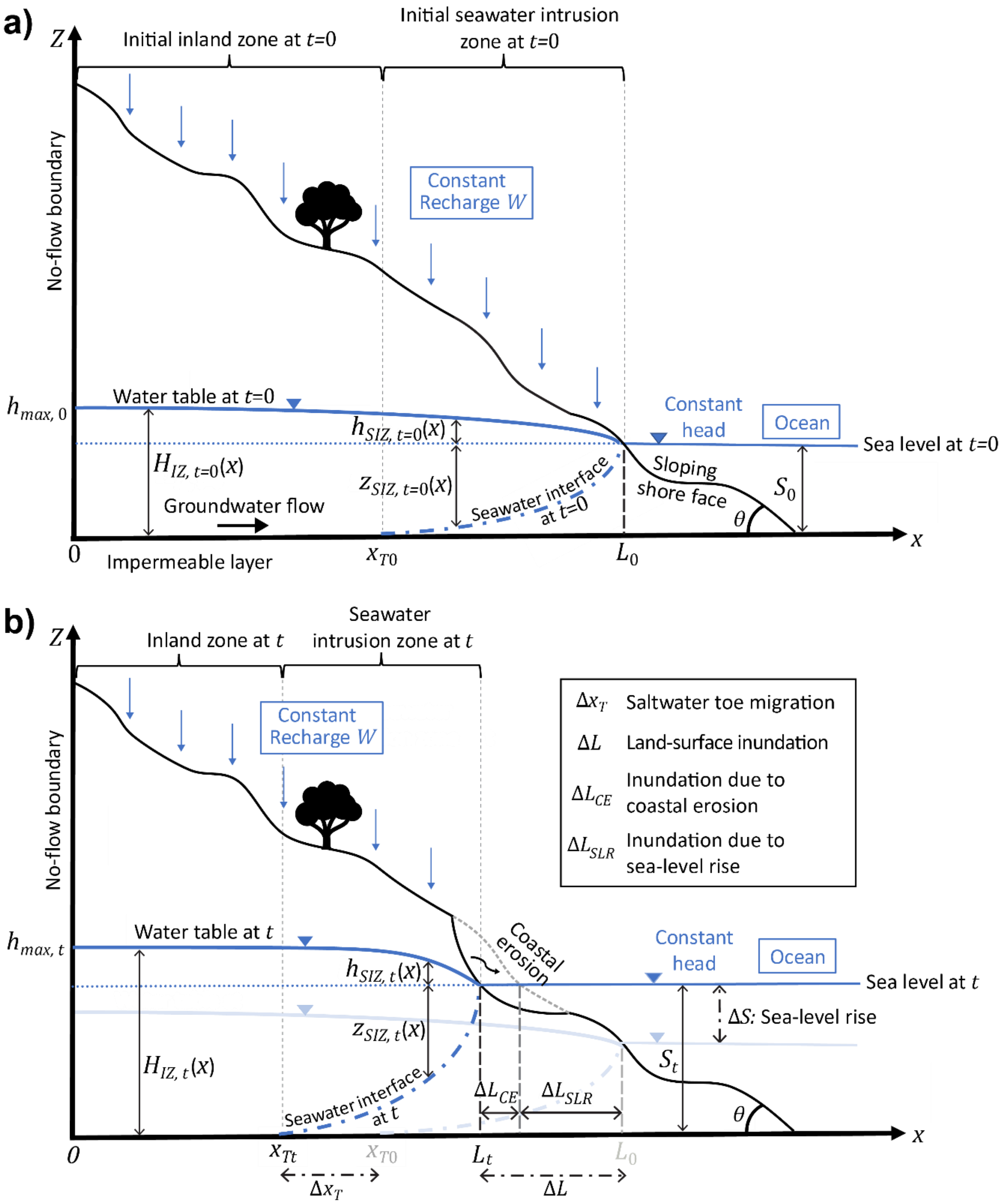

Figure 30 - Conceptual model for evaluating the cumulative effects of sea-level rise and coastal erosion on seawater intrusion in coastal aquifers. a) Conditions at initial time t=0. b) Conditions caused by sea level rise and coastal erosion that have occurred at time t, with conditions at time t=0 also shown in light blue and light gray. The change in water table position results from the combined effects of land-surface inundation and reduction of total recharge, which are controlled in part by the seashore angle, θ. The unconfined aquifer has hydraulic conductivity K.

According to Figure 30, S [L] is defined as the depth below sea level of the aquifer basement—the impermeable bottom. ΔS is the change of sea level over time t: $\Delta S = S_t - S_0$ with S_0 and S_t the initial and final sea level after time t, respectively. If $\Delta S > 0$, sea level has risen during t and conversely if $\Delta S < 0$, sea level has dropped during t. Assuming L [L] to be the length of the aquifer, at time t=0 L=L_0 and at time t L=L_t. Therefore, ΔL=L_t−L_0 is the change in length of the aquifer during t due to land-surface inundation caused by both sea-level rise and coastal erosion. For example, a change ΔS will cause a change ΔL depending on θ, the slope—or angle of the shore face compared to horizontal—and the coastal erosion of the coastal aquifer (Equation (85)).

Two different behaviors of the aquifer are observed concurrently with land-surface inundation: 1) the seawater intrusion zone where $x_T \leq x \leq L$ experiences a rise of the water table resulting from both a rise of the same amount of sea-level rise and the loss of land-surface due to erosion and inundation; and 2) the inland zone where $0 \leq x < x_T$ experiences a rise of the water table that only results from the loss of land-surface because this zone is not directly under the influence of seawater intrusion. In the next two sub-sections, solutions are developed for the water table position change for the two different parts of the coastal aquifer.

Seawater intrusion zone

Equation (113) defines $I_{SIZ}(x)$ as the change of water table elevation at t in the seawater intrusion zone where $x_T \leq x \leq L$ with $\Delta h_{SIZ}(x) = h_{SIZ,t}(x) - h_{SIZ,t=0}(x)$ as shown in Figure 30.

$$I_{SIZ}(x) = \Delta S + \Delta h_{SIZ}(x) \tag{113}$$

Replacing $h_{SIZ}(x)$ in Equation (113) with the expression given by Equation (55) yields Equation (114).

$$I_{SIZ}(x) = \Delta S + \sqrt{\frac{\Delta\rho}{\rho_s}\frac{W}{K}}\left(\sqrt{{L_t}^2 - x^2} - \sqrt{{L_0}^2 - x^2}\right) \quad \text{with } x_{Tt} \leq x \leq L_t \tag{114}$$

Replacing L_t by ΔL+L_0 in Equation (114) yields Equation (115).

$$I_{SIZ}(x) = \Delta S + \sqrt{\frac{\Delta\rho}{\rho_s}\frac{W}{K}}\left(\sqrt{(\Delta L + L_0)^2 - x^2} - \sqrt{{L_0}^2 - x^2}\right) \quad \text{with } x_{Tt} \leq x \leq L_t \tag{115}$$

Combining Equations (112) and (115) gives Equation (116).

$$I_{SIZ}(x) = \Delta S + \sqrt{\frac{\Delta\rho}{\rho_s}\frac{W}{K}}\left(\sqrt{\left(-\frac{\Delta S}{tan\theta} - \Delta L_{CE} + L_0\right)^2 - x^2} - \sqrt{{L_0}^2 - x^2}\right) \quad \text{with } x_{Tt} \leq x \leq L_t \tag{116}$$

Equation (116) is the closed-form analytical solution for the fluctuation in height of the water table at any position x in the seawater intrusion zone of the coastal aquifer when sea level rises and coastal erosion occurs (Figure 30). Knowing sea-level rise ΔS, the coastal erosion ΔL_{CE}, the slope of the shore θ, the recharge W (assumed constant) and the initial length of the aquifer L_0 (distance from the water divide), Equation (116) can calculate the new position of the water table after land-surface inundation. It can be verified that if the shoreline is vertical (θ=90°) and if there is no coastal erosion (ΔL_{CE}=0), $I_{SIZ}(x) = \Delta S$. In this case—such as a vertical rock cliff—an increase in sea-level of ΔS leads to an increase in the water table of the same amount ΔS at any position x.

Inland zone

In the inland zone, where $0 \le x \le x_T$, $I_{IZ}(x)$ is defined as the change in elevation of the water table at t (Equation (117)) with $\Delta H_{IZ}(x) = H_{IZ,t}(x) - H_{IZ,t=0}(x)$, as shown in Figure 30.

$$I_{IZ}(x) = \Delta H_{IZ}(x) \tag{117}$$

Replacing $H_{IZ}(x)$ in Equation (117) with the expression given by Equation (59) yields Equation (118).

$$I_{IZ}(x) = \sqrt{\frac{W}{K}\,(L_t^2 - x^2) + \frac{\rho_s}{\rho_f}\,S_t^2} - \sqrt{\frac{W}{K}\,(L_0^2 - x^2) + \frac{\rho_s}{\rho_f}\,S_0^2} \quad \text{with } 0 \le x \le x_{Tt} \tag{118}$$

Replacing L_t by ΔL+L_0 and S_t by ΔS+S_0 in Equation (118) yields Equation (119).

$$I_{IZ}(x) = \sqrt{\frac{W}{K}\,((\Delta L + L_0)^2 - x^2) + \frac{\rho_s}{\rho_f}\,(\Delta S + S_0)^2} - \sqrt{\frac{W}{K}\,(L_0^2 - x^2) + \frac{\rho_s}{\rho_f}\,S_0^2} \quad \text{with } 0 \le x \le x_{Tt} \tag{119}$$

Combining Equations (112) and (119) gives Equation (120):

$$\begin{aligned} I_{IZ}(x) = &\sqrt{\frac{W}{K}\left(\left(-\frac{\Delta S}{tan\theta} - \Delta L_{CE} + L_0\right)^2 - x^2\right) + \frac{\rho_s}{\rho_f}\,(\Delta S + S_0)^2} \\ &- \sqrt{\frac{W}{K}\,(L_0^2 - x^2) + \frac{\rho_s}{\rho_f}\,S_0^2} \\ &\text{with } 0 \le x \le x_{Tt} \end{aligned} \tag{120}$$

Equation (120) is the closed-form analytical solution for the fluctuation in height of the water table at any position x in the inland zone of the coastal aquifer when sea level rises and coastal erosion occurs (Figure 30).

I_{SIZ} and I_{IZ} are both positive when ΔS is positive, meaning that the water table elevation increases in both zones of the aquifer concurrently with climate change and land-surface inundation.

6.2.2 Saltwater Toe Migration

The shift of the saltwater toe position Δx_T during time t when there is land-surface inundation (Figure 30) is given by Equation (121) with x_{T0} and x_{Tt} the positions of the seawater intrusion toe at initial time (t=0) and time t, respectively.

$$\Delta x_T = x_{Tt} - x_{T0} \tag{121}$$

Replacing x_{T0} and x_{Tt} in Equation (121) with the expression given in Equation (57) yields Equation (122).

$$\Delta x_T = \sqrt{L_t^2 - \frac{\rho_s \Delta\rho}{\rho_f^2}\frac{K}{W}S_t^2} - \sqrt{L_0^2 - \frac{\rho_s \Delta\rho}{\rho_f^2}\frac{K}{W}S_0^2} \tag{122}$$

Replacing L_t by ΔL+L_0 and S_t by ΔS+S_0 in Equation (122) yields Equation (123).

$$\Delta x_T = \sqrt{(\Delta L + L_0)^2 - \frac{\rho_s \Delta\rho}{\rho_f^2}\frac{K}{W}(\Delta S + S_0)^2} - \sqrt{L_0^2 - \frac{\rho_s \Delta\rho}{\rho_f^2}\frac{K}{W}S_0^2} \tag{123}$$

Combining Equation (112) with Equation (123) yields Equation (124).

$$\Delta x_T = \sqrt{(-\frac{\Delta S}{tan\theta} - \Delta L_{CE} + L_0)^2 - \frac{\rho_s \Delta\rho}{\rho_f^2}\frac{K}{W}(\Delta S + S_0)^2} - \sqrt{L_0^2 - \frac{\rho_s \Delta\rho}{\rho_f^2}\frac{K}{W}S_0^2} \tag{124}$$

Equation (124) is the closed-form analytical solution for the change in position x_T of the seawater toe when both the sea level changes and coastal erosion occur over a period t. In other words, Equation (124) allows us to measure the scale of seawater intrusion in coastal aquifers. With land-surface inundation, Δx_T is negative according to the assumed positive direction of the x-axis (Figure 30).

6.2.3 Change in Groundwater Velocities

As mentioned earlier, land-surface inundation of the coastal aquifer resulting from sea-level rise and coastal erosion will diminish the length of the aquifer ($L_t < L_0$) and at the same time will diminish the total recharge across the aquifer. The decrease in recharge will decrease the groundwater flux within the aquifer and therefore the discharge rate of fresh groundwater to the ocean. At the same time, the water table position will also change by the values I_{SIZ} and I_{IZ} presented in Section 6.2.1. The change of groundwater velocity in the seawater intrusion zone and the inland zone will result from the combination of the changes in the discharge flux and in the water table position, both variables being interdependent.

Seawater intrusion zone

Groundwater velocities in the seawater intrusion zone are expressed by Equation (60) developed in Section 4. The change in groundwater velocity $\Delta v_{SIZ}(x)$ in the seawater intrusion zone can be calculated for position x between x_{T0} and L_t (Figure 30) and is expressed by Equation (125).

$$\Delta v_{SIZ}(x) = v_{SIZ,t}(x) - v_{SIZ,t=0}(x) = \frac{1}{n_e}\sqrt{\frac{\Delta\rho W K}{\rho_s}}\left(\frac{x}{\sqrt{L_t^2-x^2}} - \frac{x}{\sqrt{L_0^2-x^2}}\right) \tag{125}$$

with $x_{T0} \leq x \leq L_t$

Because $L_t < L_0$, $\Delta v_{SIZ}(x)$ is positive. Replacing L_t by $\Delta L + L_0$ in Equation (125) and combining with Equation (112) yields Equation (126).

$$\Delta v_{SIZ}(x) = \frac{1}{n_e}\sqrt{\frac{\Delta\rho W K}{\rho_s}}\left(\frac{x}{\sqrt{\left(-\frac{\Delta S}{tan\theta} - \Delta L_{CE} + L_0\right)^2 - x^2}} - \frac{x}{\sqrt{L_0^2 - x^2}}\right) \tag{126}$$

with $x_{T0} \leq x \leq L_t$

Equation (126) is the closed-form analytical solution for the change in groundwater velocity at any position x in the seawater intrusion zone of the coastal aquifer when sea level rises and coastal erosion occurs (Figure 30). $\Delta v_{SIZ}(x)$ is positive (because ΔS and ΔL_{CE} are positive), meaning that land-surface inundation causes an increase of groundwater velocities in the seawater intrusion zone of the coastal aquifer.

Inland zone

Groundwater velocities in the inland zone are expressed by Equation (61) developed in Section 4. The variation of groundwater velocities $\Delta v_{IZ}(x)$ in the inland zone can be calculated for a position x between 0 and x_{Tt} (Figure 30) and is expressed by Equation (127).

$$\Delta v_{IZ}(x) = v_{IZ,t}(x) - v_{IZ,t=0}(x) = \frac{W}{n_e}\left(\frac{x}{\sqrt{\frac{W}{K}\cdot(L_t^2-x^2)+\frac{\rho_s}{\rho_f}S_t^2}} - \frac{x}{\sqrt{\frac{W}{K}\cdot(L_0^2-x^2)+\frac{\rho_s}{\rho_f}S_0^2}}\right) \tag{127}$$

$$\text{with } 0 \leq x \leq x_{Tt}$$

As shown in Figure 30, $L_t < L_0$ and $S_t > S_0$. Replacing L_t by $\Delta L + L_0$ and S_t by $\Delta S + S_0$ in Equation (127) and combining with Equation (112) yields Equation (128).

$$\Delta v_{IZ}(x) = \frac{W}{n_e}\left(\frac{x}{\sqrt{\frac{W}{K}\cdot\left(\left(-\frac{\Delta S}{tan\theta}-\Delta L_{CE}+L_0\right)^2-x^2\right)+\frac{\rho_s}{\rho_f}(\Delta S+S_0)^2}}-\frac{x}{\sqrt{\frac{W}{K}\cdot(L_0^2-x^2)+\frac{\rho_s}{\rho_f}S_0^2}}\right) \quad (128)$$

$$\text{with } 0 \leq x \leq x_{Tt}$$

Equation (128) is the closed-form analytical solution for the change in groundwater velocity at any position x in the inland zone of the coastal aquifer when sea level rises and coastal erosion occurs. In the case of the inland zone, the sign of the groundwater velocity change is not obvious as it is for the seawater intrusion zone. It will depend on the values of ΔS and ΔL. Indeed, the loss of recharge due to the land-surface inundation—decrease of L—is compensated by the increase of S—sea-level rise and coastal erosion—as can be seen in Equations (127) and Equation (128).

6.2.4 Change in Groundwater Travel Times

Changes in groundwater velocity directly affect changes in groundwater travel times in the different zones of the coastal aquifer.

Seawater intrusion zone

Groundwater travel time in the seawater intrusion zone is expressed by Equation (63) developed in Section 4. The difference in groundwater travel time $\Delta t_{SIZ}(x)$ in the seawater intrusion zone between a particle of water traveling in groundwater conditions at initial time t=0 and a particle traveling in conditions at time t after land-surface inundation is expressed by Equation (129). The two particles depart from the same position x_i ($x_{T0} \leq x_i \leq L_t$) and travel to the same position x ($x_i \leq x \leq L_t$) (Figure 31).

$$\Delta t_{SIZ}(x) = t_{SIZ,t}(x) - t_{SIZ,t=0}(x) = n_e\sqrt{\frac{\rho_s}{\Delta\rho WK}}\left[\left(\sqrt{L_t^2-x^2}-\sqrt{L_t^2-x_i^2}-L_t\, ln\left(\frac{L_t+\sqrt{L_t^2-x^2}}{L_t+\sqrt{L_t^2-x_i^2}}\,\frac{x_i}{x}\right)\right)-\left(\sqrt{L_0^2-x^2}-\sqrt{L_0^2-x_i^2}-L_0\, ln\left(\frac{L_0+\sqrt{L_0^2-x^2}}{L_0+\sqrt{L_0^2-x_i^2}}\,\frac{x_i}{x}\right)\right)\right] \quad (129)$$

$$\text{with } x_{T0} \leq x_i \leq L_t \text{ and } x_i \leq x \leq L_t$$

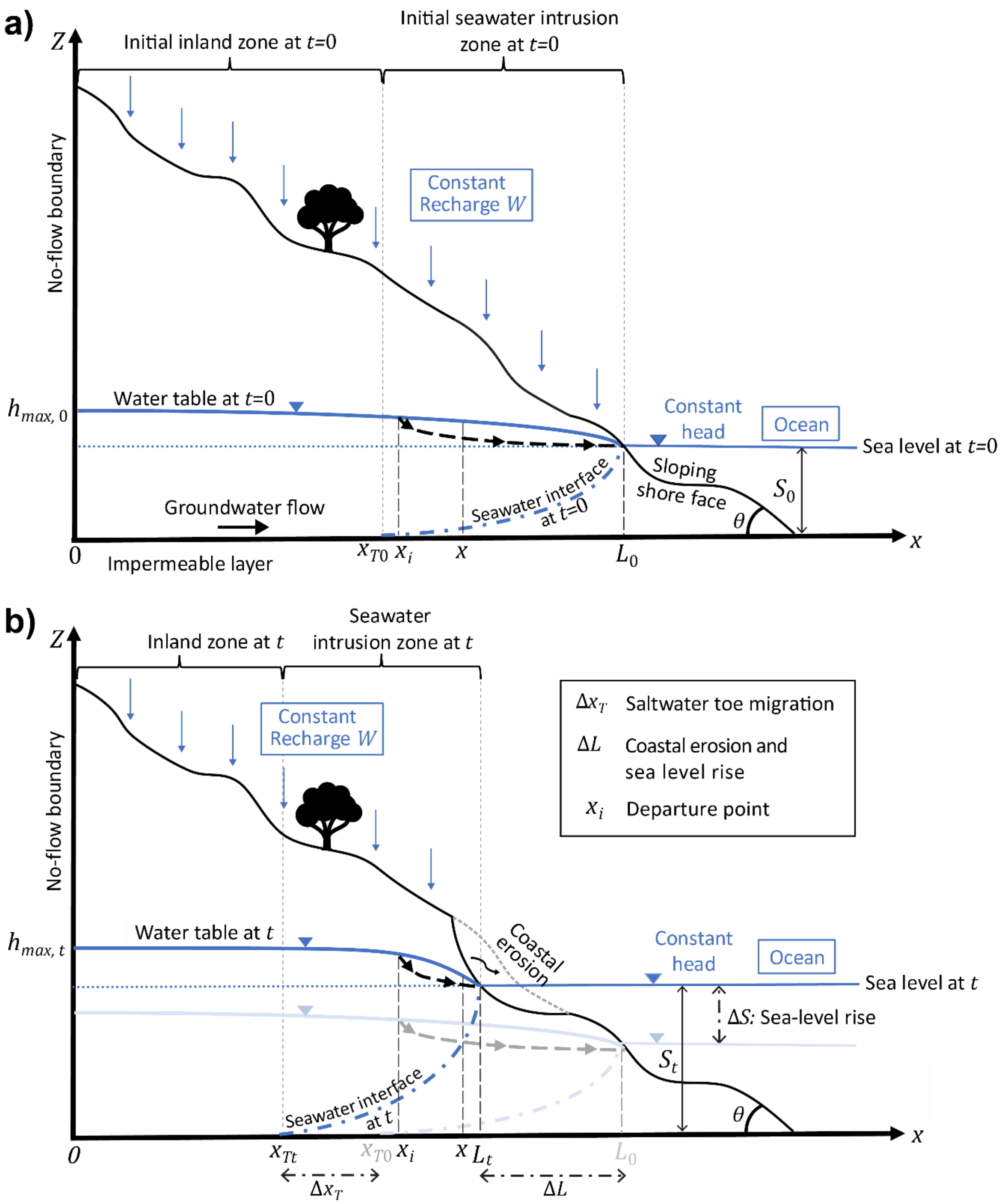

Figure 31 - Comparison of the travel paths of two groundwater particles in the seawater intrusion zone that both start at position x_i. a) The path trajectory at initial time t=0. b) The trajectory at time t after sea level rise and land-surface inundation, with the path at time t=0 also shown in light gray. The two particles travel between x_i, where $x_{T0} \leq x_i \leq L_t$, and the oceanic boundary of the aquifer, L_0 or L_t. The equation for the difference in travel times between the two particles is developed for the case of both particles traveling to the same position x, where $x_i \leq x \leq L$.

Replacing L_t by ΔL+L_0 in Equation (129) and combining with Equation (112) yields Equation (130).

$$\Delta t_{SIZ}(x) = n_e\sqrt{\frac{\rho_s}{\Delta\rho WK}}\left[\left(\sqrt{\left(L_0 - \frac{\Delta S}{tan\theta} - \Delta L_{CE}\right)^2 - x^2} - \sqrt{\left(L_0 - \frac{\Delta S}{tan\theta} - \Delta L_{CE}\right)^2 - x_i^2} - \left(L_0 - \frac{\Delta S}{tan\theta} - \Delta L_{CE}\right) ln\left(\frac{L_0 - \frac{\Delta S}{tan\theta} - \Delta L_{CE} + \sqrt{\left(L_0 - \frac{\Delta S}{tan\theta} - \Delta L_{CE}\right)^2 - x^2}}{L_0 - \frac{\Delta S}{tan\theta} - \Delta L_{CE} + \sqrt{\left(L_0 - \frac{\Delta S}{tan\theta} - \Delta L_{CE}\right)^2 - x_i^2}}\frac{x_i}{x}\right)\right) - \left(\sqrt{L_0^2 - x^2} - \sqrt{L_0^2 - x_i^2} - L_0\, ln\left(\frac{L_0 + \sqrt{L_0^2 - x^2}}{L_0 + \sqrt{L_0^2 - x_i^2}}\frac{x_i}{x}\right)\right)\right] \tag{130}$$

with $x_{T0} \leq x_i \leq L_t$ and $x_i \leq x \leq L_t$

Equation (130) is the closed-form analytical solution for the change in groundwater travel time with land-surface inundation in the seawater intrusion zone of the coastal aquifer. $\Delta t_{SIZ}(x)$ is negative according to Equations (129) and (130), which agrees with $\Delta v_{SIZ}(x)$ being positive, as previously determined. In other words, groundwater travel times decrease with climate change and land-surface inundation in the seawater intrusion zone of the coastal aquifer. This implies shorter travel times of potential contaminants, potentially exposing the seawater intrusion zone to reduced contaminant decay over time.

Inland zone

Groundwater travel time in the inland zone is expressed by Equation (64) developed in Section 4. The difference in groundwater travel time $\Delta t_{IZ}(x)$ in the inland zone between a particle of water traveling in groundwater conditions at initial time t=0 and a particle traveling in conditions at time t after land-surface inundation is expressed by Equation (131). The two particles of water depart from the same position x_i $(0 < x_i \leq x_{Tt})$ and travel to the same position x $(x_i \leq x \leq x_{Tt})$ (Figure 32).

$$\Delta t_{IZ}(x) = t_{IZ,t}(x) - t_{IZ,t=0}(x) = n_e\sqrt{\frac{1}{WK}}\left[\left(\sqrt{L_t^2+\left(\frac{K}{W}\,\frac{\rho_s}{\rho_f}\,S_t^2\right)-x^2} - \sqrt{L_t^2+\left(\frac{K}{W}\,\frac{\rho_s}{\rho_f}\,S_t^2\right)-x_i^2} - \sqrt{\left(L_t^2+\left(\frac{K}{W}\,\frac{\rho_s}{\rho_f}\,S_t^2\right)\right)}\;ln\left(\frac{\sqrt{L_t^2+\left(\frac{K}{W}\frac{\rho_s}{\rho_f}\cdot S_t^2\right)}+\sqrt{L_t^2+\left(\frac{K}{W}\frac{\rho_s}{\rho_f}S_t^2\right)-x^2}}{\sqrt{L_t^2+\left(\frac{K}{W}\frac{\rho_s}{\rho_f}S_t^2\right)}+\sqrt{L_t^2+\left(\frac{K}{W}\frac{\rho_s}{\rho_f}S_t^2\right)-x_i^2}}\,\frac{x_i}{x}\right)\right) - \left(\sqrt{L_0^2+\left(\frac{K}{W}\,\frac{\rho_s}{\rho_f}\,S_0^2\right)-x^2} - \sqrt{L_0^2+\left(\frac{K}{W}\,\frac{\rho_s}{\rho_f}\,S_0^2\right)-x_i^2} - \sqrt{\left(L_0^2+\left(\frac{K}{W}\,\frac{\rho_s}{\rho_f}\,S_0^2\right)\right)}\;ln\left(\frac{\sqrt{L_0^2+\left(\frac{K}{W}\frac{\rho_s}{\rho_f}S_0^2\right)}+\sqrt{L_0^2+\left(\frac{K}{W}\frac{\rho_s}{\rho_f}S_0^2\right)-x^2}}{\sqrt{L_0^2+\left(\frac{K}{W}\frac{\rho_s}{\rho_f}S_0^2\right)}+\sqrt{L_0^2+\left(\frac{K}{W}\frac{\rho_s}{\rho_f}S_0^2\right)-x_i^2}}\,\frac{x_i}{x}\right)\right)\right] \qquad (131)$$

with $0 < x_i \leq x_{Tt}$ and $x_i \leq x \leq x_{Tt}$

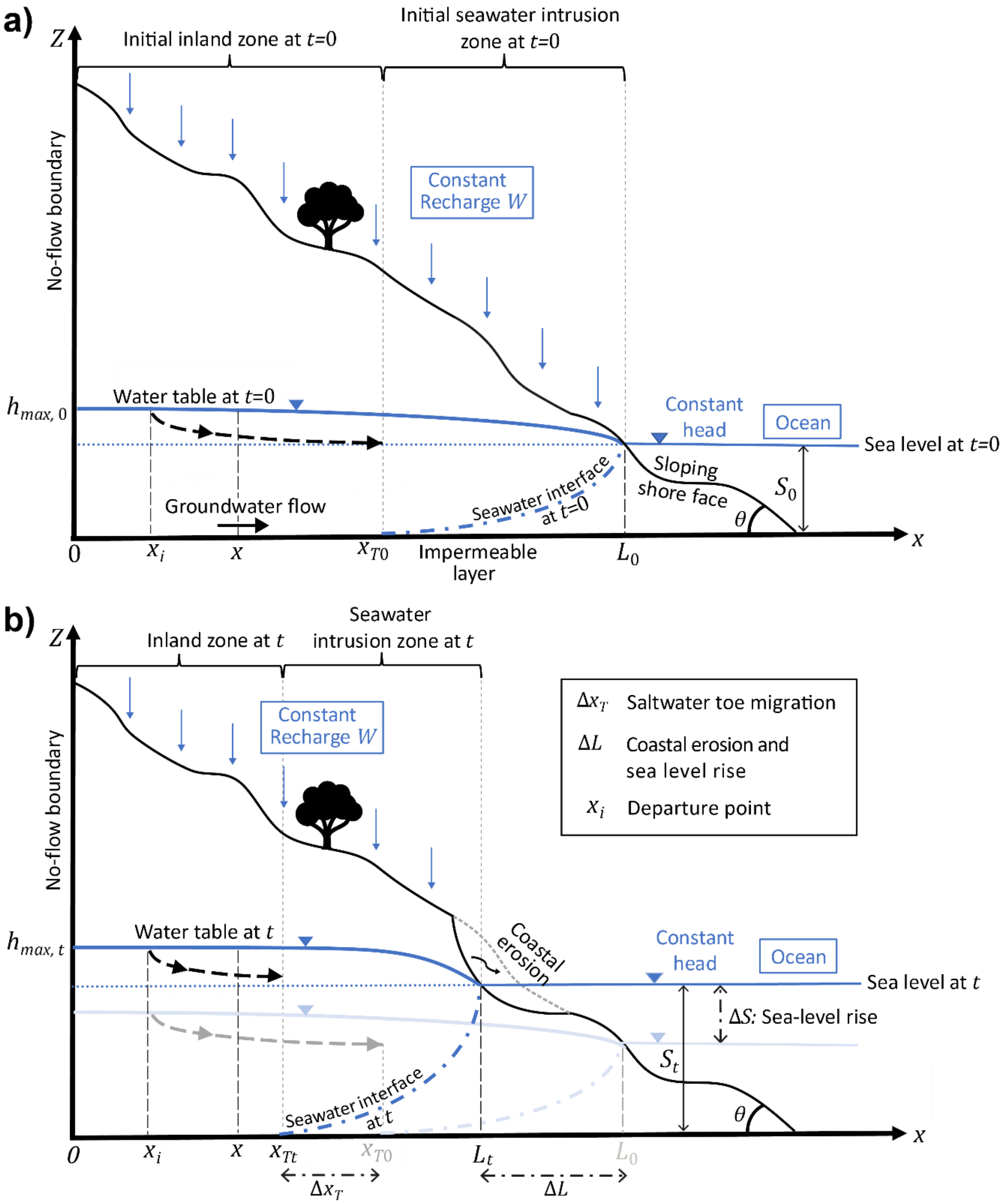

Figure 32 - Comparison of the travel paths of two groundwater particles in the inland zone, one at initial time t=0 and the other at time *t* after land-surface inundation. The two particles have the same starting position x_i ($0 < x_i \leq x_{Tt}$) and travel to the saltwater toe (x_{Tt} or x_{T0}) at their respective times. The equation for the difference in travel times between the two particles is developed for the case of both particles traveling to the same position *x*, where $x_i \leq x \leq x_{Tt}$.

Replacing L_t by ΔL+L_0 and S_t by ΔS+S_0 in Equation (131) and combining with Equation (112) yields Equation (132).

$$\Delta t_{IZ}(x) =$$

$$n_e\sqrt{\frac{1}{WK}}\left[\left(\sqrt{\left(L_0-\frac{\Delta S}{tan\theta}-\Delta L_{CE}\right)^2+\left(\frac{K}{W}\frac{\rho_s}{\rho_f}\,(\Delta S+S_0)^2\right)-x^2}-\sqrt{\left(L_0-\frac{\Delta S}{tan\theta}-\Delta L_{CE}\right)^2+\left(\frac{K}{W}\frac{\rho_s}{\rho_f}\,(\Delta S+S_0)^2\right)-x_i^2}\right.\right.$$
$$\left.-\sqrt{\left(\left(L_0-\frac{\Delta S}{tan\theta}-\Delta L_{CE}\right)^2+\left(\frac{K}{W}\frac{\rho_s}{\rho_f}\,(\Delta S+S_0)^2\right)\right)}\,ln\left(\frac{\sqrt{\left(L_0-\frac{\Delta S}{tan\theta}-\Delta L_{CE}\right)^2+\left(\frac{K}{W}\frac{\rho_s}{\rho_f}\,S_t^2\right)}+\sqrt{\left(L_0-\frac{\Delta S}{tan\theta}-\Delta L_{CE}\right)^2+\left(\frac{K}{W}\frac{\rho_s}{\rho_f}S_t^2\right)-x^2}}{\sqrt{\left(L_0-\frac{\Delta S}{tan\theta}-\Delta L_{CE}\right)^2+\left(\frac{K}{W}\frac{\rho_s}{\rho_f}\,S_t^2\right)}+\sqrt{\left(L_0-\frac{\Delta S}{tan\theta}-\Delta L_{CE}\right)^2+\left(\frac{K}{W}\frac{\rho_s}{\rho_f}\,S_t^2\right)-x_i^2}}\,\frac{x_i}{x}\right)\right) \tag{132}$$
$$\left.-\left(\sqrt{L_0^2+\left(\frac{K}{W}\frac{\rho_s}{\rho_f}\,S_0^2\right)-x^2}-\sqrt{L_0^2+\left(\frac{K}{W}\frac{\rho_s}{\rho_f}\,S_0^2\right)-x_i^2}-\sqrt{L_0^2+\left(\frac{K}{W}\frac{\rho_s}{\rho_f}\,S_0^2\right)}\,ln\left(\frac{\sqrt{L_0^2+\left(\frac{K}{W}\frac{\rho_s}{\rho_f}\,S_0^2\right)}+\sqrt{L_0^2+\left(\frac{K}{W}\frac{\rho_s}{\rho_f}\,S_0^2\right)-x^2}}{\sqrt{L_0^2+\left(\frac{K}{W}\frac{\rho_s}{\rho_f}\,S_0^2\right)}+\sqrt{L_0^2+\left(\frac{K}{W}\frac{\rho_s}{\rho_f}\,S_0^2\right)-x_i^2}}\,\frac{x_i}{x}\right)\right)\right]$$

with $0 < x_i \leq x_{Tt}$ and $x_i \leq x \leq x_{Tt}$

Equation (132) is the closed-form analytical solution for the change in groundwater travel time with land-surface inundation in the inland zone of the coastal aquifer. As mentioned earlier with the change in groundwater velocities, the sign of this change will depend on the values of ΔL and ΔS, which have opposing effects on the velocities and travel times in this zone.

Change of groundwater travel time for a water particle circulating both in the inland and seawater intrusion zones

Groundwater travel time in the coastal aquifer for a particle of water circulating in both the inland zone and the seawater intrusion zone is expressed by Equation (66) developed in Section 4. The groundwater particle travels first from x_i to x_T in the inland zone and then from x_T to x in the seawater intrusion zone. The difference in groundwater travel time $\Delta t_{CA}(x)$ in the coastal aquifer (both zones) between a particle of water traveling in groundwater conditions at initial time t=0 and a particle traveling in conditions at time t after land-surface inundation is expressed by Equation (133). The two particles of water depart from the same position x_i ($0 < x_i \leq x_{Tt}$) and travel to the same position x ($x_{Tt} \leq x \leq L_t$) (Figure 33).

$$\Delta t_{CA}(x) = t_{CA,t}(x) - t_{CA,t=0}(x) =$$

$$n_e\sqrt{\frac{1}{WK}}\left[S_t\frac{\rho_s}{\rho_f}\sqrt{\frac{W}{K}} - \sqrt{L_t^2+\left(\frac{K}{W}\frac{\rho_s}{\rho_f}S_t^2\right)-x_i^2} - \sqrt{L_t^2+\left(\frac{K}{W}\frac{\rho_s}{\rho_f}S_t^2\right)}\,ln\left(\frac{\sqrt{L_t^2+\left(\frac{K}{W}\frac{\rho_s}{\rho_f}S_t^2\right)}+S_t\frac{\rho_s}{\rho_f}\sqrt{\frac{W}{K}}}{\sqrt{L_t^2+\left(\frac{K}{W}\frac{\rho_s}{\rho_f}S_t^2\right)}+\sqrt{L_t^2+\left(\frac{K}{W}\frac{\rho_s}{\rho_f}S_t^2\right)-x_i^2}}\,\frac{x_i}{\sqrt{L_t^2-\frac{\rho_s\Delta\rho}{\rho_f^2}\frac{K}{W}S_t^2}}\right)\right]$$

$$+n_e\sqrt{\frac{\rho_s}{\Delta\rho WK}}\left[\sqrt{L_t^2-x^2} - S_t\sqrt{\frac{\rho_s\Delta\rho}{\rho_f^2}\frac{K}{W}} - L_t^2\,ln\left(\frac{L_t+\sqrt{L_t^2-x^2}}{L_t+S_t\sqrt{\frac{\rho_s\Delta\rho}{\rho_f^2}\frac{K}{W}}}\,\frac{\sqrt{L_t^2-\frac{\rho_s\Delta\rho}{\rho_f^2}\frac{K}{W}S_t^2}}{x}\right)\right]$$

$$-n_e\sqrt{\frac{1}{WK}}\left[S_0\frac{\rho_s}{\rho_f}\sqrt{\frac{W}{K}} - \sqrt{L_0^2+\left(\frac{K}{W}\frac{\rho_s}{\rho_f}S_0^2\right)-x_i^2} - \sqrt{L_0^2+\left(\frac{K}{W}\frac{\rho_s}{\rho_f}S_0^2\right)}\,ln\left(\frac{\sqrt{L_0^2+\left(\frac{K}{W}\frac{\rho_s}{\rho_f}S_0^2\right)}+S_0\frac{\rho_s}{\rho_f}\sqrt{\frac{W}{K}}}{\sqrt{L_0^2+\left(\frac{K}{W}\frac{\rho_s}{\rho_f}S_0^2\right)}+\sqrt{L_0^2+\left(\frac{K}{W}\frac{\rho_s}{\rho_f}S_0^2\right)-x_i^2}}\,\frac{x_i}{\sqrt{L_0^2-\frac{\rho_s\Delta\rho}{\rho_f^2}\frac{K}{W}S_0^2}}\right)\right] \quad (133)$$

$$-n_e\sqrt{\frac{\rho_s}{\Delta\rho WK}}\left[\sqrt{L_0^2-x^2} - S_0\sqrt{\frac{\rho_s\Delta\rho}{\rho_f^2}\frac{K}{W}} - L_0^2\,ln\left(\frac{L_0+\sqrt{L_0^2-x^2}}{L_0+S_0\sqrt{\frac{\rho_s\Delta\rho}{\rho_f^2}\frac{K}{W}}}\,\frac{\sqrt{L_0^2-\frac{\rho_s\Delta\rho}{\rho_f^2}\frac{K}{W}S_0^2}}{x}\right)\right]$$

with $0 < x_i \leq x_{Tt}$ and $x_{Tt} < x \leq L_t$

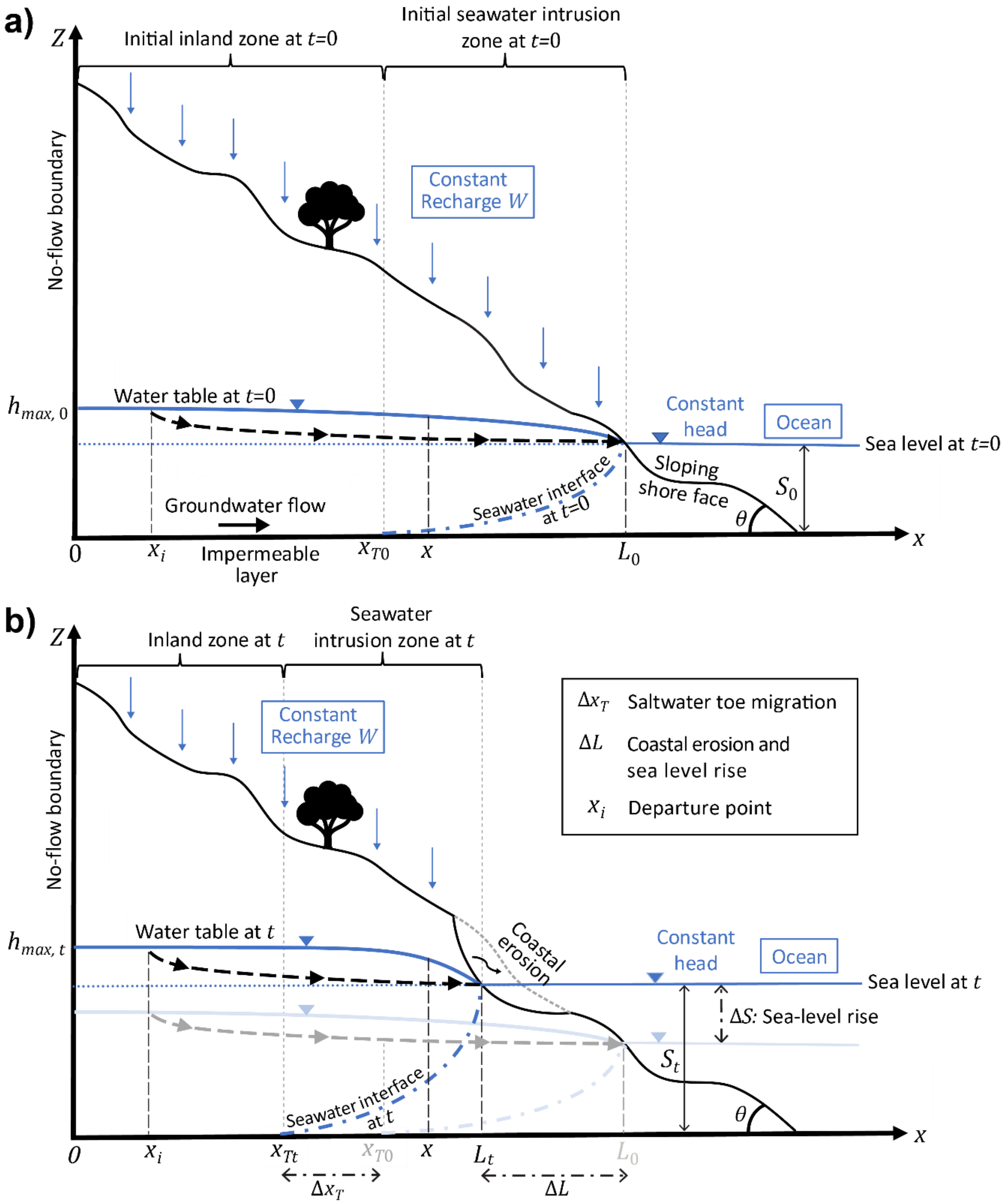

Figure 33 - Comparison of the paths of two groundwater particles that start at position x_i and travel within both the inland zone and the seawater intrusion zone. a) The path trajectory at initial time t=0. b) The trajectory at time t after sea level rise and land-surface inundation, with the path at time t=0 also shown in light gray. The two particles travel from position x_i, where $0 < x_i \leq x_{Tt}$, to the oceanic boundary of the aquifer (L_0 or L_t) that exists at their respective times. The equation for the difference in travel times between the two particles is developed for the case of both particles traveling to the same position x, where $x_{Tt} \leq x \leq L_t$.

Replacing L_t by ΔL+L_0 and S_t by ΔS+S_0 in Equation (133) and combining with Equation (112) yields Equation (134).

$$
\begin{aligned}
&\Delta t_{CA}(x) = \\
&n_e\sqrt{\frac{1}{WK}}\left[(\Delta S+S_0)\,\frac{\rho_s}{\rho_f}\sqrt{\frac{W}{K}}-\sqrt{\left(L_0-\frac{\Delta S}{tan\theta}-\Delta L_{CE}\right)^2+\left(\frac{K}{W}\,\frac{\rho_s}{\rho_f}\,(\Delta S+S_0)^2\right)-x_i^2}-\sqrt{\left(\left(L_0-\frac{\Delta S}{tan\theta}-\Delta L_{CE}\right)^2+\left(\frac{K}{W}\,\frac{\rho_s}{\rho_f}\,(\Delta S+S_0)^2\right)\right)}\right.\\
&\left.ln\left(\frac{\sqrt{\left(L_0-\frac{\Delta S}{tan\theta}-\Delta L_{CE}\right)^2+\left(\frac{K}{W}\,\frac{\rho_s}{\rho_f}\,(\Delta S+S_0)^2\right)}+(\Delta S+S_0)\,\frac{\rho_s}{\rho_f}\sqrt{\frac{W}{K}}}{\sqrt{\left(L_0-\frac{\Delta S}{tan\theta}-\Delta L_{CE}\right)^2+\left(\frac{K}{W}\,\frac{\rho_s}{\rho_f}\,(\Delta S+S_0)^2\right)}+\sqrt{\left(L_0-\frac{\Delta S}{tan\theta}-\Delta L_{CE}\right)^2+\left(\frac{K}{W}\,\frac{\rho_s}{\rho_f}\,(\Delta S+S_0)^2\right)-x_i^2}}\;\frac{x_i}{\sqrt{\left(L_0-\frac{\Delta S}{tan\theta}-\Delta L_{CE}\right)^2-\frac{\rho_s\Delta\rho}{\rho_f^2}\,\frac{K}{W}\,(\Delta S+S_0)^2}}\right)\right]\\
&+n_e\sqrt{\frac{\rho_s}{\Delta\rho WK}}\left[\sqrt{\left(L_0-\frac{\Delta S}{tan\theta}-\Delta L_{CE}\right)^2-x^2}-(\Delta S+S_0)\sqrt{\frac{\rho_s\Delta\rho}{\rho_f^2}\,\frac{K}{W}}\right.\\
&\left.-\left(L_0-\frac{\Delta S}{tan\theta}-\Delta L_{CE}\right)^2 ln\left(\frac{L_0-\frac{\Delta S}{tan\theta}-\Delta L_{CE}+\sqrt{\left(L_0-\frac{\Delta S}{tan\theta}-\Delta L_{CE}\right)^2-x^2}}{L_0-\frac{\Delta S}{tan\theta}-\Delta L_{CE}+(\Delta S+S_0)\sqrt{\frac{\rho_s\Delta\rho}{\rho_f^2}\,\frac{K}{W}}}\;\frac{\sqrt{\left(L_0-\frac{\Delta S}{tan\theta}-\Delta L_{CE}\right)^2-\frac{\rho_s\Delta\rho}{\rho_f^2}\,\frac{K}{W}\,(\Delta S+S_0)^2}}{x}\right)\right]\\
&-n_e\sqrt{\frac{1}{WK}}\left[S_0\,\frac{\rho_s}{\rho_f}\sqrt{\frac{W}{K}}-\sqrt{L_0^2+\left(\frac{K}{W}\,\frac{\rho_s}{\rho_f}\,S_0^2\right)-x_i^2}-\sqrt{\left(L_0^2+\left(\frac{K}{W}\,\frac{\rho_s}{\rho_f}\,S_0^2\right)\right)}\,ln\left(\frac{\sqrt{L_0^2+\left(\frac{K}{W}\,\frac{\rho_s}{\rho_f}\,S_0^2\right)}+S_0\,\frac{\rho_s}{\rho_f}\sqrt{\frac{W}{K}}}{\sqrt{L_0^2+\left(\frac{K}{W}\,\frac{\rho_s}{\rho_f}\,S_0^2\right)}+\sqrt{L_0^2+\left(\frac{K}{W}\,\frac{\rho_s}{\rho_f}\,S_0^2\right)-x_i^2}}\;\frac{x_i}{\sqrt{L_0^2-\frac{\rho_s\Delta\rho}{\rho_f^2}\,\frac{K}{W}\,S_0^2}}\right)\right]\\
&-n_e\sqrt{\frac{\rho_s}{\Delta\rho WK}}\left[\sqrt{L_0^2-x^2}-S_0\sqrt{\frac{\rho_s\Delta\rho}{\rho_f^2}\,\frac{K}{W}}-L_0^2\,ln\left(\frac{L_0+\sqrt{L_0^2-x^2}}{L_0+S_0\sqrt{\frac{\rho_s\Delta\rho}{\rho_f^2}\,\frac{K}{W}}}\;\frac{\sqrt{L_0^2-\frac{\rho_s\Delta\rho}{\rho_f^2}\,\frac{K}{W}\,S_0^2}}{x}\right)\right]
\end{aligned}
\tag{134}
$$

with $0 < x_i \leq x_{Tt}$ and $x_{Tt} < x \leq L_t$

Equation (134) is the closed-form analytical solution for the change in groundwater travel time with land-surface inundation in the coastal aquifer for a particle of water traveling both in the inland zone and the seawater intrusion zone. The increase or decrease of the groundwater travel times for particles of water circulating both in the inland and seawater intrusion zones will depend on the values of travel times in the inland zone and the seawater intrusion zone. As discussed previously, an increase in sea-level rise will cause travel time to decrease in the seawater intrusion zone, but in the inland zone the increase in water table elevation due to an increase in S is compensated by the decrease of the total aquifer recharge caused by the decrease of L with land-surface inundation.

6.2.5 Change in the Total Groundwater Volumes of the Aquifer

The changes in the fresh groundwater volumes of the inland zone, the seawater intrusion zone and of the entire coastal aquifer are critical because they will affect the availability of the resource and the future possible developments in coastal environments.

Seawater intrusion zone

The fresh groundwater volume contained in the seawater intrusion zone of the coastal aquifer V_{SIZ} is expressed by Equation (70) developed in Section 4. The difference of groundwater volume ΔV_{SIZ} in the seawater intrusion zone after land-surface inundation (Figure 34) is expressed by Equation (135).

$$\Delta V_{SIZ} = V_{SIZ,t}(x) - V_{SIZ,t=0}(x) = \frac{n_e}{2}\sqrt{\frac{\rho_s}{\Delta\rho}\frac{W}{K}}\ \left[\left(L_t^2\left(\frac{\pi}{2} - sin^{-1}\left(\frac{x_{Tt}}{L_t}\right)\right) - x_{Tt}\sqrt{L_t^2 - {x_{Tt}}^2}\right) - \left(L_0^2\left(\frac{\pi}{2} - sin^{-1}\left(\frac{x_{T0}}{L_0}\right)\right) - x_{T0}\sqrt{L_0^2 - {x_{T0}}^2}\right)\right] \tag{135}$$

with $x_{Tt} = \sqrt{L_t^2 - \frac{\rho_s \Delta\rho}{\rho_f^2}\frac{K}{W}S_t^2}$ and $x_{T0} = \sqrt{L_0^2 - \frac{\rho_s \Delta\rho}{\rho_f^2}\frac{K}{W}S_0^2}$

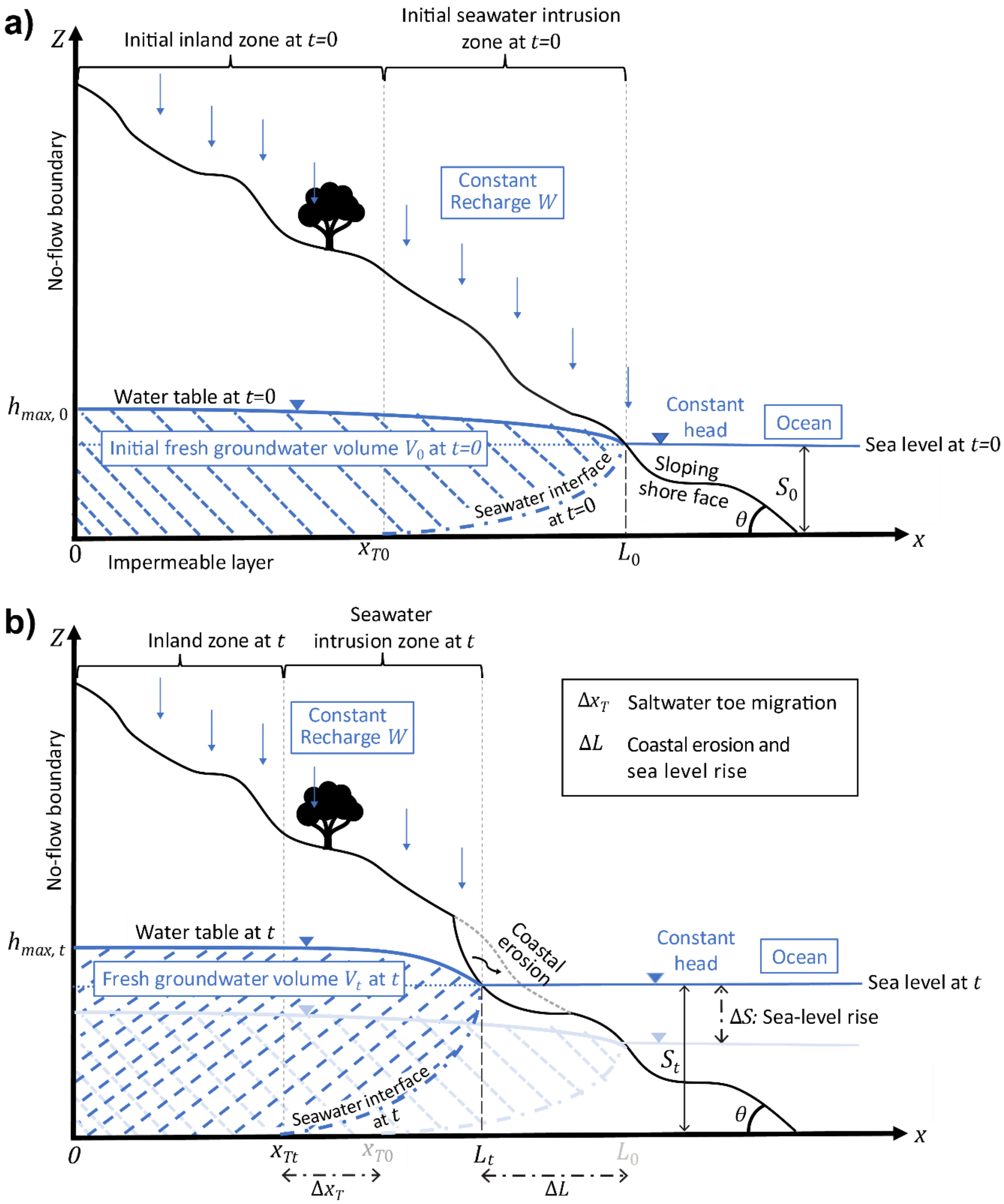

Figure 34 - Visualizing the change in groundwater volumes caused by land-surface inundation in an oceanic coastal aquifer. a) Freshwater volume V_0 at time t=0. b) Freshwater volume V_t, at time t, with volume V_0 also shown in light blue.

Replacing L_t by ΔL+L_0 and S_t by ΔS+S_0 in Equation (135) and combining with Equation (112) yields Equation (136).

$$\Delta V_{SIZ} = \frac{n_e}{2}\sqrt{\frac{\rho_s}{\Delta\rho}\frac{W}{K}}\left[\left(\left(L_0 - \frac{\Delta S}{tan\theta} - \Delta L_{CE}\right)^2\left(\frac{\pi}{2} - sin^{-1}\left(\frac{x_{Tt}}{L_0 - \frac{\Delta S}{tan\theta} - \Delta L_{CE}}\right)\right) - x_{Tt}\sqrt{\left(L_0 - \frac{\Delta S}{tan\theta} - \Delta L_{CE}\right)^2 - {x_{Tt}}^2}\right) - \left(L_0^2\left(\frac{\pi}{2} - sin^{-1}\left(\frac{x_{T0}}{L_0}\right)\right) - x_{T0}\sqrt{L_0^2 - {x_{T0}}^2}\right)\right] \quad (136)$$

$$\text{with } x_{Tt} = \sqrt{\left(L_0 - \frac{\Delta S}{tan\theta} - \Delta L_{CE}\right)^2 - \frac{\rho_s\Delta\rho}{\rho_f^2}\frac{K}{W}(\Delta S + S_0)^2} \quad and \; x_{T0} = \sqrt{L_0^2 - \frac{\rho_s\Delta\rho}{\rho_f^2}\frac{K}{W}S_0^2}$$

Equation (136) is the closed-form analytical solution that calculates the change in fresh groundwater volume with land-surface inundation in the seawater intrusion zone of the coastal aquifer.

Inland zone

The fresh groundwater volume contained in the inland zone of the coastal aquifer V_{IZ} is expressed by Equation (75) developed in Section 4. The difference of groundwater volume ΔV_{IZ} in the inland zone after land-surface inundation (Figure 34) is expressed by Equation (137).

$$\Delta V_{IZ} = V_{IZ,t}(z) - V_{IZ,t=0}(x) = \frac{n_e}{2}\sqrt{\frac{W}{K}}\left[\left(\begin{array}{c} x_{Tt}\sqrt{L_t^2 + \left(\frac{K}{W}\frac{\rho_s}{\rho_f}S_t^2\right) - {x_{Tt}}^2} + \\ \left(L_t^2 + \left(\frac{K}{W}\frac{\rho_s}{\rho_f}S_t^2\right)\right)sin^{-1}\left(\frac{x_{Tt}}{\sqrt{L_t^2 + \left(\frac{K}{W}\frac{\rho_s}{\rho_f}S_t^2\right)}}\right)\end{array}\right) - \left(\begin{array}{c} x_{T0}\sqrt{L_0^2 + \left(\frac{K}{W}\frac{\rho_s}{\rho_f}S_0^2\right) - {x_{T0}}^2} + \\ \left(L_0^2 + \left(\frac{K}{W}\frac{\rho_s}{\rho_f}S_0^2\right)\right)sin^{-1}\left(\frac{x_{T0}}{\sqrt{L_0^2 + \left(\frac{K}{W}\frac{\rho_s}{\rho_f}S_0^2\right)}}\right)\end{array}\right)\right] \quad (137)$$

$$\text{with } x_{Tt} = \sqrt{L_t^2 - \frac{\rho_s\Delta\rho}{\rho_f^2}\frac{K}{W}S_t^2} \text{ and } x_{T0} = \sqrt{L_0^2 - \frac{\rho_s\Delta\rho}{\rho_f^2}\frac{K}{W}S_0^2}$$

Replacing L_t by ΔL+L_0 in Equation (137) and combining with Equation (112) yields Equation (138).

$$\Delta V_{IZ} = \frac{n_e}{2}\sqrt{\frac{W}{K}}$$

$$\left[\left(x_{Tt}\sqrt{\left(L_0 - \frac{\Delta S}{tan\theta} - \Delta L_{CE}\right)^2 + \frac{K}{W}\frac{\rho_s}{\rho_f}(\Delta S + S_0)^2 - x_{Tt}^{\;2}} + \left(\left(L_0 - \frac{\Delta S}{tan\theta} - \Delta L_{CE}\right)^2 + \frac{K}{W}\frac{\rho_s}{\rho_f}(\Delta S + S_0)^2\right) sin^{-1}\left(\frac{x_{Tt}}{\sqrt{\left(L_0 - \frac{\Delta S}{tan\theta} - \Delta L_{CE}\right)^2 + \left(\frac{K}{W}\frac{\rho_s}{\rho_f}S_0^2\right)}}\right)\right)\right. \tag{138}$$

$$\left. - \left(x_{T0}\sqrt{L_0^2 + \left(\frac{K}{W}\frac{\rho_s}{\rho_f}S_0^2\right) - x_{T0}^{\;2}} + \left(L_0^2 + \left(\frac{K}{W}\frac{\rho_s}{\rho_f}S_0^2\right)\right) sin^{-1}\left(\frac{x_{T0}}{\sqrt{L_0^2 + \left(\frac{K}{W}\frac{\rho_s}{\rho_f}S_0^2\right)}}\right)\right)\right]$$

with $x_{Tt} = \sqrt{\left(L_0 - \frac{\Delta S}{tan\theta} - \Delta L_{CE}\right)^2 - \frac{\rho_s \Delta\rho}{\rho_f^2}\frac{K}{W}(\Delta S + S_0)^2}$ and $x_{T0} = \sqrt{L_0^2 - \frac{\rho_s \Delta\rho}{\rho_f^2}\frac{K}{W}S_0^2}$

Equation (138) is the closed-form analytical solution for the change in fresh groundwater volume with land-surface inundation in the inland zone of the coastal aquifer.

Total volume (seawater intrusion zone + inland zone)

The total fresh groundwater volume V_{CA} contained in the coastal aquifer is expressed by Equation (77) developed in Section 4. The difference of groundwater volume ΔV_{CA} in the seawater intrusion zone after land-surface inundation (Figure 34) is expressed by Equation (139) obtained by combining Equations (135) and (137).

$$\Delta V_{CA} = V_{CA,t}(x) - V_{CA,t=0}(x) = \Delta V_{SIZ} + \Delta V_{IZ} =$$

$$\frac{n_e}{2}\sqrt{\frac{\rho_s}{\Delta\rho}\frac{W}{K}}\left[\left(L_t^2\left(\frac{\pi}{2} - sin^{-1}\left(\frac{x_{Tt}}{L_t}\right)\right) - x_{Tt}\sqrt{L_t^2 - {x_{Tt}}^2}\right) - \left(L_0^2\left(\frac{\pi}{2} - sin^{-1}\left(\frac{x_{T0}}{L_0}\right)\right) - x_{T0}\sqrt{L_0^2 - {x_{T0}}^2}\right)\right] +$$

$$\frac{n_e}{2}\sqrt{\frac{W}{K}}\left[\left(x_{Tt}\sqrt{L_t^2 + \left(\frac{K}{W}\frac{\rho_s}{\rho_f}S_t^2\right) - {x_{Tt}}^2} + \left(L_t^2 + \left(\frac{K}{W}\frac{\rho_s}{\rho_f}S_t^2\right)\right) sin^{-1}\left(\frac{x_{Tt}}{\sqrt{L_t^2 + \left(\frac{K}{W}\frac{\rho_s}{\rho_f}S_t^2\right)}}\right)\right) - \left(x_{T0}\sqrt{L_0^2 + \left(\frac{K}{W}\frac{\rho_s}{\rho_f}S_0^2\right) - {x_{T0}}^2} + \left(L_0^2 + \left(\frac{K}{W}\frac{\rho_s}{\rho_f}S_0^2\right)\right) sin^{-1}\left(\frac{x_{T0}}{\sqrt{L_0^2 + \left(\frac{K}{W}\frac{\rho_s}{\rho_f}S_0^2\right)}}\right)\right)\right] \tag{139}$$

$$\text{with } x_{Tt} = \sqrt{L_t^2 - \frac{\rho_s\Delta\rho}{\rho_f^2}\frac{K}{W}S_t^2} \text{ and } x_{T0} = \sqrt{L_0^2 - \frac{\rho_s\Delta\rho}{\rho_f^2}\frac{K}{W}S_0^2}$$

Replacing L_t by ΔL+L_0 in Equation (139) and combining with Equation (112) yields Equation (140).

$$
\begin{aligned}
\Delta V_{CA} = {} & \frac{n_e}{2}\sqrt{\frac{\rho_s}{\Delta\rho}\frac{W}{K}} \\
& \left[\left(\left(L_0-\frac{\Delta S}{tan\theta}-\Delta L_{CE}\right)^2\left(\frac{\pi}{2}-sin^{-1}\left(\frac{x_{Tt}}{L_0-\frac{\Delta S}{tan\theta}-\Delta L_{CE}}\right)\right)-x_{Tt}\sqrt{\left(L_0-\frac{\Delta S}{tan\theta}-\Delta L_{CE}\right)^2-{x_{Tt}}^2}\right)-\left(L_0^2\left(\frac{\pi}{2}-sin^{-1}\left(\frac{x_{T0}}{L_0}\right)\right)-x_{T0}\sqrt{L_0^2-{x_{T0}}^2}\right)\right]+ \\
& \frac{n_e}{2}\sqrt{\frac{W}{K}}\left[\left(x_{Tt}\sqrt{\left(L_0-\frac{\Delta S}{tan\theta}-\Delta L_{CE}\right)^2+\frac{K}{W}\frac{\rho_s}{\rho_f}(\Delta S+S_0)^2-{x_{Tt}}^2}+\left(\left(L_0-\frac{\Delta S}{tan\theta}-\Delta L_{CE}\right)^2+\frac{K}{W}\frac{\rho_s}{\rho_f}(\Delta S+S_0)^2\right)sin^{-1}\left(\frac{x_{Tt}}{\sqrt{\left(L_0-\frac{\Delta S}{tan\theta}-\Delta L_{CE}\right)^2+\left(\frac{K}{W}\frac{\rho_s}{\rho_f}S_0^2\right)}}\right)\right)-\right. \\
& \left.\left(x_{T0}\sqrt{L_0^2+\left(\frac{K}{W}\frac{\rho_s}{\rho_f}S_0^2\right)-{x_{T0}}^2}+\left(L_0^2+\left(\frac{K}{W}\frac{\rho_s}{\rho_f}S_0^2\right)\right)sin^{-1}\left(\frac{x_{T0}}{\sqrt{L_0^2+\left(\frac{K}{W}\frac{\rho_s}{\rho_f}S_0^2\right)}}\right)\right)\right]
\end{aligned}
\tag{140}
$$

with $x_{Tt}=\sqrt{\left(L_0-\frac{\Delta S}{tan\theta}-\Delta L_{CE}\right)^2-\frac{\rho_s\Delta\rho}{\rho_f^2}\frac{K}{W}(\Delta S+S_0)^2}$ and $x_{T0}=\sqrt{L_0^2-\frac{\rho_s\Delta\rho}{\rho_f^2}\frac{K}{W}S_0^2}$

Equation (140) is the closed-form analytical solution for the change in fresh groundwater volume with land-surface inundation in the entire coastal aquifer.

6.2.6 Change in Mean Residence Time

Seawater intrusion zone

The change of the mean residence time ΔRT_{SIZ} in the seawater intrusion zone with land-surface inundation can be expressed by Equation (141).

$$\Delta RT_{SIZ} = RT_{SIZ}(t) - RT_{SIZ}(t=0) = \frac{V_{SIZ}(t)}{W\,(L_t - x_{Tt})} - \frac{V_{SIZ}(t=0)}{W\,(L_0 - x_{T0})} \qquad (141)$$

The expression of RT_{SIZ} is given by Equation (79) in Section 4. Replacing L_t by ΔL+L_0, x_{Tt} by Δx_T+x_{T0} and $V_{SIZ}(t)$ *by* ΔV_{SIZ}+$V_{SIZ}(t$=0) in Equation (141) and combining with Equation (112) yields Equation (142).

$$\Delta RT_{SIZ} = \frac{1}{W}\left(\frac{\Delta V_{SIZ} + V_{SIZ}(t=0)}{\left(-\frac{\Delta S}{tan\theta} - \Delta L_{CE} + L_0 - \Delta x_T - x_{T0}\right)} - \frac{V_{SIZ}(t=0)}{(L_0 - x_{T0})}\right) \qquad (142)$$

Equation (142) gives the solution for the change of the mean residence time of groundwater in the seawater intrusion zone with combined sea-level rise and coastal erosion. The equation can be solved by first calculating the following quantities: ΔV_{SIZ} using Equation (136), $V_{SIZ}(t$=0) using Equation (71), Δx_T using Equation (124), and x_{T0} using Equation (57). Then, these calculated quantities and the values of other variables are substituted into Equation (142).

Inland zone

The change of the mean residence time ΔRT_{IZ} in the inland zone with land-surface inundation can be expressed by Equation (143).

$$\Delta RT_{IZ} = RT_{IZ}(t) - RT_{IZ}(t=0) = \frac{V_{IZ}(t)}{W\,x_{Tt}} - \frac{V_{IZ}(t=0)}{W\,x_{T0}} \qquad (143)$$

The expression of RT_{IZ} is given by Equation (81) in Section 4. Replacing x_{Tt} by Δx_T+x_{T0} and $V_{IZ}(t)$ by ΔV_{IZ}+$V_{IZ}(t$=0) in Equation (143) and combining with Equation (112) yields Equation (144).

$$\Delta RT_{IZ} = \frac{1}{W}\left(\frac{\Delta V_{IZ} + V_{IZ}(t=0)}{(\Delta x_T + x_{T0})} - \frac{V_{IZ}\,(t=0)}{(L_0 - x_{T0})}\right) \qquad (144)$$

Equation (144) gives the solution for the change of the mean residence time of groundwater in the inland zone with combined sea-level rise and coastal erosion. The equation can be solved by first calculating the following quantities: ΔV_{IZ} using

Equation (138), $V_{IZ}(t{=}0)$ using Equation (76) Δx_T using Equation (124), and x_{T0} using Equation (57). Then, these calculated quantities and the values of other variables are substituted into Equation (144).

Global coastal aquifer (seawater intrusion zone + inland zone)

The change of the mean residence time ΔRT_{IZ} in the coastal aquifer can be expressed by Equation (145).

$$\Delta RT_{CA} = RT_{CA}(t) - RT_{CA}(t=0) = \frac{V_{CA}(t)}{W\ L_t} - \frac{V_{CA}(t=0)}{W\ L_0} \tag{145}$$

The expression of RT_{CA} is given by Equation (83) in Section 4.

Replacing L_t by ΔL+L_0 and $V_{CA}(t)$ by ΔV_{CA}+$V_{CA}(t{=}0)$ in Equation (145) and combining with Equation (112) yields Equation (146).

$$\Delta RT_{CA} = \frac{1}{W}\left(\frac{\Delta V_{CA} + V_{CA}(t=0)}{\left(-\frac{\Delta S}{tan\theta} - \Delta L_{CE} + L_0\right)} - \frac{V_{CA}(t=0)}{L_0}\right) \tag{146}$$

Equation (146) gives the solution for the change of the mean residence time of groundwater in the entire coastal aquifer with combined sea-level rise and coastal erosion. The equation can be solved by replacing ΔV_{CA} by its expression given in Equation (140), and by replacing $V_{CA}(t{=}0)$ by its expression in Equation (78).

The behaviors of the change of the residence times in the different zones of the coastal aquifer are the same as the behaviors of the travel times as described previously with the opposing effects of the changes of ΔL and ΔS.

6.2.7 Change in Total Groundwater Recharge

Groundwater recharge rates W_t [LT^{-1}] may change (compared to W_{t0}) with changes in climate that cause sea level rise, but the total recharge, RE_{CA} [L^2], may decrease with climate change due to the loss of land surface caused by inundation. At time t, the total groundwater recharge to the coastal aquifer (per unit width) during a period of time Δt is the product of Δt, the recharge rate W_t, and by the length L_t of the coastal aquifer (Equation (147)).

$$RE_{CA} = L_t\ W_t\ \Delta t \tag{147}$$

The total recharge RE_{CA} over Δt indicates the amount of freshwater that is renewed in the coastal aquifer over this time period. This amount theoretically corresponds to the maximum amount of water that can be withdrawn from the aquifer without depleting the resource—with the rate of uptake not exceeding the rate of renewal. Consequently, characterizing the value of RE_{CA} in a context of climate change and land-surface inundation is of crucial interest and importance for decision-makers. RE_{CA} represents a threshold value when planning future scenarios of possible water use that consider the effects of climate change on both land inundation and groundwater recharge rates.

Exercise 5 provides the opportunity to apply the main previously presented equations to a specific case to calculate the impacts of climate change on a coastal unconfined Dupuit-type aquifer.

6.3 Case of Oceanic Island Aquifers

The closed-form analytical solutions presented in this section are based on derivations by Chesnaux (2016) and Chesnaux and others (2021). However, the solutions presented here are more comprehensive because they also include the cumulative effects of coastal erosion and sea-level rise as well as a larger variety of changes of the hydraulic parameters.

The solutions presented in Section 5 for both strip and circular oceanic islands for the different groundwater quantities (e.g., travel times, volumes) under study will be used to develop the equations for the change in these quantities with land-surface inundation caused by sea-level rise and coastal erosion.

6.3.1 Strip Oceanic Islands

Change in the thickness of the freshwater lens

A change of S (ΔS) caused by sea level rise combined with coastal erosion will cause land-surface inundation of the strip island aquifer, producing a change of L ($\Delta L = L_t - L_0$) that depends on θ, the slope of the shore face (Figure 35). The resulting inundation in the case of sea-level rise ΔS and coastal erosion ΔL_{CE} during a period t will cause a loss of length of the strip island of $|\Delta S/tan\theta|$+$|\Delta L_{CE}|$ (Figure 35).

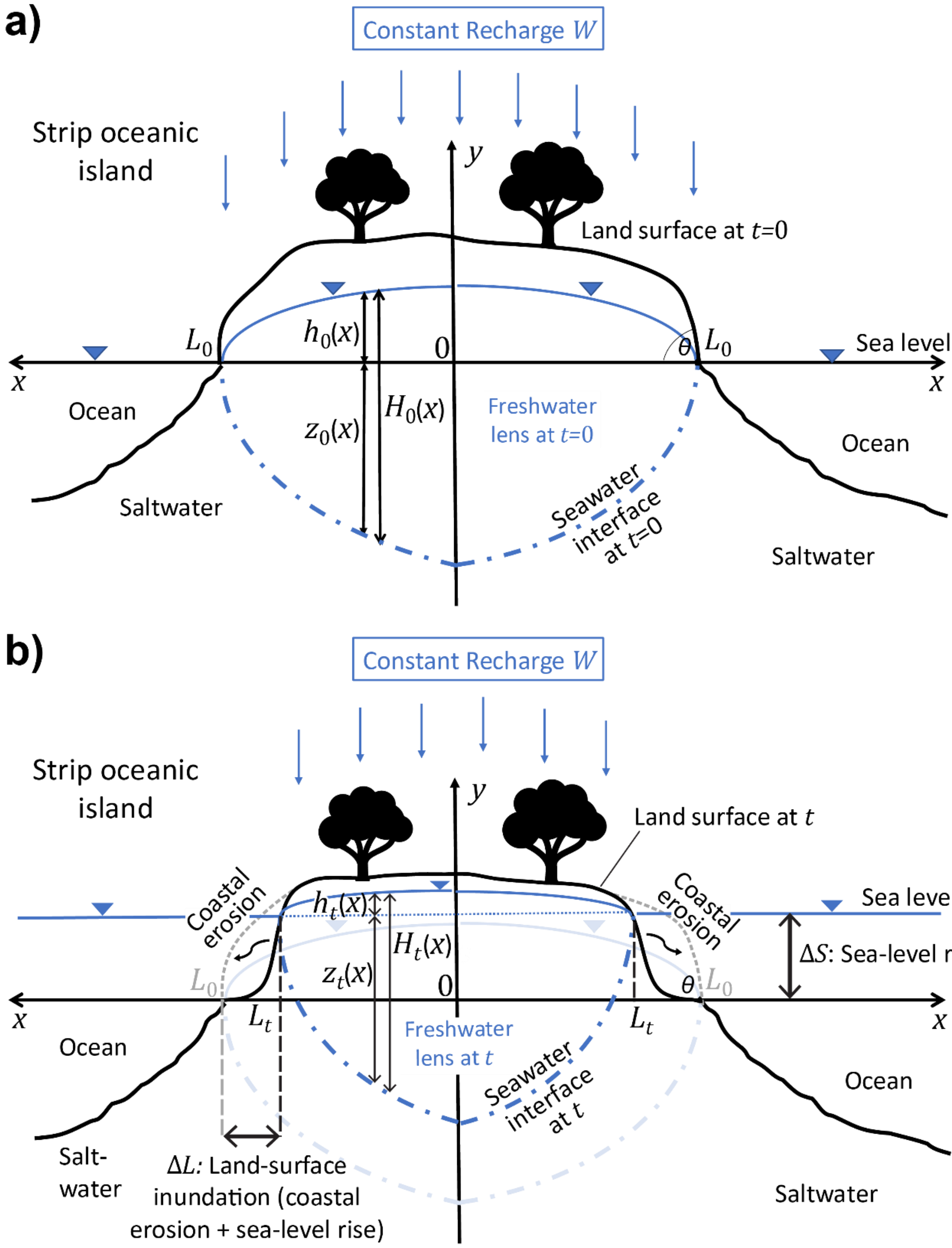

Figure 35 - Conceptual model for evaluating the cumulative effects of sea-level rise and coastal erosion on seawater intrusion in a strip oceanic island aquifer, showing the change in land surface, water table, and seawater interface. a) Conditions at initial time t=0. b) Conditions due to sea level rise that has occurred at time t, with conditions at time t=0 also shown, in light blue and light gray. The change in water table position results from the combined effects of land-surface inundation and decrease in total recharge, which are controlled in part by the seashore angle θ.

The change in thickness of the freshwater lens $\Delta H_{SOI}(x)$ can be written using Equation (90), giving $H_{SOI}(x)$, the freshwater lens thickness of the strip oceanic island presented earlier in Section 5. $\Delta H_{SOI}(x)$ is expressed by Equation (148) (Chesnaux, 2016).

$$\Delta H_{SOI}(x) = H_{SOI}(t) - H_{SOI}(t=0) = \sqrt{\frac{\rho_s}{\Delta\rho}\frac{W}{K}}\left[\left(\sqrt{L_t^2 - x^2}\right) - \left(\sqrt{L_0^2 - x^2}\right)\right] \quad (148)$$

$$\text{with } x \leq L_t$$

Replacing L_t by $\Delta L + L_0$ in Equation (148) and combining with Equation (112) for ΔL yields Equation (149) with L_0 the initial length of the aquifer at time t=0.

$$\Delta H_{SOI}(x) = \sqrt{\frac{\rho_s}{\Delta\rho}\frac{W}{K}}\left[\left(\sqrt{\left(L_0 - \frac{\Delta S}{tan\theta} - \Delta L_{CE}\right)^2 - x^2}\right) - \left(\sqrt{L_0^2 - x^2}\right)\right] \quad (149)$$

$$\text{with } x \leq L_t$$

Equation (149) is the closed-form analytical solution for calculating the change in thickness of the freshwater lens at a distance x from the water divide in strip islands of coastal slope θ when sea level rises by a value of ΔS and when the erosion of the coast is ΔL_{CE}. $\Delta H_{SOI}(x)$ is negative when sea level rises, meaning that the thickness of the freshwater lens diminishes. Also, $\Delta H_{SOI}(x)$=0 when θ=90° and there is no coastal erosion (ΔL_{CE}=0).

Change in groundwater velocities

Groundwater velocities in strip oceanic islands are expressed by Equation (95) developed in Section 5. The change in groundwater velocity $\Delta v_{SOI}(x)$ in strip islands can be calculated for a position x between 0 and L_t (Figure 35) and is expressed by Equation (150).

$$\Delta v_{SOI}(x) = v_{SOI}(t) - v_{SOI}(t=0) = \frac{1}{n_e}\sqrt{\frac{\Delta\rho W K}{\rho_s}}\left(\frac{x}{\sqrt{L_t^2 - x^2}} - \frac{x}{\sqrt{L_0^2 - x^2}}\right) \quad (150)$$

$$\text{with } x \leq L_t$$

Replacing L_t by $\Delta L + L_0$ in Equation (150) and combining with Equation (112) yields Equation (151).

$$\Delta v_{SOI}(x) = \frac{1}{n_e}\sqrt{\frac{\Delta\rho W K}{\rho_s}}\left(\frac{x}{\sqrt{\left(L_0 - \frac{\Delta S}{tan\theta} - \Delta L_{CE}\right)^2 - x^2}} - \frac{x}{\sqrt{L_0^2 - x^2}}\right) \quad (151)$$

$$\text{with } x \leq L_t$$

Equation (151) is the closed-form analytical solution for calculating the change of groundwater travel time in the freshwater lens of a strip oceanic island of coastal slope θ at a distance x from the water divide when sea level rises by a value of ΔS and the erosion of the coast is ΔL_{CE}. $\Delta v_{SOI}(x)$ is positive when sea level rises, meaning that groundwater velocities increase. Also, $\Delta v_{SOI}(x)$=0 when θ=90° and there is no coastal erosion (ΔL_{CE}=0).

Change in groundwater travel times

Groundwater travel times in strip oceanic islands are expressed by Equation (99) developed in Section 5. The difference in groundwater travel time $\Delta t_{SOI}(x)$ in the strip oceanic island between a particle of water traveling in groundwater conditions at initial time t=0 and a particle traveling in conditions at time t after land-surface inundation is expressed by Equation (152) (Chesnaux, 2016). The two particles depart from the same position x_i ($0 < x_i \leq L_t$) and travel to the same position x ($x_i \leq x \leq L_t$) (Figure 36).

$$\Delta t_{SOI}(x) = t_{SOI}(t) - t_{SOI}(t=0) =$$

$$n_e\sqrt{\frac{\rho_s}{WK\Delta\rho}}\left[\left(\sqrt{L_t^2 - x^2} - \sqrt{L_t^2 - x_i^2} - L_t\ ln\left(\frac{L_t+\sqrt{L_t^2-x^2}}{L_t+\sqrt{L_t^2-x_i^2}}\ \frac{x_i}{x}\right)\right) - \left(\sqrt{L_0^2 - x^2} - \sqrt{L_0^2 - x_i^2} - L_0\ ln\left(\frac{L_0+\sqrt{L_0^2-x^2}}{L_0+\sqrt{L_0^2-x_i^2}}\ \frac{x_i}{x}\right)\right)\right] \quad (152)$$

$$\text{with } x_i \leq x \leq L_t$$

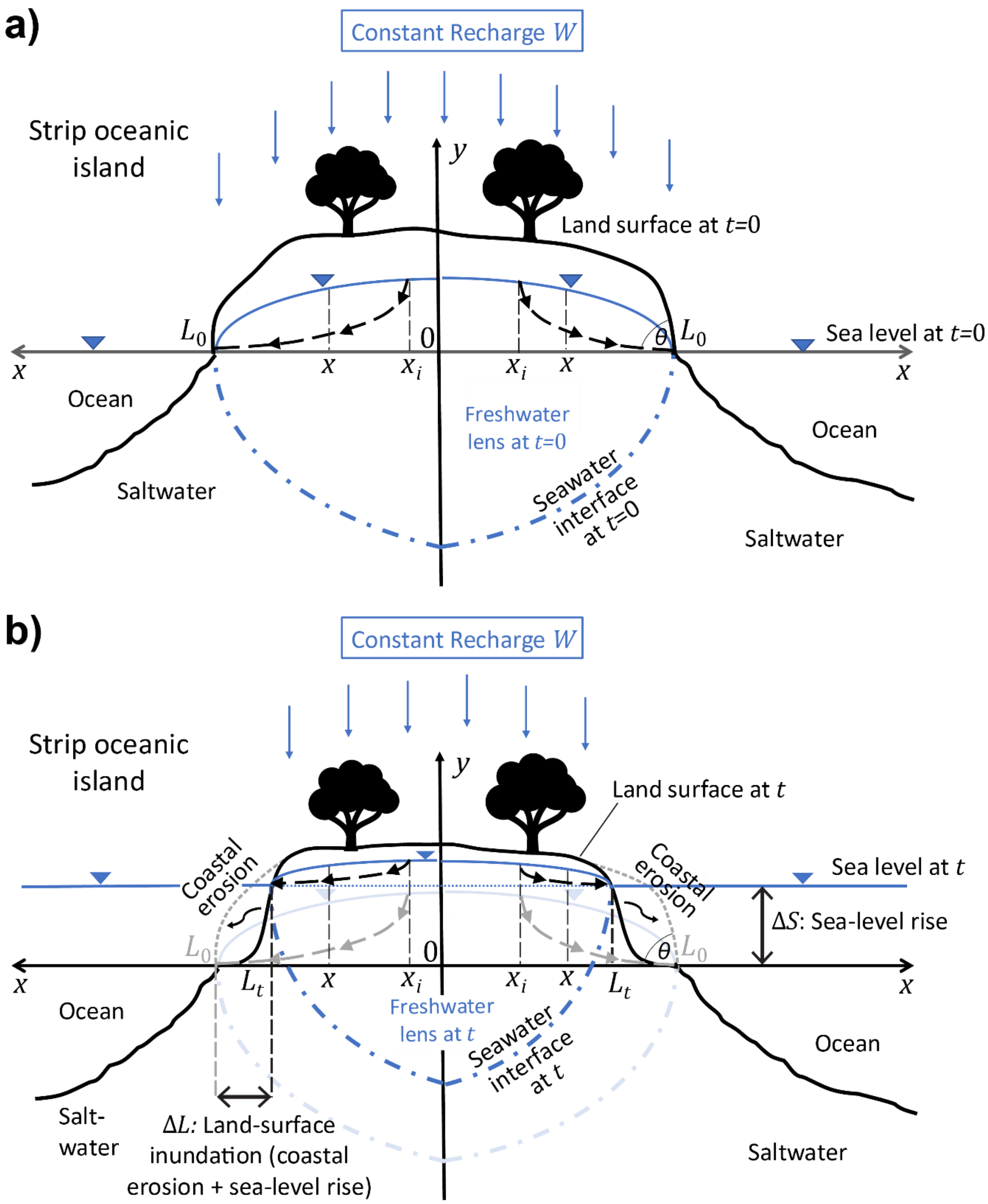

Figure 36 - Comparison of the travel paths of two groundwater particles within a strip oceanic island, before (time t=0) and after (time t) sea-level rise. a) Conditions at time t=0 before sea-level rise, showing particle paths that start at position x_i and travel to the sea. Two different paths are shown, each with a different starting position x_i. b) Conditions at time t after land-surface inundation, showing particle paths that start at the same positions x_i; the paths at time t=0 are also shown, in light gray. The equation for the difference in travel times between the particles at t=0 and at t is developed for the case of the particles traveling from the same starting point x_i to the same position x where $0 < x_i \le L_t$ and $x_i \le x \le L_t$.

Replacing L_t by $\Delta L + L_0$ in Equation (152) and combining with Equation (112) yields Equation (153).

$$\Delta t_{SOI}(x) = n_e\sqrt{\frac{\rho_s}{WK\Delta\rho}}\left[\left(\sqrt{\left(L_0 - \frac{\Delta S}{tan\theta} - \Delta L_{CE}\right)^2 - x^2} - \sqrt{\left(L_0 - \frac{\Delta S}{tan\theta} - \Delta L_{CE}\right)^2 - x_i^2} - \left(-\frac{\Delta S}{tan\theta} - \Delta L_{CE} + L_0\right) ln\left(\frac{-\frac{\Delta S}{tan\theta} - \Delta L_{CE} + L_0 + \sqrt{\left(L_0 - \frac{\Delta S}{tan\theta} - \Delta L_{CE}\right)^2 - x^2}}{-\frac{\Delta S}{tan\theta} - \Delta L_{CE} + L_0 + \sqrt{\left(L_0 - \frac{\Delta S}{tan\theta} - \Delta L_{CE}\right)^2 - x_i^2}}\frac{x_i}{x}\right)\right) - \left(\sqrt{L_0^2 - x^2} - \sqrt{L_0^2 - x_i^2} - L_0\ ln\left(\frac{L_0 + \sqrt{L_0^2 - x^2}}{L_0 + \sqrt{L_0^2 - x_i^2}}\frac{x_i}{x}\right)\right)\right] \tag{153}$$

with $x_i \leq x \leq L_t$

Equation (153) is the closed-form analytical solution for the change in groundwater travel time with land-surface inundation in the strip oceanic island when sea level rises by a value of ΔS and when the erosion of the coast is ΔL_{CE}. $\Delta t_{SOI}(x)$ is negative when sea level rises meaning that groundwater travel times decrease. Also, $\Delta t_{SOI}(x)=0$ when $\theta=90^o$ and there is no coastal erosion ($\Delta L_{CE}=0$).

Change of volume of the fresh groundwater lens

Define V_{SOI} $(t=0)$ (Equation (105)) to be the initial volume of the freshwater lens of the strip island at $t=0$. At time t, the change of volume $\Delta V_{SOI}=V_{SOI}(t)-V_{SOI}(t=0)$ after land-surface inundation (Figure 37) is provided in Equation (154).

$$\Delta V_{SOI} = \frac{\pi n_e}{2}\sqrt{\frac{\rho_s}{\Delta\rho}\frac{W}{K}}\,(L_t^2 - L_0^2) \tag{154}$$

(per unit width of aquifer)

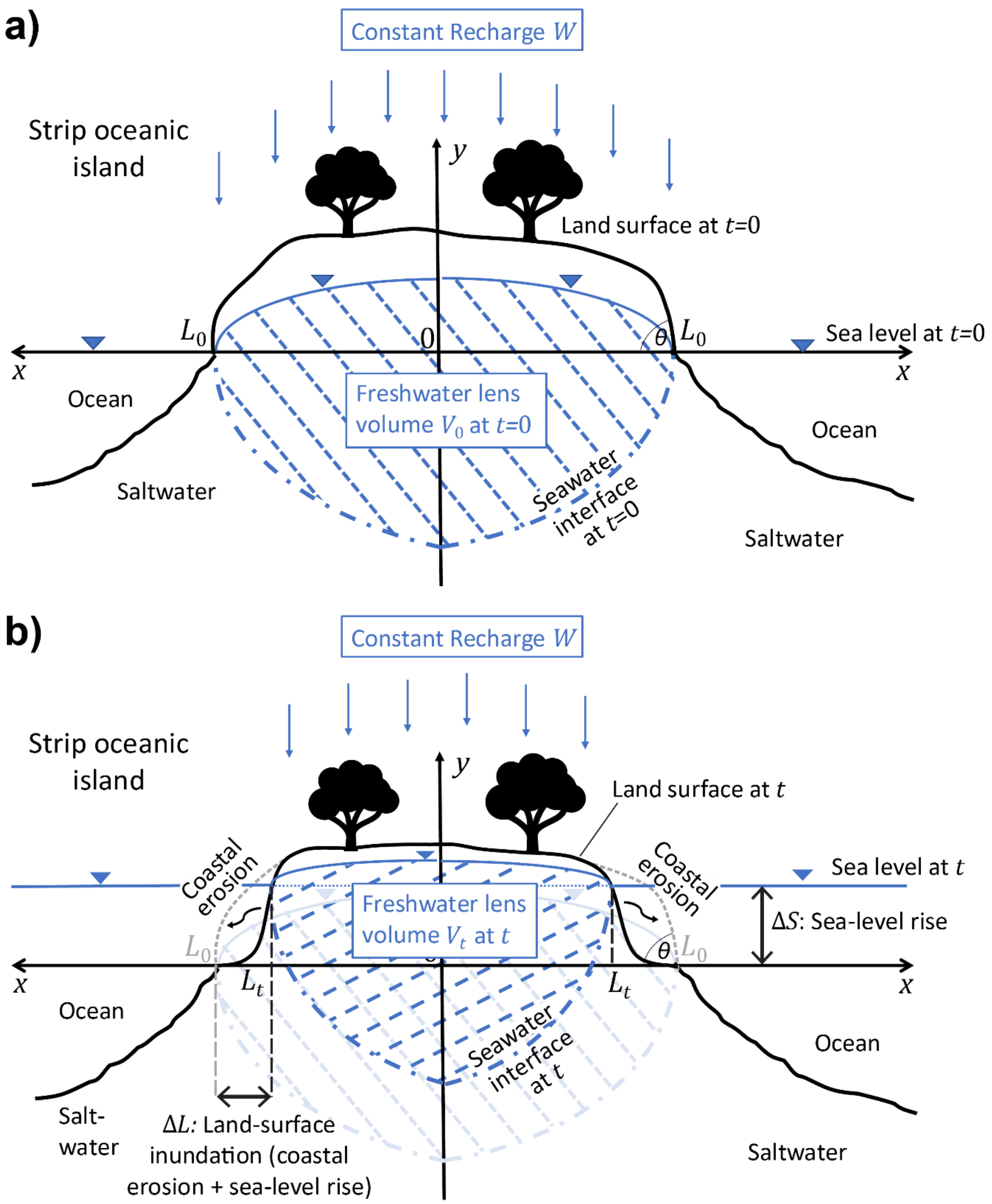

Figure 37 - Visualizing the change in groundwater volumes caused by land-surface inundation in a strip oceanic island aquifer. a) Freshwater volume V_0 at time t=0. b) Freshwater volume V_t at time t, with volume V_0 also shown in light blue.

Replacing L_t by ΔL+L_0 in Equation (154) and combining with Equation (112) yields Equation (155).

$$\Delta V_{SOI} = \frac{\pi n_e}{2}\sqrt{\frac{\rho_s}{\Delta\rho}\frac{W}{K}}\left(\left(L_0 - \frac{\Delta S}{tan\theta} - \Delta L_{CE}\right)^2 - L_0^2\right) \tag{155}$$

(per unit width of aquifer)

Equation (155) can be developed to yield Equation (156).

$$\Delta V_{SOI} = -\frac{\pi n_e}{2}\sqrt{\frac{\rho_s}{\Delta\rho}\frac{W}{K}}\left(2L_0 - \frac{\Delta S}{tan\theta} - \Delta L_{CE}\right)\left(\frac{\Delta S}{tan\theta} + \Delta L_{CE}\right) \tag{156}$$

(per unit width of aquifer)

Equation (156) is the closed-form solution for calculating the volume change of the freshwater lens in a strip oceanic island as a function of the initial half-length L_0 of the island and the slope θ of the coast when sea level rises by ΔS and coastal erosion increases by ΔL_{CE}. ΔV_{SOI} is negative for $0 < \theta < 90$, and is equal to zero when θ equals 90 degrees (i.e., no land surface inundation) and there is no coastal erosion.

Change in mean groundwater residence time

The change in mean residence time ΔRT_{SOI} in the strip oceanic island with land-surface inundation is expressed by Equation (157), which is based on Equation (109) developed in Section 5.

$$\Delta RT_{SOI} = RT_{SOI}(t) - RT_{SOI}(t=0) = \frac{V_{SOI}(t)}{W \cdot L_t} - \frac{V_{SOI}(t=0)}{W \cdot L_0} = \frac{\pi n_e}{2}\sqrt{\frac{\rho_s}{\Delta\rho}\frac{1}{WK}}\,[L_t - L_0] \tag{157}$$

Replacing L_t by $\Delta L+L_0$ in Equation (157) and combining with Equation (112) yields Equation (158).

$$\Delta RT_{SOI} = -\frac{\pi n_e}{2}\sqrt{\frac{\rho_s}{\Delta\rho}\frac{1}{WK}}\left[\frac{\Delta S}{tan\theta} + \Delta L_{CE}\right] \tag{158}$$

Equation (158) is the closed-form solution for calculating the change of the groundwater residence time within the freshwater lens in a strip oceanic island. ΔRT_{SOI} is negative for a seashore slope angle $0 < \theta < 90$ and is equal to zero when θ equals 90 degrees (i.e., no land surface inundation) and there is no coastal erosion.

Change in groundwater recharge

Groundwater recharge rates W_t [LT^{-1}] may change (compared to W_{t0}) with changes in climate that cause sea level rise, but the total recharge of the strip oceanic island, RE_{SOI} [L^2], may decrease with climate change due to the loss of land surface caused by inundation. At time t, the total groundwater recharge to the freshwater lens (per unit width) during a period of time Δt is the product of Δt, the recharge rate W_t, and the length $2L_t$ of the strip island aquifer (Equation (159)).

$$RE_{SOI} = 2\ L_t\ W_t\ \Delta t \tag{159}$$

The total recharge RE_{SOI} during Δt represents the amount of freshwater that is renewed during this time. This amount theoretically corresponds to the maximum amount of water that can be withdrawn from the lens without depleting the resource—with the rate of uptake not exceeding the rate of renewal. Consequently, characterizing the value of RE_{SOI} in a context of climate change is of crucial interest and importance for decision-makers. RE_{SOI} represents a threshold value when planning future scenarios of possible water use that consider the effects of climate change on both land inundation and groundwater recharge rates.

6.3.2 Circular Oceanic Islands

Change in the thickness of the freshwater lens

A change of S (ΔS) combined with coastal erosion will cause land-surface inundation of a circular island aquifer, producing a change of R (ΔR=R_t−R_0) that depends on θ, the slope of the shore face, of the coastal aquifer according to Equation (112) presented earlier (Figure 38). The resulting inundation ΔR of the island in the case of sea-level rise ΔS and coastal erosion ΔR_{CE} during t will cause a loss of radius of the circular island of $|\Delta S/tan\theta|$+$|\Delta R_{CE}|$ (Figure 38).

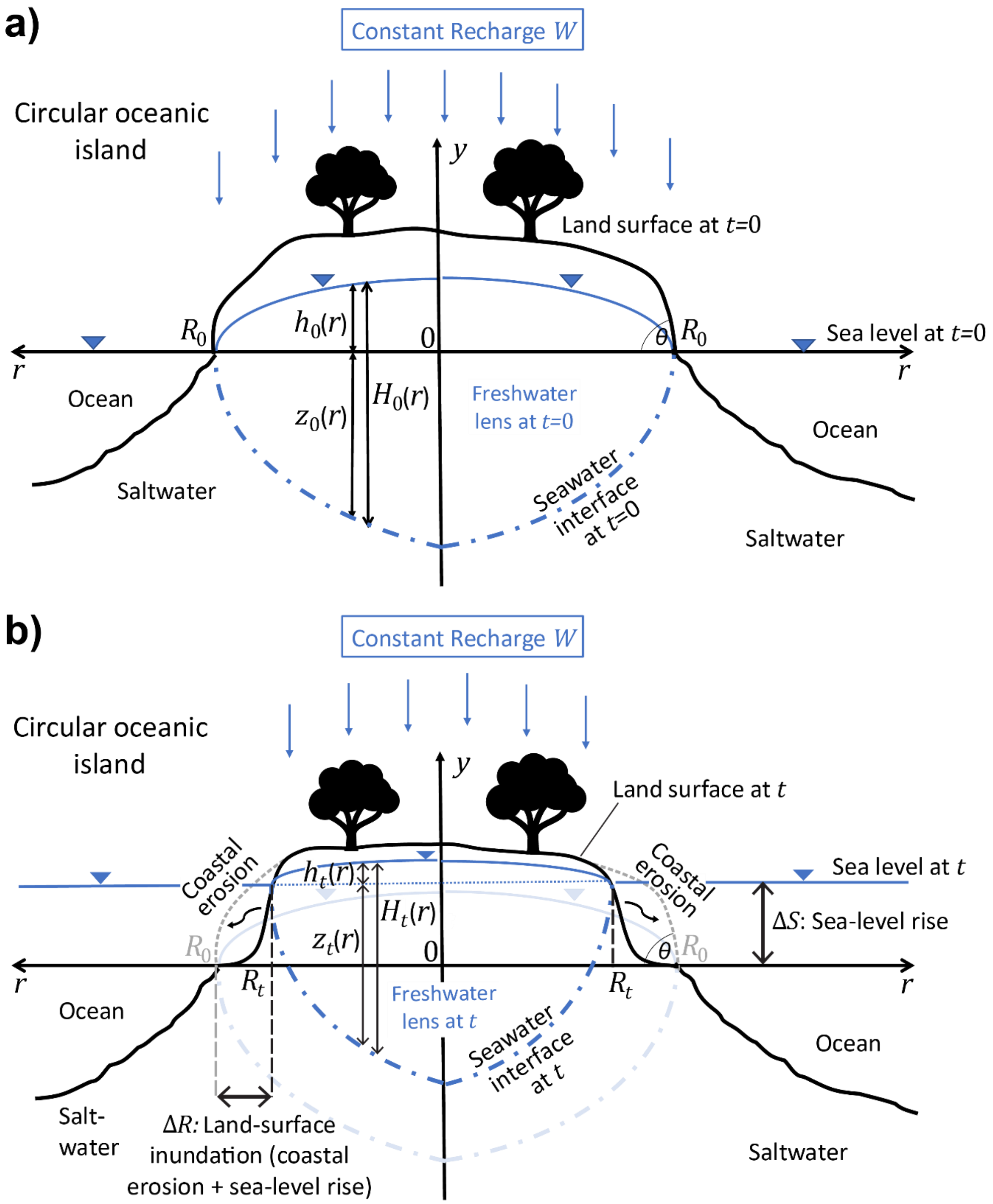

Figure 38 - Conceptual model for evaluating the cumulative effects of sea-level rise and coastal erosion on seawater intrusion in a circular oceanic island aquifer, showing the change in land surface, water table, and seawater interface. a) Conditions at initial time t=0. b) Conditions due to sea level rise that has occurred at time t, with conditions at time t=0 also shown, in light blue and light gray. The change in water table position results from the combined effects of land-surface inundation and decrease in total recharge, which are controlled in part by the seashore angle θ.

The change in thickness of the freshwater lens $\Delta H_{COI}(r)$ can be written using Equation (94), giving $H_{COI}(r)$, the freshwater lens thickness of the circular oceanic island presented earlier in Section 5 presented earlier in Section 5. $\Delta H_{COI}(r)$ is expressed by Equation (160) (Chesnaux, 2016).

$$\Delta H_{COI}(r) = H_{COI}(t) - H_{COI}(t=0) = \sqrt{\frac{\rho_s}{\Delta\rho}\frac{W}{2K}}\left[\left(\sqrt{R_t^2 - r^2}\right) - \left(\sqrt{R_0^2 - r^2}\right)\right] \tag{160}$$

$$\text{with } r \leq R_t$$

Replacing R_t *by* ΔR+R_0 in Equation (160) and combining with Equation (112) yields Equation (161) with R_0 the initial radius of the aquifer at time t=0.

$$\Delta H_{COI}(r) = \sqrt{\frac{\rho_s}{\Delta\rho}\frac{W}{2K}}\left[\left(\sqrt{\left(R_0 - \frac{\Delta S}{tan\theta} - \Delta R_{CE}\right)^2 - r^2}\right) - \left(\sqrt{R_0^2 - r^2}\right)\right] \tag{161}$$

$$\text{with } r \leq R_t$$

Equation (161) is the closed-form analytical solution for calculating the change in thickness of the freshwater lens at a distance r from the water divide when sea level rises by a value of ΔS and the erosion of the coast is ΔR_{CE}, with $r \leq R_t$, the radius of the aquifer after sea level rise at time t. $\Delta H_{COI}(x)$ is negative when sea level rises, meaning that the thickness of the freshwater lens diminishes. Also, $\Delta H_{COI}(x)$=0 when θ=90^o and there is no coastal erosion (ΔR_{CE}=0).

Change in groundwater velocities

Groundwater velocities in circular oceanic islands are expressed by Equation (96) developed in Section 5. The change in groundwater velocity $\Delta v_{COI}(r)$ in circular islands can be calculated for a position r comprised between 0 and R_t (Figure 38) and is expressed by Equation (162).

$$\Delta v_{COI}(r) = v_{COI}(t) - v_{COI}(t=0) = \frac{1}{n_e}\sqrt{\frac{\Delta\rho WK}{2\rho_s}}\left[\left(\frac{r}{\sqrt{R_t^2 - r^2}}\right) - \left(\frac{r}{\sqrt{R_0^2 - r^2}}\right)\right] \tag{162}$$

$$\text{with } r \leq R_t$$

Replacing R_t by ΔR+R_0 in Equation (162) and combining with Equation (112) yields Equation (163).

$$\Delta v_{COI}(x) = \frac{1}{n_e}\sqrt{\frac{\Delta\rho WK}{2\rho_s}}\left[\left(\frac{r}{\sqrt{\left(R_0 - \frac{\Delta S}{tan\theta} - \Delta R_{CE}\right)^2 - r^2}}\right) - \left(\frac{r}{\sqrt{R_0^2 - r^2}}\right)\right] \tag{163}$$

$$\text{with } r \leq R_t$$

Equation (163) is the closed-form analytical solution for calculating the change of groundwater travel time in the lens of the circular oceanic island of coastal slope θ at a distance r from the water divide when sea level rises by a value of ΔS and the erosion of the coast is ΔR_{CE}. $\Delta v_{COI}(r)$ is positive when sea level rises, meaning that groundwater velocities increase. Also, $\Delta v_{COI}(\mathrm{r})=0$ when $\theta=90^{\circ}$ and there is no coastal erosion ($\Delta R_{CE}=0$).

Change in groundwater travel times

Groundwater travel times in circular oceanic islands are expressed by Equation (102) developed in Section 5. The difference in groundwater travel times $\Delta t_{COI}(r)$ in a circular oceanic island between a particle of water traveling in groundwater conditions at initial time $t=0$ and a particle traveling in conditions at time t after land-surface inundation is expressed by Equation (164) (Chesnaux, 2016). The two particles of water depart from the same position r_i ($0 < r_i \leq R_t$) and travel to the same position r ($r_i \leq r \leq R_t$) (Figure 39).

$$\Delta t_{COI}(r) = t_{COI}(t) - t_{COI}(t=0) = n_e\sqrt{\frac{2\rho_s}{WK\Delta\rho}}\left[\left(\sqrt{R_t^2 - r^2} - \sqrt{R_t^2 - r_i^2} - R_t\ ln\left(\frac{R_t + \sqrt{R_t^2 - r^2}}{R_t + \sqrt{R_t^2 - r_i^2}}\frac{r_i}{r}\right)\right) - \left(\sqrt{R_0^2 - r^2} - \sqrt{R_0^2 - r_i^2} - R_0\ ln\left(\frac{R_0 + \sqrt{R_0^2 - r^2}}{R_0 + \sqrt{R_0^2 - r_i^2}}\frac{r_i}{r}\right)\right)\right] \quad (164)$$

$$\text{with } r_i \leq r \leq R_t$$

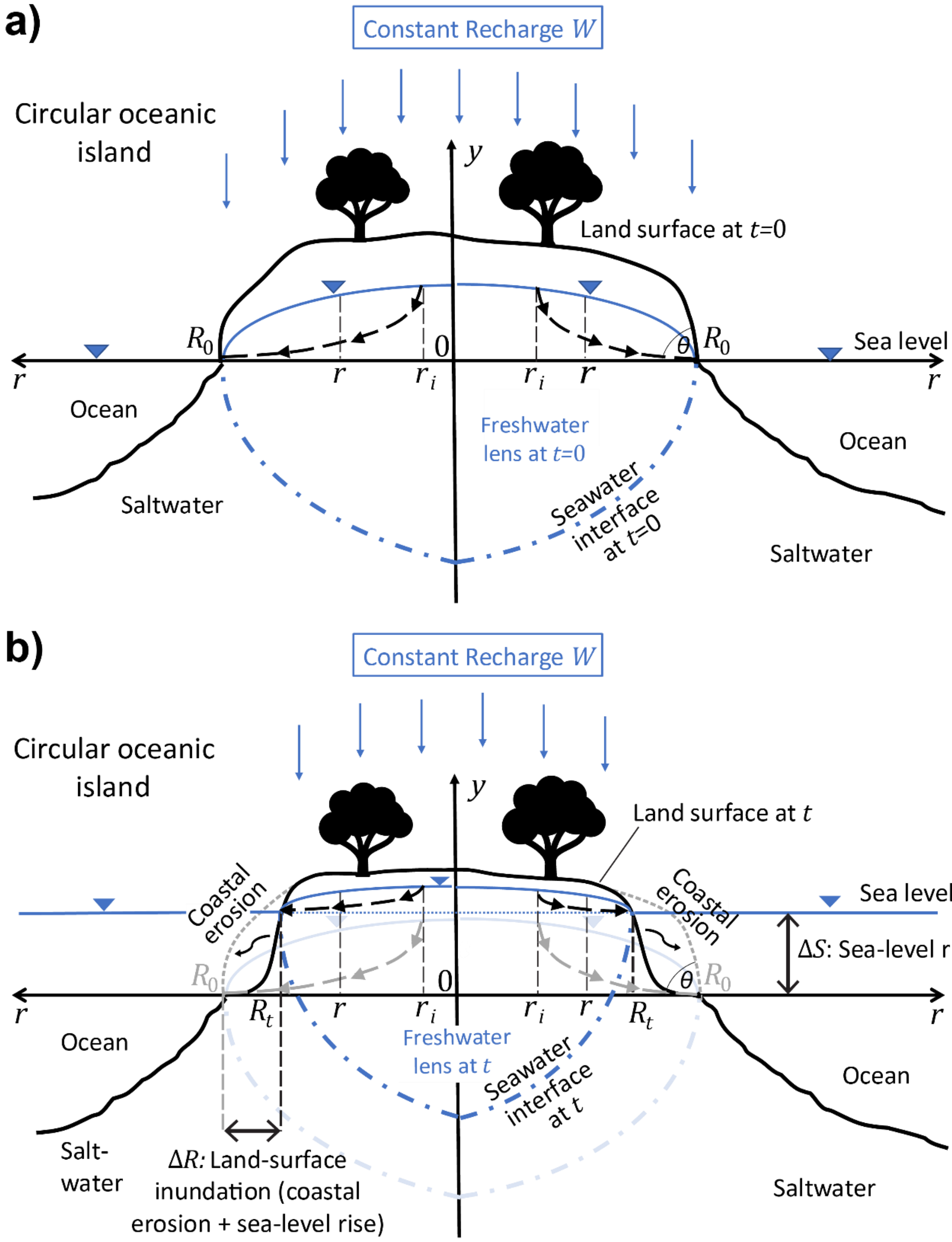

Figure 39 - Comparison of the travel paths of groundwater particles within a circular oceanic island before (time t=0) and after (time t) sea-level rise. A) Conditions at time t=0 before sea-level rise, showing particle paths that start at position r_i and travel to the sea. Two different paths are shown, each with a different starting position r_i. B) Conditions at time t after land-surface inundation, showing particle paths that start at the same positions r_i; the paths at time t=0 are also shown in light gray. The equation for the difference in travel times between the particles at t=0 and at t is developed for the case of the particles traveling from the same starting point r_i to the same position r where $0 < r_i \leq R_t$ and $r_i \leq r \leq R_t$.

Replacing R_t by ΔR+R_0 in Equation (164) and combining with Equation (112) yields Equation (165).

$$\Delta t_{COI}(r) = n_e\sqrt{\frac{2\rho_S}{WK\Delta\rho}}\left[\left(\sqrt{\left(R_0 - \frac{\Delta S}{tan\theta} - \Delta R_{CE}\right)^2 - r^2} - \sqrt{\left(R_0 - \frac{\Delta S}{tan\theta} - \Delta R_{CE}\right)^2 - r_i^2} - \left(R_0 - \frac{\Delta S}{tan\theta} - \Delta R_{CE}\right)\ ln\left(\frac{R_0 - \frac{\Delta S}{tan\theta} - \Delta R_{CE} + \sqrt{\left(R_0 - \frac{\Delta S}{tan\theta} - \Delta R_{CE}\right)^2 - r^2}}{R_0 - \frac{\Delta S}{tan\theta} - \Delta R_{CE} + \sqrt{\left(R_0 - \frac{\Delta S}{tan\theta} - \Delta R_{CE}\right)^2 - r_i^2}}\ \frac{r_i}{r}\right)\right) - \left(\sqrt{R_0^2 - r^2} - \sqrt{R_0^2 - r_i^2} - R_0\ ln\left(\frac{R_0 + \sqrt{R_0^2 - r^2}}{R_0 + \sqrt{R_0^2 - r_i^2}}\ \frac{r_i}{r}\right)\right)\right] \quad (165)$$

$$\text{with } r_i \le r \le R_t$$

Equation (165) is the closed-form analytical solution for the change in groundwater travel time with land-surface inundation in a circular oceanic island when sea level rises by a value of ΔS and when the erosion of the coast is ΔR_{CE}. $\Delta t_{COI}(r)$ is negative when sea level rises meaning that groundwater travel times decrease. Also, $\Delta t_{COI}(r)=0$ when $\theta=90^o$ and there is no coastal erosion ($\Delta R_{CE}=0$).

Change of volume of the fresh groundwater lens

Define $V_{COI}(t=0)$ (Equation (108)) to be the initial volume of the freshwater lens of the circular island at $(t=0)$. At time t, the change of volume $\Delta V_{COI}=V_{COI}(t)-V_{COI}(t=0)$ after land-surface inundation (Figure 40) is expressed by Equation (166).

$$\Delta V_{COI} = \frac{\pi n_e \sqrt{2}}{3} \sqrt{\frac{\rho_s}{\Delta\rho} \frac{W}{K}} \left(R_t^3 - R_0^3\right) \tag{166}$$

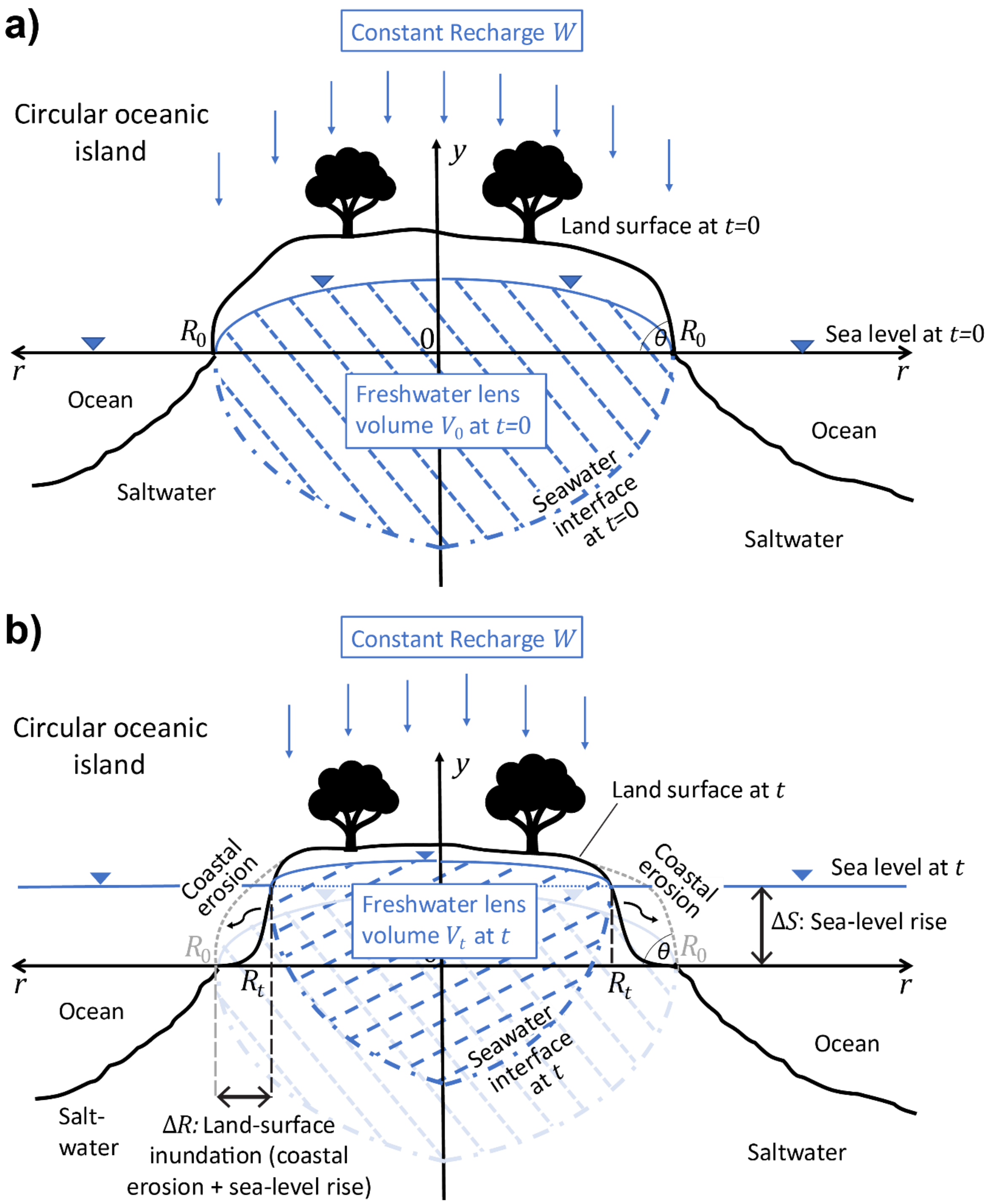

Figure 40 - Visualizing the change in groundwater volumes with land-surface inundation in a circular oceanic island aquifer. a) Freshwater volume V_0 at time t=0. b) Freshwater volume V_t at time t, with volume V_0 also shown in light blue.

Replacing R_t by ΔR+R_0 in Equation (166) and combining with Equation (112) yields Equation (167).

$$\Delta V_{COI} = \frac{\pi n_e \sqrt{2}}{3}\sqrt{\frac{\rho_s}{\Delta\rho}\frac{W}{K}}\left(\left(R_0 - \frac{\Delta S}{tan\theta} - \Delta R_{CE}\right)^3 - R_0^3\right) \tag{167}$$

Equation (167) is the closed-form solution for calculating the volume change of the freshwater lens in a circular oceanic island as a function of the initial radius R_0 of the island and the coastal slope angle θ when sea level rises by ΔS and coastal erosion increases by ΔR_{CE}. ΔV_{COI} is negative for $0 < \theta < 90$, and is equal to zero when θ equals 90 degrees—i.e., no land surface inundation—and there is no coastal erosion.

Change in mean groundwater residence time

The change in mean residence time ΔRT_{COI} in the circular oceanic island with land-surface inundation is expressed by Equation (168), which is based on Equation (110) developed in Section 5.

$$\Delta RT_{COI} = RT_{COI}(t) - RT_{COI}(t=0) = \frac{V_{COI}(t)}{\pi\, R_t^2\, W} - \frac{V_{COI}(t=0)}{\pi\, R_0^2\, W} = \frac{n_e\sqrt{2}}{3}\sqrt{\frac{\rho_s}{\Delta\rho}\frac{1}{WK}}\,(R_t - R_0) \tag{168}$$

Replacing R_t by ΔR+R_0 in Equation (168) and combining with Equation (112) yields Equation (169).

$$\Delta RT_{COI} = -\frac{n_e\sqrt{2}}{3}\sqrt{\frac{\rho_s}{\Delta\rho}\frac{1}{WK}}\left[\frac{\Delta S}{tan\theta} + \Delta R_{CE}\right] \tag{169}$$

Equation (169) is the closed-form solution for calculating the change of the groundwater residence time in the freshwater lens in a circular oceanic island. ΔRT_{COI} is negative for a seashore slope angle $0 < \theta < 90$, and is equal to zero when θ equals 90 degrees (i.e., no land surface inundation) and there is no coastal erosion.

Change in groundwater recharge

Groundwater recharge rates W_t [LT^{-1}] may change (compared to W_{t0}) with changes in climate that cause sea level rise, but the total recharge of the circular oceanic island, RE_{COI} [L^3], may decrease with climate change due to the loss of land surface caused by inundation. At time t, the total groundwater recharge to the freshwater lens RE_{COI} during a time period Δt is the product of Δt, the recharge rate W_t, and the surface area of the circular island of radius R_t (Equation (170)).

$$RE_{COI} = \pi\, R_t^2\, W_t\, \Delta t \tag{170}$$

The total recharge RE_{COI} during Δt represents the amount of freshwater that is renewed in the lens during this time. This amount theoretically corresponds to the maximum amount of water that can be withdrawn from the lens without depleting the resource—with the rate of uptake not exceeding the rate of renewal. Consequently, characterizing the value of RE_{COI} in a context of climate change is of crucial interest and importance for decision-makers. RE_{COI} represents a threshold value when planning future scenarios of possible water use that consider the effects of climate change on both land inundation and groundwater recharge rates.

Exercise 6⤵ provides the opportunity to apply the main previously presented equations to a specific case to calculate the impacts of climate change on coastal strip and circular oceanic islands containing an unconfined Dupuit-type aquifer.

6.4 Climate Change Prediction and Scenarios of Land-Surface Inundation

The Intergovernmental Panel on Climate Change (IPPCC) assesses the evolution of climate change and provides regularly updated results of the latest scientific observations and predictions (Parmesan et al., 2022). The National Aeronautics and Space Administration (NASA) has established different models, based on the different scenarios of climate change provided by the IPPC, to predict sea-level rise at different coastal stations worldwide. The results of these models are available on a website that can be consulted for free (NASA, n.d.). This web interface can be very useful for obtaining the rate of sea-level rise predicted for the next 100 years.

These predictions can be used as input data (specifically for the parameter ΔS) in the closed-form analytical solutions. Sensitivity analyses can be conducted on the equations presented in this book, not only with the different hydrogeological parameters (K, W, n_e, θ, L, $\Delta\rho$ and boundary conditions), but also with different scenarios of sea-level rise ΔS and coastal erosion ΔL_{CE}. For assessing coastal erosion, a hydrogeologist will need to consult other sources, usually local, such as geotechnical and coastal engineering reports (Chesnaux et al., 2021). Although the equations assume fixed recharge rates, as the climate changes an aquifer's recharge may change significantly, which should also be considered. The effect of a change in recharge can be considered in the equations, for example, by calculating the quantity of interest for a base case recharge rate, and then for a recharge rate expected during a change in climate. Again, sensitivity analyses can be conducted with recharge. The equations are very versatile and can be used to estimate the hydrogeological consequences of multiple scenarios of variations in the controlling parameters under climate change.

6.5 Discussion

Some analytical solutions developed in this book—for both inland and oceanic aquifers—have been verified against numerical modeling (Chesnaux et al., 2005; Chesnaux et al., 2021; Miled et al., 2023) or geochemical methods (Chesnaux et al., 2018) with conceptual or real-case situations.

Evaluating changes in fresh groundwater resource volumes and in groundwater travel times in coastal and oceanic island aquifers, as well as changes in coastal erosion, constitute useful tools for practitioners and decision-makers. Anticipating fresh groundwater volume changes is of particular interest for the management of the resource. It has been shown that the loss of freshwater constitutes an important impact of sea-level rise and coastal erosion.

Changes in groundwater travel time due to sea-level rise can be used to determine the implications of advection in the fate of a contaminant plume in coastal aquifers. It is expected that the advective behavior of a contaminant plume in a coastal aquifer could be considerably impacted by sea-level rise and coastal erosion.

Land reclamation can lower the impacts of sea-level rise, because reclamation displaces the groundwater divide of a coastal aquifer inland. This causes the saltwater–freshwater interface to move seaward which also increases fresh groundwater volume. As rain falls over a larger area, reclaimed land increases the recharge in the aquifer (Guo & Jiao, 2007).

From the closed-form analytical solutions proposed in this book, a general-scale evaluation could be conducted by measuring the changes occurring in coastal and island fresh groundwater resources caused by sea-level rise and coastal erosion. This would provide a first estimate for the prediction of the future fresh groundwater availability in oceanic aquifers. The developed models, together with their analytical solutions, could be used by managers of coastal aquifers and watersheds to assess their vulnerability to saltwater intrusion on a regional scale.

Seawater intrusion into groundwater is happening all over the world. Oceanic islands are probably the most threatened because they are surrounded by saltwater and are therefore more exposed to land-surface inundation. Also, fresh groundwater is often the sole source of water for drinking and irrigation on small islands which depend on a freshwater lens floating above the seawater—for example, the Magdalen Islands, Quebec, Canada (Lemieux et al., 2015). Chesnaux and others (2021) provide a methodology—as applied to an example with a strip island located in western Canada—to evaluate the consequences of climate change with analytical solutions. This study presents the evolution of the volume of a freshwater lens with different scenarios of sea-level rise as predicted by the IPCC, combined with different scenarios of coastal erosion. It illustrates how analytical solutions can be useful for such predictions.

Finally, the restrictive assumptions in these solutions must be acknowledged and should be kept in mind, including assumptions about Dupuit-type flow, the sharp interface between freshwater and seawater, and natural flow conditions—that is, the assumption of limited effects of pumping or injecting.

7 Summary and Examples

This section provides (1) a summary of the analytical equations for calculating groundwater quantities for inland and oceanic Dupuit-type aquifers and (2) examples that illustrate the use of the analytical solutions presented in this book. All the equations can be solved with Excel spreadsheets. Basic spreadsheets are provided with this book, and the user can build additional spreadsheets for custom purposes.

7.1 Summary of the Closed-Form Analytical Solutions

The tables presented in Section 7.1.1 and 7.1.2 provide a summary of the equations presented in this book.

7.1.1 Inland and Oceanic Dupuit-Type Aquifers

Table 1 summarizes the equations useful for inland and oceanic unconfined Dupuit-type aquifers.

Table 1 - Summary table of equations for inland and oceanic unconfined Dupuit-type aquifers.

	Aquifer type		**Water table elevation** (Saturated thickness for inland aquifers and IZ of coastal aquifers) or freshwater lens thickness (coastal SIZ and oceanic island aquifers)	**Ground-water velocity**	**Ground-water travel time**	**Aquifer recharge**	**Fresh ground-water volume**	**Ground-water mean-residence time**
Inland aquifers	Inland aquifer (I)		h_I (Eq. (8))	v_I (Eq. (9))	t_I (Eq. (19))	W_I (Eq. (20))	V_I (Eq. (23))	RT_I (Eq. (24) or (25))
	Island aquifer	Strip (SII)	h_{SII} (Eq. (26))	v_{SII} (Eq. (27))	t_{SII} (Eq. (28))	W_{SII} (Eq. (29))	V_{SII} (Eq. (30))	RT_{SII} (Eq. (31))
		Circular (CII)	h_{CII} (Eq. (35))	v_{CII} (Eq. (38))	t_{CII} (Eq. (41))	W_{CII} (Eq. (42))	V_{CII} (Eq. (45))	RT_{CII} (Eq. (47))
Oceanic aquifers	Coastal aquifer	Seawater intrusion zone (SIZ)	H_{SIZ} (Eq. (56))	v_{SIZ} (Eq. (60))	t_{SIZ} (Eq. (63))	*NA*	V_{SIZ} (Eq. (70) or (71))	RT_{SIZ} (Eq. (79) or (80))
		Inland zone (IZ)	H_{IZ} (Eq. (59))	v_{IZ} (Eq. (61))	t_{IZ} (Eq. (65))	*NA*	V_{IZ} (Eq. (75) or (76))	RT_{IZ} (Eq. (81) or (82))
		Entire coastal aquifer (CA)	*NA*	*NA*	t_{CA} (Eq. (67))	*NA*	V_{CA} (Eq. (77) or (78))	RT_{CA} (Eq. (83) or (84))
	Island aquifer	Strip (SOI)	H_{SOI} (Eq. (90))	v_{SOI} (Eq. (95))	t_{SOI} (Eq. (99))	*NA*	V_{SOI} (Eq. (105))	RT_{SOI} (Eq. (109))
		Circular (COI)	H_{COI} (Eq. (94))	v_{COI} (Eq. (96))	t_{COI} (Eq. (102))	*NA*	V_{COI} (Eq. (108))	RT_{COI} (Eq. (110))

7.1.2 Impacts of Climate Change on Inland and Oceanic Dupuit-Type Aquifers

Table 2 summarizes the equations for assessing the impacts of climate change, including sea-level rise and coastal erosion, on oceanic aquifers.

Table 2 - Summary table of equations for investigating the impacts of climate change on oceanic unconfined Dupuit-type aquifers.

	Aquifer type		**Variation of the position of the saltwater toe**	**Variation of the position of the water table (coastal aquifers) or of the freshwater lens thickness (island aquifers)**	**Change of the ground-water velocity**	**Change of the ground-water travel time**	**Change of fresh ground-water volume**	**Change of ground-water mean residence time**	**Change in the aquifer total recharge**
Oceanic aquifers	Coastal aquifer	Sea-water intrusion zone (SIZ)		I_{SIZ} (Eq. (114), (115) or (116))	Δv_{SIZ} (Eq. (125) or (126))	Δt_{SIZ} (Eq. (129) or (130))	ΔV_{SIZ} (Eq. (135) or (136))	ΔRT_{SIZ} (Eq. (141) or (142))	*NA*
		Inland zone (IZ)	Δx_T (Eq. (122), (123) or (124))	I_{IZ} (Eq. (118), (119) or (120))	Δv_{IZ} (Eq. (127) or (128))	Δt_{IZ} (Eq. (131) or (132))	ΔV_{IZ} (Eq. (137) or (138))	ΔRT_{IZ} (Eq. (143) or (144))	*NA*
		Entire coastal aquifer (CA)		*NA*	*NA*	Δ_{CA} (Eq. (133) or (134))	ΔV_{CA} (Eq. (139) or (140))	ΔRT_{CA} (Eq. (145) or (146))	RE_{CA} (Eq. (147))
	Island aquifer	Strip (SOI)	*NA*	ΔH_{SOI} (Eq. (148) or (149))	Δv_{SOI} (Eq. (150) or (151))	Δt_{SOI} (Eq. (152) or (153))	ΔV_{SOI} (Eq. (154), (155) or (156))	ΔRT_{SOI} (Eq. (157) or (158))	RE_{SOI} (Eq. (159))
		Circular (COI)	*NA*	ΔH_{COI} (Eq. (160) or (161))	Δv_{COI} (Eq. (162) or (163))	Δt_{COI} (Eq. (164) or (165))	ΔV_{COI} (Eq. (166) or (167))	ΔRT_{COI} (Eq. (168) or (169))	RE_{COI} (Eq. (170))

7.2 Building the Spreadsheets for Solving the Equations

Several examples are shown for the different types of aquifers presented in Sections 3, 4, 5 and 6. The examples use the same flow system parameter values for the different aquifer types—inland, island, and coastal, and calculate several of the quantities listed in Table 1 and Table 2. The main results are presented in figures that illustrate how these quantities vary with distance in the aquifers. Excel spreadsheets that calculate the quantities and make the associated figures are available on the book page↗. These spreadsheets are each associated with a section of this book.

- *Section-3_Dupuit-type-inland-and-island-aquifers.xlsx*
- *Section-4_Dupuit-type-oceanic-coastal-aquifers.xlsx*
- *Section-5_Dupuit-type-oceanic-island-aquifers.xlsx*

- *Section-6_Climate-change_Coastal-oceanic-aquifers.xlsx*
- *Section-6_Climate-change_Island-oceanic-aquifers.xlsx*

7.2.1 Inland Aquifers (Referring to the Solutions Given in Section 3)

The example for inland aquifers refers to the conceptual model shown in Figure 6. For the calculations here, a value is assigned to L', the distance between the no-flow boundary and the constant head boundary. When applying the analytical equations to real aquifers, L' can be calculated as discussed following Figure 6, and requires first calculating x_{WD} using Equation (2).

Table 3 indicates the values used for the basic parameters of the inland aquifer taken for the example.

Table 3 - Parameters for the example of an inland aquifer.

W [mm/y]	W [m/s]	L' [m]	K [m/s]	n_e	x_i [m]	h_L [m]
500	1.59x10^{-8}	1,000	1 x10^{-4}	0.35	10	50

Hydraulic heads, groundwater velocity, and groundwater travel times of an inland Dupuit-type unconfined aquifer can be calculated using the Excel spreadsheet *Section-3_Dupuit-type-inland-and-island-aquifers.xlsx*. The results are shown in Figure 41, Figure 42 and Figure 43, using Equations (8), (9) and (19), respectively.

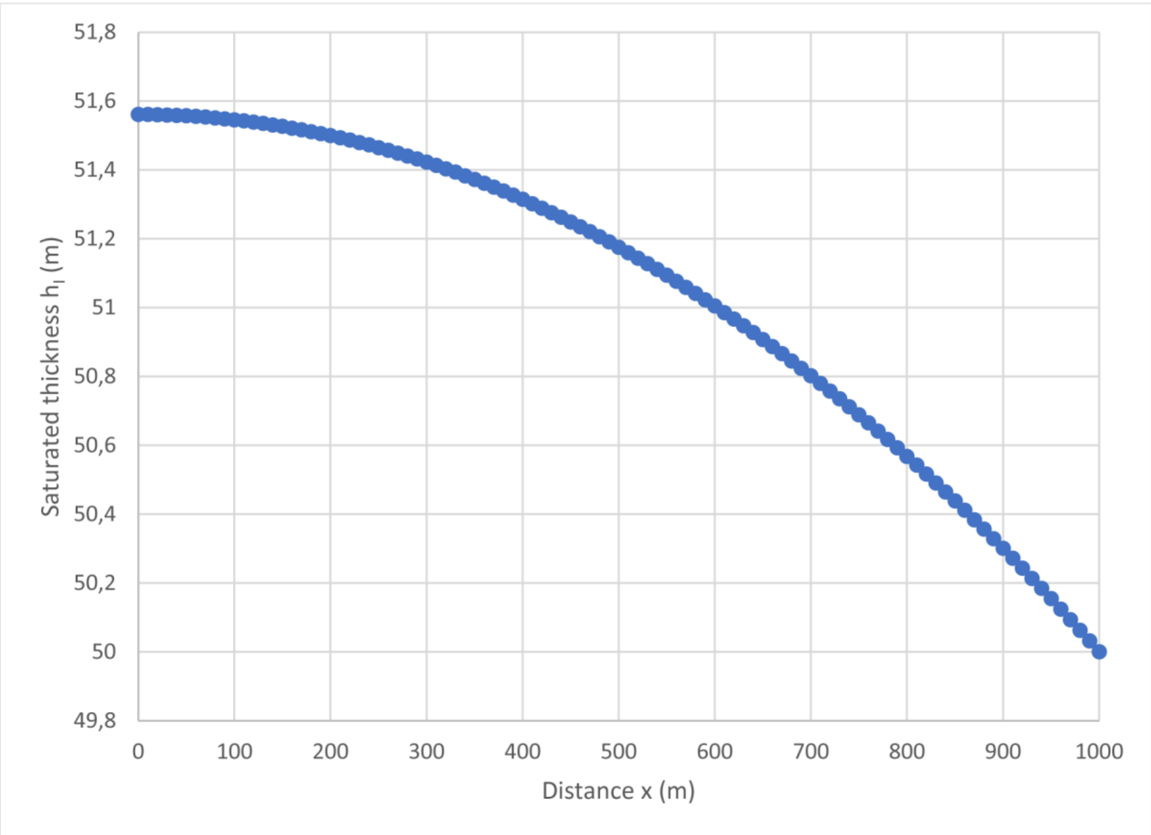

Figure 41 - Hydraulic head profile (saturated thickness) in an inland aquifer (Equation (8)).

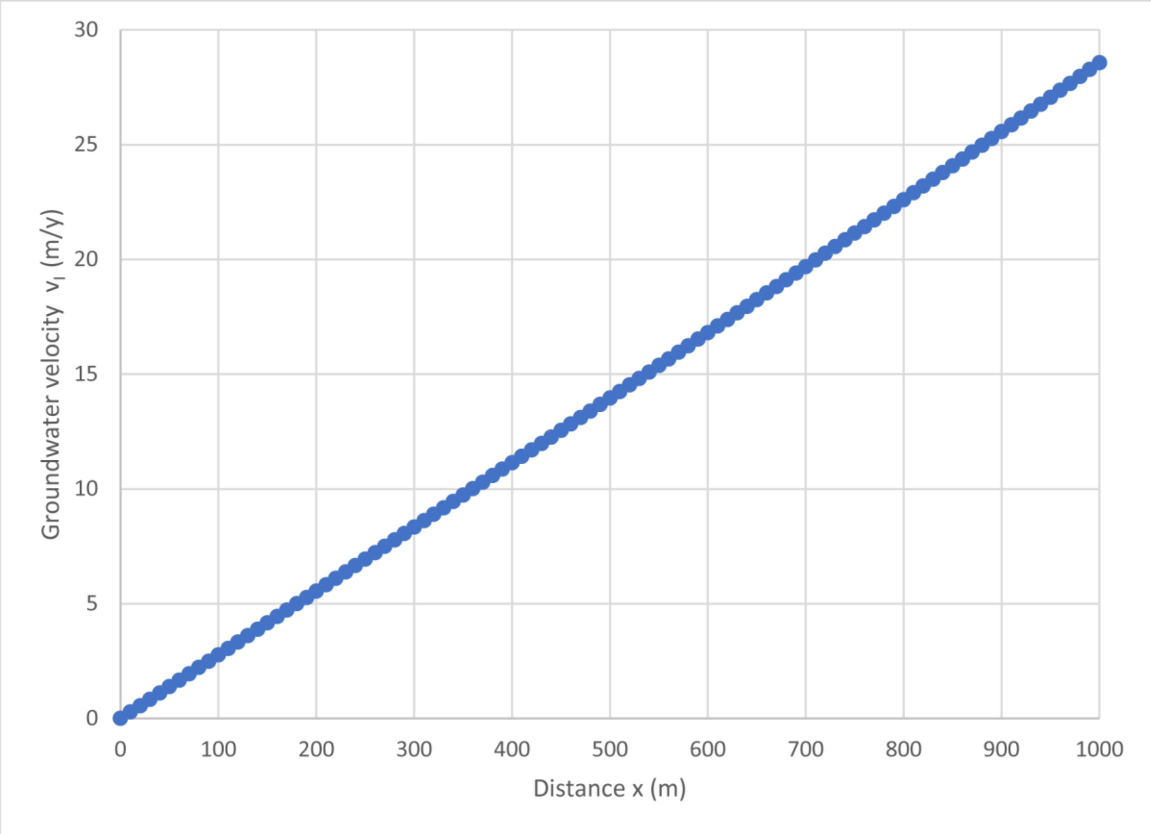

Figure 42 - Groundwater velocity profile in an inland aquifer (Equation (9)).

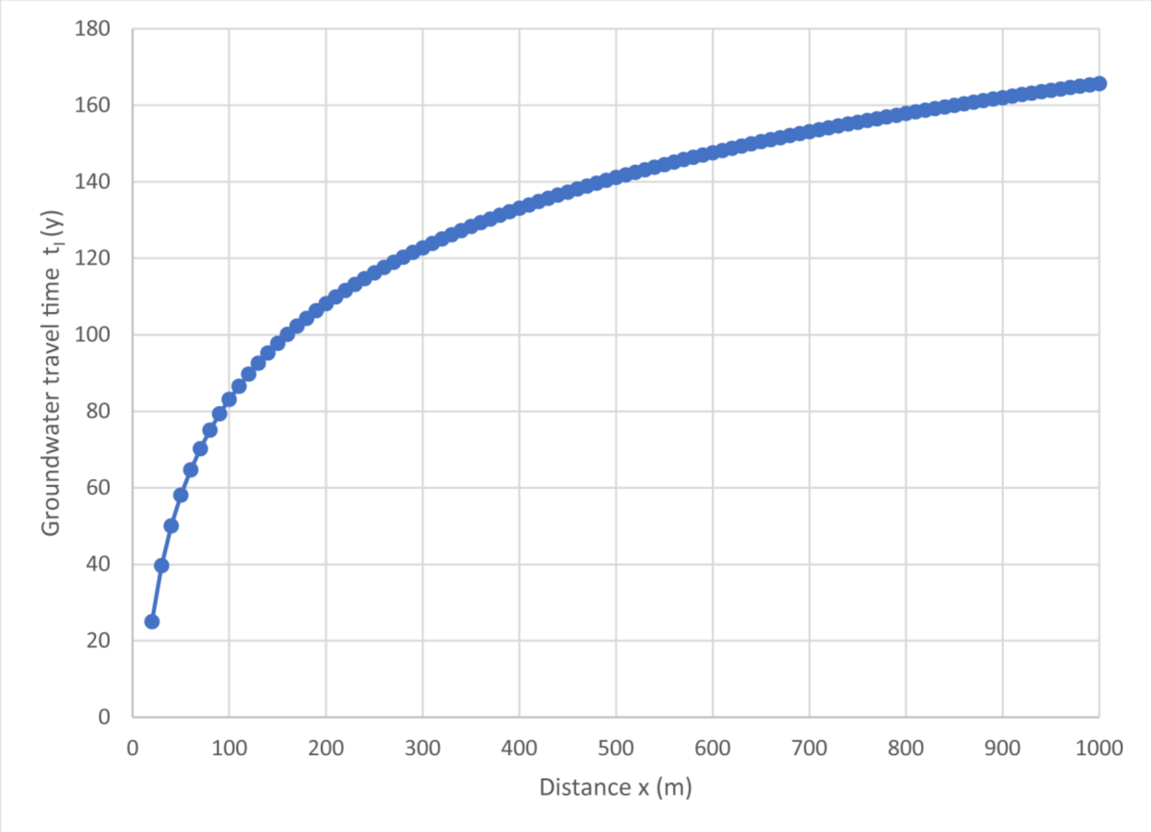

Figure 43 - Groundwater travel time of a particle of water departing from position x_i=10 m and arriving at position x in an inland aquifer (Equation (19)).

The hydraulic head profile presented in Figure 41 reflects the parabolic behavior as a function of distance as represented by Equation (8). The velocity profile (Figure 42) shows that the groundwater velocity increases when the particle gets closer to its discharge (downstream fixed-head boundary), and Figure 43 shows that the time to travel a given distance decreases accordingly (slope of the curve diminishing with distance x).

Table 4 presents the results for the calculation of the volume and residence time in the example inland aquifer. These quantities can also be calculated using the Excel spreadsheet *Section-3_Dupuit-type-inland-and-island-aquifers.xlsx*.

Table 4 - Volume and residence time in an inland aquifer.

V_I [m³/m] Eq. (23)	RT_I [s] Eq. (24)	RT_I [y] Eq. (24)
17,865	1.13x10^{-9}	36

The specific cases of inland-island (strip and circular) aquifers are not illustrated in this section because they are similar to the case of inland aquifers.

7.2.2 Coastal Oceanic Aquifers (Referring to the Solutions Given in Section 4)

The example for coastal oceanic aquifers refers to the conceptual model shown in Figure 17. A value is again assigned to L' for this example. When applying the analytical equations to real aquifers, L' can be calculated as discussed following Figure 17, with x_{WD} calculated using Equation (2).

Table 5 indicates the values used for the basic parameters of the example coastal oceanic aquifer.

Table 5 - Parameters for the example of a coastal oceanic aquifer. H_T=S (ρ_s/ρ_f).

W [mm/y]	W [m/s]	S [m]	L' [m]	K [m/s]	ρ_f	ρ_s	$\Delta\rho$	x_T [m] Eq. (57)	H_T [m]	n_e	x_i [m] for SIZ	x_i [m] for IZ
500	$1.59\text{x}10^{-8}$	50	1,000	$1\text{x}10^{-4}$	1	1.025	0.025	771.97	51.25	0.35	780	10

Freshwater saturated thickness, groundwater velocity and groundwater travel times of a coastal Dupuit-type unconfined aquifer can be calculated using the Excel spreadsheet *Section-4_Dupuit-type-oceanic-coastal-aquifers.xlsx*. Results are shown in Figure 44, Figure 45, Figure 46 and Figure 47, using Equations (56), (59), (60), (61), (63), (65) and (67). The results show that the behaviors of these different quantities are significantly different between the inland zone and the seawater intrusion zone.

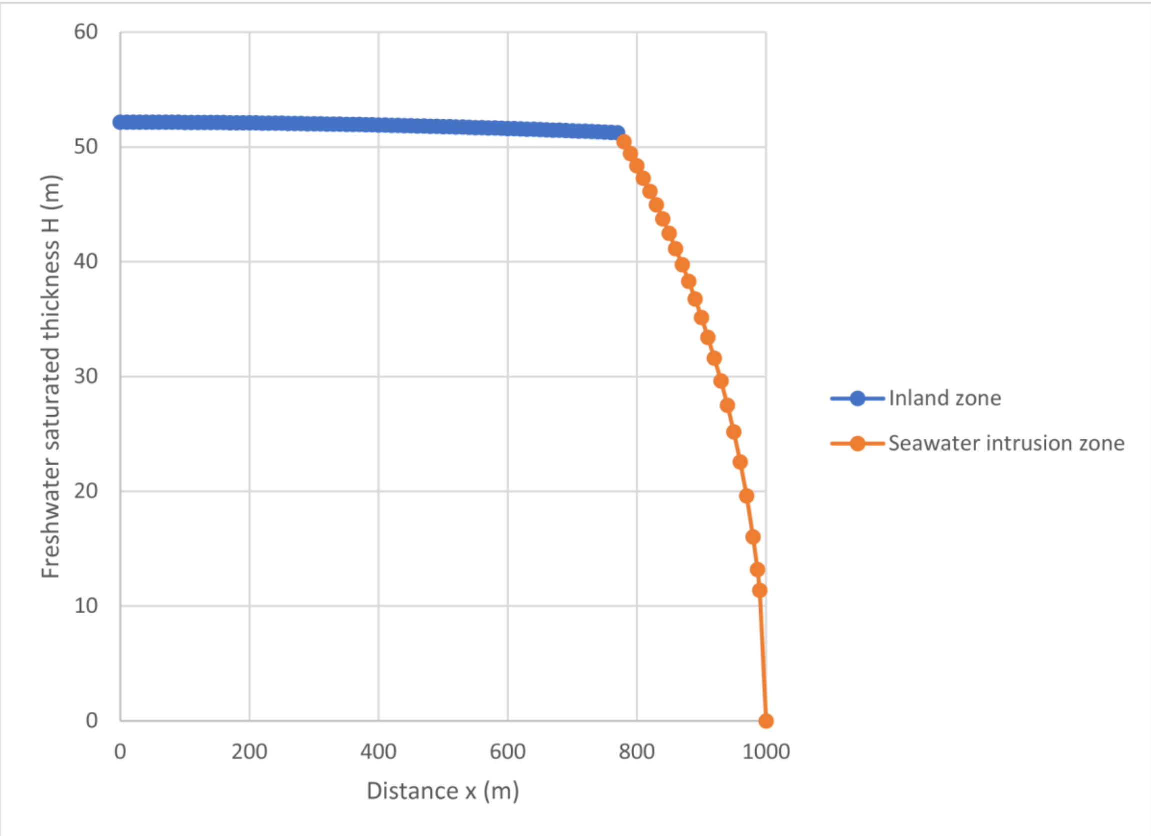

Figure 44 - Freshwater saturated thickness in a coastal aquifer (Equations (56) and (59)).

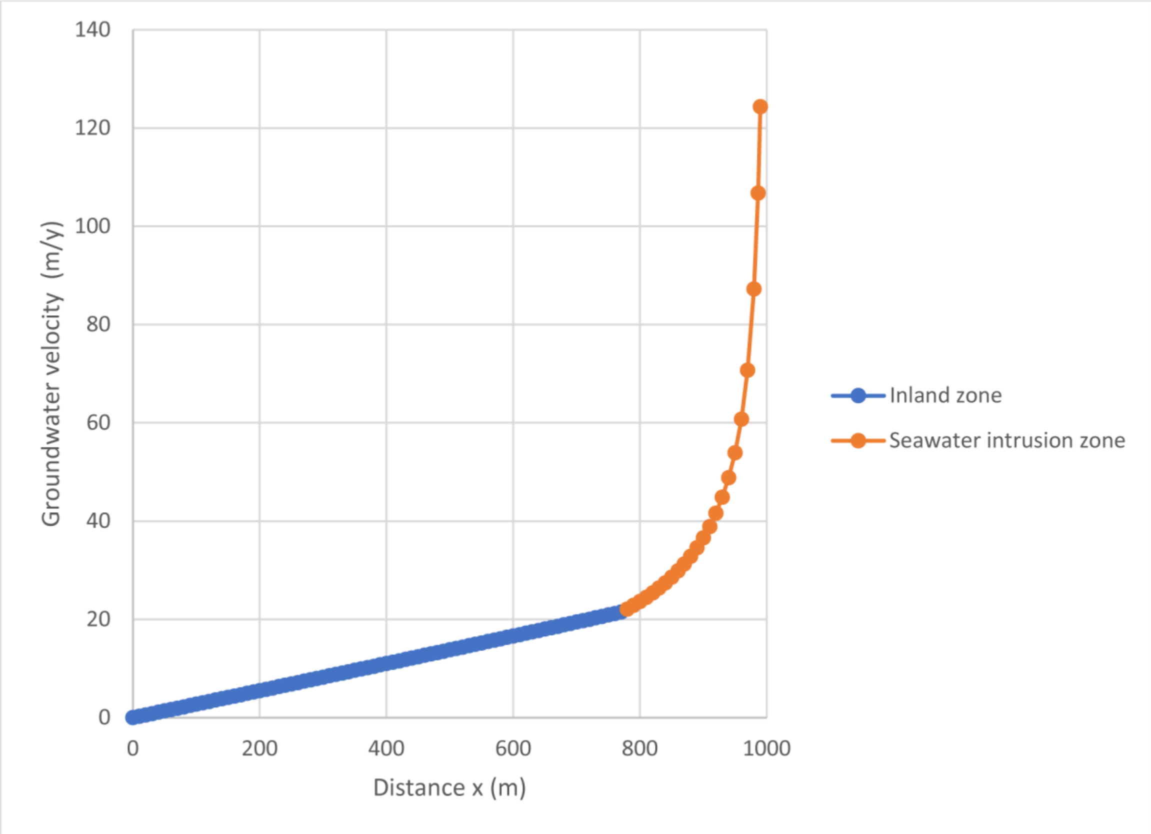

Figure 45 - Groundwater velocity profile in a coastal aquifer (Equations (60) and (61)).

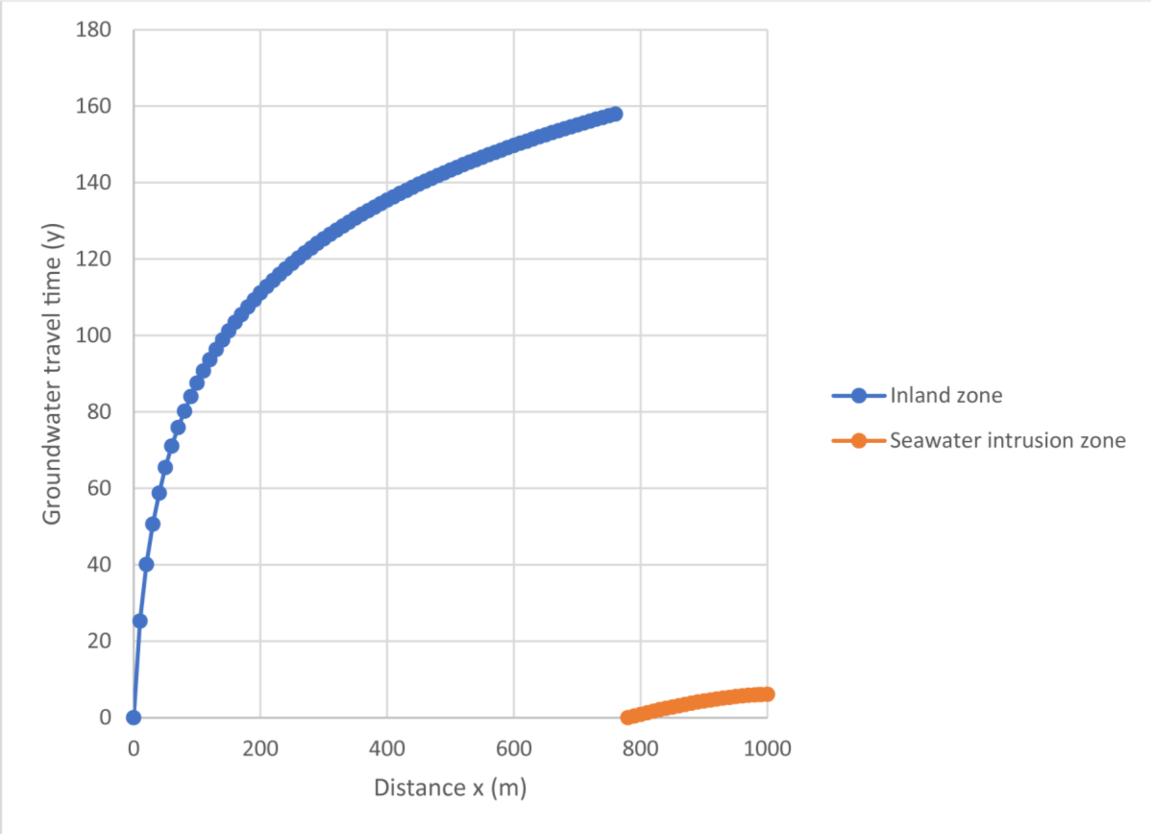

Figure 46 - Groundwater travel time of a particle of water departing from position x_i=10 m and arriving at position x in the inland zone and of another particle of water departing from x_i=780 m and arriving at position x in the seawater intrusion zone of a coastal aquifer (Equations (63) and (65).

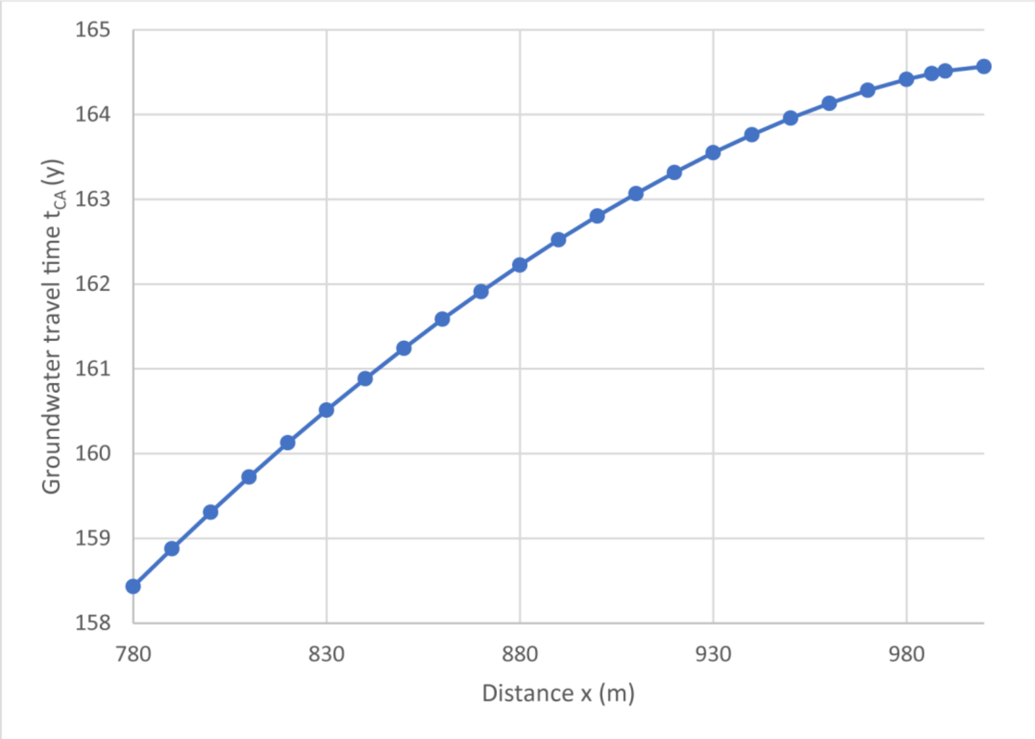

Figure 47 - Groundwater travel time within the seawater intrusion zone of a particle of water departing from position x_i=10 m in the inland aquifer and arriving at position x in the seawater intrusion zone of the coastal aquifer (Equation (67)).

Figure 44 shows the decrease of the freshwater thickness with distance x in the seawater intrusion zone due to the inland intrusion of saltwater. This decrease causes the groundwater velocity to increase along the flow path to the ocean (Figure 45), due to the reduction of the groundwater flow thickness near the ocean. In accordance with the increase of groundwater velocity, the time for a water particle to travel a given distance decreases as the particle moves closer to the ocean as shown in Figure 46 and Figure 47. Otherwise, the behaviors of the groundwater quantities in the inland zone are similar to what is observed for inland aquifers as described previously in Section 7.1.1.

Table 6 and Table 7 present respectively the results for the calculation of the freshwater volume and residence time in the example coastal aquifer. The Excel spreadsheet *Section-4_Dupuit-type-oceanic-coastal-aquifers.xlsx* shows these calculations.

Table 6 - Freshwater volumes per unit width of a coastal aquifer.

V_{SIZ} [m³/m] Eq. (70) or (71)	V_{IZ} [m³/m] Eq. (75) or (76)	V_{CA} [m³/m] Eq. (77) or (78)
2,796	14,213	17,009

Table 7 - Freshwater residence times in a coastal aquifer.

RT_{SIZ} [s] Eq. (79) or (80)	RT_{SIZ} [y] Eq. (79) or (80)	RT_{IZ} [s] Eq. (81) or (82)	RT_{IZ} [y] Eq. (81) or (82)	RT_{CA} [s] Eq. (83) or (84)	RT_{CA} [y] Eq. (83) or (84)
7.73 x10^{+8}	25	1.14 x10^{+9}	37	1.06 x10^{+9}	34

7.2.3 Oceanic Island Aquifers (Referring to the Solutions Given in Section 5)

The examples given in this section refer to the conceptual models presented in Figure 22 and Figure 23, representing a strip oceanic island and a circular oceanic island, respectively. Table 8 gives the values used for the basic parameters of the example oceanic island aquifers.

Table 8 - Parameters for the example of strip and circular oceanic island aquifers.

W [mm/y]	W [m/s]	L or R [m]	K [m/s]	ρ_f	ρ_s	$\Delta\rho$	n_e	x_i or r_i [m]
500	1.59×10^{-8}	1,000	1×10^{-4}	1	1.025	0.025	0.35	10

Freshwater saturated thickness, groundwater velocity and groundwater travel time of both strip and oceanic islands can be calculated using the Excel spreadsheet *Section-5_Dupuit-type-oceanic-island-aquifers.xlsx*. Results are shown in Figure 48, Figure 49 and Figure 50, using Equations (90), (94), (95), (96), (99), and (102).

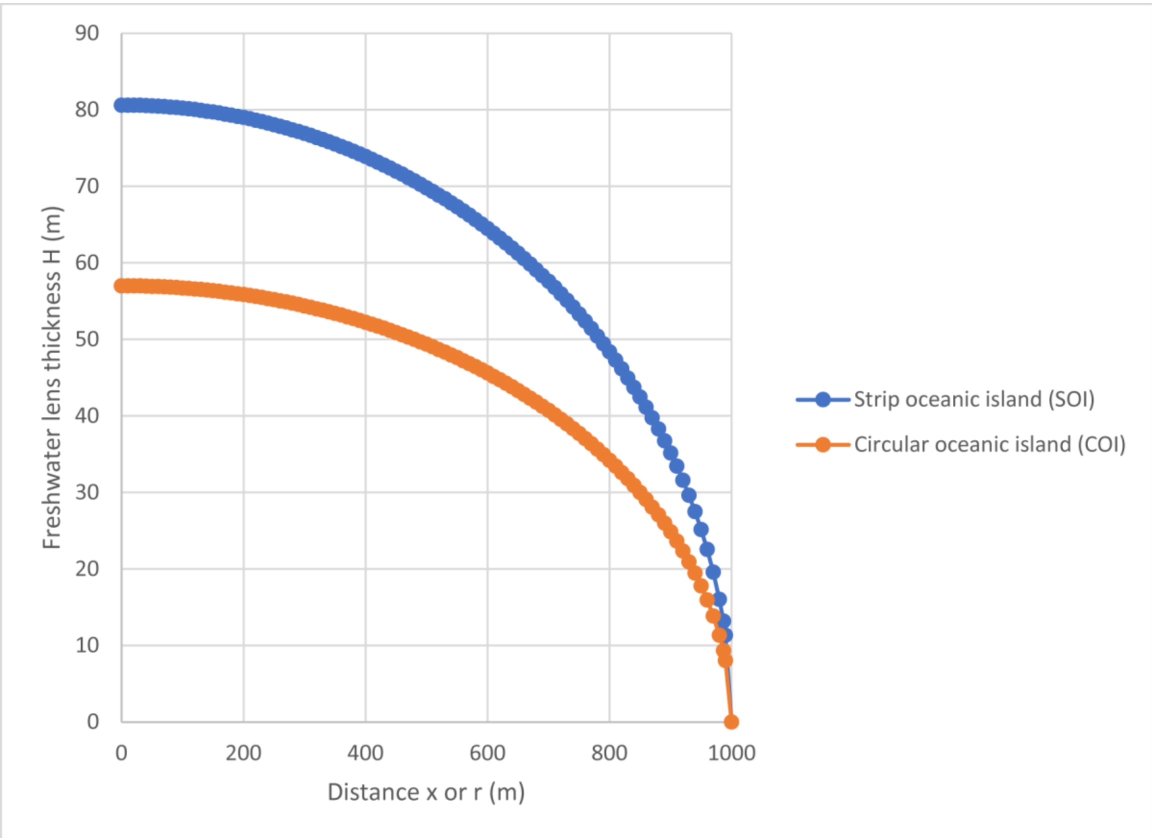

Figure 48 - Freshwater lens thickness in a strip and a circular oceanic island (Equations (90) and (94)).

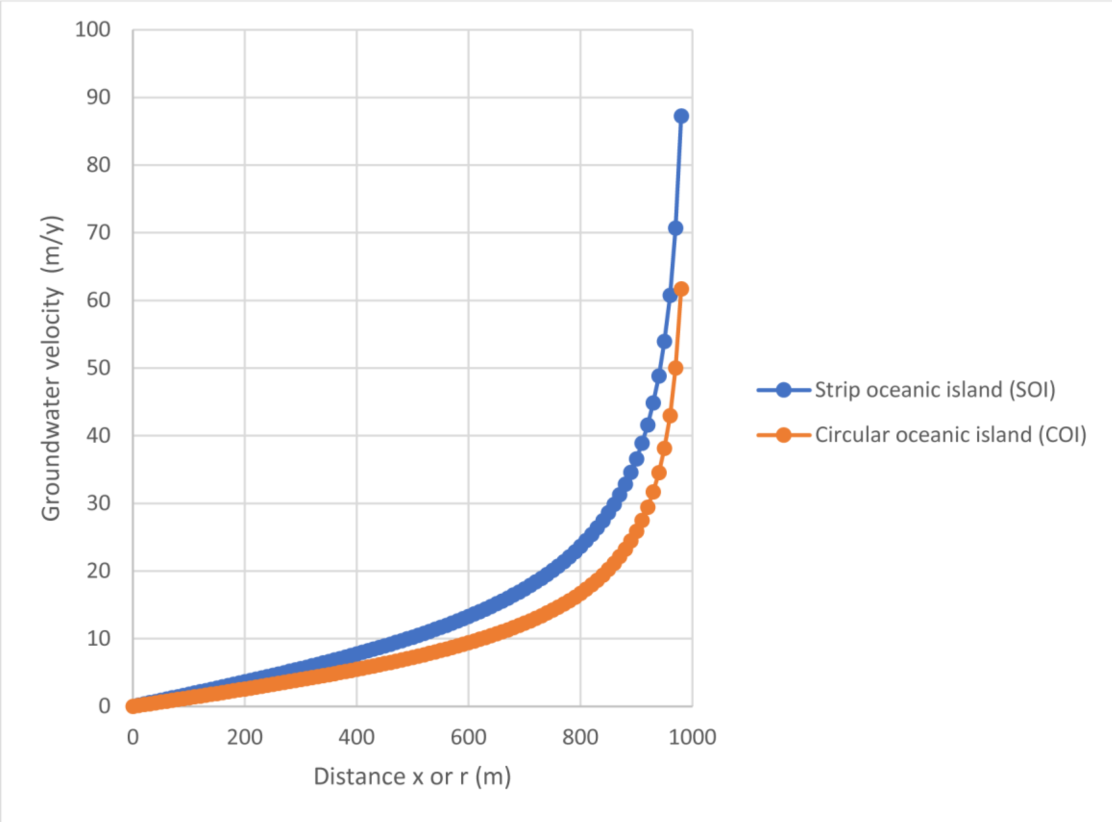

Figure 49 - Groundwater velocities in the freshwater lenses of a strip and a circular oceanic island (Equations (95) and (96)).

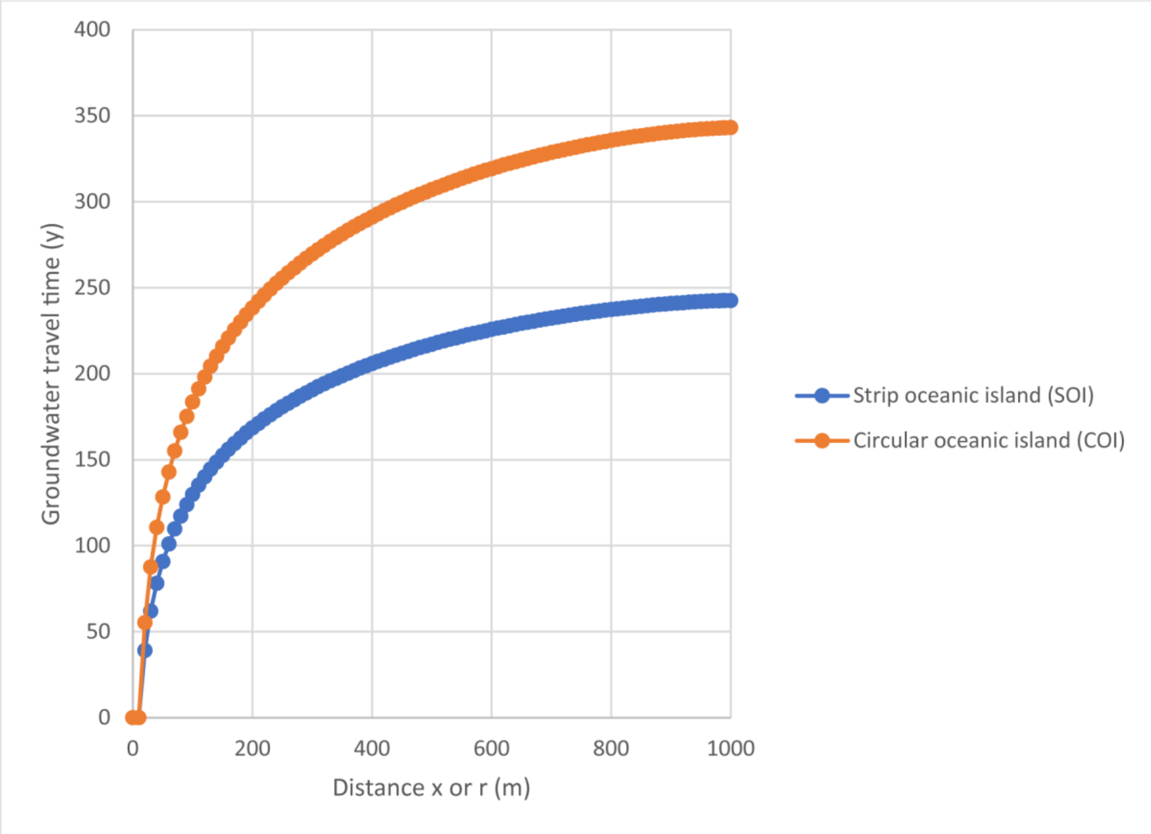

Figure 50 - Groundwater travel times in the freshwater lenses of a strip and a circular oceanic island for a particle of water departing from position x_i or r_i (10 m in the present case) and arriving at position x or r (Equations (99) and (102)).

Figure 48 shows that the freshwater lens thickness is larger in the strip oceanic island than in the circular oceanic island. This is due to the difference in geometry considering that the circular island is surrounded by saltwater, which favors the extent of the saltwater intrusion compared with the strip island which only offers two shore sides for the saltwater intrusion. The groundwater velocity is higher in the strip oceanic island than in the circular oceanic island (Figure 49) making groundwater travel time shorter (Figure 50).

Table 9 and Table 10 present respectively the results for the calculation of the freshwater volume and residence time in both strip and circular example oceanic islands. The Excel spreadsheet *Section-5_Dupuit-type-oceanic-island-aquifers.xlsx* shows these calculations.

Table 9 - Freshwater volumes of the lenses in a strip and circular oceanic island.

V_{SOI} [m^3/m] Eq. (105)	V_{COI} [m^3] Eq. (108)
44,326	41,791,243

Table 10 - Freshwater residence times in a strip and circular oceanic island.

RT_{SOI} [s] Eq. (109)	RT_{SOI} [y] Eq. (109)	RT_{COI} [s] Eq. (110)	RT_{COI} [y] Eq. (110)
$2.80\times10^{+9}$	89	$8.39\times10^{+8}$	27

7.2.4 Impacts of Climate Change (Referring to the Solutions Given in Section 6)

Coastal oceanic aquifers

The example given in this section refers to the conceptual model presented in Figure 30. Table 11 gives the values used for the basic parameters of the coastal oceanic aquifer affected by climate change.

Table 11 - Parameters for the example of a coastal oceanic aquifer.

W [mm/y]	W [m/s]	S_0 [m]	S_t [m]	ΔS [m]	L_0 [m]	L_t [m]	ΔL_{SR} [m]	ΔL_{CE} [m]	ΔL [m]	K [m/s]	Slope tanθ [m/m]
500	1.59×10^{-8}	50	50.5	0.5	1,000	986.5	12.5	1	-13.5	1×10^{-4}	0.04

ρ_f	ρ_s	$\Delta\rho$	x_{T0} [m] Eq. (57)	x_{Tt} [m] Eq. (57)	Δx_T [m] Eq. (122)	n_e	x_i [m] for SIZ	x_i [m] for IZ
1	1.025	0.025	771.97	749.00	-22.97	0.35	780	10

The effects of climate change on the water table elevation, groundwater velocity and groundwater travel times of the example coastal aquifer can be calculated using the spreadsheet *Section-6_Climate-change_Coastal-oceanic-aquifers.xlsx*. Results are shown in Figure 51, Figure 52, Figure 53 and Figure 54, using Equations (114), (118), (125), (127), (129), (131) and (133).

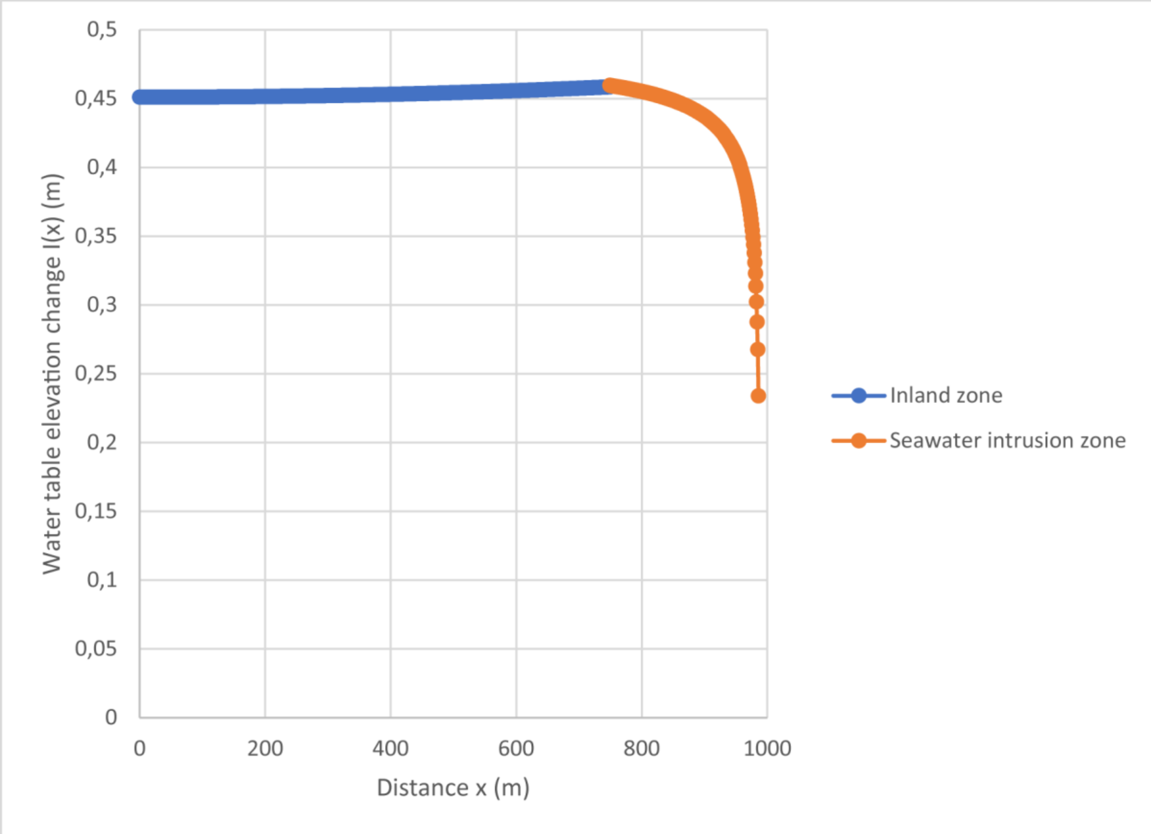

Figure 51 - Water table elevation change with land-surface inundation in a coastal aquifer (Equations (114) and (118)).

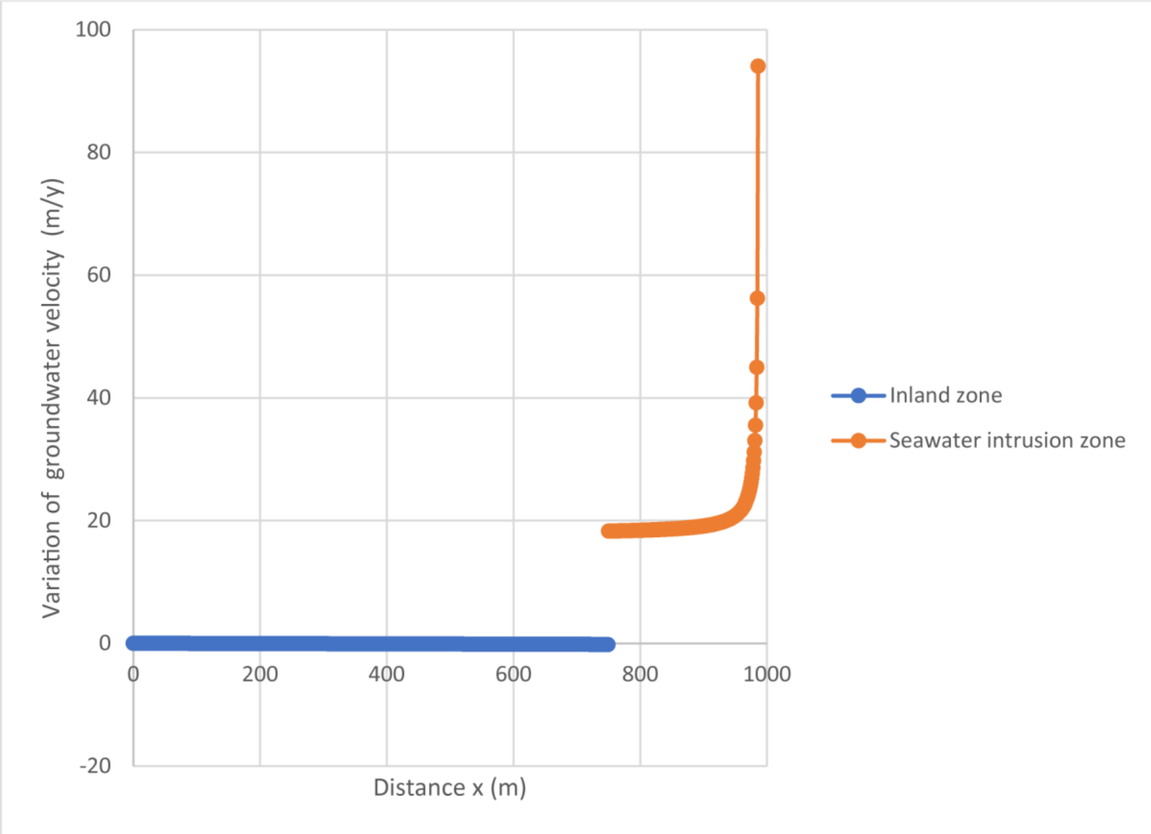

Figure 52 - Groundwater velocity profile changes with land-surface inundation in a coastal aquifer (Equations (125) and (127)).

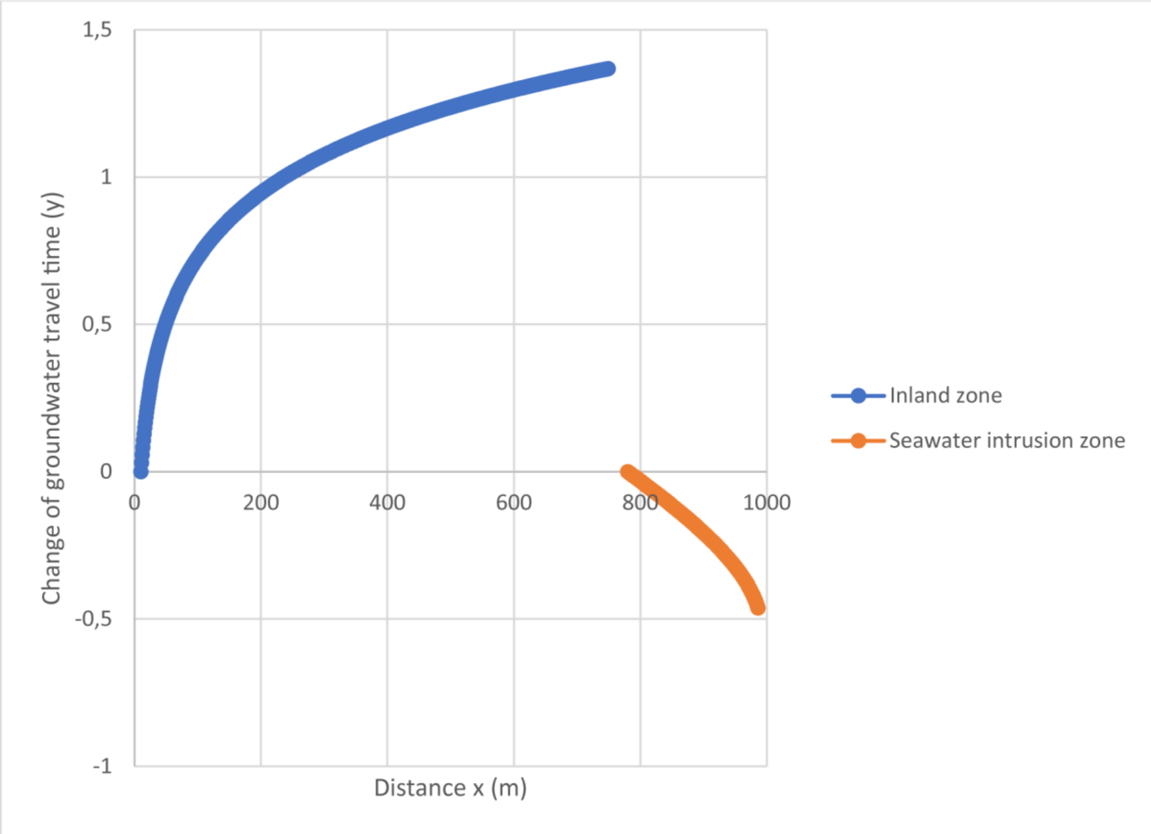

Figure 53 - Groundwater travel time changes with land-surface inundation of a particle of water departing from position x_i=10 m and arriving at position x in the inland zone and of another particle of water departing from x_i=780 m and arriving at position x in the seawater intrusion zone of a coastal aquifer (Equations (129) and (131)).

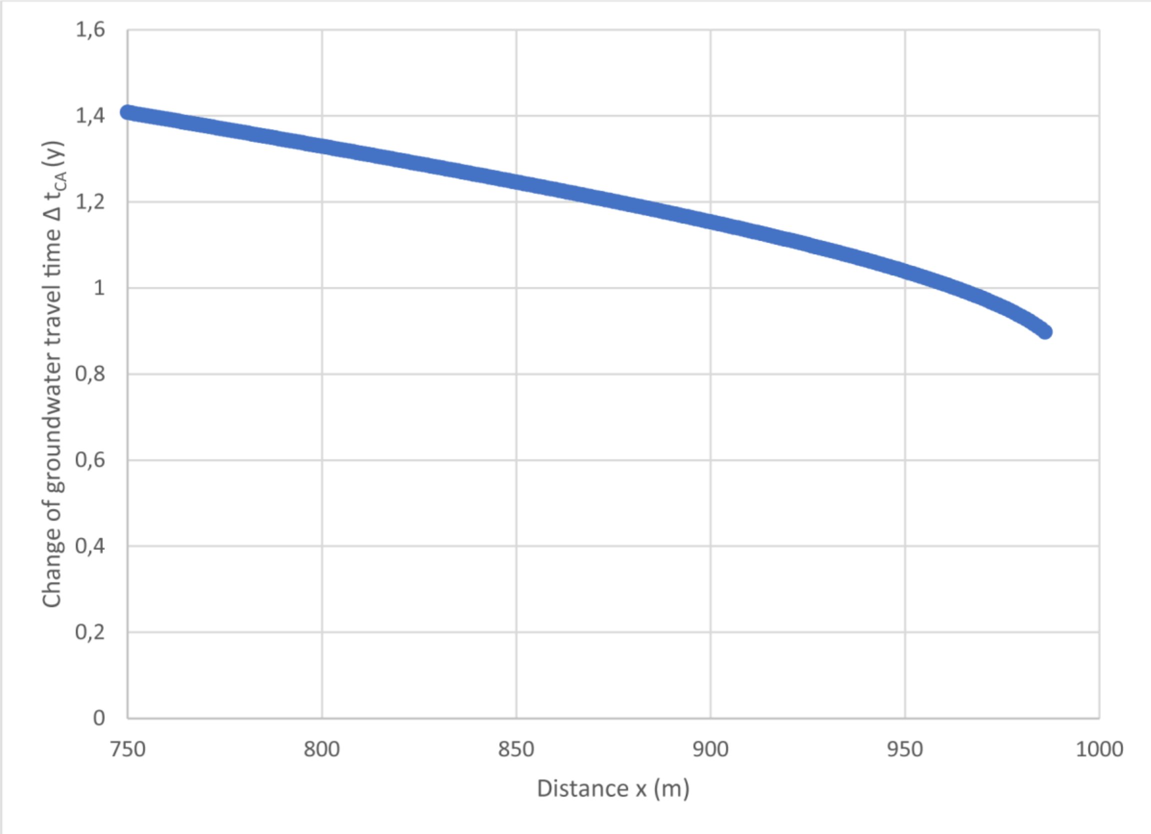

Figure 54 - Groundwater travel time changes with land-surface inundation of a particle of water departing from position x_i=10 m in the inland zone of the coastal aquifer and arriving at position x in the seawater intrusion zone of the coastal aquifer (Equation (133)).

The water table elevation change with land-surface inundation in the coastal aquifer is positive (rise of the water table) and the change is larger in the inland zone than in the seawater intrusion zone (Figure 51). In the seawater intrusion zone, the rise of the water table diminishes with distance, as x approaches the sea shore (Figure 51). The groundwater velocity does not vary significantly in the inland zone whereas it increases with distance, x, in the seawater intrusion zone with the maximum increase at the ocean (Figure 52). Figure 53 shows that the change in groundwater travel time with distance is reversed in the inland and seawater intrusion zones as illustrated by the example of travel times of a water particle departing from one position, x_i, in both zones. Indeed, the groundwater travel time increases in the inland zone (positive change) as the particle migrates toward the ocean whereas it diminishes in the seawater intrusion zone (negative change). Finally, Figure 54 shows that the overall change of groundwater travel time for a particle of water departing from the inland zone and arriving in the seawater intrusion zone is small compared to the initial travel time (before land-surface inundation) in the specific example considered. Indeed, the change is on the order of one to two years whereas Figure 47 shows that for initial conditions (before land surface inundation) the groundwater travel time varied from 150 years to 165 years.

Table 12 and Table 13 present respectively the results for the calculation of the effects of climate change on the volume and residence time the costal aquifer.

Table 12 - Changes of freshwater volumes with land-surface inundation in a coastal aquifer.

ΔV_{SIZ} [m³/m] Eq. (135)	ΔV_{IZ} [m³/m] Eq. (137)	ΔV_{CA} [m³/m] Eq. (139)
149.76 (increase of 5.35%)	-293.39 (decrease of 1.68%)	-143.63 (decrease of 0.08%)

Table 13 - Changes of residence times with land-surface inundation in a coastal aquifer.

ΔRT_{SIZ} [s] Eq. (141)	ΔRT_{SIZ} [y] Eq. (141)	ΔRT_{IZ} [s] Eq. (143)	ΔRT_{IZ} [y] Eq. (143)	ΔRT_{CA} [s] Eq. (145)	ΔRT_{CA} [y] Eq. (145)
$8.93 \times 10^{+6}$	0.28 (increase of 1.12%)	$1.04 \times 10^{+7}$	0.33 (increase of 0.89%)	$5.32 \times 10^{+6}$	0.17 (increase of 0.50%)

An overall decrease of groundwater volume in the coastal aquifer is observed. However, the situation in the inland zone and the seawater intrusion zone is not the same: the groundwater volume in the inland zone decreases, whereas the groundwater volume in the seawater intrusion zone increases. This opposing situation is explained by the fact that the inland progression of the saltwater toe ($\Delta x_T = -22.97$ m) is greater than the inland progression of land-surface inundation (ΔL=-13.5 m). This difference makes the volume of the inland zone decrease while the volume of the seawater intrusion zone increases.

An increase of the mean residence time (ΔRT_{IZ} is positive) is observed in the inland zone, although there is a decrease of groundwater volume (ΔV_{IZ} is negative) in this zone. An opposite observation would have been expected considering the mean residence time is proportional to the volume. However, the mean residence time is also inversely proportional to the flow rate. The decrease of the groundwater flow rate in the inland zone is large enough to compensate for the decrease in volume of this zone, and causes the mean residence time to increase.

Oceanic island aquifers

The examples given in this section refer to the conceptual models presented in Figure 37 and Figure 38, representing a strip oceanic island and a circular oceanic island, respectively. Table 14 gives the values used for the basic parameters of the oceanic island aquifers (strip and circular) undertaking climate change.

Table 14 - Parameters for the example of strip and circular oceanic island aquifers.

W [mm/y]	W [m/s]	S_0 [m]	S_t [m]	ΔS [m]	L_0 or R_0 [m]	L_t or R_t [m]	ΔL_{SR} [m]	ΔL_{CE} [m]	ΔL [m]	K [m/s]	Slope $\tan\theta$ [m/m]
500	1.59×10^{-8}	50	50.5	0.5	1,000	986.5	12.5	1	-13.5	1×10^{-4}	0.04

ρ_f	ρ_s	$\Delta\rho$	n_e	x_i or r_i [m]
1	1.025	0.025	0.35	10

The effects of climate change on freshwater lens saturated thickness, groundwater velocity, and groundwater travel time of both a strip and oceanic islands can be calculated using the spreadsheet *Section-6_Climate-change_Island-oceanic-aquifers.xlsx*. Results are presented in Figure 55, Figure 56 and Figure 57, using Equations (148), (160), (154), (162), (152), and (164).

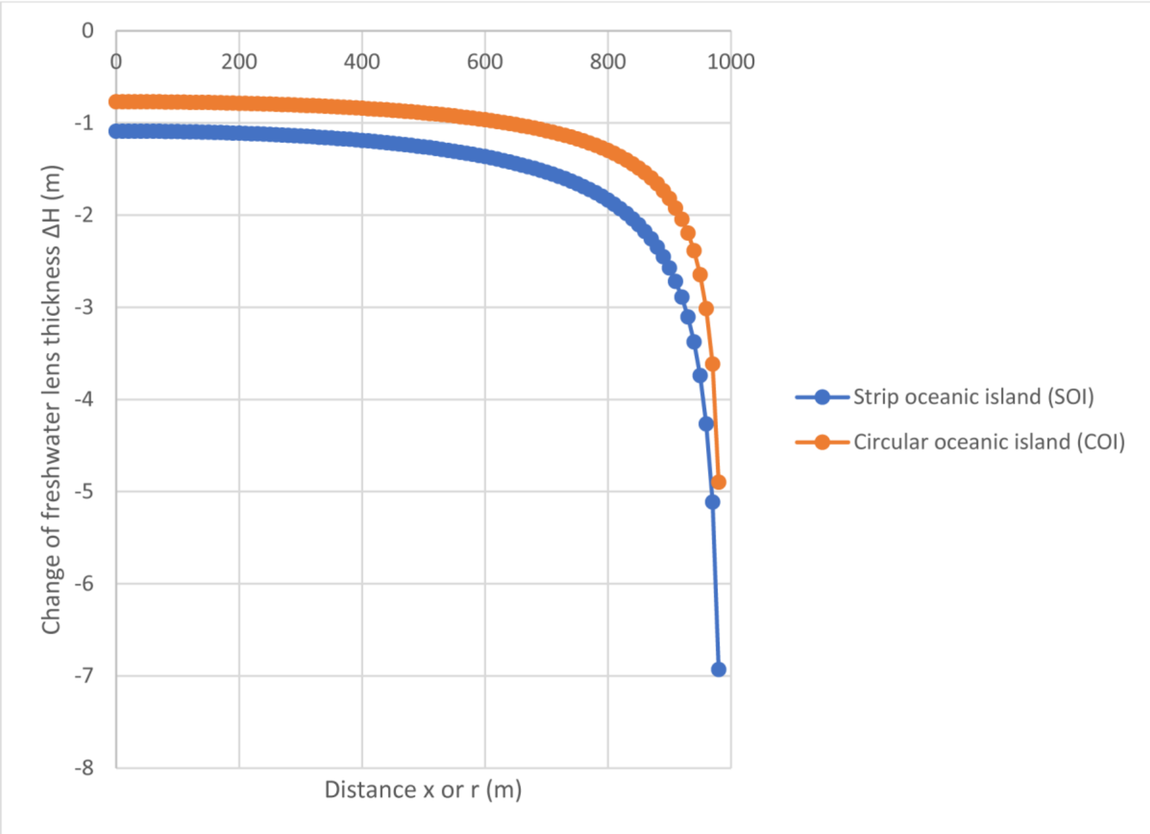

Figure 55 - Freshwater lens thickness changes with land-surface inundation in a strip and circular oceanic island (Equations (148) and (160)).

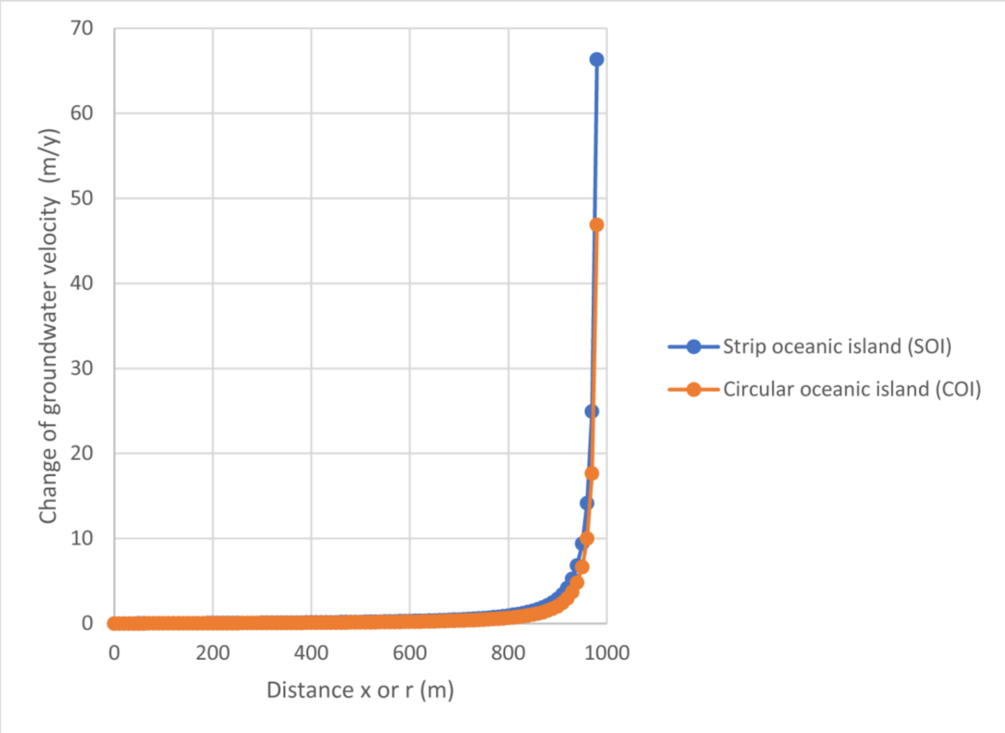

Figure 56 - Groundwater velocity changes in the freshwater lenses of a strip and circular oceanic island with land-surface inundation (Equations (154) and (162)).

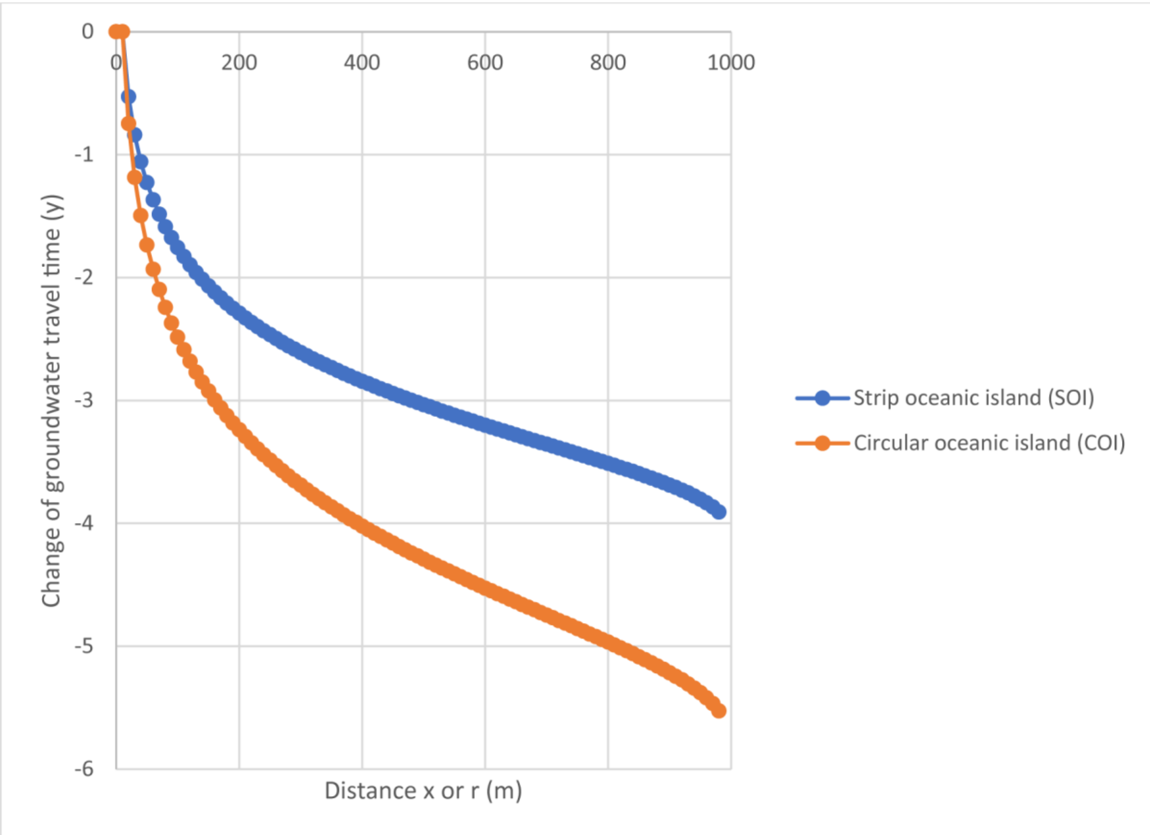

Figure 57 - Groundwater travel times changes in the freshwater lenses of a strip and circular oceanic island for a particle of water departing from position x_i or r_i and arriving at position x or r with land-surface inundation (Equations (152) and (164)).

Figure 55 shows that the change of the thickness of the freshwater lens is negative in both cases (i.e., strip and circular oceanic islands) meaning that the freshwater thickness diminishes with land-surface inundation. Consequently, the groundwater velocity increases in both cases as shown in Figure 56, thus groundwater travel time diminishes (Figure 57).

Table 15 and Table 16 respectively present the results for the calculation of the changes of the volume and residence time in both strip and circular oceanic islands taken as examples.

Table 15 - Freshwater volume changes of lenses in strip and circular oceanic islands with land-surface inundation.

ΔV_{SOI} [m^3/m] Eq. (154)	ΔV_{COI} [m^3] Eq. (166)
-1,189 (decrease of 2.7 %)	-1,669,799 (decrease of 4.0%)

Table 16 - Freshwater residence time changes of the lenses in a strip and circular oceanic island with land-surface inundation.

ΔRT_{SOI} [s] Eq. (157)	ΔRT_{SOI} [y] Eq. (157)	ΔRT_{COI} [s] Eq. (168)	ΔRT_{COI} [y] Eq. (168)
$-3.77 \times 10^{+7}$	-1.20 (decrease of 1.35%)	$-1.13 \times 10^{+7}$	-0.36 (decrease of 1.35%)

8 Wrap-Up/Conclusion

Analytical solutions have proven to be efficient in solving a broad spectrum of groundwater problems by considering simplified groundwater flow models based on simplified assumptions. The user is required to first determine if an analytical solution may be applied to a specific situation to be resolved. When possible, in hydrogeology, it is always recommended to verify the results obtained using one tool with the results that can be obtained using another, different tool. Verifying a solution obtained analytically against a result obtained from numerical modeling, when applied to the same problem, is a very enriching scientific exercise. The comparison is not mandatory but it is recommended, when possible, to provide credibility, confirmation, confidence, or perspective when analyzing results.

Analytical solutions retain an important place in hydrogeology and there is still room today for developing or extending new analytical or semi-analytical solutions. Hydrogeologists are encouraged to use analytical tools more extensively despite the availability of advanced computerized tools, not only because they are easy to access and use at lower cost but also because the application of analytical solutions requires a good understanding of the physical bases of groundwater flow systems.

It is critical for hydrogeologists to better understand how aquifer and climate parameters affect groundwater levels, total recharge, groundwater velocity, travel time, residence time, and freshwater volume. Hydrogeologists are active participants in society's complex adaptations to climate change. They are often required to determine the impacts of these changes on groundwater resources, not only in inland aquifers but also in coastal and island aquifers. This book has been designed to provide a wide range of analytical tools that contribute to scientific understanding, qualification, and quantification of hydrogeological phenomena.

9 References

Bear, J. (1972). *Dynamics of fluids in porous media.* Dover Publications, Inc.

Chesnaux, R. (2013). Regional recharge assessment in the crystalline bedrock aquifer of the Kenogami Uplands, Canada. *Hydrological Sciences Journal*, *58*(2), 421–436. https://doi.org/10.1080/02626667.2012.754100↗.

Chesnaux, R. (2015). Closed-form analytical solutions for assessing the consequences of sea-level rise on groundwater resources in sloping coastal aquifers. *Hydrogeology Journal, 23*(7), 1399–1413. https://doi.org/10.1007/s10040-015-1276-8↗.

Chesnaux, R. (2016). Closed-form analytical solutions for assessing the consequences of sea-level rise on unconfined sloping island aquifers. *Global & Planetary Change,* 139, 109–115. https://doi.org/10.1016/j.gloplacha.2016.01.005↗.

Chesnaux, R., & Allen, D.M. (2008). Ground water travel times for unconfined aquifers bounded by freshwater or seawater. *Hydrogeology Journal*, *16*(3), 437-445. https://doi.org/10.1007/s10040-007-0241-6↗.

Chesnaux, R., Marion, D., Boumaiza, L., Richard, S. & Walter, J. (2021). An analytical methodology to estimate the changes of fresh groundwater resources with sea-level rise and coastal erosion in strip island unconfined aquifers: illustration with Savary Island, Canada. *Hydrogeology Journal, 29*, 1355–1364. https://doi.org/10.1007/s10040-020-02300-0↗.

Chesnaux, R., Molson, J. W., & Chapuis, R. P. (2005). An analytical solution for ground water transit time through unconfined aquifers. *Groundwater, 43*(4), 511–517. https://doi.org/10.1111/j.1745-6584.2005.0056.x↗.

Chesnaux, R., Santoni, S., Garel, E., & Huneau, F. (2018). An analytical method for assessing recharge using groundwater travel time in Dupuit flow aquifers. *Groundwater*, *56*(6), 986–992. https://doi.org/10.1111/gwat.12794↗.

Drabbe, J., & Badon Ghijben, W. (1889). Nota in verband met de voorgenomen putboring nabij Amsterdam [Note in connection with the proposed wellbore near Amsterdam]. *Tijdschrift van het Koninklijk Instituut Van Ingenieurs 1888–1889*, 8–22.

Dupuit, J. (1863). *Études Théoriques et Pratiques sur le Mouvement des Eaux dans les Canaux Découverts et à Travers les Terrains Perméables* [Theoretical and practical studies on water movement in open canals and through permeable ground] (2nd ed., pp. 229–293). Dunod.

Ferguson, G., & Gleeson, T. (2012). Vulnerability of coastal aquifers to groundwater use and climate change. *Nature Climate Change 2*, 342–345. https://doi.org/10.1038/nclimate1413↗.

Fetter, C. W., Jr. (1972). Position of the saline water interface beneath oceanic islands. *Water Resources Research*, *8*(5), 1307–1315. https://doi.org/10.1029/WR008i005p01307↗.

Forchheimer, P. (1886). Über die Ergiebichkeit von Brunnen-Anlagen und Sickerschlitzen [On the yield of well systems and drainage ditches]. *Zeitschrift des Architectenund Ingenieurs Vereins zu Hannover*, *32*, 539–564.

Forchheimer, P. (1901). Wasserbewegung durch Boden [Water movement through soil]. *Zeitschrift des Vereines Deutscher Ingenieure*, *45*(50), 1781–1788.

Glass, J. Jain, R., Junghanns, R., Salley, J., Fichtner, T., & Stefan, C. (2018). Web-based tool compilation of analytical equations for groundwater management applications. *Environmental Modelling & Software*, *108*, 1–7. https://doi.org/10.1016/j.envsoft.2018.07.008↗.

Guo, H., & Jiao, J. J. (2007). Impact of coastal land reclamation on ground water level and the seawater interface. *Groundwater*, *45*(3), 362–367. https://doi.org/10.1111/j.1745-6584.2006.00290.x↗.

Haitjema, H. M. (1995). *Analytical element modeling of groundwater flow*. Academic Press.

Haitjema, H. M. (2006). The role of hand calculations in ground water flow modeling. *Groundwater*, *44*(6), 786–791. https://doi.org/10.1111/j.1745-6584.2006.00189.x↗.

Haitjema, H. M., & Mitchell-Bruker, S. (2005). Are water-tables a subdued replica of the topography? *Groundwater* *43*(6), 781–786. https://doi.org/10.1111/j.1745-6584.2005.00090.x↗.

Herzberg, A. (1901). Die Wasserversorgung einiger Nordseebaden [The water supply of the North Sea baths]. *Zeitung Gasbeleuchtung und Wasserversorgung* [Journal of gas lighting and water supply], *44*, 815–819.

INOWAS. (2018). *T9: Simple saltwater intrusion equations*. https://www.inowas.com/tools/t09-simple-saltwater-intrusion-equations/↗. *T13. Travel time through unconfined aquifer*. https://www.inowas.com/tools/t13-travel-time-through-unconfined-aquifer/↗.

Jiao, J. J., & Post, V. (2019). *Coastal hydrogeology*. Cambridge University Press.

Kirkham, D. (1967). Explanation of paradoxes in Dupuit-Forchheimer seepage theory. *Water Resources Research*, 3, 609–622. https://doi.org/10.1029/WR003i002p00609↗.

Lemieux, J-M., Hassaoui, J., Molson, J., Therrien, R., Therrien, P., Chouteau, M., & Ouellet, M. (2015). Simulating the impact of climate change on the groundwater resources of the Magdalen Islands, Québec, Canada. *Journal of Hydrology: Regional Studies*, *3*, 400–423. https://doi.org/10.1016/j.ejrh.2015.02.011↗.

Miled, C., Chesnaux, R., Walter, J., Boumaiza, L., & Paré, M. (2023). Multi-technique approach for estimating groundwater transit time through the saturated zone of an unconfined granular aquifer. *Hydrogeology Journal*, *31*, 1847–1861. https://doi.org/10.1007/s10040-023-02663-0↗.

NASA. (n.d). Sea level change, observations from space. Retrieved on May 2025 from https://sealevel.nasa.gov/↗.

Parmesan, C., Morecroft, M. D., Trisurat, Y., & Mezzi, D. (2022) *Climate Change 2022:Impacts, Adaptation and Vulnerability*. [Research Report] GIEC; IPCC. 2022. https://hal.science/hal-03774939v1↗.

Poeter, E. (2007). All models are wrong, how do you know which are useful? *Groundwater 45*(4), 390–391. https://doi.org/10.1111/j.1745-6584.2007.00350.x↗.

Strack, O. D. L. (1989). *Groundwater Mechanics.* Prentice Hall.

10 Exercises

To complete these exercises, spreadsheets with the relevant equations from this book can be developed. Alternatively, for exercises 2 to 6, the equations are available in the following spreadsheets: *Section-3_Dupuit-type-inland-and-island-aquifers.xlsx*, *Section-4_Dupuit-type-oceanic-coastal-aquifers.xlsx*, *Section-5_Dupuit-type-oceanic-island-aquifers.xlsx*, *Section-6_Climate-change_Coastal-oceanic-aquifers.xlsx*, and *Section-6_Climate-change_Island-oceanic-aquifers.xlsx*. These spreadsheets are available on the book page↗. Saving the downloaded spreadsheets under different names than the originals is recommended. This allows original copies to be maintained while working in revised copies.

Exercise 1

In this exercise, the location of the groundwater divide (no-flow boundary) in an inland Dupuit-type unconfined aquifer is to be determined from the conceptual model presented in Figure 1. For this aquifer, two different scenarios are considered depending on the values of the two fixed-head boundaries. For each scenario, first determine if the groundwater divide is either real (located between the two fixed-head boundaries of the aquifer as shown in Figure 2) or imaginary (external to the aquifer system as shown in Figure 5). Then, for each scenario, determine the different cases that should be considered to transform the initial flow system into a final transformed system (Figure 6), according to the explanations given in Section 3.1. The determination of the final transformed system in every scenario is necessary prior to developing the general analytical solutions presented in the book.

1. Scenario 1: The table below gives the properties of the aquifer and the values of the two fixed-head boundaries.

W [mm/y]	L [m]	K [m/s]	h_0 [m]	h_L [m]
500	2,000	$1\text{x}10^{-4}$	35	15

2. Scenario 2: The table below gives the properties of the aquifer and the values of the two fixed-head boundaries.

W [mm/y]	L [m]	K [m/s]	h_0 [m]	h_L [m]
500	2,000	$1\text{x}10^{-4}$	20	15

Solution to Exercise 1↴

Return to where text linked to Exercise 1↥

Exercise 2

Following the completion of Exercise 1, consider the right subdomain of Scenario 2 as the final transformed system. In this case, according to Figure 6, the aquifer extends from x=0 (no-flow boundary) to $x=L'$ where $h=h_{L'}$. The table below provides the values to be considered following the calculations conducted for the previous exercise.

W [mm/y]	L' [m]	K [m/s]	$h_{L'}$ [m]
500	1,276	$1\text{x}10^{-4}$	15

The value of effective porosity is n_e=0.35. The spreadsheet *Section-3_Dupuit-type-inland-and-island-aquifers.xlsx* can be used to do the calculations below. You may need to change some of the input parameters in the spreadsheet provided. Or you can build your own spreadsheet using the appropriate equations.

1. Calculate the hydraulic heads at x=10 m, x=500 m, and x=1,200 m.
2. Calculate the groundwater velocities at x=10 m, x=500 m, and x=1,200 m.
3. Calculate the groundwater travel times for a particle of water starting at position x_i=50 m and traveling to positions x=100 m, x=500 m, x=1,000 m, and x=1,276 m.
4. Calculate the groundwater volume per unit width of the aquifer.
5. Calculate the groundwater mean residence time in the aquifer.

Solution to Exercise 2⤵

Return to where text linked to Exercise 2⤴

Exercise 3

Consider an unconfined oceanic coastal Dupuit-type aquifer satisfying the conceptual model presented in Figure 17. The conditions are summarized in the table below.

W [mm/y]	S [m]	L' [m]	K [m/s]	ρ_f [g/cm^3]	ρ_s [g/cm^3]	$\Delta\rho$ [g/cm^3]	n_e [dimensionless]
500	30	1,000	1x10^{-4}	1	1.025	0.025	0.35

The spreadsheet entitled *Section-4_Dupuit-type-oceanic-coastal-aquifers.xlsx* can be used to solve the questions below. Or you can build your own spreadsheet using the appropriate equations.

1. Determine the location, x_T, of the saltwater toe (separating the inland zone from the seawater intrusion zone) as well as the freshwater saturated thickness, H_T, at this same location.
2. Calculate the water table elevation (inland zone) or the saturated freshwater thickness (seawater intrusion zone) at x=10 m, x=500 m, x=950 m, and x=990 m.
3. Calculate the fresh groundwater velocities at x=10 m, x=500 m, x=950 m, and x=990 m.
4. Calculate the fresh groundwater travel times required for a particle of water starting at position x_i=50 m and traveling to the positions x=100 m, x=500 m, x=950 m, and x=1,000 m.
5. Calculate the fresh groundwater travel times required for a particle of water starting at position x_i =930 m and traveling to the positions x=950 m, x=970 m, and x=1,000 m.
6. Calculate the fresh groundwater volumes per unit width of the aquifer in the seawater intrusion zone and the inland zone, as well as the total volume of freshwater contained in the coastal aquifer per unit width of aquifer.
7. Calculate the fresh groundwater mean residence times in the seawater intrusion zone, the inland zone, and in the coastal aquifer.

Solution to Exercise 3⤵

Return to where text linked to Exercise 3⤴

Exercise 4

Consider the cases of both strip and circular oceanic islands containing an unconfined oceanic island Dupuit-type aquifer. Conceptual models of the strip and circular oceanic islands are shown in Figure 23 and Figure 24, respectively. The conditions for both oceanic island aquifers are summarized in the table below.

W [mm/y]	L or R [m]	K [m/s]	ρ_f [g/cm³]	ρ_s [g/cm³]	$\Delta\rho$ [g/cm³]	n_e [dimensionless]
500	1,000	1×10^{-5}	1	1.025	0.025	0.35

The spreadsheet entitled *Section-5_Dupuit-type-oceanic-island-aquifers.xlsx* can be used to solve the questions below. Or you can build your own spreadsheet using the appropriate equations.

1. Calculate the freshwater lens saturated thickness in the strip and the circular islands at the locations (x, r)=10 m, (x, r)=100 m, (x, r)=500 m, (x, r)=900 m, and (x, r)=990 m.
2. Calculate the groundwater velocities at the same locations.
3. Calculate the groundwater travel times for a particle of water departing at (x_i, r_i)=20 m and arriving at (x, r)=100 m, (x, r)=500 m, and (x, r)=1,000 m.
4. Calculate the total freshwater volume per unit width of the strip island and of the circular island.
5. Calculate the freshwater mean residence times in the strip island and in the circular island.

Solution to Exercise 4↴

Return to where text linked to Exercise 4↥

Exercise 5

Consider the unconfined oceanic coastal Dupuit-type aquifer described in Exercise 3. Consider also that the slope of the aquifer is 0.02 m/m (2%). Evaluate the impacts of a sea-level rise of 0.6 m combined with a coastal erosion of 3 m on the same variables as presented in the 7 questions of Exercise 3: 1) change of the saltwater toe location and change of the freshwater saturated thickness at the saltwater toe; 2) change of the water table elevation (inland zone) or the saturated freshwater thickness (seawater intrusion zone); 3) change of the fresh groundwater velocities; 4) & 5) change of the fresh groundwater travel times; 6 change of the fresh groundwater volumes, and 7) change of the fresh groundwater mean residence times.

An additional question is:

8) Consider that the coastal aquifer undergoes different levels of land-surface inundation due to the combination of sea-level rise and coastal erosion. Consider that the sea-level rises by increments of 0.1 m from 0 to 1 m. Consider also that land-surface inundation due to coastal erosion ΔL_{CE} is 1 m for each increment of 0.1 m of sea-level rise. Determine the values of the change Δx_T of the position of the saltwater toe as a function of ΔL. Draw on a graph Δx_T versus ΔL.

The spreadsheet *Section-6_Climate-change_Coastal-oceanic-aquifers.xlsx* can be used to complete this exercise. Or you can build your own spreadsheet using the appropriate equations.

Solution to Exercise 5↴

Return to where text linked to Exercise 5↥

Exercise 6

Consider strip and circular oceanic islands containing an unconfined Dupuit-type aquifer, as described in Exercise 4. Consider also that the slope of the aquifer is 0.02 m/m (2%). Evaluate the impacts of a sea-level rise of 0.6 m combined with a coastal erosion of 3 m on the same variables as those in the 5 questions of Exercise 4:: 1) change of the freshwater lens saturated thickness in the strip and the circular islands; 2) change of the groundwater velocities; 3) change of the fresh groundwater travel times; 4) change of the fresh groundwater volumes, and 5) change of the fresh groundwater mean residence times.

The Excel spreadsheet entitled *Section-6_Climate-change_Island-oceanic-aquifers.xlsx* can be used to complete this exercise. Or you can build your own spreadsheet using the appropriate equations.

Solution to Exercise 6↴

Return to where text linked to Exercise 6↑

11 Exercise Solutions

Solution Exercise 1

The location of the groundwater divide x_{WD} is calculated from Equation (3), with W first converted to m/s, and the following results are obtained:

1. Scenario 1: x_{WD}=–577 m

In this first scenario, because x_{WD} is negative, the flow divide is imaginary and is located upgradient of the constant head boundary at x=0. Scenario 1 then refers to the conceptual model presented in Figure 5, which is Case II in Section 3.1. This scenario transforms into the system presented in Figure 6 between x=0 and $x=L'=L+|x_{WD}|$=2,000+577=2,577 m. Groundwater flow in this case will be only meaningful between $x=|x_{WD}|$=577 m and $x=L'$=2,577 m.

2. Scenario 2: x_{WD}=724 m

In this second scenario, since x_{WD} is positive, the flow divide is located between the two constant head boundaries. This scenario refers to the conceptual model presented in Figure 2, which is Case I in Section 3.1. The regional system can now be separated into two subdomains on either side of the water divide. Both subdomains can be reduced to the single problem shown in Figure 6, with a length L' of either $L'=x_{WD}$=724 m for the left subdomain of Figure 2 or $L'=L-x_{WD}$=2,000 – 724=1,276 m for the right subdomain of Figure 2. In both transformed systems, the origin x=0 now represents the upgradient no-flow boundary and the downgradient fixed-head boundaries are h'=20 m and h'=15 m for the left and right subdomains, respectively.

Return to Exercise 1
Return to where text linked to Exercise 1

Solution Exercise 2

1. The hydraulic heads (saturated thicknesses) are solved using Equation (8). The hydraulic heads at x=10 m, x=500 m, and x=1,200 m are h_I=21.98 m, h_I=21.06 m, and h_I=15.96 m, respectively.
2. The groundwater velocity is solved with Equation (9). The groundwater velocities at x=10 m, x=500 m, and x=1,200 m are v_I=0.65 m/y, v_I=33.92 m/y, and v_I=107.39 m/y, respectively.
3. The groundwater travel time is solved with Equation (19). The groundwater travel times for a particle of water starting at position x_i=50 m and traveling to position x=100 m, x=500 m, x=1,000 m, and x=1,276 m are t_I=10.65 y, t_I=35.11 y, t_I=44.78 y, and t_I=47.62 y, respectively.
4. The groundwater volume per unit width of the aquifer is calculated from Equation (23) and is V_I=8,854 m^3/m.
5. The groundwater mean residence time in the aquifer is calculated from Equation (24) or Equation (25) and is RT_I=14 y.

Return to Exercise 2

Return to where text linked to Exercise 2

Solution Exercise 3

1. The location of the saltwater toe, $x_{T,}$ is solved with Equation (57); x_T=924.41 m and the freshwater saturated thickness, $H_{T,}$ is calculated from Equation (48); H_T=30.75 m.
2. The locations x=10 m and x=500 m are situated in the inland zone and the water table elevation is calculated with Equation (59); H_{IZ}(x=10 m)=32.88 m and H_{IZ} (x=500 m)=32.27 m. The locations x=950 m, and x=990 m are situated in the seawater intrusion zone and the saturated freshwater thickness is calculated with Equation (56); H_{SIZ}(x=950 m)=25.17 m and H_{SIZ}(x=990 m)=11.37 m.
3. v_{IZ} is calculated from Equation (61) for x=10 m and x=500 m located in the inland zone: v_{IZ}(x=10 m)=0.43 m/y and v_{IZ}(x=500 m)=22.13 m/y. v_{SIZ} is calculated from Equation (60) for x=950 m and x=990 m located in the seawater intrusion zone: v_{SIZ} (x=950 m)=53.91 m/y and v_{SIZ} (x=990 m)=124.37 m/y.
4. The departure point x_i=50 m is located in the inland zone. The arrival points x=100 m and x=500 m are also located in the inland zone. Groundwater travel times in the inland zone are solved with Equation (65), yielding t_{IZ}(x=100 m)=15.94 y and t_{IZ}(x=500 m)=52.57 y. The arrival points x=950 m and x=1,000 m (this latter position corresponding to the discharge location in the ocean) are located in the seawater intrusion zone. In these two cases, the groundwater particle travels in both the inland and seawater intrusion zones and groundwater travel times are solved with Equation (67) to obtain t_{CA}(x=950 m)=66.19 y and t_{CA}(x=1,000 m)=66.80 y.
5. The departure point x_i=930 m is this time located in the seawater intrusion zone and Equation (63) is used to solve the travel times, yielding t_{SIZ}(x=950 m)=0.41 y, t_{SIZ}(x=970 m)=0.74 y and t_{SIZ}(x=1,000 m)=1.02 y.
6. The fresh groundwater volumes per unit width of the aquifer in the seawater intrusion zone, the inland zone and the entire coastal aquifer are calculated from Equations (71), (76), and (78), respectively. The calculations yield V_{SIZ}=547 m^3/m, V_{IZ}=10,411 m^3/m and V_{CA}=10,958 m^3/m.
7. The fresh groundwater mean residence times in the seawater intrusion zone, the inland zone, and in the coastal aquifer are calculated from Equations (80), (82), and (84), respectively. The calculations yield RT_{SIZ}=14.46 y, RT_{IZ}=22.53 y, and RT_{CA}=21.92 y.

Return to Exercise 3↥

Return to where text linked to Exercise 3↥

Solution Exercise 4

1. The freshwater lens saturated thickness in the strip island is calculated from Equation (90): H_{SOI}(x=10 m)=254.95 m, H_{SOI}(x=100 m)=253.68 m, H_{SOI}(x=500 m)=220.80 m, H_{SOI}(x=900 m)=111.13 m, and H_{SOI}(x=990 m)=35.97 m. The freshwater lens saturated thickness in the circular island are calculated from Equation (94): H_{COI}(r=10 m)=180.28 m, H_{COI}(r=100 m)=179.38 m, H_{COI}(r=500 m)=156.13 m, H_{COI}(r=900 m)=78.58 m, and H_{COI}(r=990 m)=25.43 m.
2. The freshwater velocities in the strip island are calculated from Equation (95): v_{SOI}(x=10 m)=0.07 m/y, v_{SOI}(x=100 m)=0.56 m/y, v_{SOI}(x=500 m)=3.23 m/y, v_{SOI}(x=900 m)=11.57 m/y, and v_{SOI}(x=990 m)=39.32 m/y. The freshwater velocities in the circular island are calculated from Equation (96): v_{COI}(r=10 m)=0.04 m/y, v_{COI}(r=100 m)=0.40 m/y, v_{COI}(r=500 m)=2.29 m/y, v_{COI}(r=900 m)=8.18 m/y, and v_{COI}(r=990 m)=27.80 m/y.
3. The groundwater travel times in the strip island (x_i=20 m) are calculated from Equation (99): t_{SOI}(x=100 m)=286.81 y, t_{SOI}(x=500 m)=562.96 y, and t_{SOI}(x=1,000 m)=643.44 y. The groundwater travel times in the circular island (r_i=20 m) are calculated from Equation (102): t_{COI}(r=100 m)=405.61 y, t_{COI}(r=500 m)=796.15 y, and t_{COI}(r=1,000 m)=909.96 y.
4. The total freshwater volume per unit width of the strip island is calculated from Equation (105): V_{SOI}=140,172 m^3/m. The total freshwater volume of the circular island is calculated from Equation (108): V_{COI}=132,155,514 m^3.
5. The freshwater mean residence time in the strip island is calculated from Equation (109): RT_{SOI}=280.34 y. The freshwater mean residence time in the circular island is calculated from Equation (110): RT_{COI}=84.13 y.

Return to Exercise 4⮥

Return to where text linked to Exercise 4⮥

Solution Exercise 5

1. The change of the location of the saltwater toe, Δx_T, is solved with Equation (122); Δx_T=–39.12 m. The new value of x_T is 885.30 m. The change of freshwater saturated thickness at the saltwater toe, ΔH_T, is calculated from Equation (116) or Equation (120). Indeed, at $x=x_T$, $I_{SIZ}(x_T)=I_{IZ}(x_T)=\Delta H_T$=0.45 m.
2. The locations x=10 m and x=500 m are still situated in the inland zone and the change of the water table elevation is calculated with Equation (116); $I_{IZ}(x$=10 m)=0.41 m and $I_{IZ}(x$=500 m)=0.42 m. The location x=950 m is still situated in the seawater intrusion zone and the change of saturated freshwater thickness is calculated with Equation (114); $I_{SIZ}(x$=950 m)=0.34 m. The location x=990 m is not situated in the seawater intrusion zone of the aquifer considering that the new length of aquifer is L_t=967 m, which is shorter than 990 m.
3. Δv_{IZ} is calculated from Equation (128) for x=10 m and x=500 m, which are still located in the inland zone: $\Delta_{vIZ}(x$=10 m)=–0.005 m/y and $\Delta v_{IZ}(x$=500 m)=-0.28 m/y. Δv_{SIZ} is calculated from Equation (126) for only x=950 m, which is still located in the seawater intrusion zone: $\Delta v_{SIZ}(x$=950 m)=30.65 m/y.
4. The departure point x_i=50 m is still located in the inland zone. The arrival points x=100 m, x=500 m and x=950 m are also still located in the inland zone. The changes in groundwater travel times in the inland zone are solved with Equation (132), yielding $\Delta t_{IZ}(x$=100 m)=0.20 y, Δt_{IZ}(x=500 m)=0.66 y and Δt_{IZ}(x=950 m)=0.86 y. The arrival point x=967 m corresponds actually to the discharge location in the ocean with the new length of the aquifer after land-surface inundation and is located in the seawater intrusion zone. In this case, the groundwater particle travels both in the inland and seawater intrusion zones and the changes in groundwater travel times are solved with Equation (134) to obtain $\Delta t_{CA}(x$=967 m)=0.46 y.
5. The departure point x_i=930 m is still located in the seawater intrusion zone and Equation (130) is used to solve the changes in travel times, yielding $\Delta t_{SIZ}(x$=950 m)=–0.14 y. The arrival points x=970 m and x=981 m are beyond the new discharge location at x=967 m.
6. The changes of fresh groundwater volumes per unit width of the aquifer in the seawater intrusion zone, the inland zone, and the entire coastal aquifer are calculated from Equations (136), (138), and (140), respectively. The calculations yield ΔV_{SIZ}=57 m^3/m, ΔV_{IZ}=–293 m^3/m, and ΔV_{CA}=–237 m^3/m.
7. The changes of fresh groundwater mean-residence times in the seawater intrusion zone, the inland zone, and in the coastal aquifer are calculated from Equations (142), (144), and (146), respectively. The calculations yield ΔRT_{SIZ}=0.30 y, ΔRT_{IZ}=0.33 y, and ΔRT_{CA}=0.26 y.

8. The variation of the saltwater toe position with land-surface inundation is given by Equation (123). The figure below shows Δx_T versus ΔL.

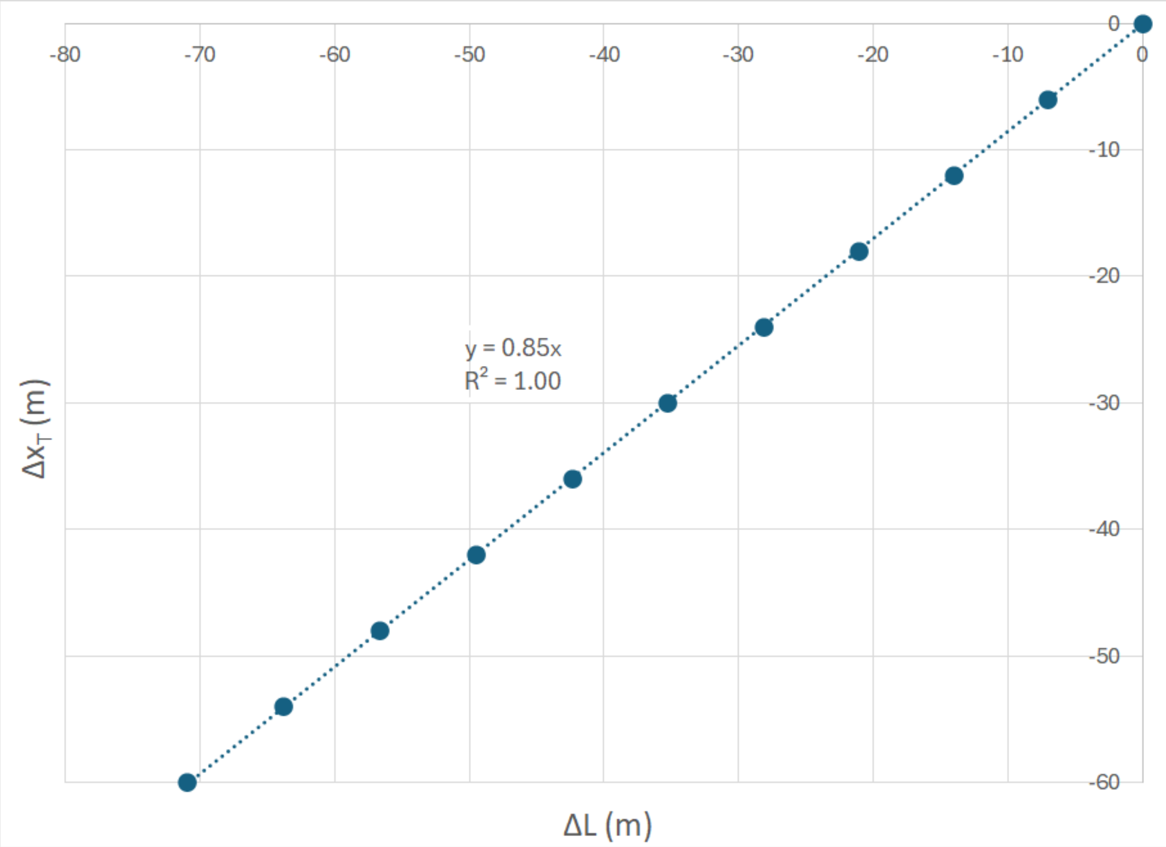

It is of particular interest that the saltwater toe appears to migrate linearly with the land-surface inundation, with $\Delta x_T \sim 0.85\Delta L$ in the given example. This means that the saltwater toe inland migration is proportional to the land-surface inundation by a factor of 0.85.

Return to Exercise 5

Return to where text linked to Exercise 5

Solution Exercise 6

1. The changes to the freshwater lens saturated thickness in the strip island are calculated from Equation (148): $\Delta H_{SOI}(x\text{=}10\text{ m})$=–8.41 m, $\Delta H_{SOI}(x\text{=}100\text{ m})$=–8.46 m, $\Delta H_{SOI}(x\text{=}500\text{ m})$=–9.77 m, $\Delta H_{SOI}(x\text{=}900\text{ m})$=–20.96 m. The location x=990 m is not situated in the aquifer considering that the new length of aquifer is L_t=967 m (inland inundation of ΔL=–33 m). The changes of the freshwater lens saturated thickness in the circular island are calculated from Equation (160): $\Delta H_{COI}(r\text{=}10\text{ m})$=–5.95 m, $\Delta H_{COI}(r\text{=}100\text{ m})$=–5.98 m, $\Delta H_{COI}(r\text{=}500\text{ m})$=6.91 m, and $\Delta H_{COI}(r\text{=}900\text{ m})$=–14.82 m. The same situation as the strip island occurs for the circular island where the new radius of the island is R_t=967 m.
2. The changes in freshwater velocities in the strip island are calculated from Equation (150): $\Delta v_{SOI}(x\text{=}10\text{ m})$=0.0019 m/y, $\Delta v_{SOI}(x\text{=}100\text{ m})$=0.02 m/y, $\Delta v_{SOI}(x\text{=}500\text{ m})$=0.15 m/y and $\Delta v_{SOI}(x\text{=}900\text{ m})$=2.69 m/y. The changes in freshwater velocities in the circular island are calculated from Equation (162): $\Delta v_{COI}(r\text{=}10\text{ m})$=0.0013 m/y, $\Delta v_{COI}(r\text{=}100\text{ m})$=0.014 m/y, $\Delta v_{COI}(r\text{=}500\text{ m})$=0.106 m/y, and $\Delta v_{COI}(r\text{=}900\text{ m})$=1.90 m/y.
3. The changes in groundwater travel times in the strip island (x_i=20 m) are calculated from Equation (152): $\Delta t_{SOI}(x\text{=}100\text{ m})$=–9.49 y and $\Delta t_{SOI}(x\text{=}500\text{ m})$=–19.38 y and $\Delta t_{SOI}(x\text{=}967\text{ m})$=–26 y. The changes in groundwater travel times in the circular island (r_i=20 m) are calculated from Equation (164): $\Delta t_{COI}(r\text{=}100\text{ m})$=13.43 y, $\Delta t_{COI}(r\text{=}500\text{ m})$=–27.41 y, and $\Delta t_{COI}(r\text{=}967\text{ m})$=–36.77 y.
4. The change in total freshwater volume per unit width of the strip island is calculated from Equation (154): ΔV_{SOI}=–9,099 m^3/m. The change in total freshwater volume of the circular island is calculated from Equation (166): ΔV_{COI}=–12,656,393 m^3.
5. The change in freshwater mean residence time in the strip island is calculated from Equation (157): ΔRT_{SOI}=–9.25 y. The change in freshwater mean residence time in the circular island is calculated from Equation (168): ΔRT_{COI}=–2.78 y.

Return to Exercise 6↥

Return to where text linked to Exercise 6↥

12 Notations

$\mathrm{d}h/\mathrm{d}r$	hydraulic gradient in the radial direction
$\mathrm{d}h/\mathrm{d}x$	hydraulic gradient in the horizontal direction
$\Delta\rho$	$\rho_s - \rho_f$
h	Equation (1), phreatic surface elevation or saturated thickness above the horizontal impervious substratum or hydraulic head [L]
h	Equation (5), hydraulic head [L]
h	Equation (48), water table elevation above sea level [L]
$h(r)$	elevation of the water table above sea level in the circular island [L]
$h(x)$	elevation of the water table above sea level in the strip island [L]
h_0	fixed-head boundary at x=0 [L]
$H=h+z$	Equation (53), freshwater saturated thickness of the unconfined aquifer in the seawater intrusion zone [L]
$H=h+z$	Equation (91), freshwater lens saturated thickness in the unconfined oceanic island [L]
h_I	hydraulic head in an inland aquifer [L]
$h_{L'}$	fixed downstream ($x=L'$) head [L]
H_T	freshwater thickness at $x=x_T$ [L]
K	saturated hydraulic conductivity of the aquifer [LT^{-1}]
L'	length of the aquifer [L]
n_e	effective porosity of the porous medium
ρ_f	density of freshwater
ρ_s	density of saltwater
q_r	Darcy flux in radial direction [LT^{-1}]
q_x	Darcy flux in horizontal direction [LT^{-1}]
$t_{CII}(x)$	travel time between position r_i and position r in the circular inland-island aquifer [T]
t_I	travel time between position x_i and position x in the inland aquifer [T]
$t_{SII}(x)$	travel time between position x_i and position x in the strip inland-island aquifer [T]
τ and ρ	the integration variables for t_{CII} (travel time in a circular inland island) and r, respectively

$v_{CII}(r)$	average linear velocity of a particle [LT^{-1}] located at *r* [L] in the circular inland island
$v_{COI}(r)$	average linear velocity of a particle [LT^{-1}] located at *r* [L] in the circular oceanic island
$v_{IZ}(x)$	average linear velocity of a particle of water [LT^{-1}] located at *x* [L] in the inland zone of a coastal aquifer
$v_{SII}(x)$	average linear velocity of a particle [LT^{-1}] located at *x* [L] in the strip inland-island
$v_{SIZ}(x)$	average linear velocity of a particle of water [LT^{-1}] located at *x* [L] in the seawater intrusion zone of a coastal aquifer
$v_{SOI}(x)$	average linear velocity of a particle [LT^{-1}] located at *x* [L] in the strip oceanic island
W	recharge rate of the aquifer [LT^{-1}]
x_i	departure point [L]
x_T	saltwater toe location [L]
x_{WD}	water divide location [L]
z	depth to the fresh-saline interface below sea level
$z(r)$	depth to the fresh-saline interface below sea level in the circular island [L]
$z(x)$	depth to the fresh-saline interface below sea level in the strip island [L]

The notations of several additional variables of groundwater are given in Table 1 and Table 2 and are not repeated here.

13 About the Author

Romain Chesnaux is a French and Canadian engineer and hydrogeologist. He earned a B.Sc. Eng. in water and environmental engineering at the "École Nationale du Génie de l'Eau et de l'Environnement de Strasbourg (ENGEES)" in France in 2000. He came to Canada in 2001 at Polytechnique Montréal for a Ph.D. specializing in groundwater research. Doctorate in hand in 2005, he moved west for a postdoctoral fellowship at Simon Fraser University in Vancouver, followed by a year away from Academia to pick wild mushrooms full-time. In 2009, he joined the faculty of the Université du Québec à Chicoutimi (UQAC) in Canada as a Professor and was promoted to Full Professor in 2020. While at UQAC, he has mentored numerous B.Sc., M.Sc., and Ph.D. students, as well as postdoctoral fellows and professional hydrogeologists. He is still mushroom picking to this day.

Please consider signing up for the GW-Project mailing list to stay informed about new book releases, events and ways to participate in the GW-Project. When you sign up for our email list it helps us build a global groundwater community. Sign up↗.

THE GROUNDWATER PROJECT